5-2016

# STUDIES IN ASYMMETRIC CATALYSIS: SUPRAMOLECULAR CATALYSIS AND BORANE-ASSISTED HYDROGENATION

Kazuya Toyama
*University of Nebraska-Lincoln*, kazuya.toyama@huskers.unl.edu

# STUDIES IN ASYMMETRIC CATALYSIS: SUPRAMOLECULAR CATALYSIS AND BORANE-ASSISTED HYDROGENATION

by

Kazuya Toyama

A DISSERTATION

Presented to the Faculty of
The Graduate College at the University of Nebraska
In Partial Fulfillment of Requirements
For the Degree of Doctor of Philosophy

Major: Chemistry

Under the Supervision of Professor James M. Takacs
Lincoln, Nebraska
May, 2016

# STUDIES IN ASYMMETRIC CATALYSIS: SUPRAMOLECULAR CATALYSIS AND BORANE-ASSISTED HYDROGENATION

Kazuya Toyama, PhD.

University of Nebraska, 2016

Adviser: James M. Takacs

Metal-catalyzed catalytic asymmetric reactions have gained enormous attentions and the utilities of such reactions have facilitated natural products syntheses to afford highly bioactive molecules. While these reactions have provided reliable methodologies to transform basic reactants into product(s) with highly enantio- and regioselective manners, the incompatibility with a many functional groups and the associated need to employ protecting groups increases the number of synthetic steps required. Herein, a solution to such an issue has been proposed in catalytic asymmetric hydroboration of styrene derivatives where supramolecular catalysts developed by Takacs *et al.* were used to achieve highly regio- and stereoselective reaction on functionalized alkenes without the usage of protection chemistry. Moreover, the usefulness of the chemo- and site selective chemistry was demonstrated by applying this methodology to carry out a total synthesis of anti-fungal compounds with no protecting group manipulations.

Organoborons have been identified as one of the most versatile and important class of molecules due to the facts that they can be transformed into many different useful functional

groups including boronic acids which are widely used as a coupling partner for Suzuki-Miyaura coupling reaction. Thus, studies of catalytic asymmetric hydroboration have shown exponential growth over the past decade. Despite many successful advancements in catalytic asymmetric hydroboration of various substrates, not much attention has been paid to a formation of hydrogenation by-product which is a common observation from various research groups around the world. In this thesis, mechanism of hydrogenation by-product was investigated by both experimentally and computationally and a boron assisted hydrogenation mechanism is proposed to account for the hydrogenation by-product.

ACKNOWLEDGEMENTS

I would like to start by thanking my advisor Professor James M. Takacs. His guidance has been indispensable during my graduate study. I have truly enjoyed being an independent scientist in the lab and the experiences have taught me very important lessons to my professional career. I would like to thank him for being patient with me and supportive for me during the difficult times of my graduate study.

I thank my committee members for their helpful comments, discussions, and supports during the PhD study. In addition, I very much appreciate the direction and advice from the committee members to organize and keep me on track toward my graduation: Professor Dussault, Professor Cheung, Professor Guo, Professor Tan, and Professor DiMagno. I would like to especially thank thesis reading committee members; professor Guo for accepting to serve as a reading committee at the last minute and professor Dussault for providing insightful feedback on my thesis

I would also like to thank all my colleagues in Takacs group for all the helpful discussions and guidance: Dr. Sean Smith, Dr. Nathan Thacker, Scott Pettibone, Mohammad Khaled, Andy Geis, Dr. Rajesh Panicker, Dr. Mark Helle, Gia Lê Hoàng, Dr. Kostiantyn Marichev, Shuyang Zhang, Suman Chakrabarty, Veronika Shoba, Ryan Carr, and Andrew Bochat. Special thanks go to Dr. Nathan Thacker who trained me well for graduate research from the beginning. I would like to also thank Dr. Rajesh Panicker for helpful discussions and being a good resource.

I thank Dr. Martha Morton and Dr. Beth Donovan for various helps on instruments to identify key intermediates for the projects.

# Table of Contents

## CHAPTER 2 SITE SELECTIVE CATALYTIC ASYMMETRIC HYDROBORATION

# Table of figures

**Chapter 1**

**Chapter 2**

**Chapter 3**

**LIST OF ABBREVIATIONS:**

Aq: Aqueous

Ar: Aryl

B: Borane

$BF_4$: Tetrafluoroborate

BINAP: 2,2'-Bis(diphenylphosphino)-1,1'-binaphthyl

BINOL: 1,1'-Bi-2,2'-naphthol

Bn: Benzylic

BOX: Bisoxazoline

CAHB: Catalyzed asymmetric hydroboration

CatBH: Catecholborane

CD: Circular dichrooism

cod: Cyclooctadiene

$D_2$: deuterium

DCE: Dichloroethane

DCM: Dichloromethane

de: Diastereomeric excess

DFT: Density functional theory

DMF: N,N-dimethylformamide

DOSY: Diffusion-ordered NMR spectroscopy

dppe: Diphenylphosphinoethane

ee: Enantiomeric excess

Eqv: Equivalent

Et: Ethyl

EtOAc: Ethyl acetate

GC: Gas chromatography

GPC: Gel-permeation chromatography

GCMS: Gas chromatography mass spec

h: Hour

$H_2$: Hydrogen

HD: hydrogen deuteride

HPLC: High-performance liquid chromatography

Hz: Hertz

IR: Infrared

L: Ligand

m-: Meta

Me: Methyl

MeOH: Methanol

min: Minutes

MOF: Metal-Organic Framework

MS: Mass spectrometry

$N_2$: Nitrogen

nbd: Norbornadiene

NHC: N-heterocyclic carbene

NMR: Nuclear magnetic resonance

o-: Ortho

Oms: Mesylate

OTf: Triflate

OTs: Tosylate

p-: Para

Ph: Phenyl

PinBH: Pinacolborane

psi: Pounds per square inch

rac: Racemic

rt: Room temperature

SAL: Self-assembled ligand

TADDOL: α, α, α, α-Tetraaryl-1,3-dioxolan-4,5-dimethanol

TBDPS: Tert-butyl diphenylsilyl

TBDMS: Tert-butyl dimetylsilyl

t-butyl: Tetra-butyl

THF: Tetrahydrofuran

TLC: Thin-layer chromatography

TMDBH: 4,5,6-trimethyl-1,3,2-dioxaborinane

TMDBD: 4,5,6-trimethyl-1,3,2-dioxaborinane-2d

TIPS: Tri-isopropylsilyl

UV-Vis: Ultraviolet-visible spectroscopy

(X)-Taddol: [(3,5-Me)2C6H3]-aryl substituted TADDOL

# CHAPTER 1. SUPRAMOLECULAR CATALYSIS

## 1.1 Supramolecular catalysis - Introduction

Catalysis is the basic tool of building molecules via breaking and making chemical bonds, a process that is necessary for transforming basic chemicals into more valuable products. Catalytic processes can be homogeneous, or heterogeneous, and the catalysts used in these processes include transition metal complexes, organocatalysts, metals and enzymes. In addition, recent efforts have led to impressive developments in the area of supramolecular catalysis. Supramolecular catalysis utilizes weak intra- and intermolecular interactions to assemble complex catalyst species. This approach has shown promising results, often achieving impressive stereoselection typically achieved only by enzymes. Such selectivity can be achieved due to the fact that supramolecular catalysts possess flexibility somewhat flexible chiral framework around a catalysis metal, which defines unique chiral topography. This chiral topography is characteristic of what makes supramolecular catalysts behave similarly to enzymes.

Supramolecular catalysts typically are large molecules. Many supramolecular catalysts developed in the past decade have a molecular weight of between 1,000 and 3,000 daltons [1]. However, the assembly of such large catalysts is rarely as complicated as the molecular weight suggests thanks to the way supramolecular catalysts utilize inter- or intramolecular interactions to bring monomeric components of the catalyst structure together. This has several advantages over traditional metal asymmetric catalysts which incorporate one binding site (monodentate) or two metal binding sites

(bidentate) within a low molecular weight scaffold. Typical monodentate and bidentate ligands are illustrated schematically by structures **101** and **102** (Figure 1). Monodentate ligands (Figure 1, structure **101**) have been used extensively in asymmetric catalysis and shown to be highly effective using two or more equivalents of the ligand. However, exploring the effect of both steric and electronic changes in ligand structure requires one to synthesize ligands one by one, a time consuming process. In addition, fine-tuning the properties of a monodentate ligated catalyst is challenging since it is often found that a relatively subtle change to the catalyst structure leads to significant changes in catalyst performance. Although bidentate ligands (Figure 1. Structure **102**) often offer more precise control relative to monodentate ligands resulting in more efficient catalysts and the catalyst of choice for many asymmetric transformations, building a ligand library of chiral bidentate ligands is often very tedious as well. The design of chiral supramolecular catalysts fill in these gaps by offering a relatively easy method to generate a large numbers of structurally closely related ligand libraries via combinatorial method. While preparation of the individual components of a supramolecular ligand can require significant effort, these individual components can now be organized. Although each of supramolecular ligand synthesis can be as tedious as bidentate ligands synthesis, prepared supramolecular catalysts can be organized via directed self-assembly using a structural metal (Figure 1, structure **103**) or complementary hydrogen bonding motifs (Figure 1, structure **104**) to produce a large numbers of ligand libraries with comparative ease.

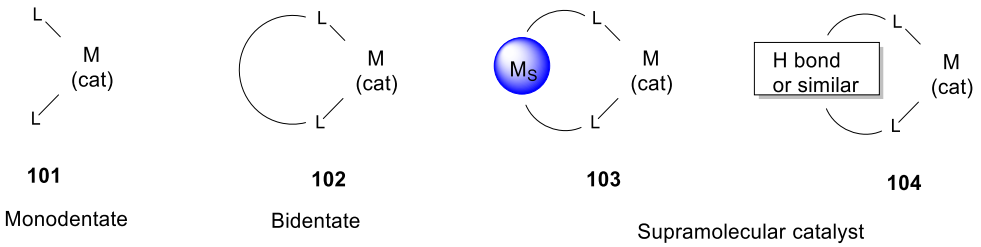


**Figure 1.** Chirality organization around a catalyst metal via traditional monodentate (**101**) and bidentate (**102**) ligands. Chirality organization around a catalyst supramolecular metal catalyst via metal complexation (**103**) and complementary hydrogen bonding (**104**). ($M_S$ represents a metal complex whose role is principally structural).

This chapter will provide a brief review of the field of asymmetric supramolecular catalysis. There are two now well established methods for utilizing intramolecular interactions to self-assemble supramolecular catalysts, namely, the use of a structural metal (Figure 1, structure **103**) and the use of complementary hydrogen bonding (Figure 1, structure **104**). Two newly developed methods for self-assembly based upon ionic or dipole-dipole interactions will be discussed briefly at the end of the chapter. As my thesis focuses on the development of asymmetric catalysts using metal-directed self-assembly, this background and literature review chapter will focus on asymmetric supramolecular catalysts. Other types of supramolecular catalysts exploit host-guest interactions wherein the uniquely constructed conformation inside a catalyst cavity can lead to a chemo-, regio-, or stereoselective chemical transformations. However, most of the host-guest supramolecular catalyst focuses on size or shape exclusion aspect of the chemistry not on asymmetric catalysis.

**1.2 Homogeneous asymmetric supramolecular catalysis – structural metal coordination to form supramolecular catalysts**

Briet, Reek and Van Leeuwen, and Takacs were the principal early contributors to the development of homogeneous asymmetric supramolecular catalysis. Reek and Van Leeuwen collaborated on supramolecular catalysis research and the first example of using a metal-directed self-assembly to construct supramolecular catalysts was published jointly from Reek and Van Leeuwen[2] in 2003. At that point hydrofoymylation research in the community had focused on the design and evaluation of novel bidentate ligands since it had been found that the "bite angle" of bidentate ligands was an important factor in giving more active and more selective catalyst systems.[3]. However, the syntheses of bidentate ligands are more complex and time-consuming; systematic investigations requiring a library of ligands were challenging tasks. A solution to this issue is to combine sets of easily prepared monodentate ligands via intra- and intermolecular interactions to create supramolecular bidentate ligand systems via metal-directed self-assembly.

Building on prior studies[4] Reek used a non-chelating bifunctional pyridine-phosphorus compound as a ligand and bis-porphyrin as a template (Figure 2. A). The secondary interaction, which is responsible for efficient assembly of supramolecular catalyst, is selective coordination of the pyridine nitrogen atoms to the porphyrin-bound zinc. (Figure 2. B. **105**). After complexing to the template, a phosphorus donor atom **106** is still available for complexation to transition metals such as rhodium. The authors turned their attention to asymmetric induction using the assembled bidentate ligand for

the hydroformylation of styrene. In the absence of the zinc porphyrin template, the bifunctional ligand **106** alone afforded only 7.2% ee of the hydroformylation product. In contrast, the assembled supramolecular catalyst showed significantly higher enantioselectivity (33% ee) along with an increase in reactivity up to 15 fold (Figure 2. C). Although the described work showed only moderate enantioselectivity and reactivity in the rhodium catalyzed hydroformylation of styrene, these results were very promising start for asymmetric supramolecular catalysis systems.

(A)

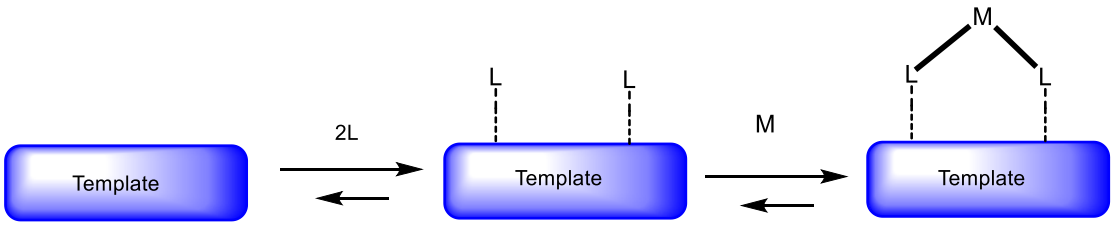


(B)

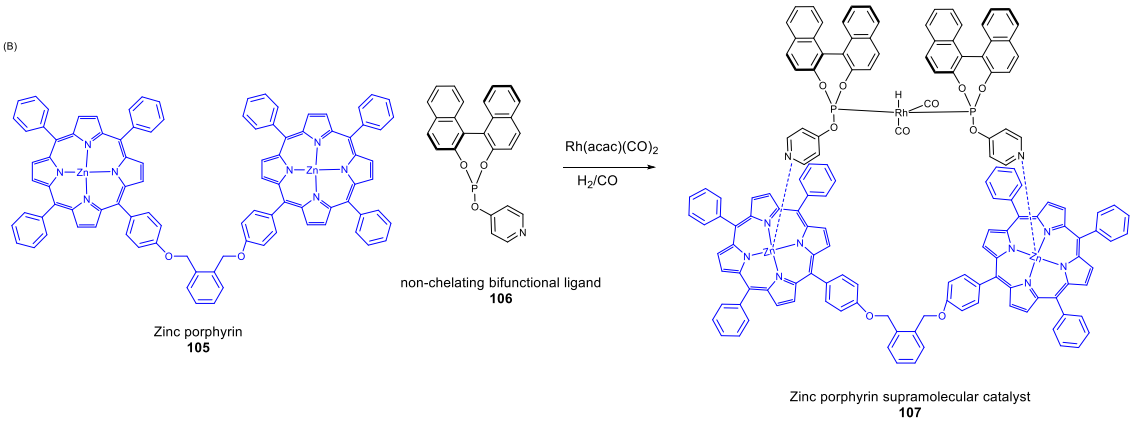

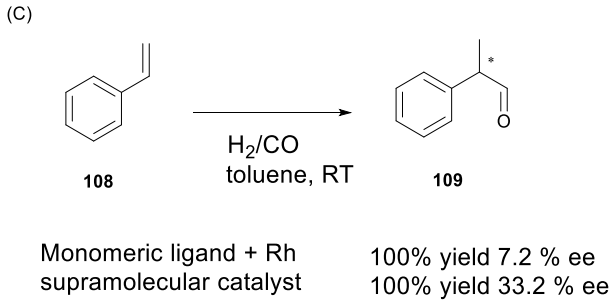


**Figure 2.** (A) Schematic representation of a self- assembled chelating ligand. L = monodentate ligand and M = transition metal. (B) Transition metal supramolecular catalyst formed by self-assembly of non-chelating bifunctional ligand on dimeric zinc porphyrin (template) and in presence of a rhodium precursor. Rhodium catalyzed hydroformylation results with supramolecular catalysts and monomeric ligand (C). Figure adapted from *Chem Commun*. **2003**, 2474.

Building from this first self-assembled asymmetric supramolecular catalyst, Reek and his colleagues developed several different supramolecular catalyst systems over the last decade[2] (Figure 3). The overall design continued to be based upon self-assembly of a supramolecular ligand for regio- and stereoselective hydroformylation based upon selective coordination of the nitrogen donor atom of the monomeric ligand to the zinc atoms of the metalloporphyrins. A second generation supramolecular catalyst (**111**) allowed the authors to combine different ligand building blocks equipped with complementary binding sites to form bidentate ligands. This was achieved by attaching one of the two non-chelating ligands to porphyrin template covalently, while a pyridine moiety of the other non-chelating ligand was coordinated to the zinc center of porphyrin template leaving a phosphorus center suitably deployed to bind to another transition metal[5] (Figure 3B). This approach provided an easy access to build a large

bidentate ligand library (i.e., 400 ligands were synthesized from 40 building blocks). It is worth noting that this system showed an unprecedented, albeit modest level (72:28) of regioselectivity for the linear aldehyde over the branched aldehyde in the rhodium-catalyzed hydroformylation of styrene. It was hypothesized that the regioselectivity is due to slow migratory insertion of CO and therefore enhanced β-hydride elimination from the branched alkyl-rhodium species. The latter intermediate reforms the rhodium alkene complex permitting the regioisomeric mode of reaction to predominate. In search for further alternative strategies the authors introduced a new class of supramolecular bidentate ligands[6] in which the two non-equivalent phosphorus and pyridine moieties are attached covalently to a chiral backbone and supramolecular interaction was used as a mean to control the steric bulk around a metal (Figure 3C. **112**). One of the interesting observations from this work was that the authors were able to fine-tune the ligand properties by utilizing electronically and sterically different zinc porphyrin templates to achieve higher levels of enantioselectivity (up to 83% ee)

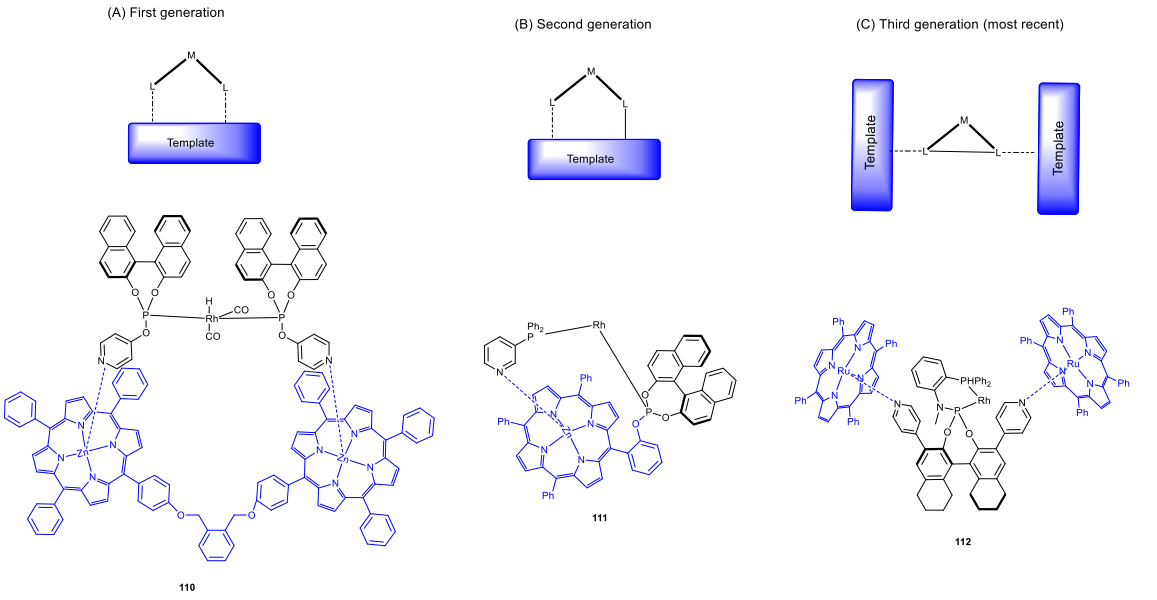


| | | | |
|---|---|---|---|
| Styrene hydroformylation best results | 99 % conv<br>b:l = 99 : 1<br>33.2 %ee | 83 % conv<br>b:l = 28 : 72 | 99 % conv<br>b:l = 95 : 5<br>82 %ee |

**Figure 3.** Selected examples of Reek's hydroformylation supramolecular catalysts in the past decade.

In 2004, only shortly after the initial publication from Reek and Van Leeuwen, Takacs and coworkers[7] reported a self-assembled ligand (SAL) system for asymmetric allylic animation. Previously, Takacs and the coworkers showed that interaction of chiral bisoxazoline (BOX) ligands (**113** & **114**) with $Zn(OAc)_2$ results in the rapid formation of a $(BOX)_2Zn$ complex (**115**) under mild conditions[8]. In Takacs' system the nitrogen atoms of BOX selectively coordinate to zinc metal to form a neutral stable complex. What makes this system unique is that in presence of racemic BOX (e.g., (R,R) BOX **114** and (S, S) BOX **113**) only heteroleptic complex (**115**) is formed. This selectivity results from the need to

achieve tetrahedral coordination around Zn while minimizing steric interactions between the phenyl groups. (Figure 4A) The favored formation of the heteroleptic complex was found to have two advantages in terms of creating self-assembled bidentate ligands. One reason is that constructing BOX moieties incorporating a pendant ligating group is fairly straightforward. Another reason is that since zinc forms the heteroleptic complex selectively, large numbers of supramolecular catalysts are easily obtainable through a combinatorial method. For example, given five different ligands linked to an (*S*, *S*)-BOX moiety and another five different ligating groups linked to an (R, R) BOX moiety, total combinations of zinc heteroleptic complex which can be produced by simple mixing is 25 so building a large numbers of self-assembled ligands (SAL) is relatively easy with this system and consequently can often be achieved within a short period of time. Each one of the ligands, in principle, has different catalytic activity and selectivity

To build a library of self-assembled ligand (SAL) systems using this approach, a series of substituted mono- or biaryl structures (tethers) are constructed to connect the BOX moiety and ligating group. Making 15 different ligands from the (S, S) BOX derivative and another 15 ligands incorporating an (R, R) BOX moieties generates 225 different bidentate ligands upon self-assembly around Zn(II). The Takacs group prepared and screened 50 of the 225 possible SAL combinations in a palladium-catalyzed asymmetric allylic amination[9-14] of a prototypical racemic allylic carbonate substrate by *N*-methyl-*p*-toluenesulfornamide (**116**). The authors found that the enantiomeric excess in product (**117**) varies tremendously, 20–97% ee, as a function of

the combinations of tethers (Figure 4B). This striking variation in enantiomeric excess demonstrates the ability to translate very subtle changes in the ligand structural backbone into rather significant changes to the chiral pocket topography around palladium. It is worth mentioning that without the supramolecular scaffold, the monodentate for the SAL ligating groups, that is, the simple TADDOL-derived phenyl monophosphite ligand, (TADDOL) POPh, afforded 48% ee. The most successful SAL (**118**) of this study afforded 82 % yield and 97 % ee for this asymmetric transformation demonstrating the significant role of the supramolecular complex in determining the enantioselectivity of the supramolecular catalyst system.

Rhodium catalyzed asymmetric hydrogenation is well-stablished area of asymmetric catalysis[15] for which new asymmetric catalysts are seemingly always in demand. Having utilized palladium catalyzed allylic amination to demonstrate proof of principle for Takacs' SAL concept for the design of asymmetric supramolecular catalysts, the authors evaluated the SAL in asymmetric hydrogenation of prototypical *N*-acyl enamide substrate (**119**)[16]. Experimentally, the SAL approach typically begins with selecting the most efficient mono- or bidentate ligands structures and then exploring how the SAL scaffold can be used to optimize selectivity. For the hydrogenation, ten different monodentate ligands were tested; the BIPHEP-derived ligand was found to be the most effective[16]. Incorporating BIPHEP ligand into Takacs' SAL and screening a library of 110 SALs in conjunction with $Rh(cod)_2BF_4$ resulted in a supramolecular catalyst (**121**) that gave 92% yield 82% ee (Figure 4. (C)). The authors and coworkers noticed wide variation in enantioselectivity (i.e., racemic to 80% ee) for 110 SALs that tested.

This spread in the enantioselectivity of the resulting chiral supramolecular catalysts is very similar to the results observed in the asymmetric aminations, and again demonstrates that subtle changes in the SAL scaffold strongly influences the chiral pocket topography and leads to variations in enantioselectivity. The results were at the time quite surprising given that the structural changes in the SAL are far from the resident chiral centers in the ligand and seemingly remote to the site of reaction. A comment in the publication was particularly interesting: "The results obtained thus far make it clear that, while the shape of the BIPHEP-phosphite ligating group within the macrocyclic metal chelate is invariant, small changes in the ligand scaffold reposition or reorient that shape to a more, or less, effective position for asymmetric catalysis. In some ways, this seemingly mimics a feature of biological catalysts; that is, Nature uses a rather limited set of structures (i.e., amino acid side chains and/or enzyme cofactors) positioned in different ways via macromolecular assemblies to define the topography and characteristics required for efficient asymmetric catalysis". This comment made clear the intent of the Takacs group to pursue enzyme-inspired supramolecular catalysts in the hopes of achieving reactivity and selectivity far superior to conventional man-made catalysts. Chapter 2 of this PhD thesis focuses on building supramolecular catalysts through self-assembly for site-selective asymmetric hydroboration where similarly situated alkenes are present but only one of them reacts with a particular supramolecular catalyst with high efficiency.

The authors further studied structure-activity and structure-selectivity relationships on asymmetric hydrogenation with two other prototypical enamide

hydrogenation substrates (**122 S1** & **S2** in Figure 4. (D)) [17]. The most efficient catalyst **124** afforded 99% yield and 96 % ee for **S1** and 96% and 93% ee for **S2** (Figure 4. (D)). However, the most valuable conclusion from this study was not the high enantioselectivity itself but the observation of the major changes in enantioselectivity that could result from even small changes made to SAL structure. The study revealed that a balance between scaffolds' rigidity and flexibility is required for effective fine-tuning of catalysts. Without sufficient rigidity, subtle changes in scaffold structure are inconsequential with respect to achieving a meaningful change (hopefully improvement) in reactivity or selectivity. Much the same is true for the case where the SAL is too rigid; it was found that small changes often lead to major shifts in catalyst performance. Thus, the enantioselectivity of the reaction is very sensitive to the selection of ligating groups and the balance between rigidity and flexibility of SAL tethers. Surprisingly, this study reveals that the structural element BOX moiety can play an important role in affecting reactivity and enantioselectivity to some extent, although the authors finds it difficult to rationalize the results on the basis of a remote conformational change passed along to the chiral ligating groups.

Having established a versatile supramolecular catalysts system based on the results of asymmetric allylic amination and asymmetric hydrogenation, Takacs and his coworkers extended the work to asymmetric hydroboration. Compared to asymmetric hydrogenation, metal catalyzed asymmetric hydroboration is much less explored, [18-19] but it has attracted much recent interest due to usefulness of the organoborane intermediates for synthetic transformations. While the reactivity of substituted

styrenes and related vinyl arenes toward metal catalyzed hydroboration is generally quite high, the level of enantioselectivity reported in the literature is often only modest[20-22]. The reaction is sensitive to both steric and electronic nature of substrates; this is especially true for *ortho*-substituted styrene series (**125**). It is not uncommon to find that different classes of chiral catalysts are required for the efficient reaction of each substituted styrenes (Figure 4E). Optimizing Takacs' SAL scaffolds for the asymmetric hydroboration of *ortho*-substituted styrene series led to catalysts (**127**) that rival or surpass the enantiomeric excess seen in previous systems [23] (Figure 4F); 91 – 96 % ee could be obtained for a series of five different *ortho*-substituted styrenes (i.e., Me, OMe, F, Cl, $CF_3$).

With the successful application of Takacs' SALs to asymmetric hydroboration of *ortho*-substituted styrene series, the authors reported a more advanced optimization method in the supramolecular SAL for meta-substituted styrene series (**128**). In prior studies it was found that subtle changes to the catalyst scaffold gave rise to supramolecular catalysts that exhibit excellent enantioselectivity. In the study of *meta*-substituted styrenes, after optimizing the catalyst scaffold, modifying the ligating groups achieved further increases in enantioselectivity (94 – 97%) [24] across a series of *meta*-substituted styrenes varying in electronic demand; the authors suggested this represented a second stage of catalyst optimization (Figure 4. (F)). The resulting supramolecular catalysts (**130**) are found to be much better in terms of turnover frequency (TOF) and turnover number (TON). In some case, the reaction was completed with as little as 0.05 mole percent catalyst within 5 h. Takacs and coworkers have been

unable to obtain a crystal structure of active supramolecular catalyst, but several data obtained in this study (e.g., circular dichroic (CD) spectra, HRFAB mass spectrometry, and DFT calculations) are consistent with a 1:1 SAL: Rh chelated structure.

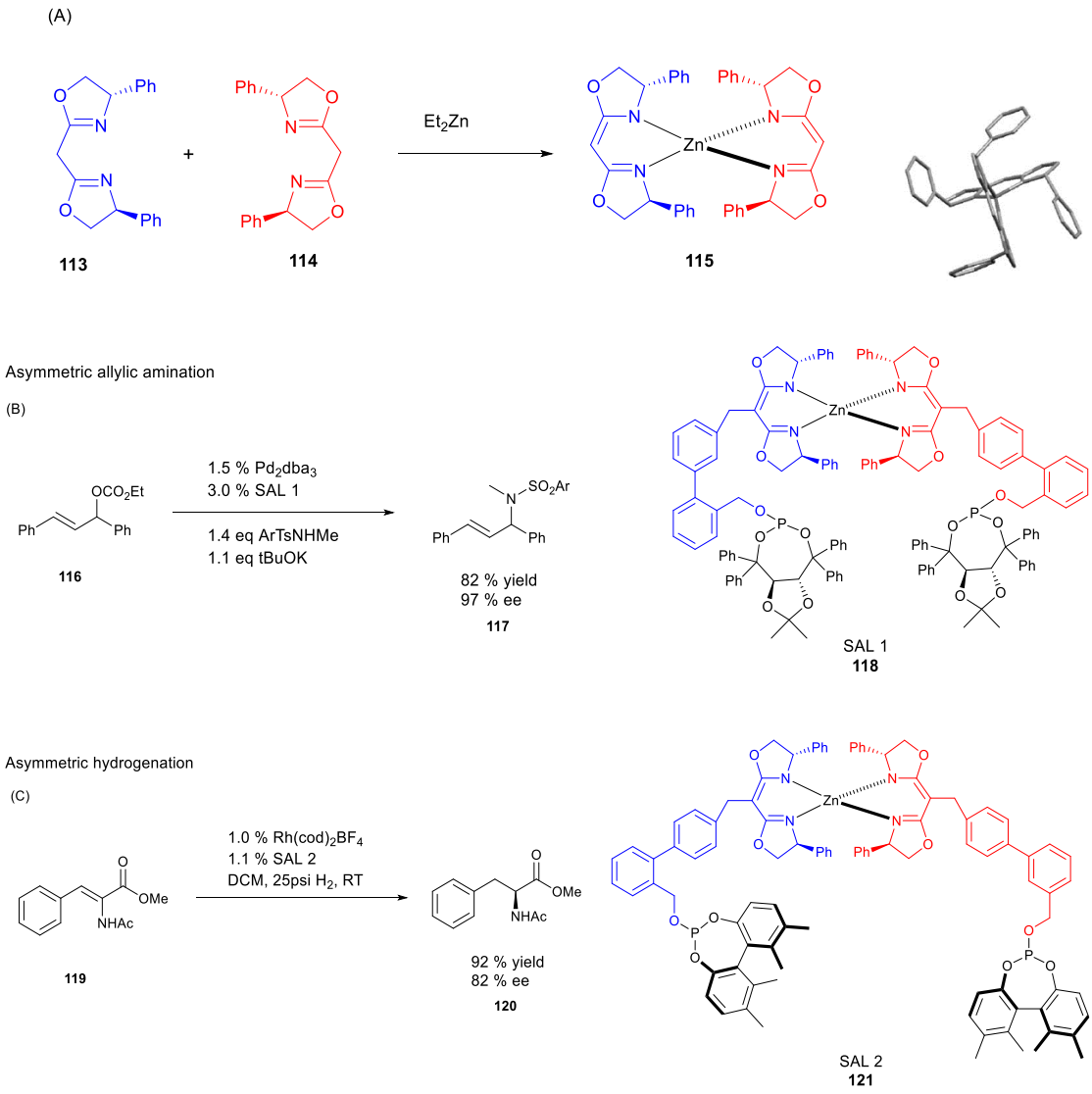

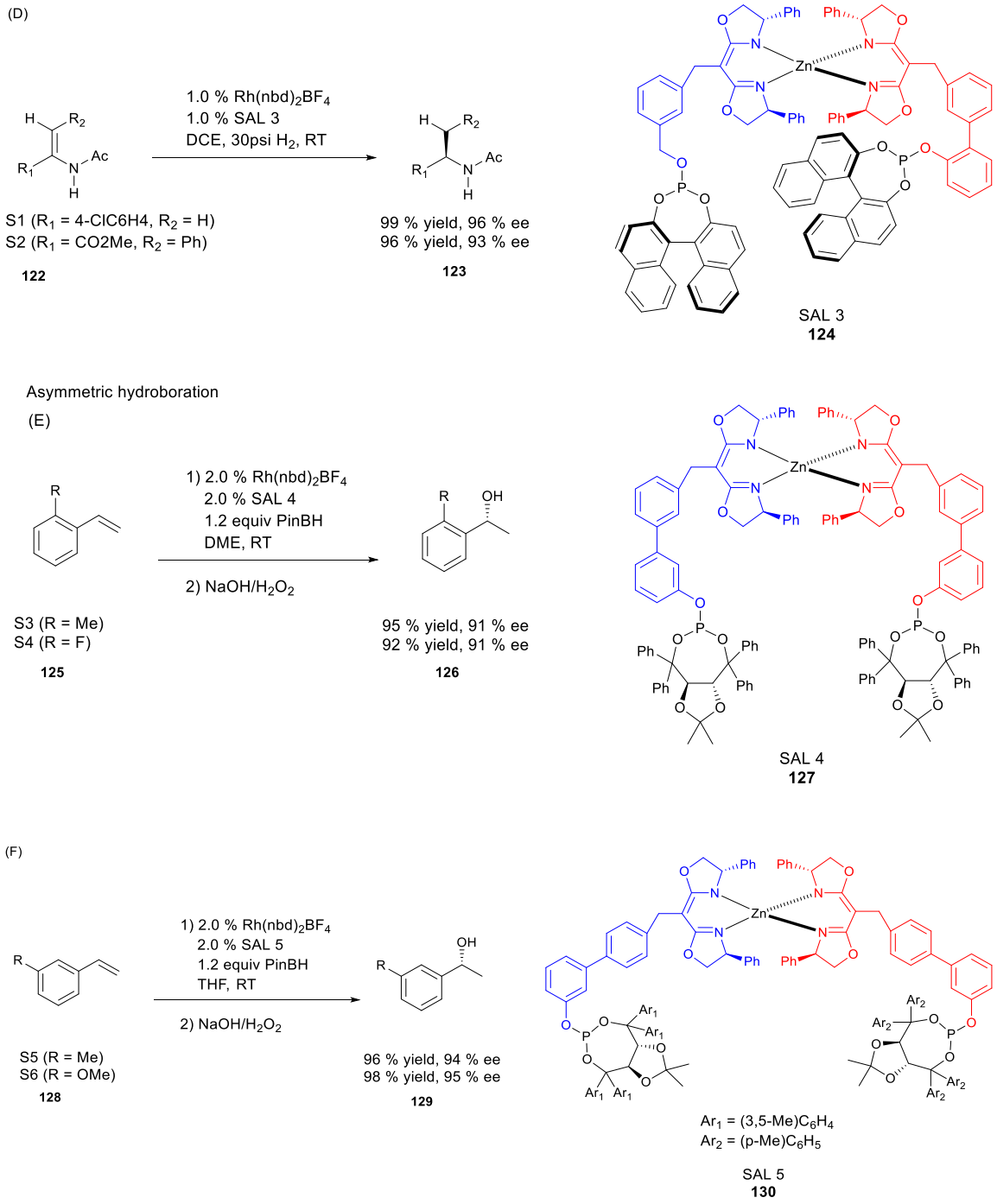


**Figure 4.** Overview of Takacs supramolecular catalysts. (A) Racemic bisoxazoline (BOX) ligands preferentially form a heteroleptic $(BOX)_2Zn$ complex. (B) Application of bisoxazoline-derived supramolecular catalyst to asymmetric allylic amination. (C) Application of same ligand system to asymmetric hydrogenation. (D) Through this study the authors found that having right combinations of rigidity (phenolic linkage between a

tether and ligating group) and flexibility (benzylic linkage between a tether and ligating group provides extra degree of flexibility to the SAL catalyst) to the ligand is necessary to afford high enantioselectivity for typical hydrogenation substrates. (E) Application of the ligand system to asymmetric hydroboration of *ortho*-substituted styrenes, resulting in the highest enantioselectivities reported. (F) Two stage optimization was applied to achieve the highest enantioselectivity reported for asymmetric hydroboration of *meta*-styrene series.

**1.2 Heterogeneous asymmetric supramolecular catalysis – Use of Metal-Organic Frameworks (MOFs) to form supramolecular catalysts**

Most highly efficient asymmetric catalysts are homogeneous catalysts. However heterogeneous catalysts have an advantage over homogeneous asymmetric catalysts by their relative ease of recyclability. This is an especially important issue for large-scale industrial processes in which the cost of precious metal catalysts is a major consideration[25]. Although traditional heterogeneous catalysts supported on resins[26] or metal particles[27] are well-precedented in industry, research into the development of supramolecular asymmetric catalysts based on Metal-Organic-Frameworks (MOFs) has seen rapid growth in the past decade. MOFs are compounds consisting of metals coordinating to organic molecules to form one-, two-, or three-dimensional structures usually having a porous core structures that can be used for size or shape exclusion of guest (often substrates). MOFs provide an excellent platform for the design of functional materials and numerous MOFs have been designed for important potential applications including gas storage[28], catalysis[29], imaging[30], sensing[31], and drug delivery[32]. Due to the mechanism by which MOFs are self-assembled, the active catalytic sites are usually exposed on or near the surface of the structure. The main difference between the homogeneous supramolecular catalysts based on structural metal coordination and the supramolecular catalysts assembled by MOF is that the latter has an extended three-dimensional structure of repeating subunits. Another key difference is that the former usually has a single reactive site, while the MOF based supramolecular catalysts usually have more than one catalytic site per structure.

The main reasons why successful asymmetric catalysts based on MOFs have been rare are that there are several requirements[33] that must be met in order to produce an efficient asymmetric catalyst. First of all, an appropriate chiral environment, or chiral binding pocket, is needed for the substrate(s) of interest. Secondly, MOF catalysts require a catalytic site(s) in close proximity to the chiral binding pocket and the substrate must interact with this site through an orientation enabling high levels of asymmetric induction. The MOF frameworks need to have large and readily permeable pores for chemicals (reagents and substrates) to exchange through MOF structure at a reasonable rate and those pores and pocket must retain their structural integrity during the reaction. A recent study demonstrates that enantioselectivity of MOF based supramolecular catalyst depends highly on both shape and size of the pores[34].

Asymmetric supramolecular catalysts based on MOF self-assembly generally fall into two types of frameworks. Type I MOF (Figure 5A), the predominant architecture of asymmetric MOF supramolecular catalyst, incorporate secondary metal binding residues onto chiral organic linkers, usually privileged ligand structures[35] such as BINOL-, BIPHEP-, or salen-ligating groups, to complex the catalytic metal. Primary functional groups selectively coordinate to structural metal ions to form the self-assembled MOF framework. Thus, the first step is the formation of basic MOF frameworks with metal ions and chiral organic linkers without the metals needed for catalysis. Afterwards, the latter are introduced. Privileged ligands often work well for a variety of asymmetric reactions so that by substituting different metals one can in principle use that MOF framework to carry out different asymmetric reactions[36]. However, a limitation to

applying this strategy is the requirement that the secondary functional groups (i.e., chiral ligating groups) be chemically orthogonal to the primary functional group so as to not disrupt self-assembly of the MOF. Type II MOF construction offers easier and perhaps more efficient strategy to synthesize a variety of catalytically active chiral MOFs for asymmetric transformations. In contrast to the Type I method, type II organic linkers are achiral, which typically simplifies their preparation. The organic linkers are mixed with metal ions to form the MOF wherein these metal centers also serve as potential catalytic sites. Chiral ligands are introduced to the MOF structure to form the chiral environment around the metal needed for asymmetric catalysis. Although this method is simpler and in principle less time consuming, slow leaching of the chiral ligands from the MOF catalysis can be a significant issue limiting catalyst stability; leaching is especially problematic when coordinating solvents such as DMF are used[37]. Another limitation inherent in this approach is that the metal must serve both structural and catalytic roles in the MOF. Therefore, a limited set of metals can be used.

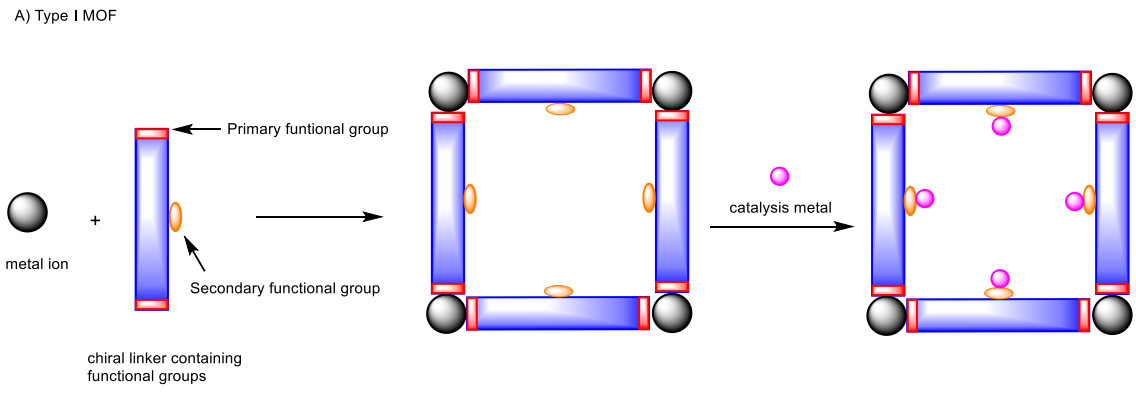

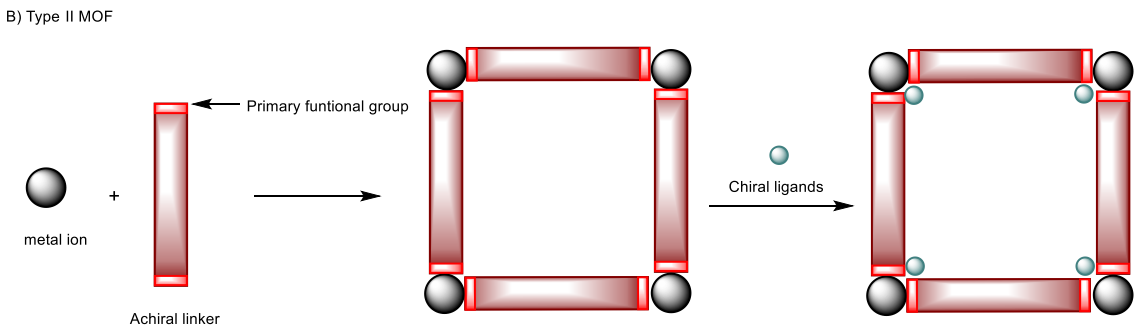


**Figure 5.** A) Type I MOF structure use chiral organic linkers possessing two orthogonal metal binding functional groups. Primary functional groups coordinate to metal ions to construct the MOF structure, while secondary functional groups are used for coordinating to the catalytic metal where asymmetric reaction occurs. B) Type II MOFs have achiral organic linkers for structural purposes. Chiral ligands are introduced after MOF structure is formed.

The first asymmetric supramolecular catalyst[34] developed based on a MOF was reported by Kim and the coworkers in 2000. This MOF was synthesized by type II method (Figure 5B). Oxo-bridged trinuclear metal carboxylates are commonly found in transition metal coordination chemistry and are easily assembled with metal and carboxylates[35]. Complexed water molecules can be easily replaced by nitrogen-containing ligands enabling the construction of extensive networks of void structures within the MOF. The chiral building block is synthesized from D-tartaric acid, which is reacted with Zn(II) ions to produce a chiral MOF based supramolecular catalyst (**135** D-POST-1). The authors used D-POST-1 (**135**) for the asymmetric transesterification of racemic 1-phenyl-2-propanol (**132**) at 10% catalyst loading. This first asymmetric reaction using a chiral MOF supramolecular catalyst was tested on only one substrate

and gave just 8% ee in product **133** (Figure 6). However, the catalyst could be reused up to three times without significant loss of its catalytic activity. Although the enantioselectivity is low, this result spurred interest in the field.

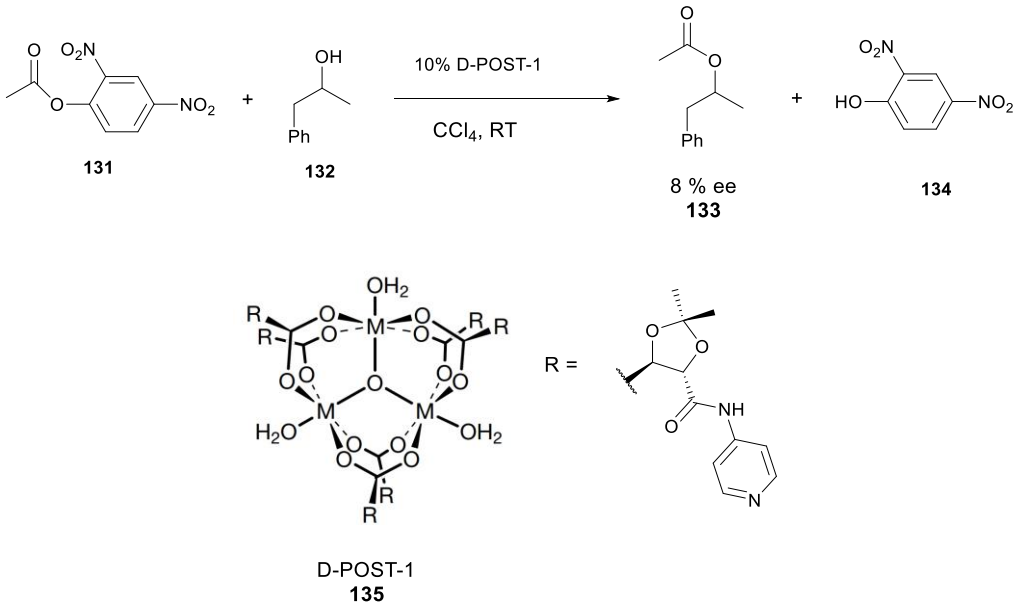


131 132 133 134 135

**Figure 6.** The first application of a MOF-based asymmetric supramolecular catalyst.

The Lin group has been the major contributor to the development of chiral MOF catalysts. They demonstrated the versatility of MOFs for asymmetric diethyl zinc additions, asymmetric hydrogenation, asymmetric 1, 4 addition of boronic acids[40], asymmetric cyclopropanation[41], and asymmetric epoxidation[42] and several publications focused on asymmetric addition of diethyl zinc to aldehydes affording chiral alcohols[38] and asymmetric hydrogenations[39]. Lin and the coworkers incorporated several metals, including Rh, Ru, Ti, and Mn, in their chiral MOF-based supramolecular structures.

MOFs containing metal-salen complexes have attracted great interest due to some promising results in asymmetric catalysis, chiral recognition and separation.[43] Utilizing metal-salen MOFs, Lin developed asymmetric MOF-based catalysts for cyclopropanation (**136** & **137**) and achieved excellent enantioselectivity, up to 98% ee (Figure 7A). MOF **1** (**140**) undergoes reversible reduction/reoxidation such that the catalytically inactive $Ru^{III}$ can be reduced to catalytic active $Ru^{II}$ to perform asymmetric cyclopropanation and can be used several times without significant loss in catalytic activity. Similar metal-salen organic linkers complexed to Mn (II) are used to construct MOF based catalyst for epoxidation; the latter achieved 84% ee for a variety of simple substrates (Figure 7C). MOF **3 (145)** is the first MOF based catalyst to undergo sequential asymmetric alkene epoxidation/epoxide ring opening reactions in one pot.

A handful of MOF-based chiral catalysts introduced by the Lin group have achieved good to excellent enantioselecitivity in asymmetric diethyl zinc addition to aldehydes. A recent report from this group describes the use of two primary functional groups in a chiral organic linker instead of one, which creates complex MOF architecture. (Figure 7 B) Although the main focus of the work was on asymmetric induction using MOF based catalysts for diethyl zinc addition, the levels of enantioselectivity was found to be dependent on the pore sizes due to the competition between enantioselective and non-enantioselective reaction.

Since the first development of MOF based chiral catalyst privileged ligands BINOL and metal/salen complex have been used for various asymmetric transformations. The corresponding phosphine, BINAP, has been successfully used as source of chirality in

many metal catalyzed reactions, beginning with Noyori's elegant asymmetric hydrogenation methodology.[45] Despite its usefulness in asymmetric catalysis, BINAP had not been incorporated into MOF based asymmetric catalysts due to the challenge of synthetic modifications and the sensitivity of phosphines to the typical MOF growth conditions. In 2014, Lin group reported the first BINAP MOF based catalysts, and their application to highly enantioselective 1, 4 addition (figure 7 D) and hydrogenation (Figure 7 E) reactions. MOF **4 (148)** was found to be three times as active as the homogeneous control catalyst. This work will most likely stimulate further developments of more BINAP based MOF catalysts for asymmetric transformations in the future.

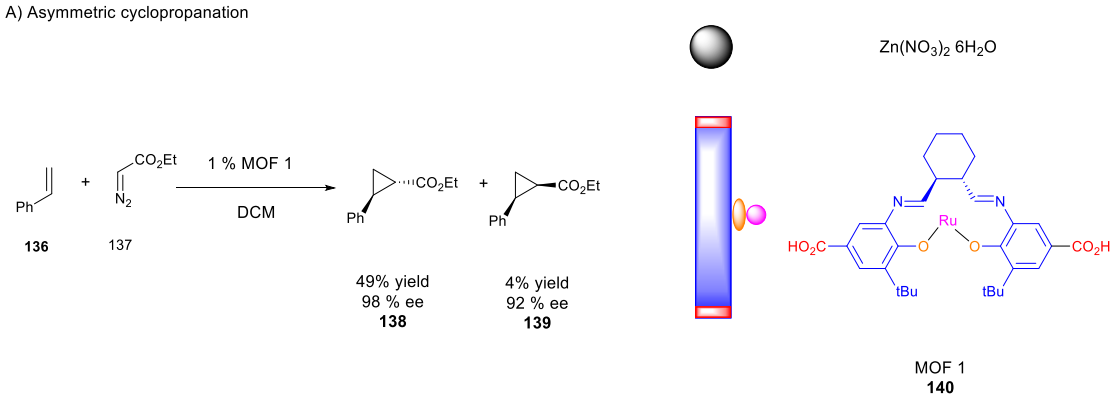

B) Asymmetric diethyl zinc addition

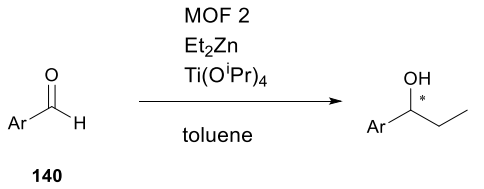


**140**

Ar = Ph 99 % yield 82 % ee
4-Me Ph 99 % yield 78% ee
4-Cl Ph 99 % yield 80 % ee
4-Br Ph 96 % yield 80 % ee
1-Naph 99 % yeild 91 % ee

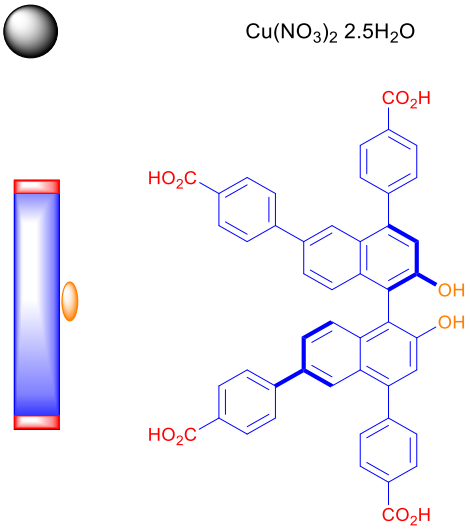


MOF 2
**141**

C) Asymmetric epoxidation

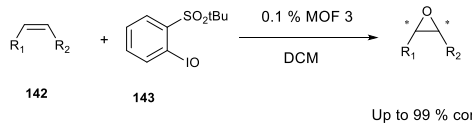


**142** **143**

Up to 99 % conv
up to 84 % ee
**144**

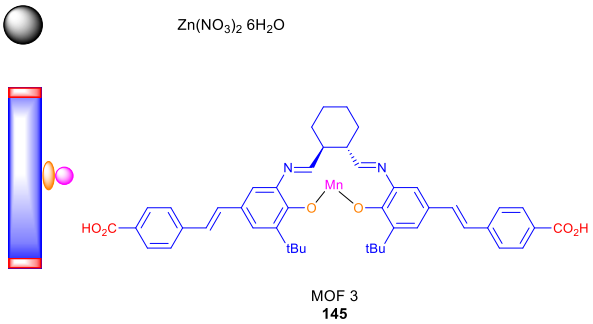


MOF 3
**145**

D) Asymmetric 1,4 addition

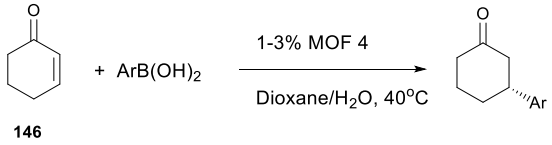


**146**

up to 99 % yield
up to 99 % ee
**147**

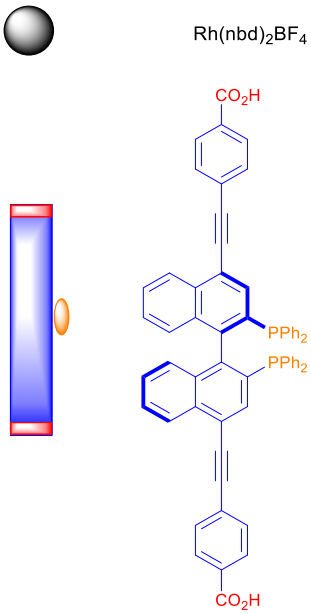


MOF 4
**148**

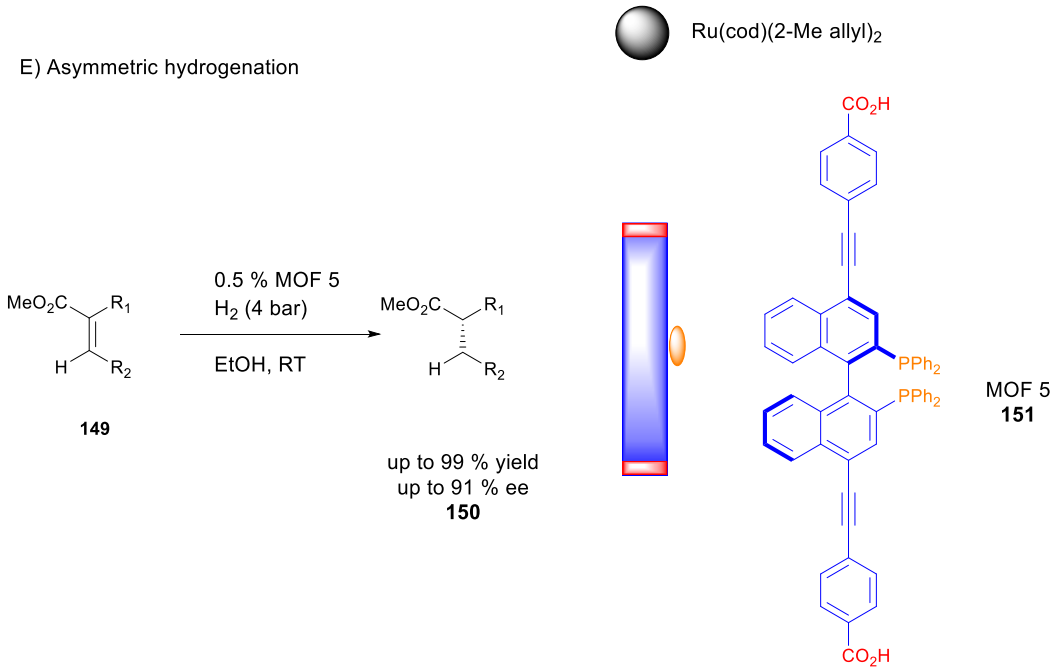


**Figure 7.** Selected examples of Lin's chiral MOF catalysts. Red color indicates primary functional group. Blue color indicates a chiral organic linker. Orange color indicates secondary functional group. Pink color indicates catalytic metal center. A) Highly enantioselective MOF-catalyzed cyclopropanation based upon Ru/salen. B) Influence of pore size on enantioselectivity. C) Mn/salen based MOF catalyzed epoxidation with 84% ee as well as sequential alkene epoxidation/ epoxide ring opening. D) First BINAP-based MOF catalyst applied to asymmetric 1, 4 addition. E) Highly enantioselective hydrogenation using a BINAP/Ru-based MOF catalyst.

After their initial breakthrough report in asymmetric catalysis in 2000, Kim and coworkers prepared a new class of MOF-based supramolecular catalyst to effect an asymmetric aldol reactions (**152**). In contrast to previous reports, Kim demonstrated that an organocatalyst MOF-based supramolecular catalyst can be easily synthesized in excellent yield (60-90%) and promoted Aldol reaction with good enantioselectivity (55-

80% ee)[46]; the performance of the MOF catalyst exceeds that of the core organocatalyst from which it is derived. The type II MOF-based catalyst architecture and MIL-101 – well-known MOF structure containing Cd as metal ions – is used as achiral MOF. This new class of MOF based catalyst proved that the MOF based organocatalyst can provide a way to induce high enantioselecitivity and high reactivity (Figure 8).

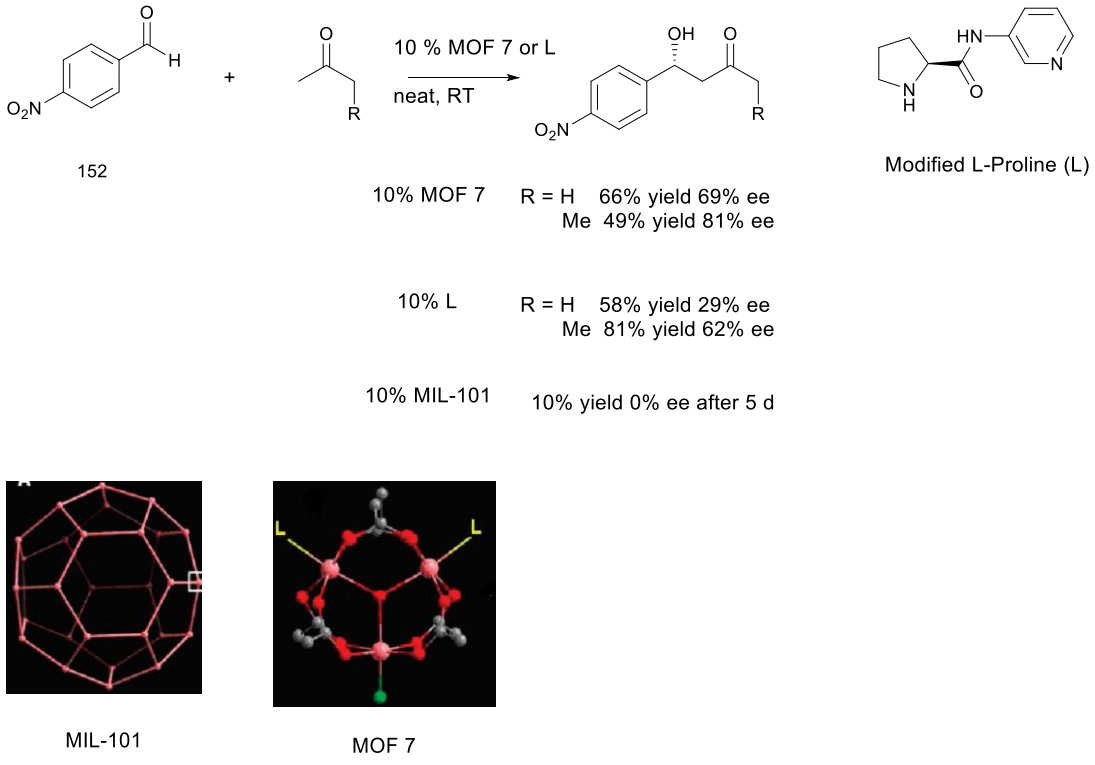


**Figure 8.** Kim's MIL-101 based MOF catalyst with L-proline as an organocatalyst moiety, which showed good enantioselecitivity. (Permission obtained from the publisher).

**1.3 Homogeneous asymmetric supramolecular catalysis – guest-host based supramolecular capsule catalyst**

Despite the long history of research toward using guest-host interactions to develop self-assemble capsules and cages for molecular recognition, reaction rate enhancement or size-selective chemistry, there has not been much attention to asymmetric guest-host supramolecular catalysts. Major figures in this field include Fujita[47] and Raymond[48]. These groups have synthesized numerous types of guest-host supramolecular structures and used them to show the effectiveness of guest-host supramolecular structures for reaction rate enhancement and size selective reactions. These supramolecular structures are usually called cages or capsules and reactions are catalyzed inside near the core of the supramolecular structure instead of the surface or near the surface. Several supramolecular capsules have been recently applied to asymmetric reactions showing moderate to good enantioselectivity. Hupp reported that a porphyrin-based capsule catalyst was able to provide up to 12 % ee for oxidation of sulfides[50]. Raymond recently reported that a chiral supramolecular cage[51] catalyzed the asymmetric cyclization of monoterpene substrates with up to 69% ee.

The most recent work on chiral caged complexes comes from Reek and coworkers[49]. Reek's supramolecular structures discussed earlier, consist of one structural metal and one metal for catalysis. In the case described here, two structural metals (Zn & Pd) embed a BINOL-derived phosphoramidite ligand-rhodium (I) complex inside the core of the capsule (Figure 9A). This differs from MOF-based supramolecular catalysts in that a single monoligated chiral rhodium complex is encapsulated rather

than multiple chiral complexes in the extended three-dimensional structure of a MOF-based catalyst. The synthesis of the capsule is straightforward. Initially, the authors envisioned that the cage, consisting of nanocage4 $(BArF)_{8\,[}(nanocage4^{8+} + (BArF)_{8}^{-})]$ would accommodate nitrogen containing ligands due to the well-known selective coordination of Zn-porphyrin to basic nitrogen atoms (Figure 9A). BINOL ligand encapsulation was supported by UV-vis, HRMS, and NMR analysis showing the formation of complex of nanocage4 $(BArF)_8$ and the ligand in 1:1 ratio. Lastly, in situ generation of the chiral Rh complex was completed by the addition of $Rh(acac)(CO)_2$, as evidenced by NMR and IR spectroscopy. The capsule catalyst catalyzes the hydroformylation of styrene in up to 79% ee (Figure 9 B). Notably, the selectivity is higher than that obtained with the monoligated rhodium catalysts in the absence of the capsule scaffold.

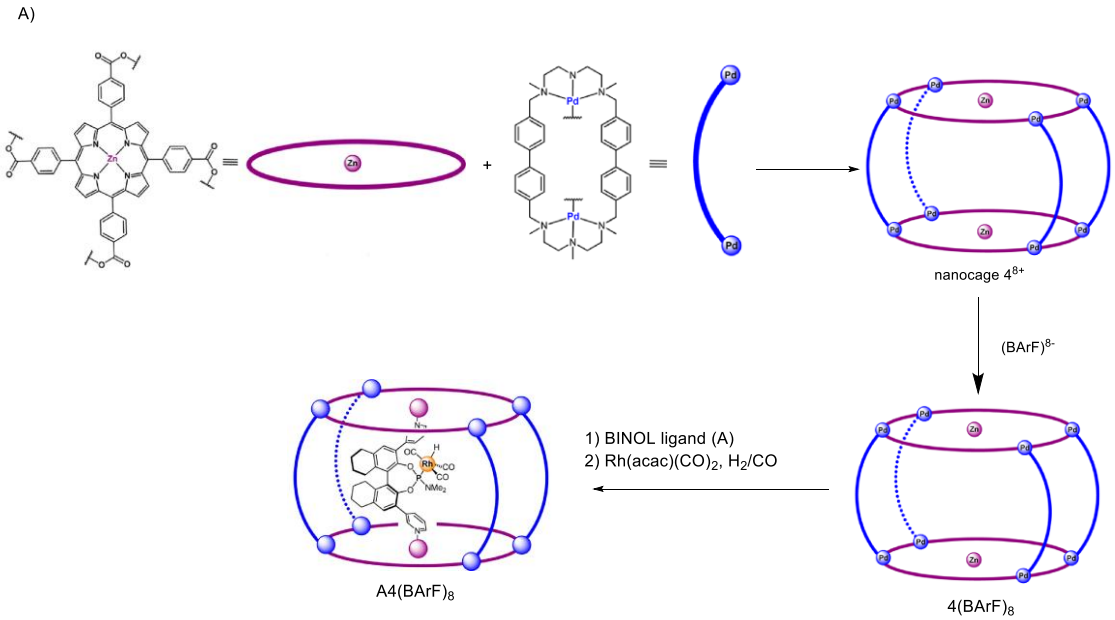

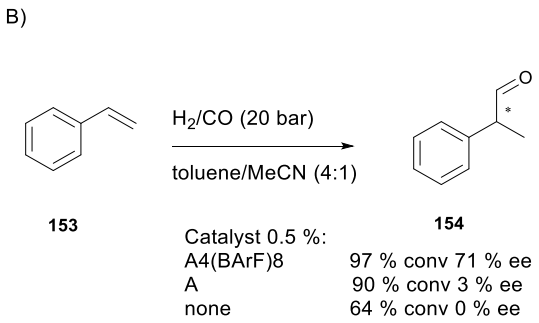


**Figure 9.** A) Synthesis route for monoligated rhodium complex with tetragonal prismatic nanocage 4(BArF)$_8$. Inclusion of BINOL ligand and complexion with Rh affords highly enantioselective encapsulated supramolecular catalyst. B) Asymmetric hydroformylation results with the encapsulated supramolecular catalyst showing that the capsule play an important role in inducing chirality. Schematic representation shown in figure 9 A is reproduced from scheme 1 & 3 in *J. Am. Chem. Soc*. **2015**, 137, 2680. (Permission obtained from the publisher).

**1.4 Homogeneous asymmetric supramolecular catalysis – self-assembled supramolecular catalysts directed by complementary hydrogen bonding motifs**

The methods for self-assembly discussed thus far focused on metal coordination-directed self-assembly, specifically exploiting the selective coordination of nitrogen ligands to Zn(II) and Fe(III) coupled with concomitant oxygen ligand coordination to Zn(II), Cu(I or II) or other metals. There has also been considerable effort directed toward developing supramolecular catalysts that self-assemble through a complementary hydrogen bonding network. The basic architecture of two types of supramolecular catalysts based upon hydrogen bonding networks is shown in Figure 10A/B. The two types differ in that catalytically active site is either a transition metal (Figure 10A) or an organocatalyst (Figure 10B). A third concept for directed self-assembly has been illustrated recently wherein electrostatic charges (i.e., cation and anion pairs) are used to link two monodentate ligand backbones together to form chiral bidentate ligands systems and/or supramolecular catalysts (Figure 10C). Although there are potential benefits to avoid the use of metals to direct self-assembly (e.g., reduced toxicity, environmental impact, and/or expense), there are several downsides as well. The reaction conditions need to be compatible with the hydrogen bond network; this limits the types of asymmetric transformations that can be performed. For example, hydrogen bonding directed self-assembled supramolecular catalysts are not good candidates for reactions which require high temperature or protic, acidic or basic solvents. Next section of the chapter briefly describes the major accomplishments in

each of the three categories of alternative methods metal-directed self-assembly for the preparation of supramolecular catalysts described above.

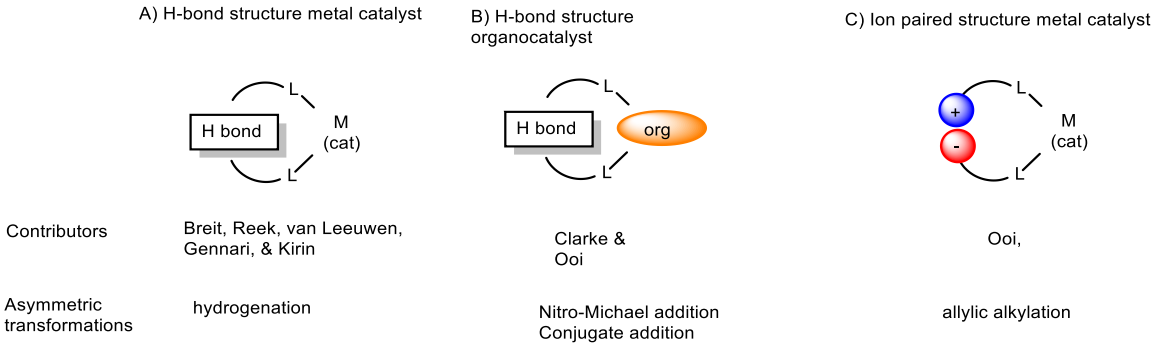


**Figure 10.** A brief overview of non-metal-directed organization of asymmetric supramolecular catalysts. A) Ligands are held together with hydrogen bonding to create bidentate ligands. A transition metals is used for a catalytic center. B) Ligands are made the same way as in A but utilize an organocatalyst such as proline as a catalytic center. C) The ligand backbone is held with ion pairs and a transition metal is used for a catalytic center.

**1.5 Hydrogen bond assembled supramolecular catalysts – Non-amino acid based hydrogen bond-directed self-assembly of organometallic supramolecular catalysts**

While there are several groups working in this area, the major contributor and initiator of the concept is Bernhard Breit. In 2003, Breit and his coworkers reported a new concept for in situ self-assembly of bidentate ligands[52] via complementary hydrogen bonding networks. These new ligands provide highly active and regioselective catalysts for the hydroformylation of terminal olefins. This idea was inspired by A-T, G-C base pairs seen in DNA and analogous self-assembly of 2-pyridone with 2-hydroxypyridine; the latter system was exploited in the early publication by Breit. Although the catalysts were achiral, Breit provided the proof of principle for this concept and series of ligands have subsequently been developed including excellent catalysts for the regioselective hydroformylation[53] and hydrocyanation[54] of alkenes and the anti-Markovnikov water addition[55] to alkynes.

Asymmetric hydrogenations using chiral supramolecular catalyst systems were reported by the Breit group in 2006[56] and 2010[57] (Figure 11). The two constituent monodentate ligands incorporate a hydrogen acceptor and donor subunits and a pendant BINOL-derived phosphonite moiety for bidentate coordination to a catalysis metal. A hydrogen acceptor and a donor units are placed side by side and alternately (Figure 11A $L^{DA}$-$L^{AD}$ complex) so that the hydrogen acceptor on one monodentate ligand form hydrogen bonding with a donor unit on another monodentate ligand. Such an arrangement positions the phosphorus atoms to coordinate to a metal to form a bidentate ligand system (Figure 11A). A crystal structure of the rhodium complex was

reported by the same group. The catalyst **156** is reported to be stable at 100 $^{o}$C[52] and exhibits enantioselectivity of 99% ee for rhodium catalyzed asymmetric hydrogenation of some prototypical substrates **155** (Figure 11 B). It is worth mentioning that when only one of the two monodentate ligands is present, the enantioselectivity is lower than self-assembled heteroleptic mixture. Other research groups actively pursuing this approach to the development of novel non-amino acid based hydrogen bond chiral supramolecular catalysts include those of Reek[58], van Leeuwen[59], and Gennari[60].

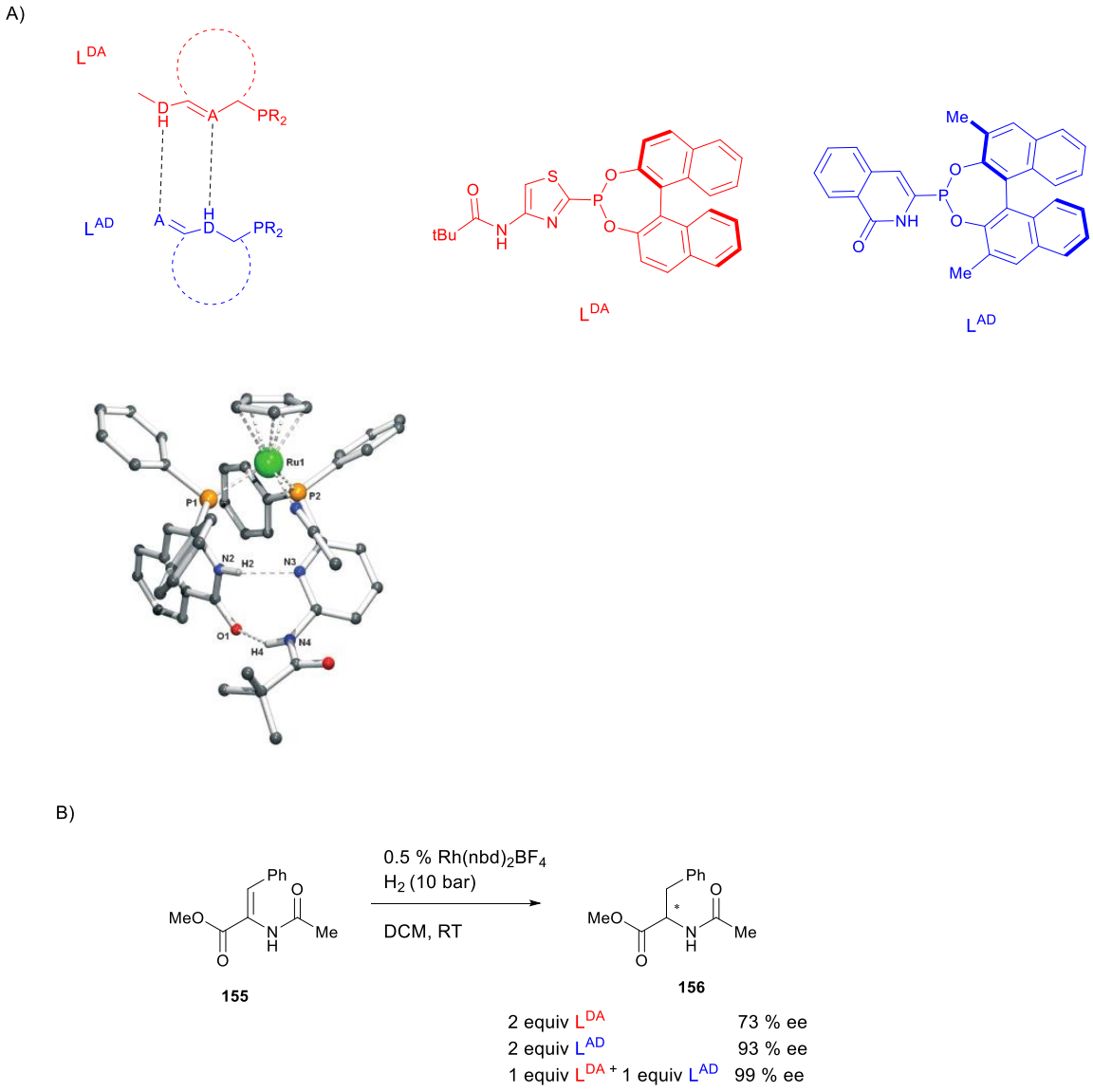


**Figure 11.** A) Self-assembled hydrogen based supramolecular catalysts. $L^{DA}$ (red) represents donor acceptor containing monodentate ligand and $L^{AD}$ (blue) represents acceptor donor containing monodentate ligands. These two form complementary hydrogen network when mixed in a solution. The crystal structure is reused with permission. B) Effectiveness of self-assembled catalysts for asymmetric hydrogenation of prototypical substrate dehydroamino acid substrate.

**1.6 Hydrogen bond assembled supramolecular catalysts – Amino acid based hydrogen bonding network assembled metal supramolecular catalysts**

Highly ordered hydrogen network exists at the core of the selective base pairing in DNA and RNA to enhance both reactivity and selectivity and therefore utilizing related hydrogen networks to construct supramolecular catalysts comes with no surprise. Complementary hydrogen bonding networks are also important in determining the tertiary structure of proteins. The Breit group was first in successfully using amino acids into ligand backbone to form efficient bidentate supramolecular ligands[61] via hydrogen bonding. Based on the results of molecular modeling Breit suggested that *meta*-carboxypepridyl substituted triarylphosphines or phosphites could be suitable candidate for directing the self-assembly of novel chiral ligands. The crystal structure of the Pt (II) complex shows that a helical hydrogen bonding network between two monodentate amino acids induces a planar chirality, a stereochemical element found in phanephos (Figure 12A). The supramolecular assembly was found to be stable in aprotic solvent such as $CDCl_3$. In addition to the helical hydrogen bonding network, it was postulated that π-π interactions contribute to the stability of the supramolecular assembly. Utilizing this nature, the authors tested the ligands **158** for the effectiveness towards asymmetric hydrogenation of prototypical substrates **157**. Three substrates exhibit excellent enantioselectivity (97 – 99% ee) and high reactivity (Figure 12B). Other examples for amino acid based supramolecular catalysts include Kirin's backdoor induction catalysts[62].

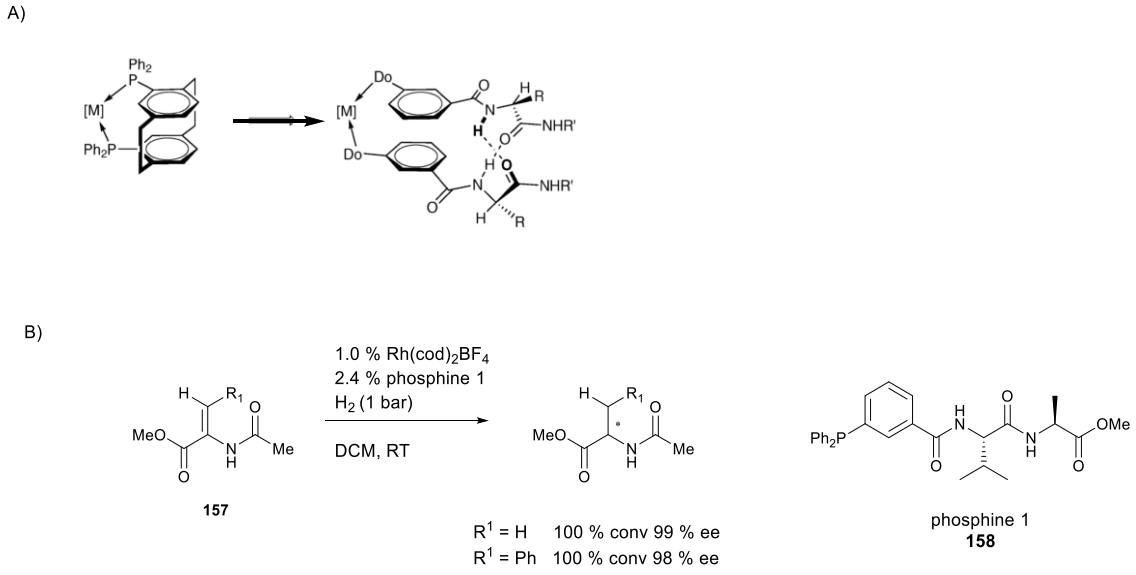


**Figure 12.** A) Schematic representation of a chiral supramolecular catalyst based upon amino acid backbones. Hydrogen network formed between backbone amino acids induce a planar chiral environment. B) Application of amino acid phosphine 1 to highly enantioselective asymmetric hydrogenation.

**1.7 Hydrogen bond assembled supramolecular catalysts - Hydrogen bond assembling organocatalytic supramolecular catalysts**

Organocatalytic reactions have attracted much interest over the past decade[63]. However, the majority of studies of supramolecular catalyst design have focused on metal catalyzed reactions. It is logical that researchers would attempt to fill the gap between supramolecular transition metal catalysts and supramolecular organocatalysts (see also Figure 10B). The Clarke group used proline analogues as an organocatalyst in conjunction with a co-catalyst. The combination forms a complementary hydrogen bonded network (Figure 13A) that both enhances reactivity and enantioselectivity in the nitro-Michael reaction[64]. Although the exact mechanism is not fully understood, the co-catalyst apparently helps organize and effectively shield one enantioface over the other to create a preferential addition site for the substrates to react. A control reaction using proline alone was shown as ineffective for the nitro-Michael reaction (**159** & **160**); only 1% of the product formed and it formed in low enantiomeric excess. A second control reaction repeated the original conditions but now in the presence of a reagent that disrupts hydrogen bonding; the result was a drastic reduction in reaction rate and enantioselectivity (Figure 13B).

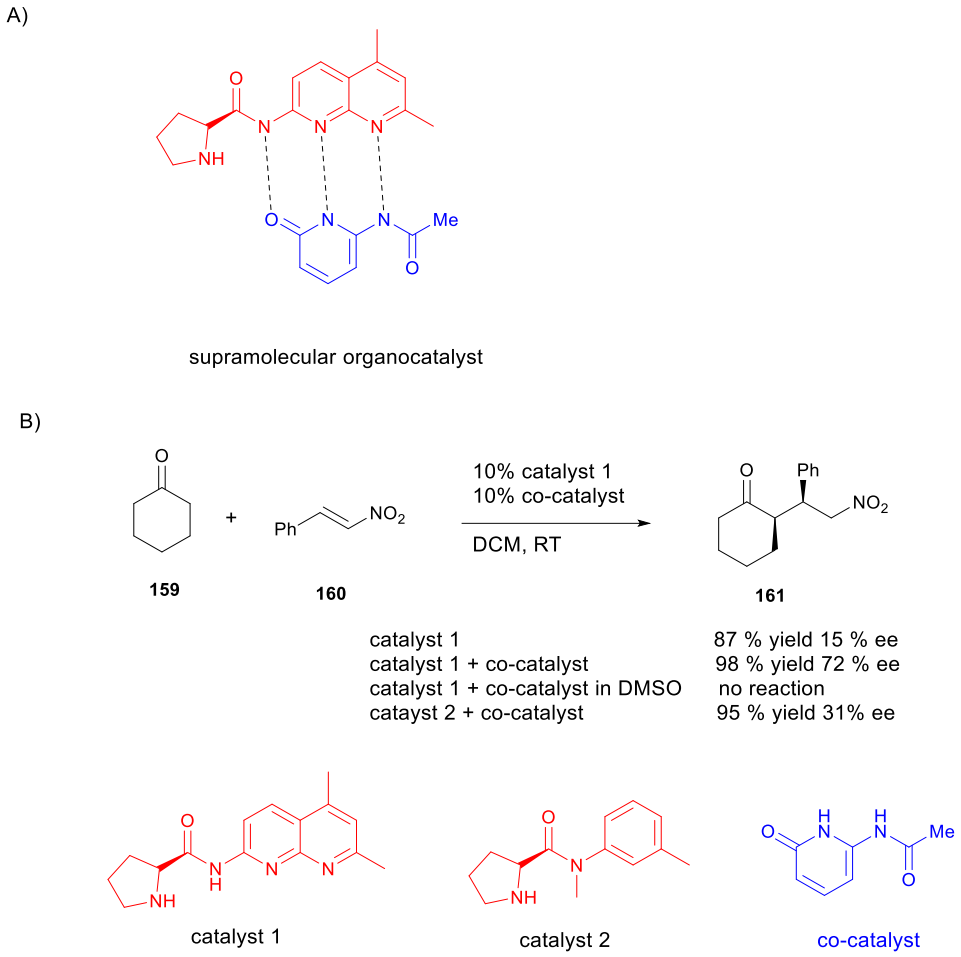


**Figure 13.** A) Supramolecular catalyst complex. Red indicates organocatalytic moiety and blue indicates co-catalyst. B) Nitro-Michael reaction with hydrogen based organocatalytic supramolecular catalyst showing good enantioselectivity. It is important to maintain hydrogen bonding network for this asymmetric reaction to have high enantioselectivity.

## 1.8 Ionic bonding (electrostatic charge-directed) self-assembled organometallic supramolecular catalysts

In 2012, Ooi and his coworkers reported a new methodology based on electrostatic interaction to direct self-assembled ligands and catalysts[65]. One potential advantage of the approach is that this methodology can use commercially available chiral bidentate ligands as long as they contain a readily ionized group. Therefore, the need to synthesize chiral ligands is minimized. The strategy is to use achiral bifunctional molecules, one bearing a ligating group such as phosphine along with a quaternary ammonium moiety. The phosphine bearing a pendant ammonium salt as its hydroxide is prepared through an anion-exchange process. Reaction of the alkyl ammonium hydroxide with chiral acids such as BINOL forms an ion-paired complex via electrostatic interactions (i.e., salt formation) (Figure 14A). The approach was used in the palladium catalyzed asymmetric allylic alkylation of α-nitrocarboxylates (**162** & **163**) with excellent levels of enantioselectivity, up to 97% ee (**164**) (Figure 14 B). The proposed mechanism hypothesizes that the anion (Nu-) hydrogen bonds with the phenolic proton of BINOL. This organization through a non-covalent bonding interaction is thought to be the key to achieve high enantiofacial discrimination of the prochiral π-allyl palladium complex (Figure 14 C).

A)

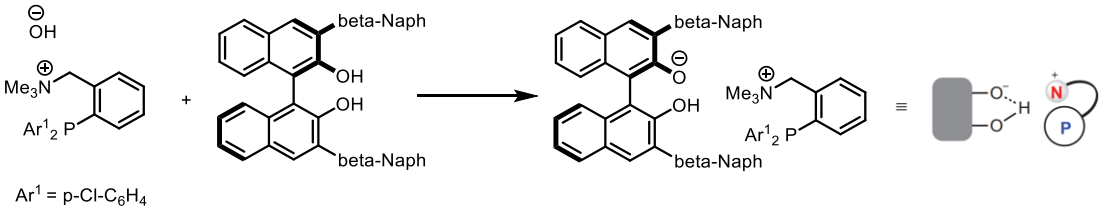

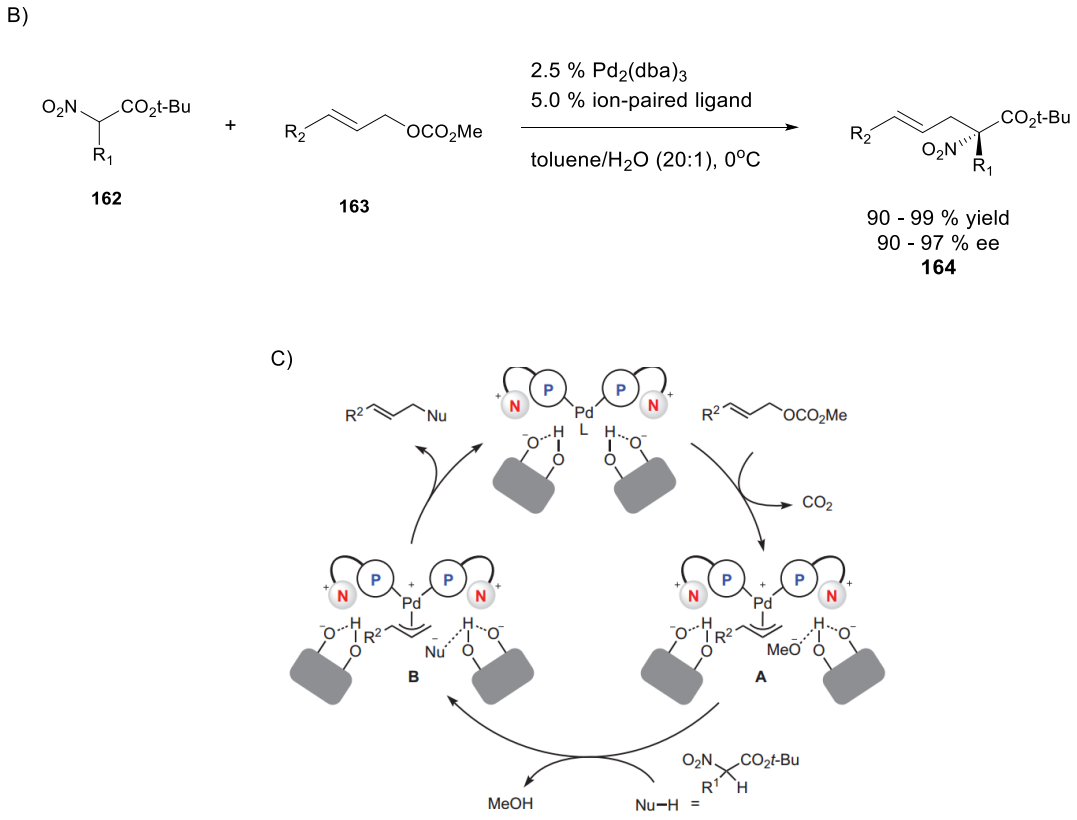


**Figure 14.** A) Strategy for constructing ion-paired chiral bidentate ligands. B) Application to asymmetric allylic alkylation. C) Proposed catalytic cycle for asymmetric allylic alkylation using ion-paired chiral catalyst. Figure 14 C is reproduced with permission from *Nature Chemistry*. **2012**, 4, 473.

**1.9 Remarks on the future of supramolecular catalysis**

Since the first report of a supramolecular chiral catalyst by Reek in 2000, various exciting and promising supramolecular methodologies for constructing chiral catalysts have been developed. These have included: metal-directed self-assembly and organization of organometallic catalysts, MOF-based organometallic catalysts, hydrogen bond network based organometallic catalysts, hydrogen bond network based organocatalysts, and ion-paired based organometallic catalysts. These advances have begun to change the way chemists synthesize chiral bidentate ligands for useful asymmetric transformations and provided much easier access to large chiral ligand libraries via combinatorial methods. Nonetheless, the field is still young and supramolecular catalysts have been applied to only a limited group of asymmetric transformations.

Supramolecular catalysts are similar to enzyme in that weakly non-bonded interactions are the key to control of reactivity and selectivity. Therefore, there is a goal to develop chemical catalysts with enzyme-like behavior[66]. I expect that since energy efficiency and green chemistry are of growing interest, reactions involving water as reaction media using supramolecular catalysts could in particular be of great future interest. The design of catalysts that can choose one reactive site over the others based on multiple weak interactions between the substrates and the catalysts is another important future goal. Several research groups, including that of Scott Miller[67-72] have already demonstrated interesting results in this regard. Much of this PhD thesis will

focus on selective chemistry developed in Takacs group utilizing the benefit of supramolecular catalysts, *vide infra*.

**1.10 References**


1. J. Meeuwissen, J. N. H. Reek, "Supramolecular catalysis beyond enzyme mimics". *Nature Chemistry.* **2010**, 2, 615
2. V. F. Slagt, P. W. N. M. van Leeuwen, J. N. H. Reek, "Bidentate ligands formed by self-assembly". *Chem Commun*. **2003,** 2474
3. P. W. N. M. van Leeuwen, P.C. J. Kamer, J. N. H. Reek, P. Dierkes, "Synthesis and Coordination Chemistry of a Novel Bidentate Phosphine". *Chem Rev*. **2000,** 100, 2741
4. V. F. Slagt, J. N. H. Reek, P.C. J. Kamer, P. W. N. M. van Leeuwen, "Assembly of Encapsulated Transition Metal Catalysts". *Angew. Chem. Int. Ed*. **2001**, 40, 4271
5. P. E. Goudriaan, M. Kuil, X. B. Jiang, P. W. N. M. van Leeuwen, J. N. H. Reek, "SUPRAPhos ligands for the regioselective rhodium catalyzed hydroformylation". *Dalton Trans*. **2009**, 1801
6. R. Bellini, J. N. H. Reek, "Application of Supramolecular Bidentate Hybrid Ligands in Asymmetric Hydroformylation". *Chem. Eur. J.* **2012**, 18, 13510
7. J. M. Takacs, D. S. Reddy, S. A. Moteki, D. Wu, H. Palencia. "Asymmetric Catalysis Using Self-Assembled Chiral Bidentate P, P-Ligands". *J. Am. Chem. Soc*. **2004**, 126, 4494
8. J. M. Atkins, S. A. Moteki, S. G. DiMagno, J. M. Takacs. "Single Enantiomer, Chiral Donor-Acceptor Metal Complexes from Bisoxazoline Pseudoracemates". *Org Lett.* **2006**, 8, 2759
9. Y. Hamada, N. Seto, Y. Takayanagi, T. Nakano, O, Hara, "Asymmetric allylic substitution reaction with nitrogen and oxygen nucleophiles using monodentate chiral phosphine 9-PBN". *Tetrahedron Lett.* **1999**, 40, 7791
10. D. A. Evans, K. R. Campos, J. S. Tedrow, F. E. Michael, M. R. Gagne. "Application of Chiral Mixed Phosphorus/Sulfur Ligands to Palladium-Catalyzed Allylic Substitutions". *J. Am. Chem. Soc.* **2000**, 122, 7905
11. O. Pamies, G. P. F. van Strijdonck, M. Dieguez, S. Deerenberg, G. Net, A. Ruiz, C. Claver, P. C. J. Kamer, P. W. N. M. van Leeuwen, "Influence of Steric Symmetry

and Electronic Dissymmetry on the Enantioselective Palladium-Catalyzed Allylic Substitutions". *J. Org. Chem*. **2003**, 68, 3258

12. A. Agarkov, E. W. Uffman, S. R. Gillbertson. "Parallel Approach to Selective Catalysts for Palladium-Catalyzed Desymmetrization of 2, 4-Cyclopentenediol". *Org. Lett*. **2003**, 5, 2091
13. J. L. Vasse, R. Stranne, R. Zalubovskis, C. Gayet, C. Moberg. "Influence of Steric Symmetry and Electronic Dissymmetry on the Enantioselective in Palladium-Catalyzed Allylic Substitutions". *J. Org. Chem*. **2003**, 68, 3258
14. J. Ansell, M. Wills, "Enantioselective catalysis using phosphorus-donor ligands containing two or three P-N or P-O bonds". *Chem. Soc. Rev*. **2002**, 31, 259
15. M. Yoshimura, S. Tanaka, M. Kitamura. "Recent topics in catalytic asymmetric hydrogenation of ketones". *Tetrahedron Lett*. **2014**, 55, 3635
16. J. M. Takacs, K. Chaiseeda, S. A. Moteki, D. S. Reddy, D. Wu, K. Chandra. "Rhodium-atayzed asymmetric hydrogenation using self-assembled chiral bidentate ligands". *Pure Appl. Chem*. **2006**, 78, 501
17. N. C. Thacker, S. A. Moteki, J. M. Takacs. "Ligand Scaffold Optimization of a Supramolecular Hydrogenation Catalyst: Analyzing the Influence of Key Structural Subunits on Reactivity and Selectivity". *ACS Catal*. **2012**, 2, 2743
18. D. Manning, H. Nöth, "Catalytic hydroboration with rhodium complexes", *Angew. Chem*. **1985**, 97, 854
19. J. M. Brown, G. C. Lloyd-Jones. "Catalytic asymmetric hydroboration with oxazaborolidines", *Tetrahedron:Asymmetry*. **1990**, 1, 869
20. H. Doucet, E. Fernandez, T. P. Layzell, J. M. Brown, "The Scope of Catalytic Asymmetric Hydroboration/Oxidation with Rhodium Complexes of 1, 1'-(2-diarylphosphino-1-naphthly) isoquinolines". *Chem Eur J*. **1999**, 5, 1320
21. T. Hayashi, Y. Yamamoto, Y, Ito. "Catalytic asymmetric hydroboration of styrenes". *J. Am. Chem. Soc*. **1989**, 111, 3426

22. T. Hayashi, Y. Yamamoto, Y, Ito. “Catalytic asymmetric hydroboration with heterotopic P-N ligands: Trends in enantioselectivity with increased steric demand”. *Tetrahedron: Asymmetry.* **1991**, 2, 601
23. S. A. Moteki, J. M. Takacs. “Exploiting Self-Assembly for Ligand-Scaffold Optimization: Substrate-Tailored Ligands for Efficient Catalytic Asymmetric Hydroboration”. *Angew. Chem. Int. Ed*. **2008**, 47, 894
24. S. A. Moteki, K. Toyama, Z. Liu, J. Ma, A. E. Holmes, J. M. Takacs. “Two-Stage Optimization of a Supramolecular Catalyst for Catalytic Asymmetric Hydroboration”. *Chem. Commun*. **2012**, 48, 263
25. B. Wang, K. Chen, K. Cai, X. Kou, L. Liang, W. Chen, Q. Tian, B. Fan, “Method for preparing intermediate compound of sitagliptin”. *PCT Int. Appl.* **2015**, WO 2015035735 A1 20150319.
26. R. Schloegl, “Heterogeneous Catalysis”, *Angew. Chem. Int. Ed*. **2015**, 54, 3465
27. A. R. Silva. “Asymmetric Heterogeneous Catalysis by Nanoporous Materials Using Privileged Ligands as Chiral Building Blocks”. *Current Organic Chemistry*. **2014**, 18, 1226
28. a) M. Dinca, J. R. Long, “Hydrogen storage in microporous metal-organic frameworks with exposed metal sites”. *Angew. Chem. Int. Ed*. **2008**. 47, 6766; b) J. L. Rowsell, O. M. Yaghi, “Strategies for Hydrogen Storage in Metal-Organic Frameworks”. *Angew. Chem. Int. Ed*. **2005**, 44, 4670; c) B. Kesanli, Y. Cui, M. R. Smith, E. W. Bittner, B. C. Bockrath, W. Lin, “Surface Modification and Functionalization of Nanoscale Metal-Organic Frameworks for Controlled Release and Luminescence Sensing”. *Angew. Chem. Int. Ed*. **2005**, 44, 72; d) W. Yang, A. Greenaway, X. Lin, R. Matsuda, A. J. Blake, C. Wilson, W. Lewis, P. Hubberstey, S. Kitagawa, N. R. Champness, M. Schroder, “Exceptional Thermal Stability in a Supramolecular Organic Frameworks: Porosity and Gas Storage”. *J. Am. Chem. Soc*. **2010**, 132, 14457
29. a) B. Kesanli, W. Lin, “Synthesis and crystal structure of the porous metal-organic coordination polymer $[Zn_4(Ndc)_4(Oxz)_2]2H_2O$”. *Coord. Chem. Rev*. **2003**, 246, 305;

b) J. Lee, O. K. Farha, J. Roberts, K. A. Scheidt, S. T. Nguyen, J. T. Hupp, "Metal-organic Framework Materials As Catalysts". *Chem. Soc. Rev*. **2009**, 38, 1450; c) L. Ma, C. Abney, W. Lin, "Enantioselective catalysis with homochiral metal-organic frameworks". *Chem. Soc. Rev*. **2009**, 38, 1248; d) G. Nickerl, A. Henschel, R. Grunker R, K. Gedrich, S. Kaskel, "Cellulose und heterogene Katalyse". *Chem. Ing. Tech*. **2011**, 83, 90

30. a) K. E. deKrafft, Z. Xie, G. Gao, S. Tran, L. Ma, O. Z. Zhou, W. Lin, "Nanoscale Metal-Organic Frameworks for Biomedical Imaging and Drug Delivery". *Angew. Chem. Int. Ed*. **2009**, 48, 9901; b) W. Lin, W. J. Rieter, K. M. Taylor, "Modular Synthesis of Functional Nanoscale Coordination Polymers". *Angew. Chem. Int. Ed*. **2009**, 48, 650
31. a) M. D. Allendorf, R. J. Houk, L. Andruszkiewicz, A. A. Talin, J. Pikarsky, A. Choudhury, K. A. Gall, P. J. Hesketh, "Stress-Induced Chemical Detection Using Flexible Metal-Organic Frameworks". *J. Am. Chem. Soc*. **2008**, 130, 14404; b) B. Chen, L. Wang, Y. Xiao, F. R. Fronczek, M. Xue, Y. Cui, G. Qian, "A Luminescent Metal-Organic Framework with Lewis basic Pyridyl Sites for the Sensing of Metal Ions". *Angew. Chem. Int. Ed*. **2009**, 48, 500; c) S. Pramanik, C. Zheng, X. Zhang, T. J. Emge, J. Li, "New Microporous Metal-Organic Framework Demonstrating Unique Selectivity for Detection of High Explosives and Aromatic Compounds". *J. Am. Chem. Soc*. **2011**, 133, 4153
32. K. M. L. Taylor-Pashow, J. Della Rocca, Z. Xie, S. Tran, W. Lin, "Postsynthetic Modifications of Iron-Carboxylate Nanoscale Metal-Organic Frameworks for Imaging and Drug Delivery". *J. A. Chem. Soc*. **2009**, 131, 14261
33. M. Yoon, R. Srirambalaji, K. Kim, "Homochiral Metal-Organic Frameworks for Asymmetric Heterogeneous Catalysis". *Chem. Rev*. **2012**, 112, 1196
34. L. Ma, J. M. Falkowski, C. Abney, W. Lin, "A series of isoreticular chiral metal-organic frameworks as a tunable platform for asymmetric catalysis". *Nature Chemistry*. **2010**, 2, 838

35. J. S. Seo, D. Whang, H. Lee, S. I. Jun, J. Oh, Y. J. Jeon, K. Kim, “A homochiral metal-organic porous material for enantioselective separation and catalysis”. *Nature*. **2000**, 404, 982
36. K. Manna, T. Zhang, F. X. Greene, W. Lin, “Bipyridine- and Phenanthroline-Based Metal-Organic Frameworks for Highly Efficient and Tandem Catalytic Organic Transformations via Directed C-H Activation”. *J. Am. Chem. Soc.*, **2015**, *137*, 3844–3851
37. H. G. Woelfler, P. F. Radaschitz, P. W. Feenstra, W. Haas, J. G. Khinast. “Synthesis, catalytic activity, and leaching studies or a heterogeneous Pd-catalyst including an immobilized bis(oxazoline) ligand”. *J. Catal.* **2012**, 286, 30
38. C. J. Simmons, B. J. Hathaway, K. Amornjarusiri, B. D. Santarsiero, A. Clearfield, “The first determination of the energy difference between solid-state conformers by x-ray diffraction”, *J. Am. Chem. Soc*. **1987**, 109, 1947
39. a) H. Jiang, A. Hu, W. Lin, “A chiral metallacyclophane for asymmetric catalysis”. *Chem. Commun*. **2003**, 96; b) S. J. Lee, A. Hu, W. Lin*, “*The First Chiral Organometallic Triangle for Asymmetric Catalysis”. *J. Am. Chem. Soc.* **2002**, 124, 12948; c) C. D. Wu, A. Hu, L. Zhang, W. Lin, “A Homochiral Porous Metal-Organic Framework for highly Enantioselective Heterogeneous Asymmetric Catalysis”. *J. Am. Chem. Soc.* **2005**, 127, 8940
40. a) A. Hu, H. L. Ngo, W. Lin, “Chiral, porous, hybrid solids for highly enantioselective heterogeneous asymmetric hydrogenation of beta-keto esters”. *Angew. Chem. Int. Ed*. **2003**, 42, 6000; b) A. Hu, H. L. Ngo, W. Lin, “Chiral Porous Hybrid Solids for Practical Heterogeneous Asymmetric Hydrogenation of Aromatic Ketones”. *J. Am. Chem. Soc*. **2003**, 125, 11490; c) A. Hu, H. L. Ngo, W. Lin, “Highly enantioselective catalytic asymmetric hydrogenation of beta-keto esters in room temperature ionic liquids”. *Chem. Commun.* **2003**, 1912
41. J. M. Falkowski, T. Sawano, T. Zhang, G. Tsun, Y. Chen, J. V. Lockard, W. Lin, “Privileged Phosphine-Based Metal-Organic Frameworks for Broad-Scope Asymmetric Catalysis”. *J. Am. Chem. Soc*. **2014**, 136, 5213

42. J. M. Falkowski, C. Wang, S. Liu, W. Lin, “Actuation of Asymmetric Cyclopropanation Catalysts: Reversible Single-Crystal to Single-Crystal Reduction of Metal-Organic Frameworks”. *Angew. Chem. Int. Ed*. **2011**, 50, 8674
43. F. Song, C. Wang, W. Lin, “A chiral metal-organic framework for sequential asymmetric catalysis”. *Chem. Commun*. **2011**, 47, 8256
44. G. Yuan, C. Zhu, W. Xuan, Y. Cui, “Enantioselective recognition and separation by a homochiral porous lamellar solid based on unsymmetrical Schiff base metal complexes”. *Chemistry*, **2009**, 15, 6428
45. R. Noyori, S. Hashiguchi, “Asymmetric Transfer Hydrogenation Catalyzed by Chiral Ruthenium Complexes”, *Accounts of Chemical Research*, **1997**, 30, 97
46. L. Yu, Z. Wang, J. Wu, S. Tu, K. Ding, “Directed Orthogonal Self-Assembly of Homochiral Coordination Polymers for Heterogeneous Enantioselective Hydrogenation”. *Angew. Chem. Int. Ed*. **2010**, 49, 3627
47. M. Banerjee, S. Das, M. Yoon, H. J. Choi, M. H. Hyun, S. M. Park, G. Seo, K. Kim, “Postsynthetic Modification Switches an Achiral Framework to Catalytically Active Homochiral Metal-Organic Porous Materials”. *J. Am. Chem. Soc*. **2009**, 131, 7524
48. a) T. Murase, S. Horiuchi, . Fujita, “Naphthalene Diels-Alder in a Self-Assembled Molecular Flask”. *J. Am. Chem. Soc*. **2010**, 132, 2866; b) T. Kawamichi, Y. Inokuma, M. Kawano, M. Fujita, “Regioselective Huisgen Cycloaddition within Porous Coordination Networks”. *Angew. Chem. Int. Ed*. **2010**, 49, 2375; c) M. Yoshizawa, S. Miyagi, M. Kawano, K. Ishiguro, M. Fujita, “Alkane Oxidation via Photochemical Excitation of a Self-Assembled Molecular Cage”. *J. Am. Chem. Soc*. **2004**, 126, 9172; d) M. Yoshizawa, Y. Takeyama, T. Okano, M. Fujita, “Cavity-Directed Synthesis within a Self-Assembled Coordination Cage: Highly Selective [2+2] Cross-Photodimerization of Olefins”. *J. Am. Chem. Soc*. **2003**, 125, 3243
49. a) C. J. Brown, G. M. Miller, M. W. Johnson, R. G. Bergman, K. N. Raymond, “high-Turnover Supramolecular Catalysis by a Protected Rhuthenium (II) Complex in Aqueous Solution”. *J. Am. Chem. Soc*. **2011**, 133, 11964; b) C. J. Jastings, M. P.

Backlund, R. G. Bergman, K. N. Raymond, “Enzyme-like Control of Carbocation Deprotonation Regioselectivity in Supramolecular Catalysis of the Nozarov Cyclization”. *Angew. Chem. Int. Ed*. **2011**, 50, 10570; c) C. J. Hastings, M. D. Pluth, R. G. Bergman, K. N. Raymond, “Enzymeline Catalysis of the Nozarov Cyclization by Supramolecular Encapsulation”. *J. Am. Chem. Soc*. **2010**, 132, 6938; d) Z. J. Wang, C. J. Brown, R. G. Bergman, K. N. Raymond, F. Dean. Toste, “Hydroalkoxylation Catalyzed by a Gold(I) Complex Encapsulated in a Supramolecular Host”. *J. Am. Chem. Soc*. **2011**, 133, 7358

50. C. G. Simon, R. G. Doria, S. Raofmoghaddam, T. Parella, M. Costas, X. Ribas, J. N. H. Reek, “Enantioselective Hydroformylation by a Rh-Catalyst entrapped in a Supramolecular Metallocage”. *J. Am. Chem. Soc*. **2015**, 137, 2680
51. S. J. Lee, S. H. Cho, K. L. Mulfort, D. M. Tiede, J. T. Hupp, S. T. Nguyen, “Cavity-Tailored, Self-Sorting Supramolecular Catalytic Boxes for Selective Oxidation”. *J. Am. Chem. Soc*. **2008**, 130, 16828
52. C. Zhao, Q. Sun, W. M. Cooper, A. G. DiPasquale, F. Dean Toste, R. G. Bergman, K. N. Raymond, “Chiral Amide Directed Assembly of a Diastereo- and Enantiopure Supramolecular Host and its Application to Enantioselective Catalysis of Neutral Substrates”. *J. Am. Chem. Soc*. **2013**, 135, 18802
53. B. Breit, W. Seiche, “Hydrogen Bonding as a Construction Element for Bidentate Donor Ligands in Homogeneous Catalysis: Regioselective Hydroformylation of Terminal Alkenes”. *J. Am. Chem. Soc.* **2003**, 125, 6608
54. J. Wieland, C. Waloch, M. Keller, B. Breit, “Reagent Directing Group Controlled Organic Synthesis: Total Synthesis of (R, R, R)-α-Tacopherol”. *Angew. Chem. Int. Ed*. **2007**,46, 3037
55. M. de Greef, B. Breit, “Self-Assembled Bidentate Ligands for the Nickel-Catalyzed Hydrocyanation of Alkenes”. *Angew. Chem. Int. Ed*. **2009**, 48, 551
56. F. Chevallier, B. Breit, “Self-Assembled Bidentate Ligands for Ru-Catalyzed anti-Markovnikov Hydration of Terminal Aklynes”. *Angew. Chem. Int. Ed*. **2006**, 45, 1599

57. M. Weis, C. Waloch, W. Seiche, B. Breit, “Self-Aseembly of Bidentate Ligands for Combinatorial Homogeneous Catalysis: Asymmetric Rhodium-Catalyzed Hydrogenation”. *J. Am. Chem. Soc*. **2006**, 128, 4188
58. J. Wieland, B. Breit, “A combinatorial approach to the identification of self-assembled ligands for rhodium-catalyzed asymmetric hydrogenation”. *Nature Chemistry*, **2010**, 2, 832
59. a) J. Meeuwissen, A. J. Sandee, B. D. Bruin, M. Siegler, A. L. Spek, J. N. H. Reek, *Organometallics*, **2010**, 29, 2413; b) F. W. Patureau, M. Kuil, A. J. Sandee, J. N. H. Reek, “METAMORPos: Adaptive Supramolecular Ligands and Their Mechanistic Consequences for Asymmetric Hydrogenation”. *Angew. Chem. Int. Ed*. **2008**, 47, 3180
60. M. Raynal, F. Portier, P. W. N. M. van Leeuwen, L. Bouteiller, “Tunable Asymmetric Catalysis through Ligand Stacking in Chiral Rigid Rods”. *J. Am. Chem. Soc*. **2013**, 135, 17687
61. L. Pignataro, M. Boghi, M. Civera, S. Carboni, U. Piarulli, C. Gennari, “Rhodium-Catalyzed Asymmetric Hydrogenation of Olefins with PhthalaPhos, a New Class of Chiral Supramolecular Ligands”. *Chem. Eur. J.* **2012**, 18, 1383
62. A. C. Laungani, B. Breit, “Supramolecular PhanePhos-analogous ligands through hydrogen-bonding for asymmetric hydrogenation”. *Chem. Commun*. **2008**, 844
63. T. Ooi, K. Maruoka, “Asymmetric organocatalysis of structurally well-defined chiral quaternary ammonium fluorides”. *Accounts of Chemical Research*. **2004**, 37, 526
64. Z. Kokan, S. I. Kirin, “The application of “backdoor induction” in bioinspired asymmetric catalysis”. *RSC Adv*. **2012**, 2, 5729
65. J. A. Fuentes, T. Lebl, A. M. Z. Slawin, M. L. Clarke, “Synthesis of organocatalysts using non-covalent chemistry: understanding the reactivity of ProNap, an enamine-type organocatalyst that can self-assemble with complementary co-catalysts”. *Chem. Sci*. **2011**, 2, 1997

66. K. Ohmatsu, M. Ito, T. Kunieda, T. Ooi, “Asymmetric catalysis: The power of pairing”. *Nature Chemistry*, **2012**, 4, 473

67. P. Dydio, J. N. H. Reek, “Supramolecular control of selectivity in transition-metal catalysis through substrate preorganization”. *Chem. Sci*. **2014**, 5, 2135

68. C. A. Lewis, S. J. Miller, “Site-Selective Derivatization and Remodeling of Erythromycin A by Using Simple Peptide-Based Chiral Catalysts”. *Angew. Chem., Int. Ed*. **2006**, 45, 5616.

69. C. A. Lewis, K. E. Longcore, S. J. Miller, P. A. “Synthesis and cytotoxicity of bidesmosidic botulin and betulinic acid saponins”. *J. Nat. Prod*. **2009**, 72, 1864

70. B. S. Fowler, K. M. Laemmerhold, S. J. Miller, “Catalytic Site-Selective Thiocarbonylations and Deoxygenations of Vancomycin Reveal Hydroxyl-Dependent Conformational Effects”. *J. Am. Chem. Soc*. **2012**, 134, 9755

71. T. P Pathak, S. J. Miller, “Site-Selective Bromination of Vancomycin”. *J. Am. Chem. Soc*. **2012**, 134, 6120

72. S. Han, S. J. Miller, “Asymmetric Catalysis at a Distance: Catalytic, Site-Selective Phosphorylation of Teicoplanin”. *J. Am. Chem. Soc*. **2013**, 135, 12414

# CHAPTER 2. SITE SELECTIVE CATALYTIC ASYMMETRIC HYDROBORATION

## 2.1 Hydroboration background

Carbon-carbon bond forming reactions are an essential tool for synthetic chemists and numerous metal-catalyzed carbon-carbon bond forming reactions have been invented in response. Among these, the Suzuki coupling, a reaction in which an organoboronic acid (or ester or equivalent) and an organic (usually aryl) halide are coupled by the action of a metal (usually palladium) catalyst, is a very powerful and reliable method that is widely used for carbon-carbon bond formation; this is especially true in the pharmaceutical industry[1]. Due to the utility of this and related cross-coupling reactions for carbon-carbon bond formation, Prof. Suzuki, along with Profs. Negishi and Heck, shared the 2010 Nobel Prize in Chemistry. Figure 1 shows a variety of stereospecific ways to utilize the carbon-boron bond in subsequent refunctionalizations, [3] including formation of carbon-carbon bonds[4].

Despite the synthetic importance of organoboron intermediates, methods for their efficient preparation, especially chiral boron compounds, are rather rare[2]. One of the most important methods for preparation of organoboron intermediates is via hydroboration of alkenes, allenes, and alkynes. This chapter will discuss our efforts to employ self-assembled catalysts for the asymmetric hydroboration of alkenes.

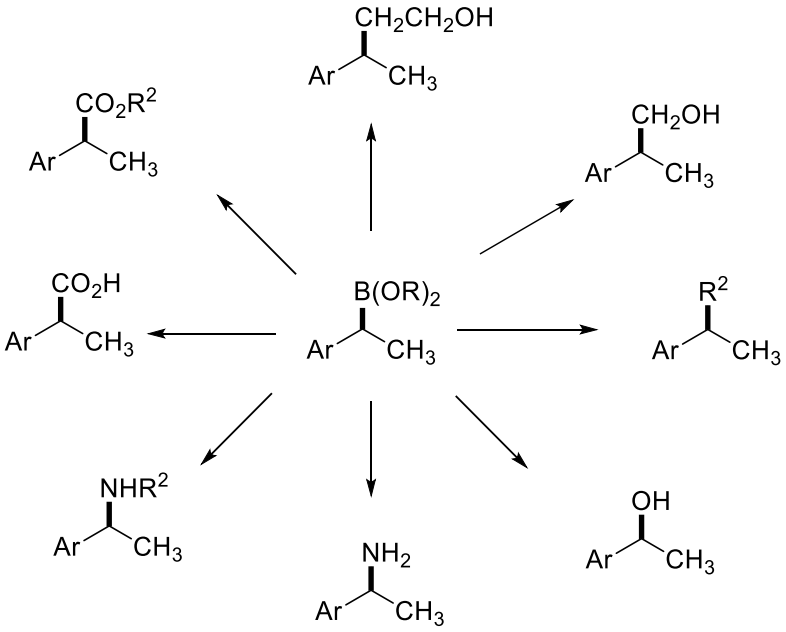


**Figure 1.** Stereospecific transformations of organoborons illustrated for a boronate.

The first hydroboration using a late transition metal catalyst was reported over 35 years ago by Wilczynski and Sneddon[5]. Building upon Wilczynski's work, Manning and Nöth described successful alkene hydroboration by catecholborane in the presence of a neutral rhodium catalyst precursor.[6] The authors observed differing chemoselectivity in the catalyzed versus non-catalyzed reactions with an unsaturated ketone; the catalyzed reaction resulted in hydroboration of the alkene while the uncatalyzed process resulted in reduction of the carbonyl (Figure 2A).

In a seminal paper, Hayashi and workers demonstrated that the combination of a cationic rhodium complex together and BINAP could produce high enantioselectivity (up to 96% ee) and excellent regioselectivity (>99:1 branched/linear) for the catalyzed hydroboration of styrene derivatives by catecholborane.[7] Excellent reactivity was

exhibited (Figure 2B); 1% catalyst was sufficient to effect complete the reaction in just 1 hour (Figure 2C).

There are several important take-home messages conveyed by the two early examples of catalyzed hydroboration described above. First, catalytic asymmetric hydroboration (CAHB) is possible. This is of interest due to a variety of chiral compounds that can be accessed via stereospecific transformations of chiral boronic esters and, particularly for reactions at scale, by the economic advantages of using chiral catalysts vs chiral reagents. Secondly, as demonstrated by both groups discussed above, unique regioselectivity can be achieved via catalyzed variant, which allows access to molecules that are not easily synthesized using other methods. Research in hydroboration of olefins has been actively pursued by a number of groups: Evans[8-15], Burgess[16-30], Guiry[31-34], Hoveyda[35-37], Crudden[38-43], Westcott[44-65], Molander[66-67], and Takacs[68-79]. Recently, even more research groups have been attracted to the catalyzed hydroboration research as judged by increasing numbers of publications in recent years.[80] (Figure 3).

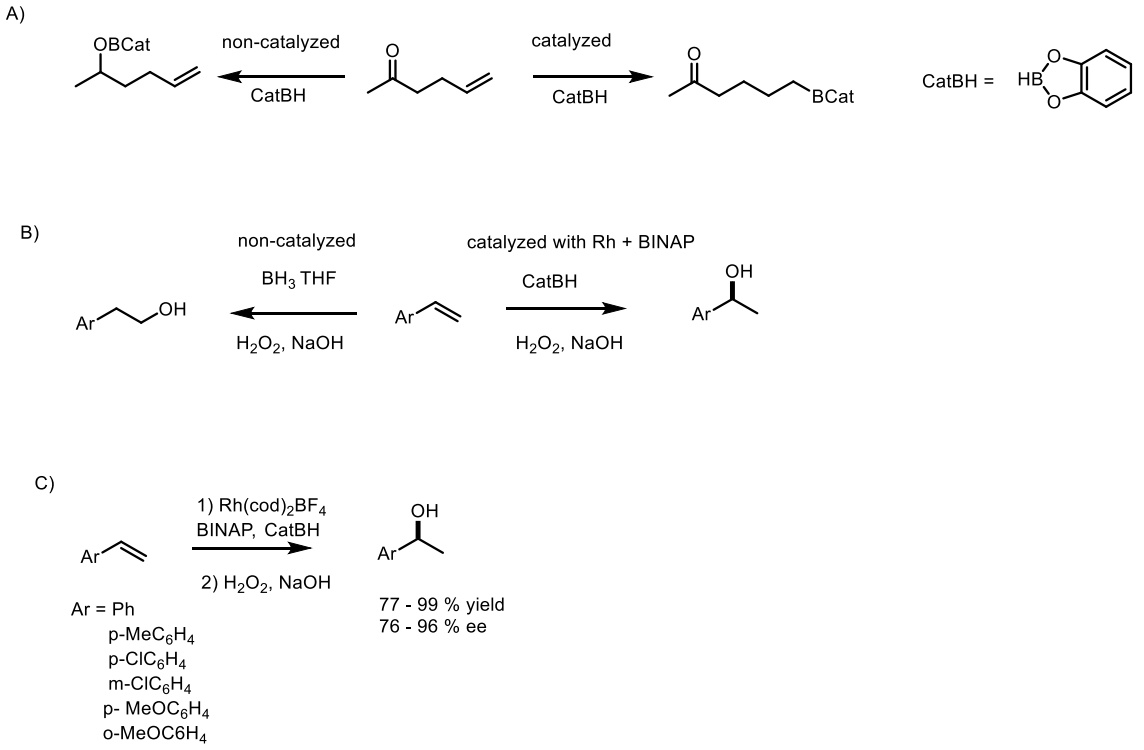


**Figure 2.** A) Comparison between catalyzed and non-catalyzed hydroboration (Manning and Nöth). B) First catalytic asymmetric hydroboration (Hayashi). C) Cationic rhodium complex and BINAP provide excellent enantioselectivity for catalytic asymmetric hydroboration.

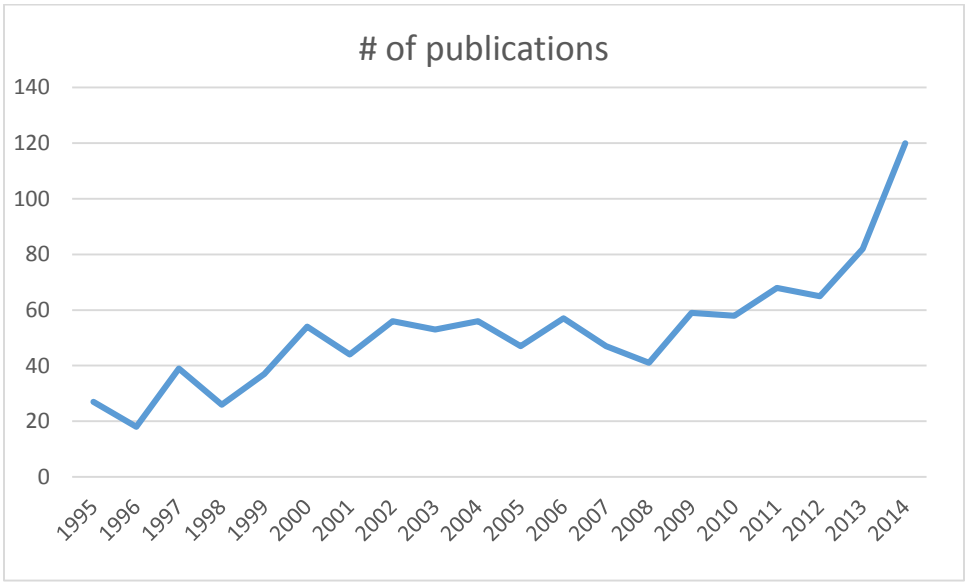

**Figure 3.** References resulting from Scifinder search by key words “catalytic hydroboration”. The sharp uptick in references in 2013 and 2014 may be related to greater awareness of organoboron chemistry following Suzuki's 2010 Nobel Prize in 2010.

**2.2 Hydroboration mechanism**

Manning and Nöth proposed a basic catalytic cycle for hydroboration using Wilkinson's catalyst (Figure 4), the most active catalyst among many they examined. The reaction starts with dissociation of one phosphine ligand from Wilkinson's catalyst to form the active Rh (I) catalyst complex **201** followed by oxidative addition of catecholborane. The five coordinate Rh (III) intermediate **202** was isolated and characterized by Kono[81] and his coworkers. The corresponding complex wherein $PPh_3$ was exchanged for $P(iPr)_3$ was isolated and its structure $[RhHCl(Bcat)(PPr^i_3)_2]$ was determined by X-ray crystallography by Westcott[82]. Intermediate **202** is expected to complex the olefin to generate intermediate **203**. Insertion of olefin into the Rh-H bond proceeds regioselectively to afford the branched intermediate **204**. Subsequent reductive elimination affords the observed branched product **205** and regenerates the active catalyst **201**. Intermediate **203** plays a key role in that it can form a minor product **207** via two different pathways. Insertion of Rh-H bond with reverse regioselectivity gives intermediate **209**, which undergoes reductive elimination to afford the linear product **207**. The other pathway involves an insertion of Rh-B bond to alkene, yielding intermediate **206**, which can undergo reductive elimination to also form linear product **207**. The latter pathway can also generate the major branched product **205** via the intermediate **208**.

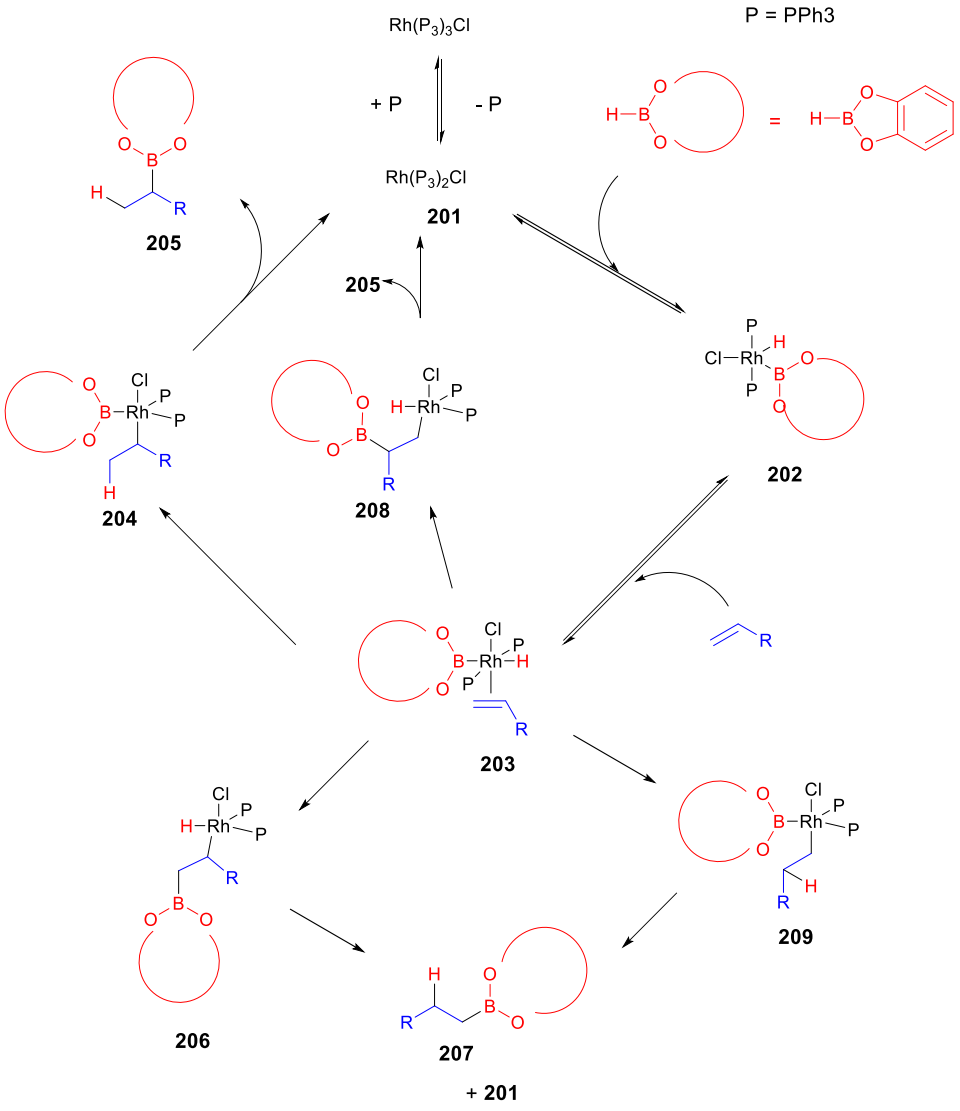


**Figure 4.** Generally accepted hydroboration mechanism of alkenes (especially vinyl arenes) with Wilkinson's catalyst (major and minor pathways).

Other researchers have suggested alternative pathways. For example, it has been suggested that alkene coordination to rhodium has two possible pathways. The original mechanism proposed by Manning and Nöth as well as a later study by Evans and Fu[83] favored a dissociative mechanism (Figure 5B). After oxidative addition of

catecholborane, coordination of the alkene to intermediate **202** takes place with simultaneous dissociation of one phosphine ligand leading to a five coordinate Rh (III) complex. Burgess and coworkers[84] favored an alternative pathway, an associative mechanism in which the alkene and two ligands are bound to rhodium to form a six coordinate Rh (III) complex (Figure 5A, intermediate **203**). Which mechanism is correct remains open to debate. Supporters of the dissociative mechanism include Dorigo and Scheleyer, [85] who conducted an ab initio study of dissociative mechanism, while Musaev and coworkers[86] favor the associative mechanism, also on the basis of computational studies.

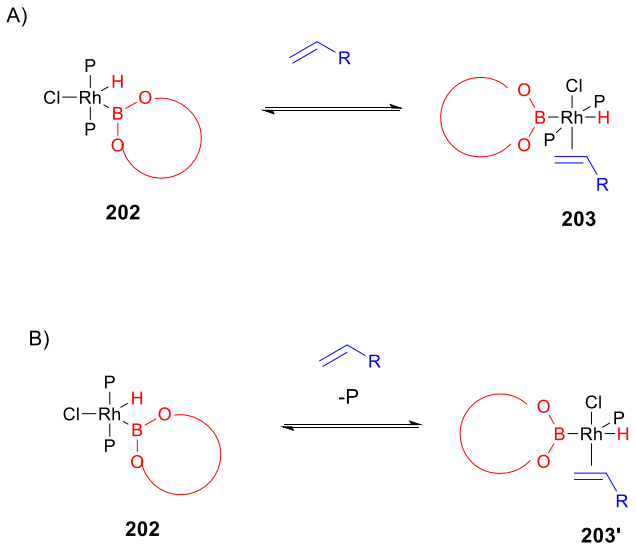


**Figure 5.** A) Associative mechanism: two phosphine containing ligands are bound to rhodium complex during alkene coordination. B) Dissociative mechanism: coordination of alkene occurs simultaneously with dissociation of one phosphine.

Widauer, Grutzmacher, and Ziegler conducted a rather extensive computational study of rhodium catalyzed hydroboration[87] focusing on the kinetics and thermodynamics of migratory insertion of the alkene into the Rh-H or Rh-B bonds from complex **209** (Figure 6A). This study revealed that the two pathways are kinetically and thermodynamically similar; both are exothermic (15-22 kcal/mol) with small barriers (< 3.5 kcal/mol). Their study on the dissociative mechanism (Figure 6B) predicts almost no barrier for insertion of the alkene into Rh-H bond; in contrast, the subsequent reductive elimination step (to form the C-B bond) has a relatively high barrier (15 kcal/mol). The opposite was observed for alkene insertion into Rh-B bond; migratory insertion has the high barrier (19.5 kcal/mol) whereas reductive elimination to form the C-H bond is predicted to be facile. Ziegler concluded that Rh-B pathway may be preferred because the high barrier for the reductive elimination step would likely hinder the product formation. This still remains for open discussion.

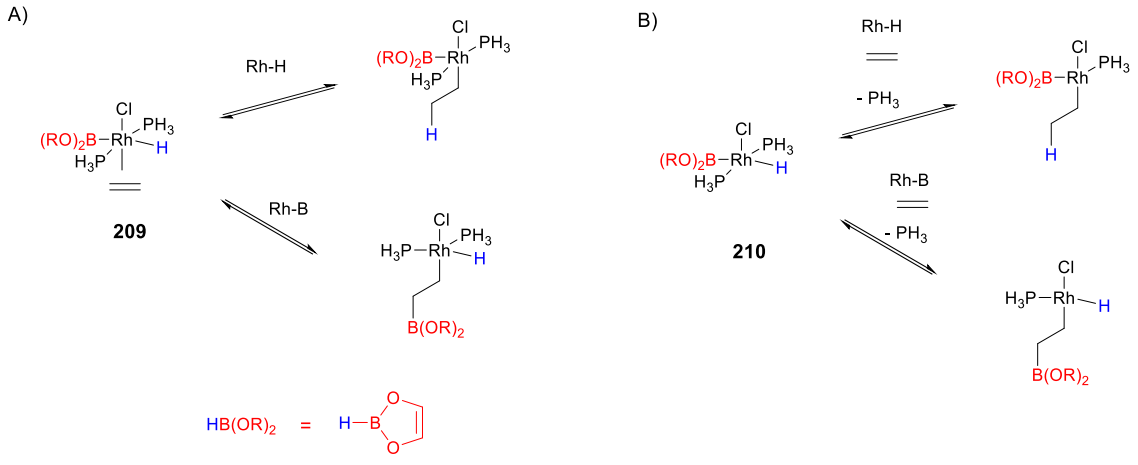


**Figure 6.** A) Theoretical study of rhodium catalyzed hydroboration for the migratory insertion of the alkene from compound **209** (associative mechanism). B) Dissociative mechanism.

Unlike mechanistically better understood metal catalyzed asymmetric transformations such as catalytic asymmetric hydrogenation (CAH), catalytic asymmetric hydroboration is still in infancy in terms of understanding of the reaction mechanism and the elements controlling selectivity. In addition to the issues discussed above, a number of mechanistic details remain clouded, particularly the differences between neutral and cationic rhodium catalysts[88] and the influence of different boranes[89]. Nonetheless, the reaction is potentially of high value to the chemistry community in that it allows straightforward accesses to chiral boronic esters, intermediate that can in turn be converted into many useful functional groups and potentially used as synthons in diversity oriented synthesis[1]. The Takacs group became interested in CAHB and has developed two approaches in its efforts including the development of supramolecular catalysts based upon self-assembled ligands (SAL) [23-24]. This chapter will describe CAHB of styrene derivatives with chiral supramolecular catalysts that led to a unique example of site selective chemistry.

**2.3 Introduction of supramolecular self-assembled ligand (SAL) system**

Nature uses enzymes to specifically and selectively catalyze the chemical reactions that are necessary for life to sustain metabolic activity. Enzymes are proteins of varying size and shape and yet often even slight changes in protein structure dramatically change enzymatic activity in terms of rate, selectivity and/or substrate specificity. The reactivity and selectivity observed with enzymes are often much greater than those with chemical catalysts. Therefore, a grand challenge for organic chemists researching in the area of asymmetric catalysis is to develop chemical catalysts that mimic some – if not all – of the desirable characteristics of enzymes. Among those desirable characteristics is the efficient use of subtle secondary interactions between the enzyme and substrate of interest to form or adapt a suitable chiral pocket to perform highly selective and specific reactions in a substrate and site-selective manner[91-92]. Supramolecular catalysts are in a size regime much smaller than typical enzymes but much larger than typical molecular catalysts[93] and thus potentially can exploit secondary interactions in a manner similar to enzymes.

Takacs and coworkers have found metal-directed self-assembly of chiral bidentate ligands (SALs) to be an efficient way to prepare and optimize chiral supramolecular catalysts for asymmetric allylic amination, asymmetric hydrogenation, and asymmetric hydroboration; in each case, supramolecular catalysts were identified that exhibited both excellent reactivity and enantioselectivity. It was decided to explore application of this approach to the rhodium-catalyzed CAHB of styrene derivatives. Takacs' SAL system can be broken down into four parts: a bisoxazoline (Box) recognition

element to direct self-assembly, scaffold-building tethers for structural diversity, ligating groups for additional structural and catalyst diversification, and an active site metal to effect the desired mode of catalysis (Figure 7A; structures based upon *R, R*- bisoxazolines are shown in red; those based upon *S,* S-scaffolds are shown in blue). In 2004 Takacs and coworkers reported[15] that equimolar mixtures of *R*,*R*- and *S*,*S*-bisoxazolines form exclusively neutral, heterochiral (heteroleptic) Zn(II) complexes (Figure 7 B). These complexes can be readily generated *in situ* or prepared and isolated. A crystal structure of a heteroleptic complex shows that each phenyl group is oriented away from other phenyl groups. This avoidance of steric interactions, which is not possible in the homochiral (homoleptic) Zn (II) complex, forms the basis for controlled self-assembly by chiral self-discrimination. The exclusive formation of the heterochiral Zn (II) complexes is used to construct chiral self-assembled ligands (SALs) and SAL-derived supramolecular rhodium catalysts for CAHB. It is worth mentioning that the heteroleptic complexes are psuedoracemic, although each bisoxazoline units is chiral. At first, the chirality of the bisoxazolines was not considered to significantly influence enantioselectivity of the catalyzed reactions; later on, this was found not to always be true for catalytic asymmetric hydrogenation reactions[94].

The scaffold-building tethers play an important role in diversifying the ultimate supramolecular structure and in positioning the ligating groups to bind to the active site metal. Suitably activated aryl- or biaryl-ring systems with different substitution patterns are prepared (Figure 7C) and are used to monoalkylate the bisoxazoline subunits thereby connecting the scaffold-building tether subunits to the bisoxazoline subunit.

The syntheses, as few as four steps and achieved with good overall yields, is straightforward. Two version of each scaffold-building tether are synthesized; one terminating in an aryl-OH (i.e., the odd numbered scaffold tethers: 1, 3, 5, 7, 9, 11, 13, & 15) and another terminating in an aryl-$CH_2OH$ (i.e., the even numbered scaffold tethers: 2, 4, 6, 8, 10, 12, 14, & 16). In comparing the homologous tethers, the additional "$CH_2$" offers an extra degree of rotational freedom so that the even numbered scaffold tethers are considered to be more flexible than the odd numbered tethers. Mixing one of each motif allows for further tuning of the resulting ligand environment and supramolecular catalysts.

The pendant "OH" group permits the facile introduction of the ligating group subunit. A variety of ligating groups, including some of the privileged chiral ligands structures, can be installed with ease; this increases the scope of reactions and substrates that can be examined with the SAL-derived supramolecular catalyst systems. Based on a previous study[78], one family of ligating groups that work especially well for the CAHB of styrene derivatives is based upon TADDOL-derived ligands[95] such as those shown in Figure 7D. The studies described below focuses exclusively on TADDOL-derived ligands.

Last but not least, the final component of a SAL-derived supramolecular catalyst is the active site metal. Previous study found that cationic Rh (I) complexes are good catalyst precursors for the CAHB of styrenes. The Rh (I) counterion affects the reactivity and selectivity of the SAL-derived catalysts. The optimal metal precursor to use for this study was found to be $Rh(nbd)_2BF_4$, which is used throughout.

Assembly of the self-assembled ligands (SALs) is straightforward (Figure 7E). First, the appropriate bifunctional (*R,R*)-Box and (*S,S*)-Box derived ligands are each prepared and then combined with an equivalent of diethyl zinc in DCM; the heteroleptic complex $(Box)_2Zn$ is formed within five minutes and ready for use. The desired catalyst precursor, $Rh(nbd)_2BF_4$ in the case at hand, is added; this affords the soluble supramolecular catalyst complex within 15 minutes. Although the supramolecular catalyst complexes can be isolated, we find their use *in situ* to be more efficient as it avoids tedious purification steps. The easy preparation of SAL facilitates the generation of a large library of SAL. For the studies described in this thesis, a combination of 16 different scaffold-building tethers were used with four different TADDOL-derived ligating groups to afford 64 different (R, R)- and (S, S)-subunits, giving us the potential to generate $(64)^2$ or 4,096 SALs. In principle, each SAL and its derived supramolecular catalyst is unique in terms of its shape (i.e., three dimensional structure). As the data will show, these differences translate into different catalytic activity and selectivity in the CAHB of a series of substituted styrenes.

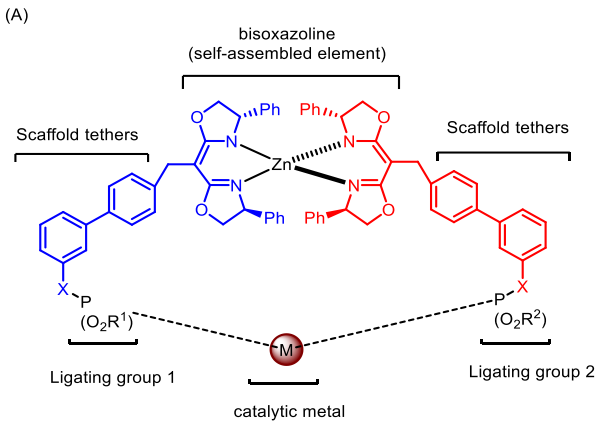

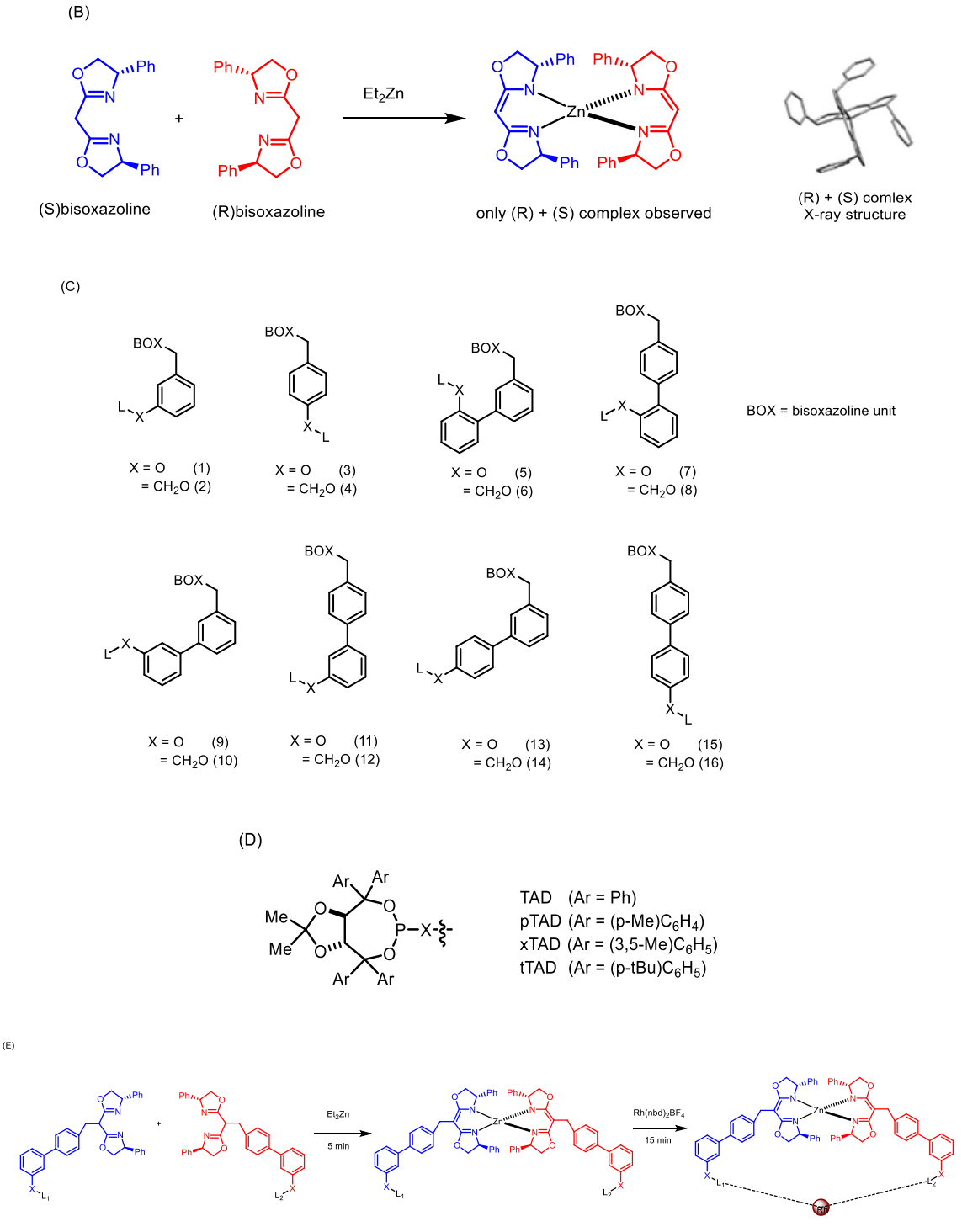


**Figure 7.** A) Takacs SAL and SAL-derived modular supramolecular catalyst system. B) Heteroleptic recognition of bisoxazoline. C) Scaffold tethers employed in construction of SALs. D) TADDOL-based chiral monodentate ligating groups attached to scaffold tethers. E) SAL synthesis procedure.

## 2.4 Catalytic asymmetric hydroboration of *ortho*- and *meta*- substituted styrenes with SAL

Styrenes are prototypical substrates for asymmetric hydroboration and are often used to test newly developed catalyst systems. Reactivity and selectivity (regio- and enantioselectivity) are sensitive to both steric and electronic natures of the substrates and *ortho*-substituted styrenes have proven to be difficult substrates on which to achieve excellent enantioselectivity[78]. The best enantioselectivities for hydroboration of *ortho*-substituted styrenes were published before 2000 and analyzing the level of enantioselectivities (Figure 8B) indicates more needs to be done. The literature best enantioselectivities ranges from 69% ee (o-F styrene) to 92% ee (o-OMe styrene).

The Takacs group tested the newly developed supramolecular SAL catalysts in the rhodium catalyzed asymmetric hydroboration across a series of *ortho*-substituted styrene derivatives (o-CF3, o-X, o-Y, o-Z, etc.) and, in each case, found catalysts that gave comparable or superior results compared to the literature (Figure 8). Enantioselectivity ranged from 91% ee (o-$CF_3$ styrene) to 96% ee (o-F styrene).[78] On one hand this suggests that perhaps the supramolecular catalyst approach may help in identifying catalysts with broader substrate scope. On the other hand each styrene substrates required a slightly different SAL catalyst for optimal results demonstrating that even structurally closely related SALs indeed have different catalytic properties.

A)

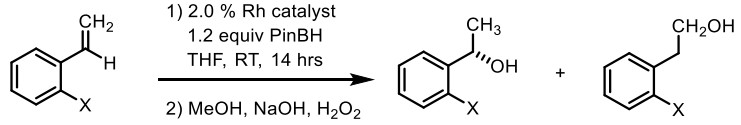


1a (X = Me)
1b (X = OMe)
1c (X = Cl)
1d (X = F)
1e (X = $CF_3$)

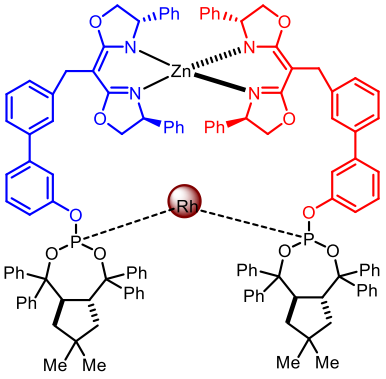


Best perfomed SAL
(S9TAR9TA)

B)

| Catalyst | 1a | 1b | 1c | 1d | 1e |
|---|---|---|---|---|---|
| Best SAL | 94% ee | 91% ee | 91% ee | 96% ee | 91% ee |
| literature | 82% ee[7] | 92% ee[96] | 83% ee[96] | 69% ee[96] | 72% ee[96] |

**Figure 8.** A) Overview of catalytic asymmetric hydroboration of *ortho*-substituted styrenes with Takacs SAL catalysts. B) Comparison of enantioselectivities with the best result previously reported.

A subsequent publication from the Takacs group described application of supramolecular SAL catalysts for catalytic asymmetric hydroboration of *meta*-substituted styrenes[73]. This time the SALs were further optimized by first optimizing scaffold tethers and then further optimizing the combination of ligating groups. The result was improvement in reactivity and enantioselectivity. The SALs identified in the study exceeded the best enantioselectivity previously reported for each of the five substrates. In addition, SAL catalysts also proved to be highly reactive. In some cases only 0.01% of the catalyst is necessary to complete the reaction within 3 hours showing that good TONs and TOFs are possible with these catalysts; In contrast, a catalyst loading of 2.0% and 14 hours of reaction is typical for other reported CAHB catalysts.

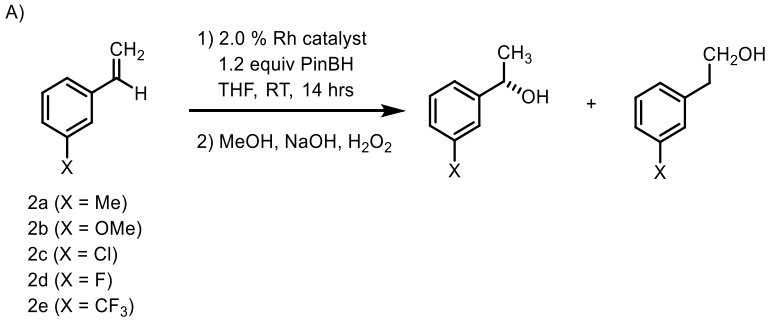


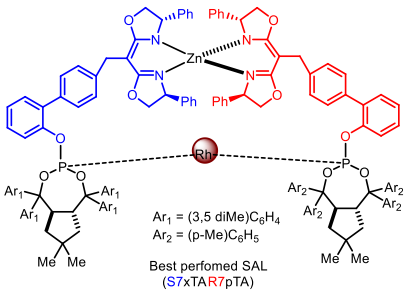

B)

| Catalyst | 2a | 2b | 2c | 2d | 2e |
|---|---|---|---|---|---|
| Best SAL | 94% ee | 95% ee | 96% ee | 96% ee | 97% ee |
| Literature | 91% ee[96] | NR | 89% ee[97] | 88% ee[97] | 83% ee[96] |

**Figure 9.** A) Catalytic asymmetric hydroboration of *meta*- substituted styrenes with Takacs SAL catalysts. B) Literature best enantioselectivities across *meta*- substituted styrenes,

**2.5 Catalytic asymmetric hydroboration of *para*- substituted styrenes with SAL**

The Takacs group has not published a paper on rhodium-catalyzed asymmetric hydroboration of *para*- substituted styrenes. This thesis will analyze and discuss data that was acquired by Dr. Shin Moteki and reported in his Ph.D. dissertation.[98] Compared to *ortho*- and *meta*- substituted styrenes, *para*- substituted styrenes are considered relative easy substrates for enantioselective CAHB. With this series of substrates, even two stage optimization failed to significantly improve upon and in one case even match the best enantioselectivities already reported in the literature. The *para*-trifluoromethyl styrene gave 89% ee with the best SAL catalyst, an improvement from the 74% ee reported in the literature. However, the *para*- methoxy styrene afforded only 93% ee, lower than the previously reported best (98% ee). Despite the less than ideal results, Takacs' SAL demonstrated that it can offer a wide variety of catalysts capable of achieving similar or better enantioselectivity across a wide range of substituted styrenes (i.e., fifteen *ortho*-, *meta*-, and *para*- substituted styrenes possessing Me-, OMe-, Cl-, F-, and $CF_3$-substitutents). No other single catalyst system reported to date shows similar scope. It is true that the Takacs' SAL can generate some of the best enantioselectivity for *ortho*-, *meta*-, and *para*- substituted styrenes, while handful of SALs were found to show rather low reactivity. The following section of chapter 2 is devoted to the discoveries and development of site selective SALs for CAHB based upon such a diverse set of data collections.

A)

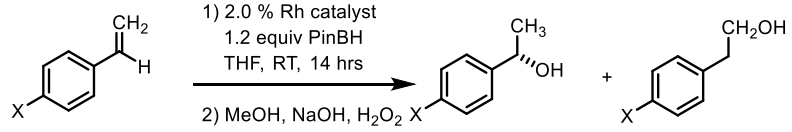


3a (X = Me)
3b (X = OMe)
3c (X = Cl)
3d (X = F)
3e (X = $CF_3$)

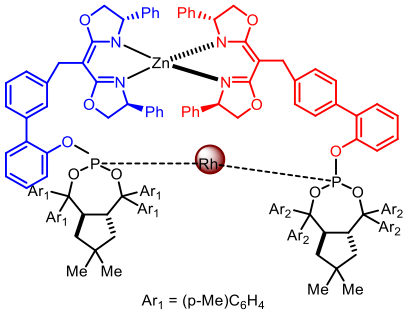


$Ar_1$ = (p-Me)$C_6H_4$
$Ar_2$ = (3,5 diMe)$C_6H_5$

Best perfomed SAL
(S5pTAR7xTA)

B)

| Catalyst | 3a | 3b | 3c | 3d | 3e |
|---|---|---|---|---|---|
| Best SAL | 92% ee | 93% ee | 92% ee | 92% ee | 89% ee |
| Literature | 94% ee[99] | 98% ee[100] | 91% ee[99] | 92% ee[100] | 74% ee[100] |

**Figure 10.** A) Catalytic asymmetric hydroboration of para- substituted styrenes with Takacs' SAL catalysts. B) Best literature results with catalyzed enantioselective hydroboration.

**2.6 Site selective hydroboration – Site selectivity toward *ortho*- and *meta*- methoxy styrenes**

Dr. Moteki generated a great deal of data in the course of his thesis studies. For example, the five *ortho*- substituted styrenes were examined with all 4,096 SAL-derived catalysts, giving 20,480 data points each on yield and enantioselectivity. The same was done for the *meta*- and *para*- substituted styrenes as well. In total, 61,440 yield and 61,440 ee data points were collected, and my goal was analyzing those data to identify useful trends and new insights into CAHB and these SAL-derived chiral supramolecular catalysts. My contribution to the site selective chemistry field begins at this point.

Analyzing the data has revealed some very interesting trends. Figure 11 shows the overall variation in individual yields obtained for *ortho*-, *meta*-, or *para*- methoxy styrene across the collection of TADDOL-derived SAL catalysts screened. In this analysis that follows, it is important to note that all of the screening reactions were carried out identically. Therefore, the yield data collected by Dr. Moteki reflects either catalyst TOF or catalyst stability under the conditions examined. The data for each substrate was independently sorted and the results graphed from the highest to the lowest yield; the three graphs are plotted together to compare the results. Even though the same set of supramolecular SALs was used, the range and distribution of yields varied considerably for the three different substitution patterns. For example, for *ortho*- methoxy styrene yields varied over a relatively narrow range, 99% to 85% (blue graph on Figure 11); almost all SAL-derived catalysts were quite efficient in terms of conversion. For *para*- methoxy styrene, SAL catalyst activity varied more widely, from 95% to 25% (gray graph

on Figure 11), and only a few catalysts were very efficient (i.e., gave above 90% yield). This is a rather drastic change in the profile of obtained yields (i.e., catalyst TOF and/or stability) and suggests that the structure of the SAL-derived catalyst strongly influences the reactivity of each different substrate. However, one could also interpret the data as simply reflecting the different inherent reactivity of the different substrates. The latter could be tested by comparing the relative reactivity of the three methoxy styrene derivatives with a chiral phosphite-modified catalyst lacking the structural bias of the SAL complex[101] in a reaction vial. Seeing that the least reactive catalyst afforded the product with 85% yield for *ortho*- methoxy styrene while the least reactive catalyst gave only 25% yield for the *para*- methoxy styrenes seemed significant and caught my attention (*vide infra*).

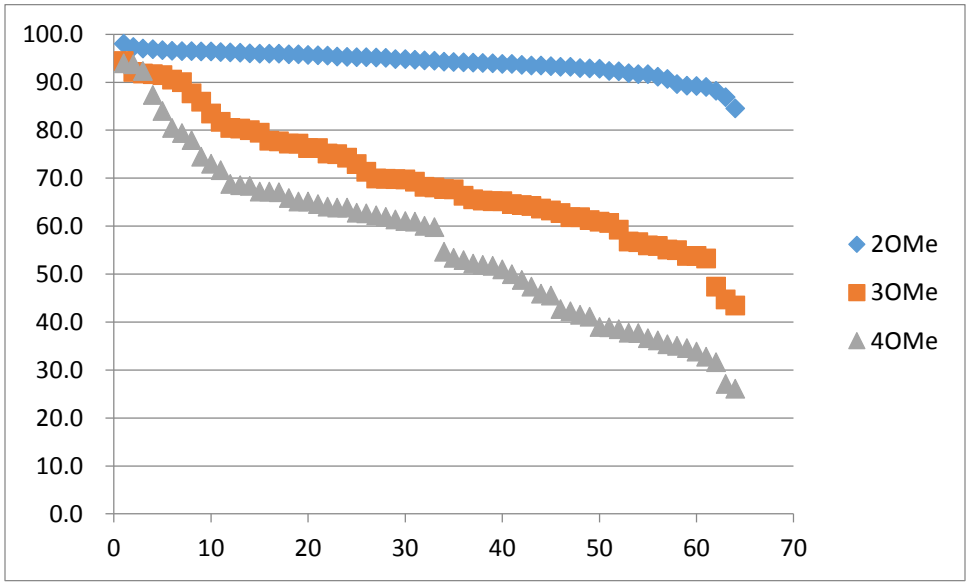


**Figure 11 (X axis: ranked series of SAL-derived catalyst. Y axis: product yields).** Individual substrate yield data are sorted from the highest to lowest for three isomeric

methoxy styrenes showing that the range of yields obtained varies considerably from substrate to substrate.

Looking at the data obtained for *ortho*-, *meta*- and *para*-methoxy styrenes led to the conclusion that the range of yields obtained varies considerably from substrate to substrate over the set of SAL-derived catalysts evaluated. For the *ortho*-substrate many catalyst structures proved very efficient while for the *para*-substrate only a few proved effective. I considered another way to analyze the yield data (Figure 12A) that led to another insight. The data in Figure 12A were first sorted in order from the highest to the lowest yield obtained with *ortho*-methoxy styrene; this gives a ranked order for the effectiveness of SAL-derived catalyst structures for *ortho*-methoxy styrene. The yield data for *meta*- and *para*-methoxy styrenes are displayed according to that same ranked order of catalyst structures; in another words, each point on x axis represents one particular SAL-derived catalyst and the three data points in that column reflect the yield obtained with that particular catalyst for the three substrates. It is readily apparent that several SAL catalysts reacted much more readily with *ortho*-methoxy styrene than the majority of the SAL catalysts and the yield differences between *ortho*-methoxy and the other two (*meta*- and *para*-) styrenes are significant enough to suggest that the *ortho* methoxy would react preferentially in presence of *meta*- and *para*- substrates. I will use this as a lead for uncovering site-selective catalysts (*vide infra*).

The data in Figure 12A was constructed from data obtained using SAL-derived catalysts in which only TADDOL-phosphite ligating groups were incorporated; recall that

Dr. Moteki's study used four different TADDOL-derivatives attached as chiral phosphite ligating groups (i.e., TADDOL, pTADDOL, xTADDOL and tTADDOL). A similar plot of data obtained for the series of (pTADDOL) SAL catalysts is shown in Figure 12B. These SAL-derived catalysts are again rank-ordered based on the yields obtained for the *ortho*-methoxy styrene substrate and the data for the *meta*- and *para*-substrates plotted accordingly. Note that by changing the nature of the ligating group, the yield obtained for the *ortho*-methoxy styrene substrate is not consistently higher than those obtained for the meta or para isomers; in some cases the yield with a particular (pTADDOL)SAL catalyst for *meta*-methoxy styrene is higher that obtained with it for the *ortho*-methoxy styrene. Thus, with the correct structure of SAL catalyst *meta*-methoxy styrene is much more reactive than *ortho*-methoxy styrene indicating that changing ligating groups and scaffold-building tethers can tune the relative reactivity of the substrates toward rhodium-catalyzed CAHB of styrenes.

A)

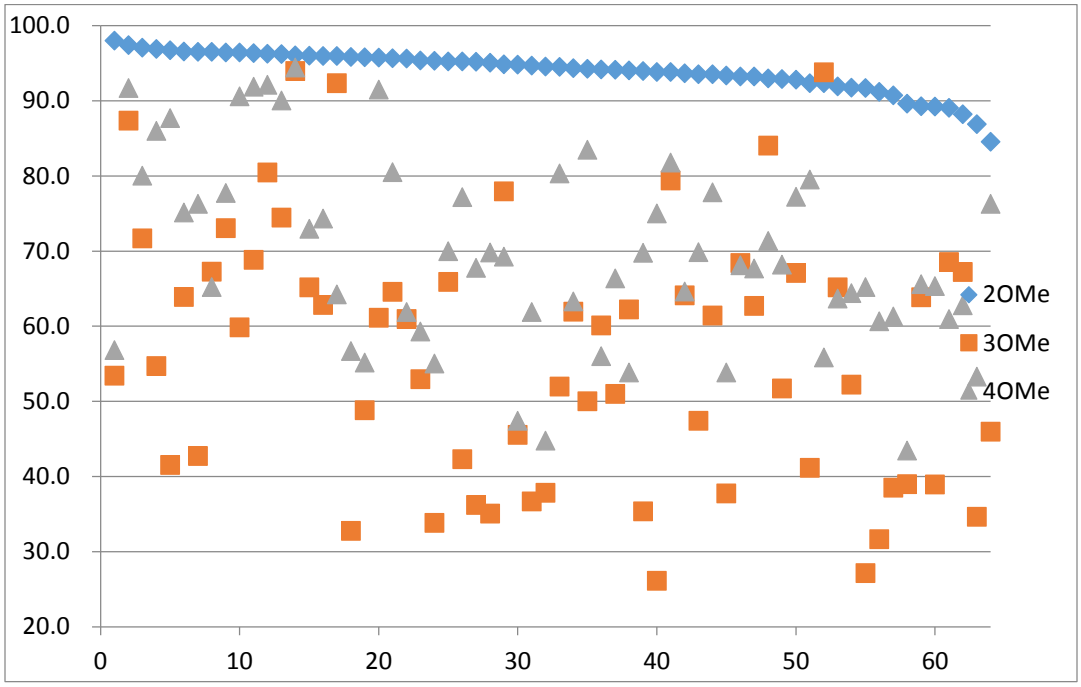
100.0
90.0
80.0
70.0
60.0
50.0
40.0
30.0
20.0
0
10
20
30
40
50
60
2OMe
3OMe
4OMe

B)

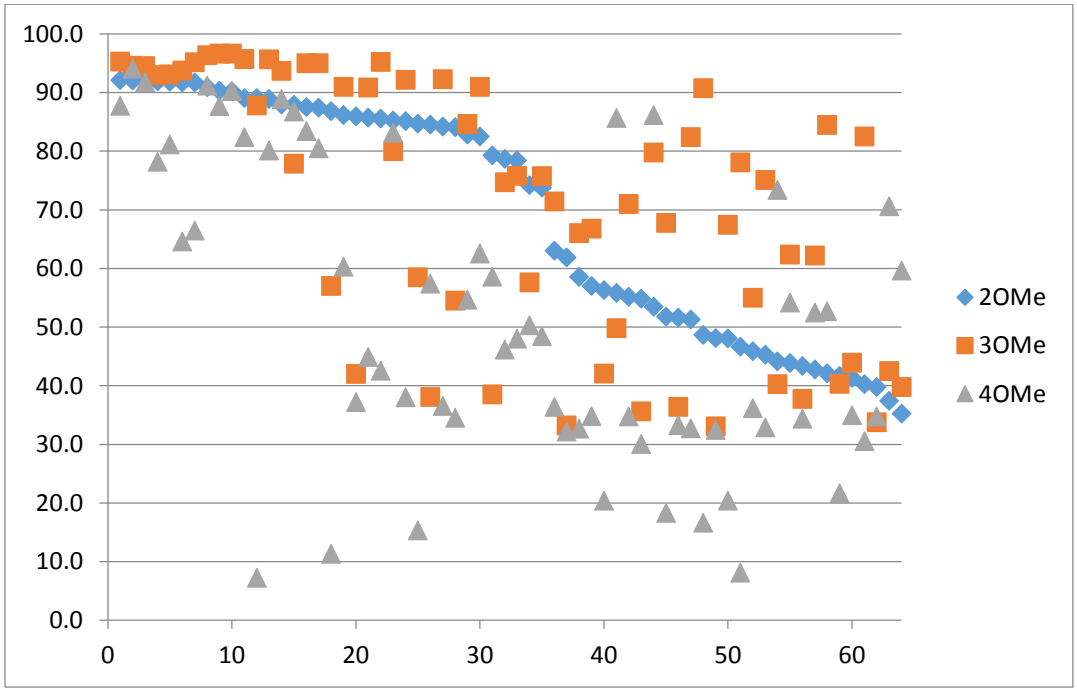
100.0
90.0
80.0
70.0
60.0
50.0
40.0
30.0
20.0
10.0
0.0
0
10
20
30
40
50
60
2OMe
3OMe
4OMe

**Figure 12 (X axis: SAL catalysts in ranked order. Y axis: yields of CAHB).** A) *ortho*-Methoxy styrene yields with TADDOL containing SAL-derived catalysts [(TADDOL)SALs] are sorted from the highest to the lowest showing that several SAL catalyst display significant yield differences among the substrates. B) Similarly constructed graph with pTADDOL as the ligating group for (pTADDOL)SAL-derived catalysts.

Analyzing the over 60,000 data points collected revealed several SAL-derived catalysts that exhibited excellent reactivity for only one substrate. Some of the SAL catalysts afforded higher levels of enantioselectivity than others and a catalyst that displays high reactivity as well as high enantioselectivity would be of particular interest in my study. The graph in Figure 13 was constructed to identify those SAL catalysts that exhibit high relative reactivity and high enantioselectivity for pairs of substrates. The X axis plots the difference of yields between *ortho*- and *meta*-methoxy styrene hydroboration products after the oxidative workup. Positive numbers mean that a particular SAL catalyst exhibited higher yield for the *ortho*- over the *meta*-isomer, while negative numbers indicate the opposite. Thus, data on the far right or far left hand side are associated with SAL-derived catalysts that are in theory more *ortho*- or *meta*-selective, respectively. The value on the Y axis indicates level of enantioselectivity (i.e., % ee) of the more abundant hydroboration product. In such a plot, data points in the top far right (*ortho*- selective with high enantioselective) and top far left (*meta*-selective with high enantioselective) of the graph represent the top candidates for further study. Colored and triangle shaped data points are the SAL-derived catalysts selected.

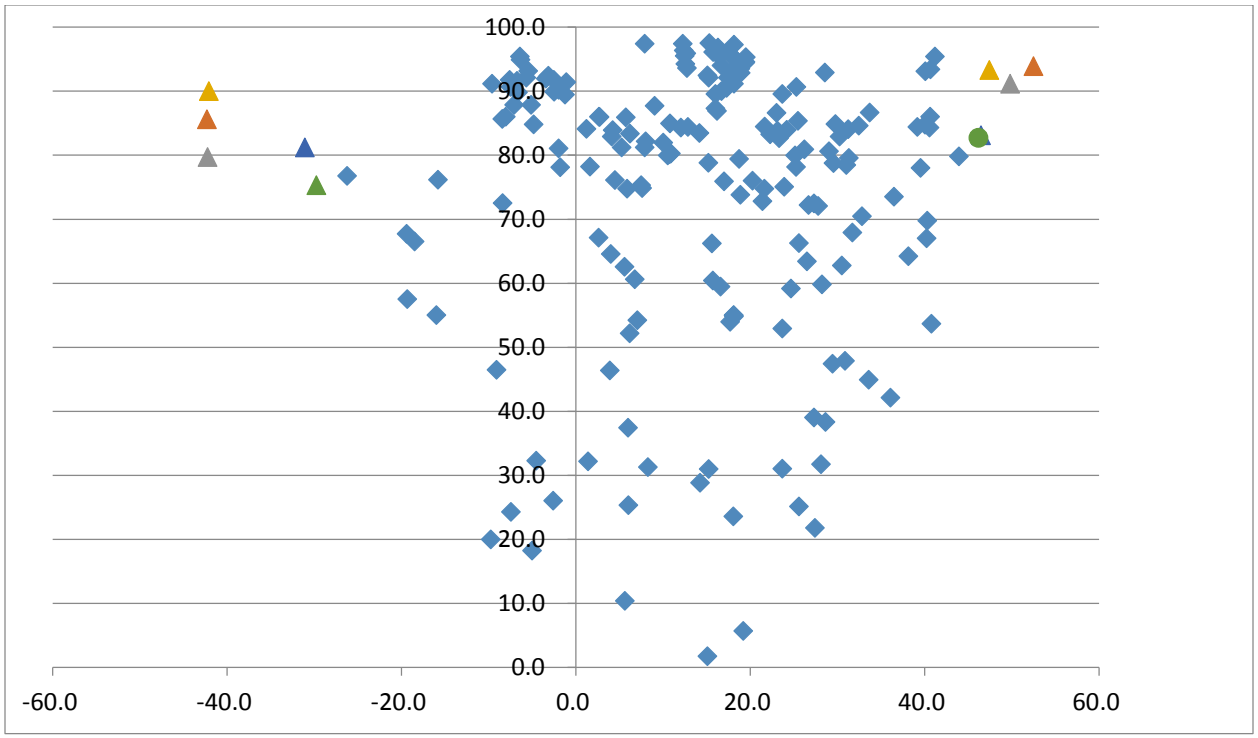


**Figure 13 (X axis: yield difference between *ortho*- and *meta*- product (*ortho* minus *meta*). Y axis: percent ee of the more abundant alcohol product).** Positive or negative numbers indicates a particular SAL catalyst gave higher yield for *ortho*- or meta- product, respectively. Colored data points reflect ligands systems were selected for further study.

The (TADDOL)SAL and (pTADDOL)SAL catalysts which exhibit the largest yield difference between *ortho*- and *meta*- methoxy styrene are summarized in Figure 14. S13TAR15TA was identified as a catalyst that would be expected to react much readily with *ortho*-methoxy styrene than *meta*- or *para*- methoxy styrene; S3pTAR7pTA was identified as a catalyst that is expected to react much readily with *meta*- methoxy styrene than *ortho*- or *para*- methoxy styrene. The yield difference observed with

S13TAR15TA and S3pTAR7pTA are 50 % and 30%, respectively. These two catalysts were examined in greater detail as described below.

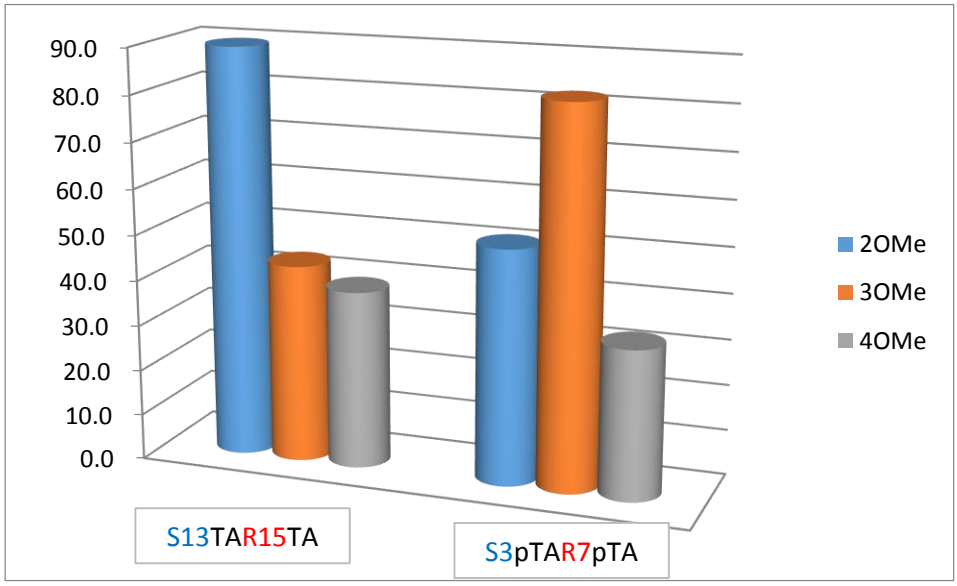


**Figure 14.** Significant yield differences are observed with two SAL catalysts for *ortho*- and *meta*- methoxy styrenes.

**2.7 Site selective hydroboration – Site selectivity trend towards other styrene derivatives**

Having focused in the previous sections on the series of methoxy-substituted substrates, I turned my attention to other substituted styrenes to learn whether similar tends prevailed and whether I might gain additional insight into the basis for the change in relative reactivity. Figure 15A–D plot data for methyl-, fluoro-, chloro- and trifluoromethyl-substituted styrenes in the manner used for Figure 11. Unlike the results discussed in Figure 11, I do not see significant differences between the isomeric substrates that are as pronounced; the data in Figure 15A-D show that the overall yield ranges are more nearly comparable for each set of isomeric substrates. Functional groups other than methoxy tend to impart lower differences in the relative reactivity of the isomeric substrates. The data used to construct the graphs in Figure 15A-D are obtained from (TADDOL)SAL-derived catalysts. Analysis of data obtained with catalysts prepared with other TADDOL derivatives led to the same conclusion (data not shown here).

A) Methyl Styrene Data

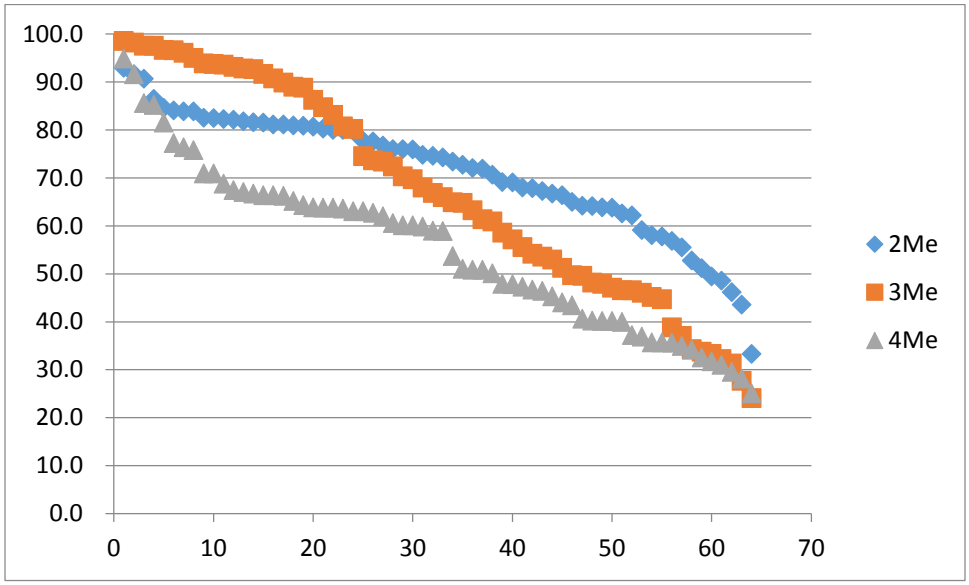


B) Fluoro styrene Data

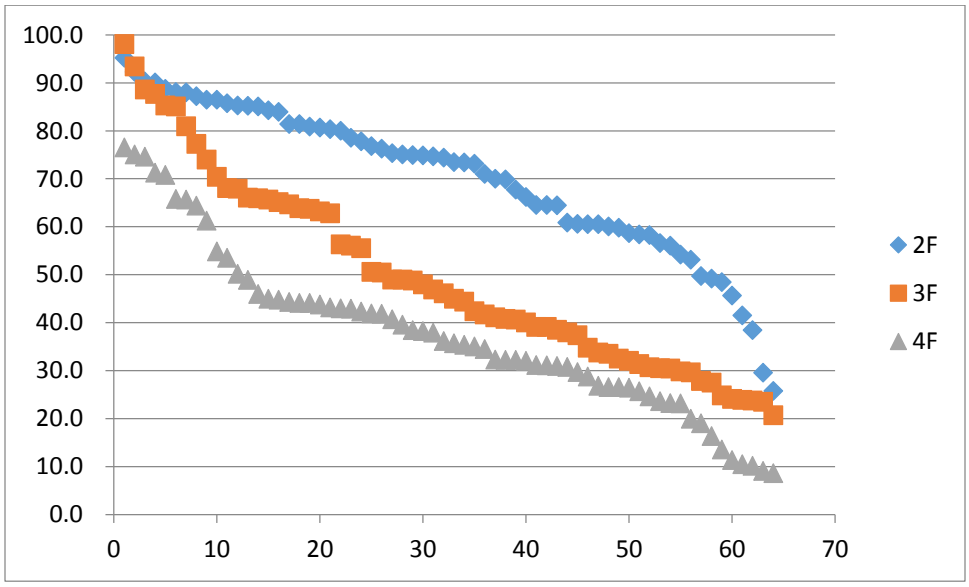

C) Chloro styrene Data

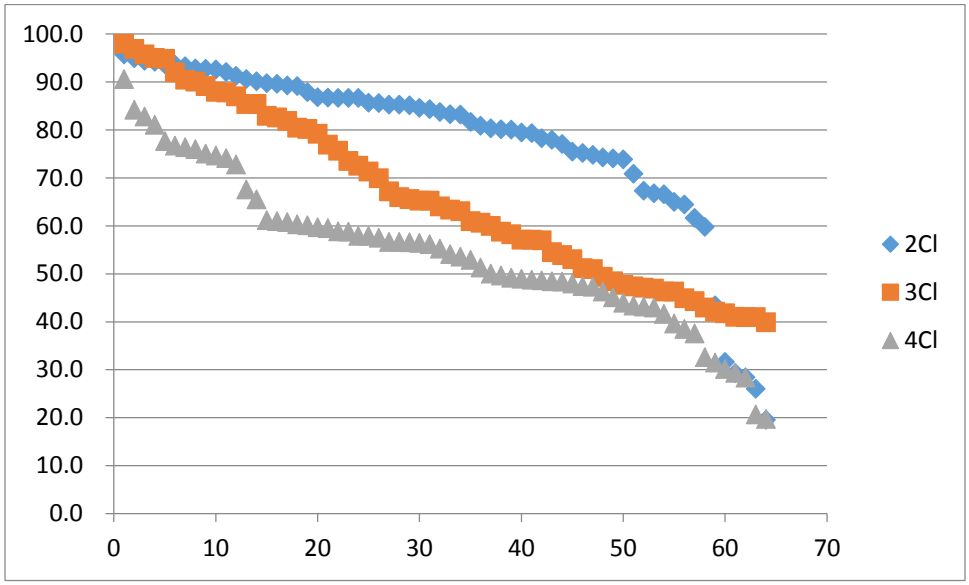


D) Trifluoromethyl Styrene Data

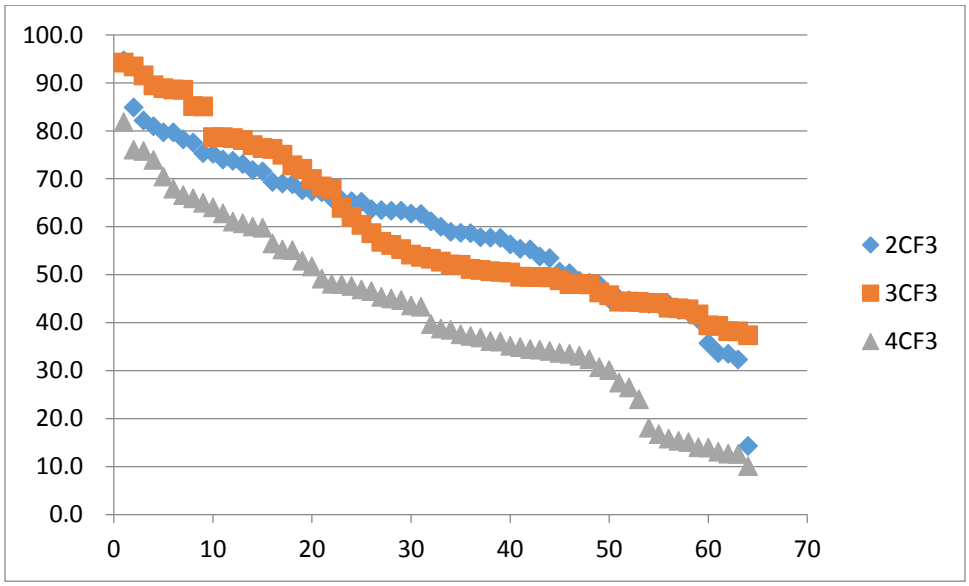


**Figure 15.** Yields for SAL-catalyzed hydroboration of sets of *o*-, m- and *p*-substituted styrenes. Yield data for a given set of isomers (e.g., methyl-substituted styrenes) are independently sorted from the highest to lowest and three graphs are plotted on the same sheet. (TADDOL)SAL-derived catalysts. This shows the variations of yields differ

considerably from substrate to substrate. X axis: SAL catalyst. Y axis: yields. A) Me substituted styrenes. B) F substituted styrenes. C) Cl substituted styrenes. D) $CF_3$ substituted styrenes.

The data from Figure 15A-D were plotted for each series of isomeric styrene derivatives as in Figure 12A sorting the data according to (TADDOL)SAL-derived catalysts and in ranked order from the highest to the lowest yield of the *ortho*-substituted styrene. Each catalyst is represented at a unique position on the X axis, with three yield data points (*ortho*-, *meta*-, and *para*-isomers) plotted on the Y axis. I was looking for wide separation (on the order of 30-50% difference) among the two of the three yields indicating another (TADDOL)SAL-derived catalyst that exhibits significant substrate discrimination. Many among the (TADDOL)SAL-derived catalysts show significant differences between the *para*-substituted (almost always more sluggish) and *ortho*- or *meta*-substituted, few differences, as striking as those uncovered for the methoxy-substituted styrenes discussed above, were found between *ortho*- and *meta*-isomers.

A) Methyl Styrene data

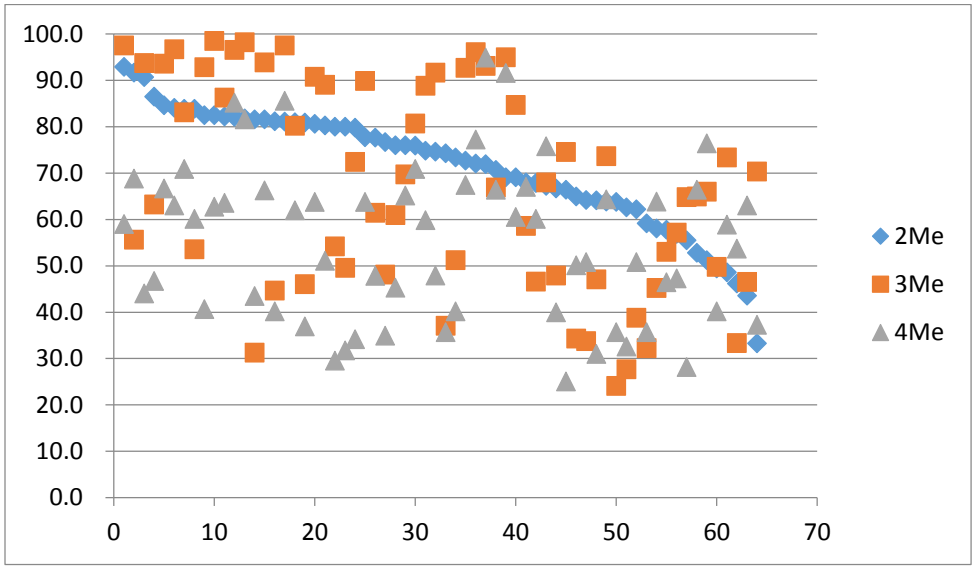


B) Fluoro Styrene data

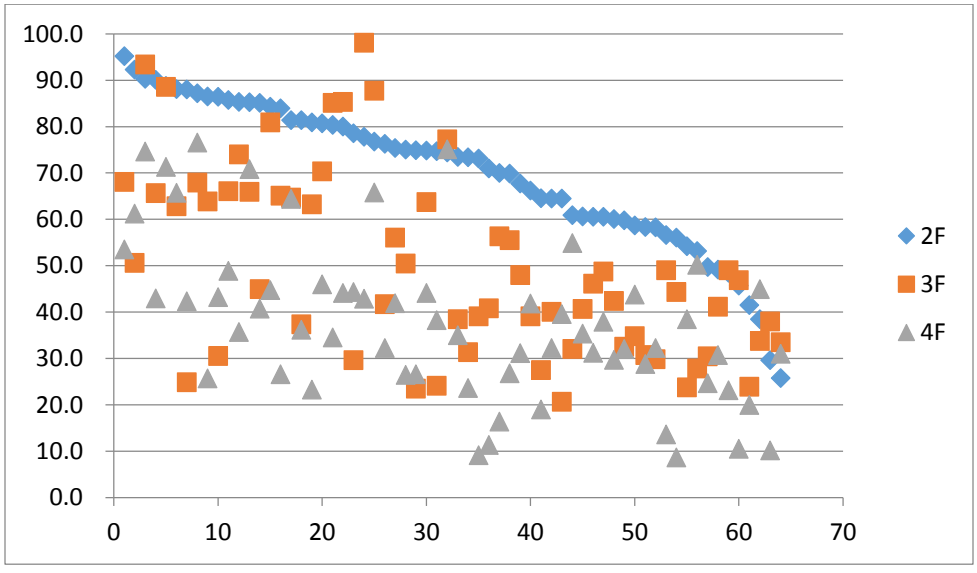

C) Chloro Styrene data

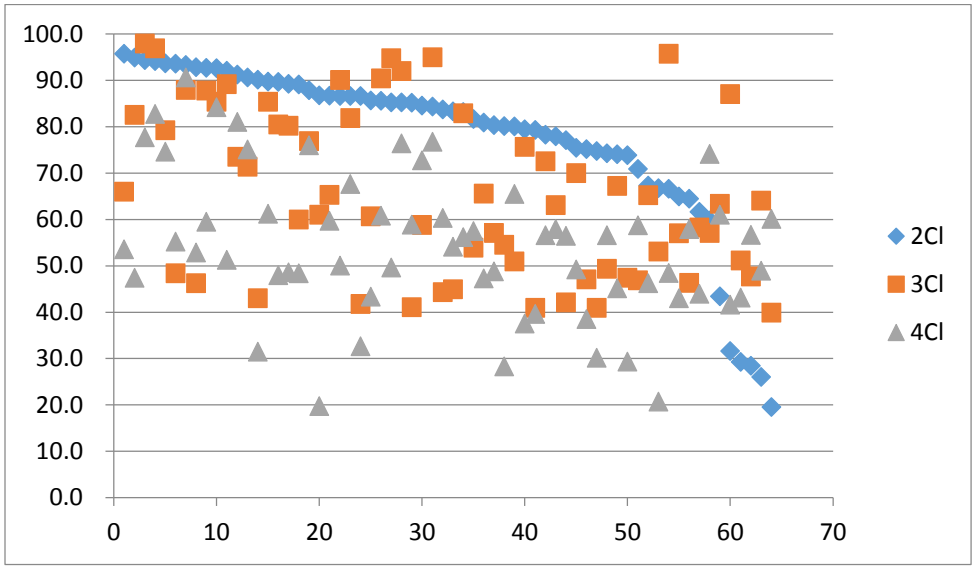


D) Trifluoromethyl Styrene data

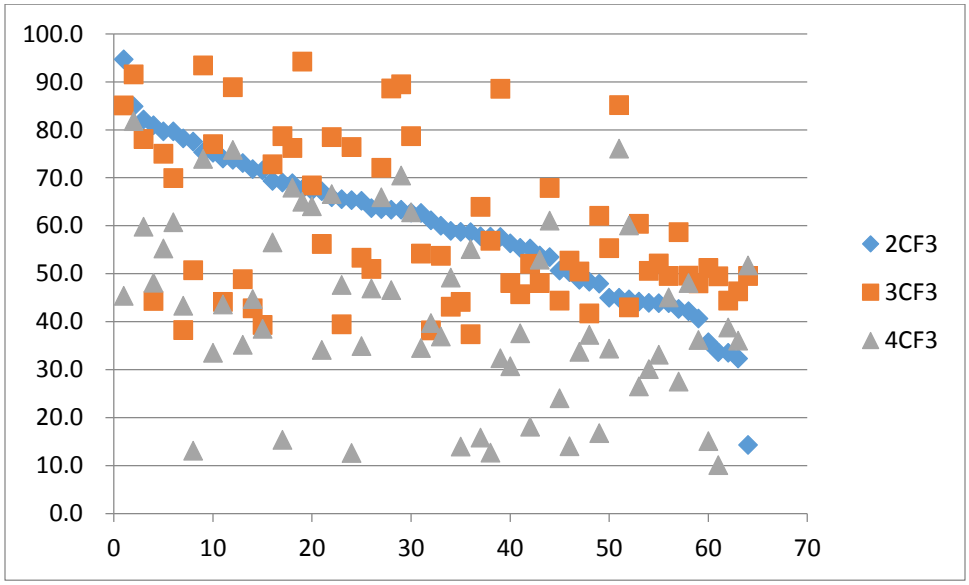


**Figure 16.** Comparison of yields within an isomeric set of styrenes. Data are sorted by individual SAL catalysts and organized from the highest to lowest yields of ortho-substituted styrenes. X axis: SAL catalyst. Y axis: yields. A) Me substituted styrenes. B) F substituted styrenes. C) Cl substituted styrenes. D) $CF_3$ substituted styrenes.

**2.8 Site selective hydroboration – finding *para*- selective SAL catalysts**

Having identified *ortho*- and *meta*- selective SAL catalysts for methoxy-substituted styrenes, I asked whether a *para*-selective catalyst be identified as well. As indicated above, finding catalysts selective for *ortho*- or *meta*-isomers over the *para*-isomer proved relatively easy. However, identifying a *para*-selective catalyst proved more difficult. This is perhaps not surprising. Figure 11 (OMe) and 15A-D (Me, F, Cl, and $CF_3$) all show that yields for *para*- substituted styrenes are almost always lower than those obtained for *ortho*- and *meta*-substituted styrenes. In another words, *para*-substituted styrenes are inherently less reactive with this catalyst system. Among all the SAL-derived catalyst combinations screened, only one catalyst showed good potential *para*-isomer selectivity. Figure 17 shows that the S13pTAR15pTA catalyst displays as high as 48 % higher yield for the *para*-methyl substituted styrene than for the other two isomers. Excepting the trifluoromethyl-substituted styrenes, the other three styrene derivatives (i.e., MeO-, Cl-, F-) also showed promising levels of substrate discrimination favoring the *para*-isomer.

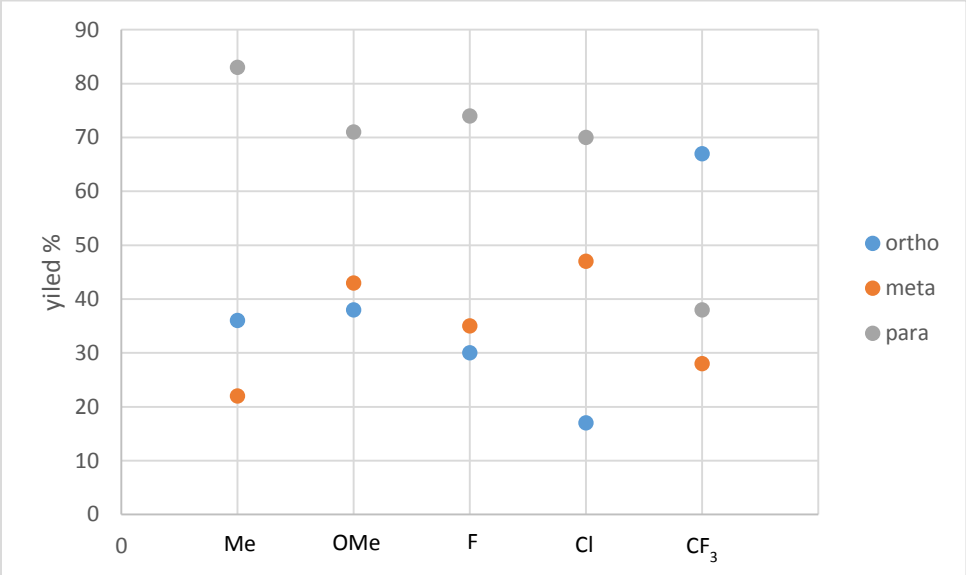


**Figure 17.** Data analysis revealed that S13pTAR15pTA SAL catalyst shows higher yields for *para*-substituted styrenes, except for the $CF_3$-substituted styrenes.

## 2.9 Site selective hydroboration – potential *ortho-*, *meta-*, and *para-* selective SAL catalyst structures

It is worth mentioning again that the data obtained by Dr. Moteki and used in the analyses described above were obtained from screening of mixtures of substrates in the presence of excess pinBH. Our next objective was to explore conditions under which substrates directly competed for a limiting amount of pinBH. The structures of the three SAL-derived catalysts identified above (i.e., *ortho-*, *meta-*, and *para*-selective catalysts S13TAR15TA, S3pTAR7pTA, and S13pTAR15pTA, respectively) are shown in Figure 18. It is interesting to note that *para-* selective catalyst S13pTAR15pTA has the same combination of scaffold-building tethers the *ortho*-selective catalyst S13TAR15TA. The only difference between the two is in the aryl-substituents on the TADDOL backbone, 4-methylphenyl versus phenyl, respectively.

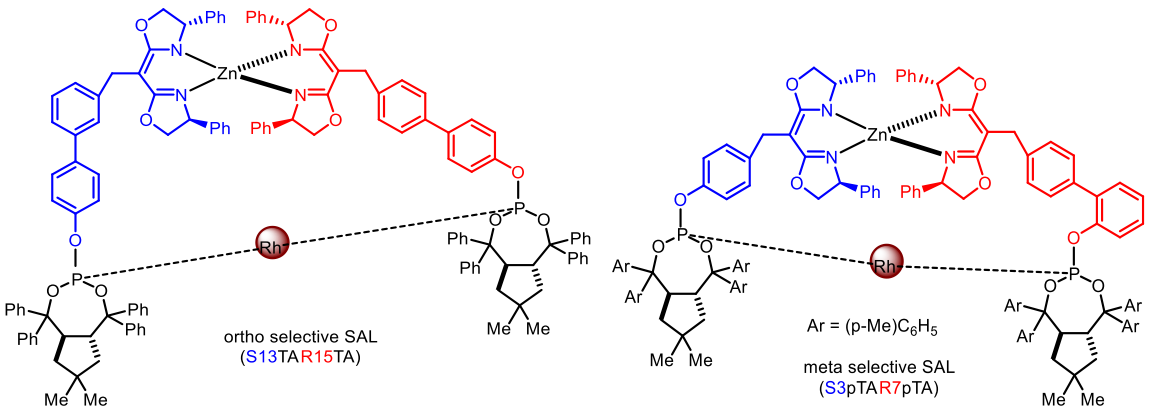

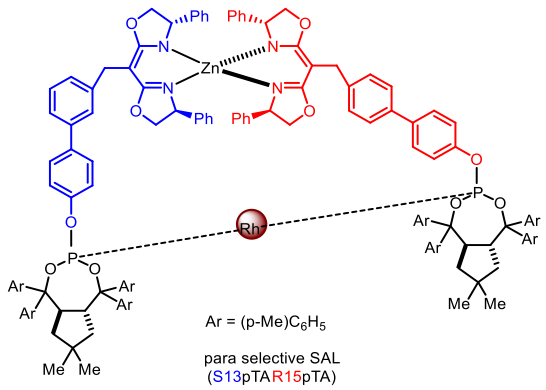


**Figure 18.** SAL catalyst structures for *ortho*-, *meta*-, and *para*-isomer selective catalysts.

**2.10 Site selective hydroboration –competition studies involving *ortho*- and *meta*-substituted substrates**

With potential substrate selective SAL catalysts identified, a series of direct substrate competition experiments were carried out. The S13TAR15TA-catalyzed CAHB of 1:1 mixtures of *ortho*- and *meta*-fluorostyrene with various amounts of pinBH was used to assess how the selectivity varied as a function conversion (Figure 19). At the limit of 1.0 equivalent of pinBH (relative to the total moles of styrenes available), both substrates reacted to give equal amounts of hydroboration products. As can be expected from a direct competition experiment, the highest level of substrate selectivity was observed at very low conversion, in this case, when the amount of pinBH was limited to 0.1 equivalents. For practical reasons, it was decided to use 0.5 equivalents of pinBH as the standard condition for our subsequent studies.

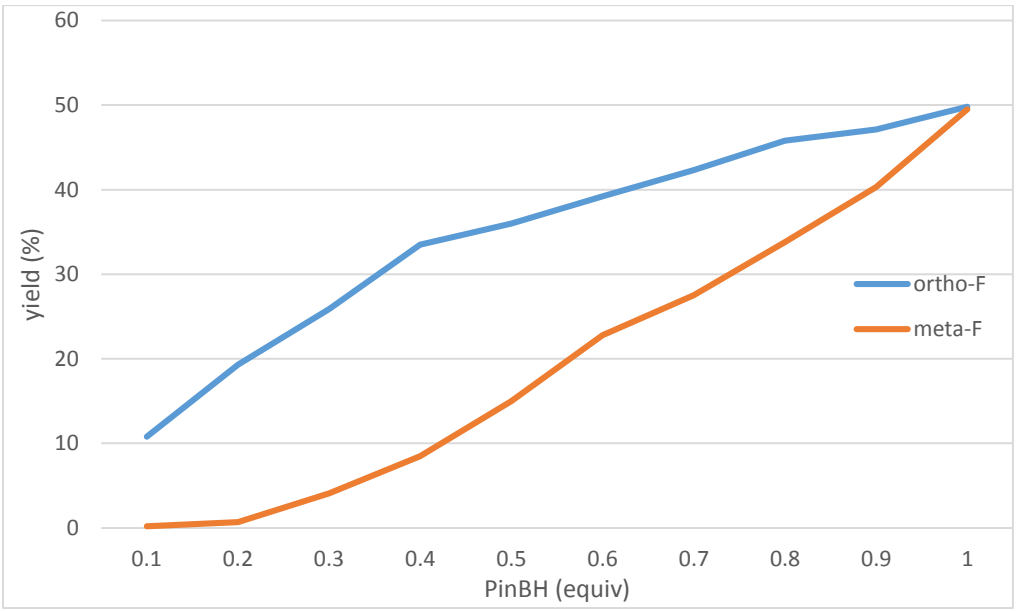

**Figure 19.** Effect of PinBH stoichiometry on substrate selectivity. The substrates used here are *ortho*-F and *meta*- F styrenes.

In order to properly evaluate the effect of SAL scaffold on substrate selectivity, TADDOL- and pTADDOL-derived phenyl monophosphites (2:1 monophosphite:Rh) were used as a control/reference point. In essence these chiral phenyl monophosphites are equivalent to the SAL-ligating groups minus the SAL scaffold. Note that the *ortho*-selective SAL catalyst (i.e., S13TAR15TA) contains the parent TADDOL-derived ligating group while the *meta*-selective SAL catalyst (i.e., S3pTAR7pTA) contains the pTADDOL-derived ligating group. It is therefore important to individually evaluate the influence of both TADDOL- and pTADDOL-derived phenyl monophosphites (2:1 monophosphite:Rh) to assess the inherent substrate selectivity imparted by the ligating groups without the SAL scaffold. The results tabulated in Figure 20 show that the ratio of the isomeric *ortho*- and *meta*-products obtained using 0.5 equivalents of pinBH is essentially 1:1 for all substituents. The exception is for *ortho*- and *meta*-phenoxy substituted styrenes, where both monophosphite ligands exhibit a modest preference for reaction of the *meta*-isomer (*ortho*:*meta* ca 1:1.5). The reasons for including the phenoxy styrenes in the study will become apparent (*vide infra*) Overall, we interpret the results as demonstrating that the ligating groups themselves, while an important component of the SAL-derived catalyst, are not the principal factor favoring selective reaction of one substrate.

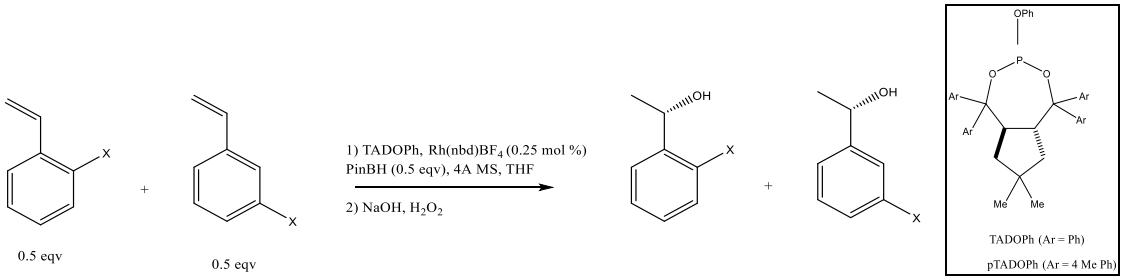


| (TADDOL)POPh | | | |
|---|---|---|---|
| | Yield (%) | | |
| X | *ortho* | *meta* | Ratio |
| F | 25.1 | 24.7 | 1 : 1 |
| Cl | 26.1 | 23 | 1.1 : 1 |
| OMe | 23.8 | 23.1 | 1 : 1 |
| Me | 24.3 | 24.7 | 1 : 1 |
| $CF_3$ | 23.1 | 24.1 | 1 : 1 |
| OPh | 19.9 | 30.1 | 1 : 1.5 |

| (pTADDOL)POPh | | | |
|---|---|---|---|
| | Yield (%) | | |
| X | *ortho* | *meta* | Ratio |
| F | 23.1 | 23.4 | 1 : 1 |
| Cl | 23.6 | 24.6 | 1 : 1 |
| OMe | 22.4 | 24.8 | 1 : 1.1 |
| Me | 24.5 | 23.6 | 1 : 1 |
| $CF_3$ | 24.9 | 24 | 1 : 1 |
| OPh | 18.2 | 31.8 | 1 : 1.7 |

**Figure 20.** Effect of TADDOL-derived chiral monophosphite ligands in a series of 1:1 direct competition experiments.

We next carried out the same set of competition experiments using the SAL-derived supramolecular catalysts S13TAR15TA and S3pTAR7pTA. As tabulated in Figure 21, the *ortho*-selective S13TAR15TA showed for each substrate a moderate but significant preference for turnover of the *ortho*-substituted styrene. The *ortho*/*meta* ratio of products was as high as 5.6 : 1 in the case of competing chlorostyrenes; recall the monophosphite ligand ((TADDOL)POPh gave a 1 : 1 ratio (see Figure 20). We conclude that the observed difference in selectivity is the consequence of the three-dimensional structure of the SAL-derived supramolecular catalyst. It is important to

note that while the substrate selectivity reported above is relatively modest, those results are under conditions in which 0.5 equivalents of pinBH are used and consumed. The observed selectivity at short reaction times can be much higher. For example, using 0.1 equivalent of pinBH, *ortho*/*meta* selectivity as high as 49 : 1 is observed for the mixture of fluorostyrenes.

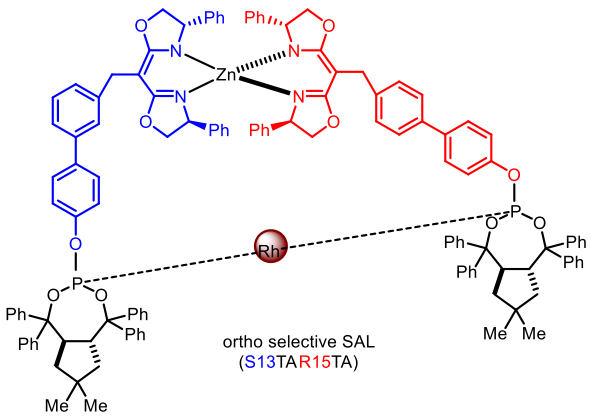


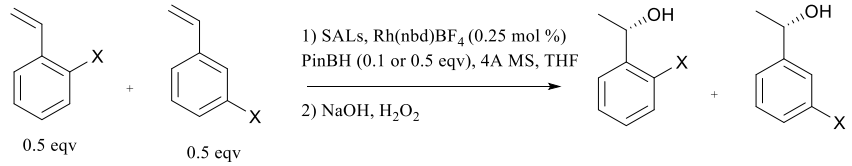


| ortho selective SAL S13TAR15TA | | | |
|---|---|---|---|
| 0.5 eq pinBH | Yield (%) | | |
| X | *ortho* | *meta* | ratio |
| F | 36 | 15 | 2.4:1 |
| Cl | 42.5 | 7.5 | 5.6:1 |
| OMe | 37.6 | 12.4 | 3.0:1 |
| Me | 22.6 | 18.4 | 1.2:1 |
| $CF_3$ | 39.4 | 12.6 | 3.1:1 |
| OPh | 34.2 | 14.7 | 2.3 : 1 |

| ortho selective SAL S13TAR15TA | | | |
|---|---|---|---|
| 0.1 eq pinBH | Yield (%) | | |
| X | *ortho* | *meta* | ratio |
| F | 9.8 | 0.2 | 49 : 1 |
| Cl | 9.7 | 0.3 | 32 : 1 |
| OMe | 9.7 | 0.3 | 32 : 1 |
| Me | 7.9 | 0.9 | 8.8 : 1 |
| $CF_3$ | 9.5 | 0.5 | 19 : 1 |
| OPh | 8.7 | 1.1 | 7.9 : 1 |

**Figure 21.** *Ortho* selective SAL S13TAR15TA showed significant substrate selectivity.

Data for the corresponding competition experiments carried out with the *meta*-selective catalyst S3pTAR7pTA are tabulated in Figure 22. Once again, recall that the monophosphite (pTADDOL)POPh exhibited no inherent reactivity preference between

*ortho*- and *meta*-substituted substrates. Nevertheless, excepting methystyrene derivatives for which the *ortho*- and *meta*-isomers are consumed at comparable rates, S3pTAR7pTA is otherwise indeed *meta*-selective. The highest substrate selectivity was observed with $CF_3$-substituted styrenes giving *ortho*-:*meta*-products in a 1 : 3.3 ratio. The lack of selectivity among the methylstyrenes may be related to their relatively slow reaction compared to other substituted styrene series that were used for this study. Qualitatively, we find that when the hydroboration reaction is slow, there tends to be little or no reactivity difference between isomers.

From the two studies discussed above we conclude that the specific combination of scaffold building tethers and ligating groups that are self-assembled by the chiral discrimination between (*R*, *R*)- and (*S*, *S*)-box derivatives creates a unique supramolecular catalyst with a unique binding pocket that can be used to discriminate between closely related substrates differing in structure relatively remote to the site of reaction. In short, closely related catalysts derived from the same family can control reactivity between very similar substrates by just changing supramolecular scaffold structure. Other than the use of chiral catalysts for enantio- and diastereoselective kinetic resolution,[102] which we argue although conceptually related is distinct in that it involves differentiation between substrates that differ at the site of reaction, there are few examples in the literature of this kind of catalyst-directed substrate selectivity (*vide infra*).

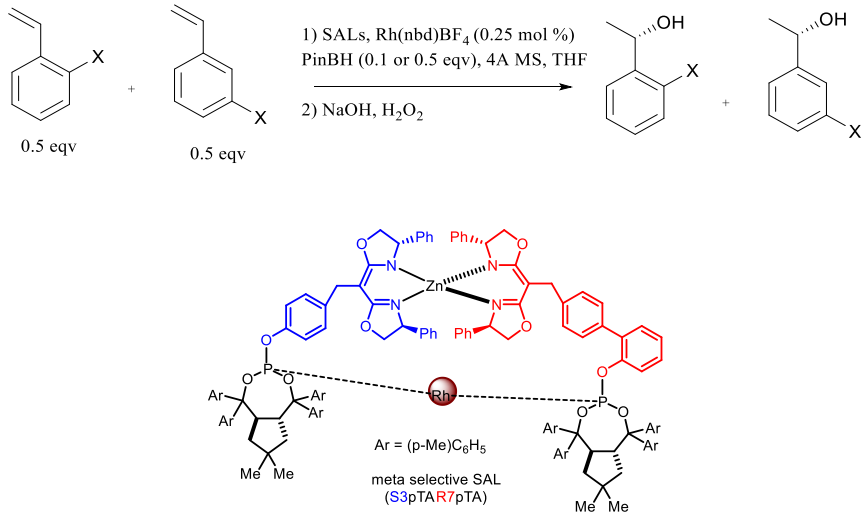


| *meta* selective SAL S3pTAR7pTA | | | |
|---|---|---|---|
| 0.5 eq pinBH | Yield (%) | | |
| X | *ortho* | *meta* | ratio |
| F | 20.6 | 31.4 | 1 : 1.5 |
| Cl | 12.8 | 38.3 | 1 : 3.0 |
| OMe | 14.1 | 35.9 | 1 : 2.5 |
| Me | 25 | 25 | 1 : 1 |
| $CF_3$ | 11.5 | 38.5 | 1 : 3.3 |
| OPh | 15.2 | 34.8 | 1 : 2.3 |

| *meta* selective SAL S3pTAR7pTA | | | |
|---|---|---|---|
| 0.1 eq pinBH | Yield (%) | | |
| X | *ortho* | *meta* | ratio |
| F | 0.3 | 9.7 | 1 : 32 |
| Cl | 0.3 | 9.7 | 1 : 32 |
| OMe | 0.3 | 9.6 | 1 : 32 |
| Me | 1.3 | 8.7 | 1 : 6.7 |
| $CF_3$ | 0.3 | 9.7 | 1 : 32 |
| OPh | 1.2 | 8.7 | 1 : 7.3 |

**Figure 22.** *Meta*-selective SAL S3pTAR7pTA showed significant substrate dependence.

**2.11 Site selective hydroboration – multi substrates competition study (*ortho*- and *para*- or *meta*- and *para*- substituted substrates)**

*para*-Substituted substrates tend to react the slowest under the hydroboration conditions. Therefore, the likelihood of finding a *para*-substrate selective SAL-derived catalyst seemed rather remote. Nonetheless, one SAL catalyst (S13pTAR15pTA) was identified via the analysis described above as having greater reactivity with *para* substituted substrates. Following the protocol described above, I first wanted to understand the inherent CAHB reactivity of the different isomers using only the monophosphite ligands (TADDOL)POPh and (pTADDOL)POPh. Two series of substrate competition experiments were carried out – completion between *ortho*- and *para*-substituted substrates and between *meta*- and *para*-substituted substrates. The reaction conditions used were identical to the previously established standard conditions.

The data tabulated in Figure 23 shows that the inherent reactivity of the *ortho*-isomer is always somewhat greater than that of the *para*-substituted isomer under the hydroboration conditions used. In addition, (TADDOL)POPh tends to prefer the *ortho*-isomer to a greater extent than (pTADDOL)POPh; this agrees with previous results shown in Figure 20. The key finding is that the *para*-substituted product was formed in lower yield than the *ortho*-substituted product based on ligating group alone.

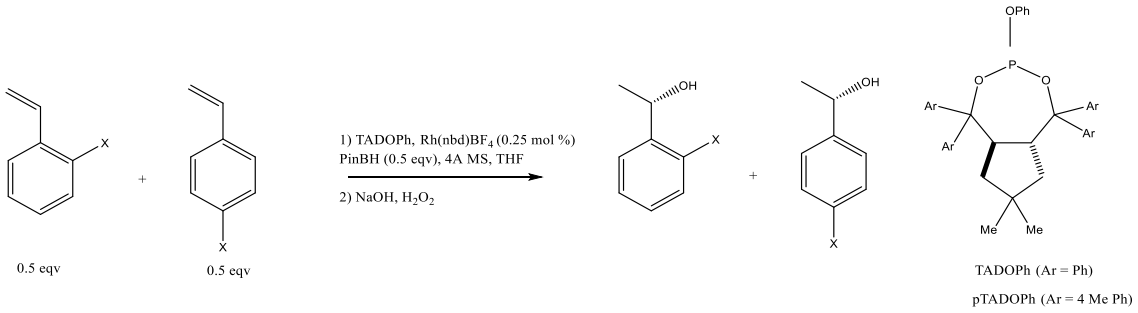


| (TADDOL)POPh | | | |
|---|---|---|---|
| | Yield (%) | | |
| X | *ortho* | *para* | ratio |
| F | 33.2 | 15.3 | 2.2 : 1 |
| Cl | 32 | 17.4 | 1.8 : 1 |
| OMe | 31.8 | 15.4 | 2.1 : 1 |
| Me | 29.8 | 18.7 | 1.6 : 1 |
| $CF_3$ | 32.7 | 16.1 | 2.0 : 1 |
| OPh | 34.2 | 12.8 | 2.7 : 1 |

| (pTADDOL)POPh | | | |
|---|---|---|---|
| | Yield (%) | | |
| X | *ortho* | *para* | ratio |
| F | 30.1 | 17.3 | 1.7 : 1 |
| Cl | 27.6 | 20.5 | 1.3 : 1 |
| OMe | 28 | 20.4 | 1.4 : 1 |
| Me | 26.3 | 22.2 | 1.2 : 1 |
| $CF_3$ | 27.4 | 21.9 | 1.3 : 1 |
| OPh | 26.4 | 18.7 | 1.4 : 1 |

**Figure 23.** TADDOL based monomer ligand screening with multi substrates (*ortho* vs *para*).

Figure 24 compares the reactivity of *meta*- and *para*-substituted substrates with chiral monophosphites (TADDOL)POPh and (pTADDOL)POPh. Once again, the *para*-substituted substrates always exhibited lower reactivity under the condition employed. The results lead to two related questions: will the *ortho*- and *meta*-selective SAL-derived catalysts promote selective reaction of those isomers over the *para*-isomer; and will the

*para*-selective SAL-derived catalyst S13pTAR15pTA indeed selective for the *para*-isomer?

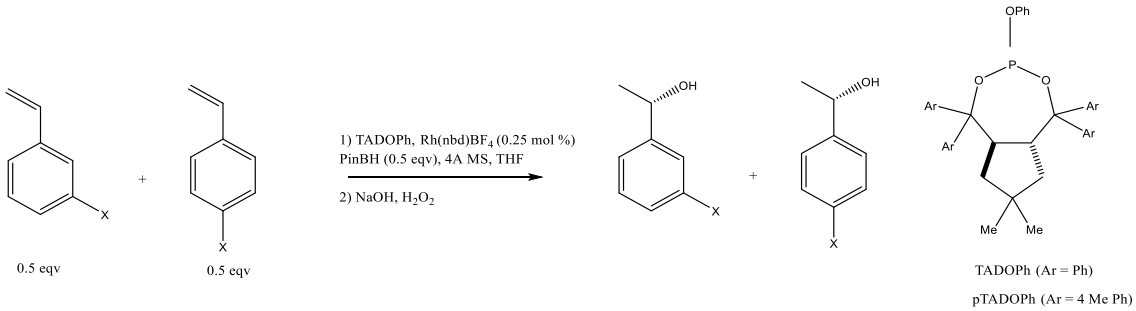


| (TADDOL)OPh | | | |
|---|---|---|---|
| | Yield (%) | | |
| X | *meta* | *para* | ratio |
| F | 26.3 | 19.6 | 1.3 : 1 |
| Cl | 27 | 20.1 | 1.3 : 1 |
| OMe | 27.5 | 17.9 | 1.5 : 1 |
| Me | 27.6 | 18.5 | 1.5 : 1 |
| $CF_3$ | 30.1 | 17.9 | 1.7 : 1 |

| (pTADDOL)OPh | | | |
|---|---|---|---|
| | Yield (%) | | |
| X | *meta* | *para* | ratio |
| F | 27.3 | 20.2 | 1.4 : 1 |
| Cl | 28.9 | 20.1 | 1.4 : 1 |
| OMe | 30.3 | 16 | 1.9 : 1 |
| Me | 27.7 | 20 | 1.4 : 1 |
| $CF_3$ | 31.5 | 17.7 | 1.8 : 1 |

**Figure 24.** TADDOL based monomer ligand screening with multi substrates (*meta* vs *para*).

Figure 25A illustrates competition reactions between equimolar amounts of *ortho*- and *para*-substituted substrates in the presence of the *ortho* selective catalyst S13TAR15TA or the *para*-selective catalyst S15pTAR13pTA. Selectivity for *ortho*- over *para*-substituted substrates in the presence of the ortho-selective catalyst was generally higher than that previously found for *ortho* over *meta* with the same catalyst. For example, the *ortho*/*para* selectivity ratio was as high as 6.3 : 1 for the isomeric

chlorostyrenes. This trend can be seen for other substituent groups as well. In contrast, the *para*-selective catalyst S15pTAR13pTA afforded little selectivity between *ortho*/*para* isomers. However, the nearly equal conversion of the two isomers suggests that the SAL catalyst clearly eliminates modest but inherent *ortho*-isomer preference imposed by the ligating group. For example, the 1.7 : 1 *ortho*/*para* preference exhibited by (pTADDOL)POPh is reduced to 1.1 : 1 *ortho*/*para* with S15pTAR13pTA. This is at least suggestive of an important role for the catalyst scaffold, although its effect does not reverse the substrate reactivity toward the para-isomer.

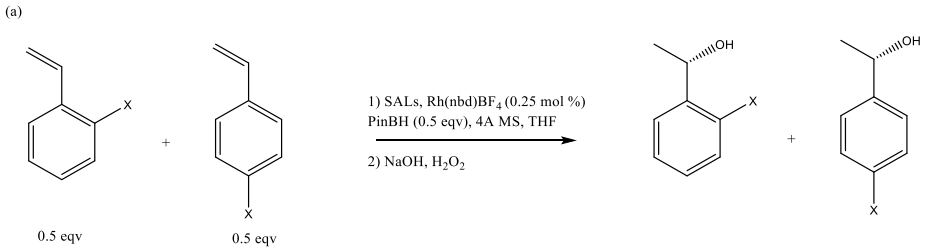


| *ortho* selective SAL | | | |
|---|---|---|---|
| | Yield (%) | | |
| X | *ortho* | *para* | ratio |
| F | 42.1 | 7.6 | 5.5: 1 |
| Cl | 43 | 6.8 | 6.3 : 1 |
| OMe | 40.1 | 9.4 | 4.3 : 1 |
| Me | 37.6 | 11.1 | 3.4 : 1 |
| $CF_3$ | 40.1 | 9.2 | 4.4 : 1 |
| OPh | 34.2 | 12.8 | 2.7 : 1 |

| *para* selective SAL S15pTAR13pTA | | | |
|---|---|---|---|
| | Yield (%) | | |
| X | *ortho* | *para* | ratio |
| F | 24.3 | 22.1 | 1.1 : 1 |
| Cl | 23.1 | 20.9 | 1.1 : 1 |
| OMe | 25.3 | 21 | 1.2 : 1 |
| Me | 24.7 | 23.8 | 1 : 1 |
| $CF_3$ | 26.9 | 21.1 | 1.3 : 1 |
| OPh | 25.3 | 23.3 | 1.1 : 1 |

(b)

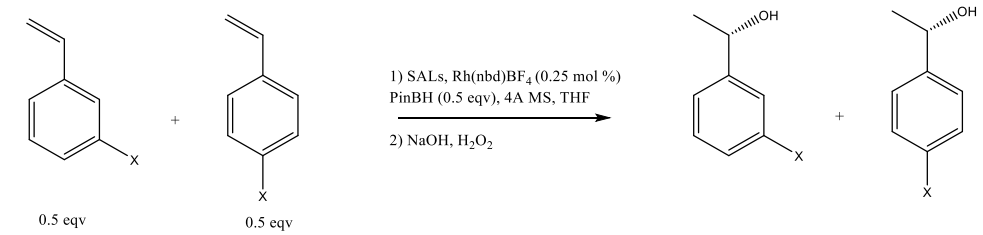


| *meta* selective SAL S3pTAR7pTA | | | |
|---|---|---|---|
| | Yield (%) | | |
| X | *meta* | *para* | ratio |
| F | 37.6 | 11.1 | 3.4 : 1 |
| Cl | 38.8 | 10.4 | 3.7 : 1 |
| OMe | 35.9 | 12.2 | 2.9 : 1 |
| Me | 34.7 | 14.6 | 2.4 : 1 |
| $CF_3$ | 38.8 | 10.9 | 3.6 : 1 |
| OPh | 34.5 | 11.7 | 2.9 : 1 |

| *para* selective SAL S15pTAR13pTA | | | |
|---|---|---|---|
| | Yield (%) | | |
| X | *meta* | *para* | ratio |
| F | 26 | 21.3 | 1.2 : 1 |
| Cl | 23.3 | 22.4 | 1 : 1 |
| OMe | 24.1 | 21.8 | 1.1 : 1 |
| Me | 23.3 | 22.2 | 1 : 1 |
| $CF_3$ | 26.9 | 22.4 | 1.2 : 1 |
| OPh | 24.3 | 24 | 1 : 1 |

**Figure 25.** (a) Competition reaction with *ortho* and *para* substituted substrates. (b) Competition reaction with *meta* and *para* substituted substrates.

Competition reactions between the isomeric *meta*- and *para*-substituted substrates tabulated in Figure 25B lead to similar conclusions to those discussed above. Without the SAL-derived catalyst scaffold, (pTADDOL)POPh showed substrate selectivity as high as 1.9 : 1 favoring *meta*- over *para*-methoxystyrene. Using the *meta*-selective S3pTAR7pTA catalyst, the ratio increased to as high as 3.7 : 1 favoring *meta*- over *para*-chlorostyrene. The *para*-selective S15pTAR13pTA again gave only near equal amounts of *meta*- and *para*-substituted products. Thus, while SAL (S15pTAR13pTA) did enhance reactivity for *para* substituted substrates, it did not prove possible to identify a SAL-

derived supramolecular catalyst the favored net reaction of the *para*-isomer over the *ortho* or *meta*.

**2.12 Site selective reaction background – literature**

There are many selectivity issues when it comes to chemical reactions: one may need to control regioselectivity, but also stereoselectivity, chemoselectivity and mode selectivity.[103] The majority of literature focuses on control of regioselectivity, stereoselectivity, and chemoselectivity. However, the concept of site selectivity was introduced by Miller's group[104] a decade ago. Their peptide-based catalysts were used to site selectively react one functional groups over another similar one in the same molecule without the need for protection/deprotection schemes. The development of efficient site selective chemistries can be especially useful in the field of medicinal chemistry. Most therapeutics for the treatment of diseases are derived from natural products and their derivatives[105]. In addition, many of the antibiotics which are in clinical applications also have been derived from natural products[106]. It is reported that synthetic endeavors to modify natural products can be a challenging task due to their structural complexity and the presence of a large array of potentially reactive functional groups[107]. Developing the ability to modify a desired site(s) in presence of other reactive moieties based on reagent- or catalyst-control is highly desirable and potentially transformative in this field. Therefore, in recent years, catalyst-controlled modification of complex drug molecules has gained great interest[108]. Two of the most prominent players in this field are Miller and coworkers, who use peptide based organocatalysts for site selective functionalization (e.g., acylation) of complex molecules and White and coworkers, who have identified metal complex capable of site selective C-H activation.

In 2001, Miller reported a peptide-based catalyst that effected the site selective phospholylation of a simple triol substrate[109]. His peptide catalyst included histidine as reactive site and employed specific hydrogen bonding motifs and interactions between peptide catalyst and the substrate to orient functionalities in a way to facilitate a particular chemical reaction. The construction of a library of potential peptide catalysts enhances the probability that one or more peptide combinations would result unique sets of secondary interactions between substrate and catalyst leading to facile reaction with differing site-selectivity. The first work was successful in identifying a peptide catalyst which was able to promote selective monophosphorylation of a triol. (Figure. 26A). Later, in 2004 Miller identified two different peptide catalysts that reacted preferentially at other different sites of the triol in good yield (56-65%) [110]. With this discoveries three different peptide catalysts identified can be used to site-selectively monophosphorylate one site at a time, which allowed them to easily access to optically pure PI3P (a product of phosphoinositide-3-kinase which is an important element in the biochemistry of cell cycle progression) and *ent*-PI3P with both saturated and unsaturated side chains[110].

In 2006, the Miller group reported a catalyst-controlled site selective acylation of erythromycin A (Figure 26 B). Erythromycin A is a well-known antibiotic compound and its modification is of interest to medicinal and synthetic chemists[111]. Erythromycin A has 5 hydroxyl groups and consequently selectively modification of only one hydroxyl is a challenging problem. For example, *N*-methylimidazole (NMI) catalyzed the selective acylation of erythromycin A to give a 4:1 mixture of **4Ac** to **11Ac** in less than 30% total

yield (Figure 26) [112]. Miller's library of peptides used in this study contained the NMI moiety. Through combinatorial screening one peptide was identified as a site selective catalyst giving 1:5 mixture of **4Ac** and **11Ac**. Overall, Miller achieved the goal of site selectively reacting one site over the others with catalysts controlled fashion. However, it is surprising that the actual yield obtained with peptide catalyst was not found in either the manuscript or the supporting information.

(A)

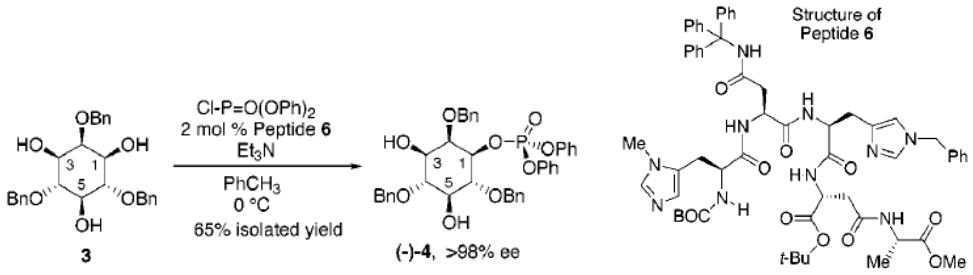


(B)

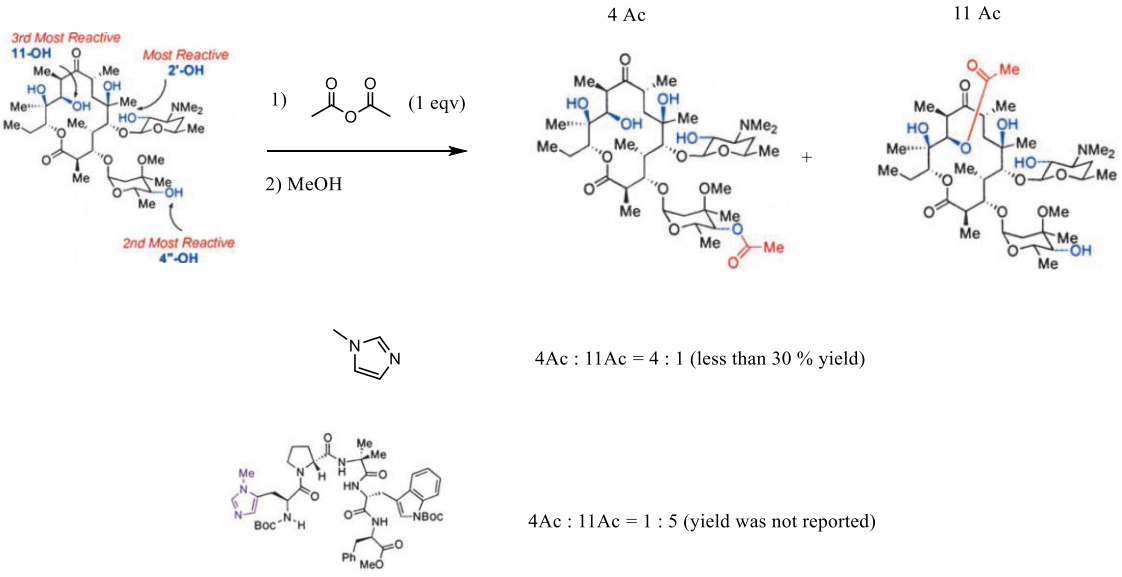

**Figure 26.** (A) First site selective chemistry reported from Miller's group. (Figures used with permission of the publisher.) (B) Miller's catalyst-controlled site selective acylation of erythromycin A. (Figures used with permission of the publisher.)

In 2012, Miller and coworkers reported the site selective epoxidation of a polyene substrate, again using peptide based catalysts[113]. Successful catalysts were identified through combinatorial synthesis and screening. They achieved a successful site selective reaction with high levels of enantioselectivity (up to 87% ee) and high yield (up to 81 % yield). The substrate, farnesol, contains three trisubstituted alkene moieties and could be predominantly epoxidized at each using mCPBA or either of two peptide catalysts (peptide A or peptide B) as shown in Figure 27. As can is done for many useful innovations, Miller filed an international patent application of this site selective modification of natural products in 2012, which can be taken as an indication of the potential utility and market value of the discovery.

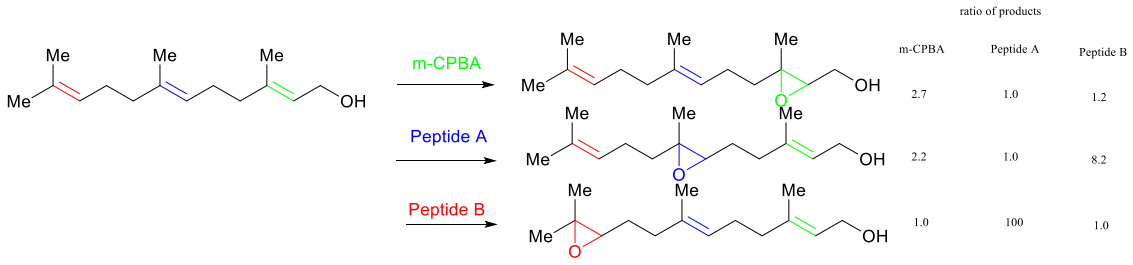


**Figure 27.** Miller's site selective epoxidation.

Among the first examples of a non-heme iron catalyst capable of site-selective C-H activation was reported by the White group in 2013 [114]. A challenge for non-peptide based catalysts in site selective chemistry field is that a small molecule catalyst has a more limited capacity to engage in secondary interactions between catalyst and substrate. Secondary interactions able to orient substrates are the key to site selective chemistry. However, small molecule catalysts are better suited to the "rational design", a designed fit between catalyst and substrate which enhances the reaction at one site over the others. White group's approach was to incorporate steric elements to restrict the approach trajectory of the catalyst reactive to certain of the C-H bonds. The author designed two catalysts (Figure 28, catalysts A and B) differing by the size of the active site or the degree to which access is restricted by sterically demanding substituents. Of the five substrates studied by White, catalysts A and B showed different selectivity for two. One example with a substituted cyclohexane (Figure 28) shows that the two catalysts each give a different major product with a roughly 3:1 preference over the minor product. C-H oxidation is achieved in excellent yield highlighting its practical applicability in a real world setting. The author also developed a quantitative structure-based catalyst reactivity model to predict site selectivity in C-H oxidations; this should further assist in the development of other site selective C-H activation reactions.

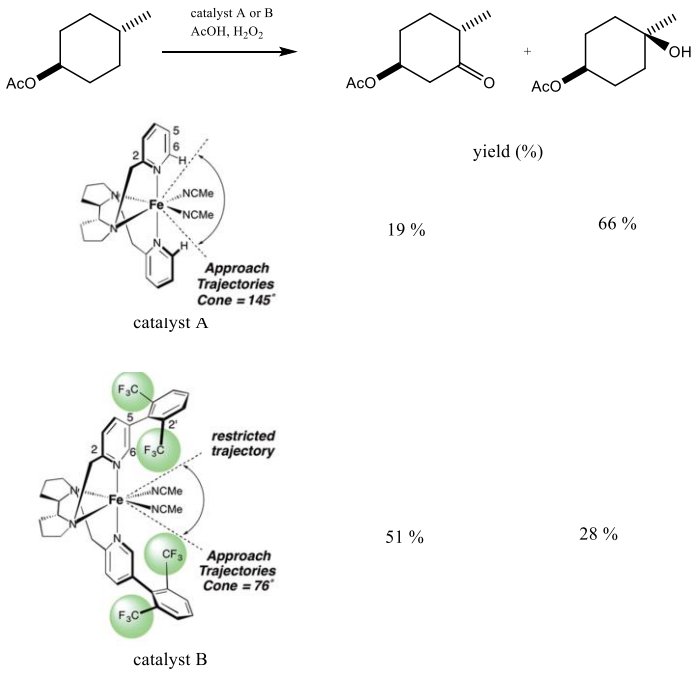


**Figure 28.** White's non-peptide based site selective catalysts (Used with permission). GIVE REF

Hermann[115] and Kawabata[116] have also reported catalyst controlled site selective reactions. The reaction scope includes transfer chemistry (acylation and phosphorylation), epoxidation, and C-H activation/oxidation. The substrate scope includes both simple model molecules and complex natural products. The methodology allows synthetic chemists to eliminate unnecessary protecting group chemistry and may ultimately complement the total synthesis of target molecules though more efficient semi-synthesis approaches. Although there is a high level of interest in this approach, the field is still in its infancy. My intention in this thesis study is to contribute to the development of site selective chemistry by exploring the use of supramolecular catalysts (non-peptide based and non-small catalysts) for site-selective CAHB. Although the work

is conducted using a simple model system, it is worth noting that no site-selective catalysts for hydroboration were known at the outset of our work.

**2.13 Site selective hydroboration –single dimeric substrate study (*ortho* and *meta* alkene substrate)**

With the exciting results obtained from CAHB intermolecular competition experiments that show potentially useful levels of substrate selectivity, it was time to face the more challenging problem of site selectivity. Intramolecular competitions for reactions at multiple sites present a profound challenge because many of the same functional groups in a molecule react similarly and because catalysts need to recognize what may be subtle differences in the environment of individual groups possessing similar inherent reactivity. To probe site-selectivity, we prepared a simple model substrate that it preserved the structural elements present in the intermolecular isomeric styrene competition reactions of styrenes; compound **221** has two vinyl arene moieties (Figure 29). For the sake of easy preparation, the two aryl groups are connected via an oxygen linker. Upon CAHB three possible products are possible: (1) the product of hydroboration of only the *ortho*-substituted vinyl group **222**; (2) the product of hydroboration of only the *meta*-substituted vinyl group **223**; and (3) diol **224** that has undergone hydroboration of both alkene moieties. The goal of the project was to be able to achieve selective reaction at one site to afford the product **223** or **224** using supramolecular SAL-derived catalysts. Note that the expected enantiomer of each product is shown in the figure; the issue of enantioselectivity will need to be addressed in due course (vide infra).

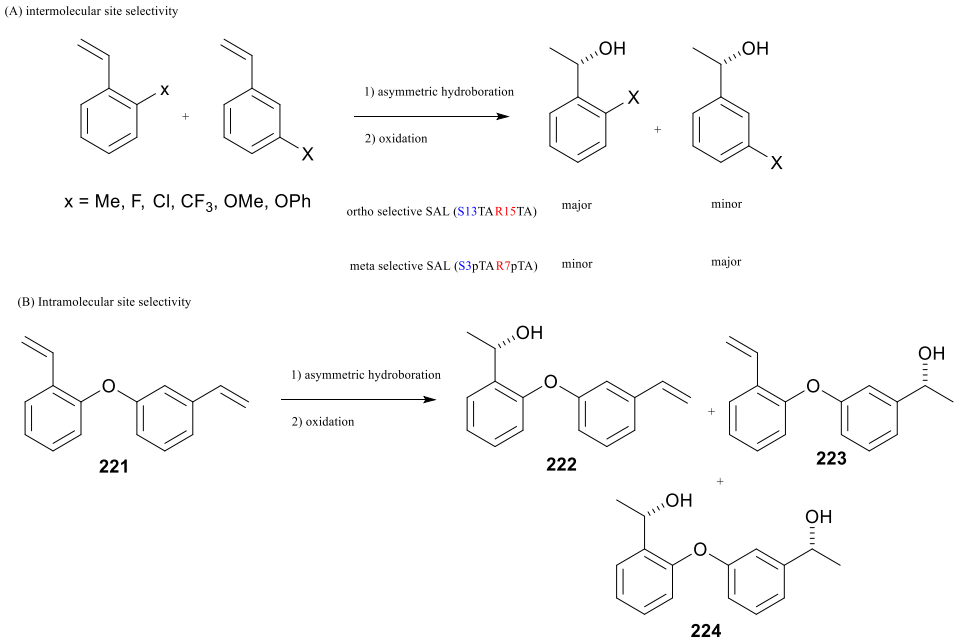


**Figure 29.** (A) Intermolecular isomer selectivity shown in previous study. (B) Intramolecular site selective reaction scheme.

The previously identified successful *ortho*- and *meta*-selective SAL catalysts were used for CAHB of bifunctional substrate **221** using 1.4 equivalents of pinBH to completely consume the starting material. The *ortho*-selective S13TAR15TA catalyst afforded three products: 74.8% of **222** derived from reaction of the *ortho*-substituted alkene; 4.1% of **223** derived from reaction of the *meta*-substituted alkene; and 20.4% of diol **224** (Figure 30) derived from reaction at both alkenes. The ratio of *ortho* to *meta* hydroborated products was 18.2 : 1. Meanwhile, the *meta*-selective S3pTAR7pTA catalyst gave the same three products but with a 1 : 21.8 ratio of *ortho* to *meta* hydroborated products. In each case roughly 20% of the diol is formed. The diol **224** can arise via two pathways: (1) the predominant isomer of the product is formed and as its

concentration builds up is slowly again hydroborated; and (2) the minor product is formed but then more quickly consumed by the faster hydroboration pathway. If the second pathway is operative, then formation of the diol effectively enhances the apparent *ortho*/*meta*-site selectivity. This is an application of the well-known Horeau Principle.[117] One way to minimize the diol formation is to use limited amount of borane source at the cost of substrate conversion and the selectivity among the isomeric products **222** and **223**.

I was pleased to find that the overall reactivity was sufficiently high that only 0.01 % of catalyst loading was needed to effect complete hydroboration within 2 hours; this translates to a TON of approximately 7500 and a TOF of approximately 60 $min^{-1}$ for formation of the major product. We feel that these high levels of reactivity and site selectivity, which constitute a significant advance over previous reports, are themselves highly significant. The 18-20 : 1 site-selectivity can perhaps be better appreciated when these data are compared to the results obtained using the corresponding chiral monophosphites lacking the supramolecular scaffold. The reaction of **221** using (TADDOL)POPh or (pTADDOL)POPh afford almost equal amounts (39.5-41.8%) of **222** and **223** along with about 18% of diol **224**. While these latter catalysts are as reactive as the SAL-derived supramolecular catalysts, they exhibit no site selectivity. It can be noted that Miller and coworkers have similarly reported striking differences in site selectivity between catalysts with peptide and without the peptide backbone.

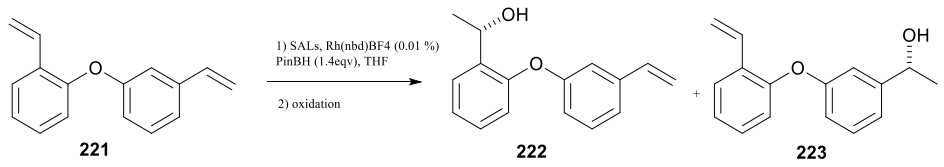


| SAL | | Yield (%) | | | ratio |
|---|---|---|---|---|---|
| | | *ortho* | *meta* | diol | (*ortho* : *meta*) |
| Ortho selective | S13TAR15TA | 74.8 | 4.1 | 20.4 | 18.2 : 1 |
| Meta selective | S3pTAR7pTA | 3.6 | 78.6 | 17.3 | 1 : 21.8 |
| monomer ligand | (TADDDOL)POPh | 40 | 41.3 | 18.5 | 1 : 1 |
| | (pTADDOL)POPh | 39.5 | 41.8 | 18 | 1 : 1.1 |

**Figure 30.** Site selective hydroboration on *ortho* and *meta* dimeric substrate (best data are shown under optimized reaction condition).

The observation that the presence of supramolecular catalyst backbone is alone responsible for the high site selectivity further prompted me to analyze what other factors are important to control site selectivity of hydroboration of the dimeric substrate. In order to understand what elements of catalysts and reaction condition impact site selectivity, first the reaction conditions were varied for optimum selectivity. The first optimization step was to analyze the effect of amount of pinBH on the product distribution using S13TAR15TA. The amount of pinBH was varied from 1.0 -1.5 equivalent in 0.1 equivalent increments. Due to the formation of diol, which consumed 2 equivalents of pinBH, the reaction with just 1.0 equivalent of pinBH left 21.6% of the starting material. Unreacted starting material persisted until 1.4 equivalents of pinBH

were used; the yield of product **222** increased, which boosted the ratio of *ortho*/*meta* product to 12.3 : 1 (Figure 31). Adding more than 1.4 equivalents of pinBH led to a reduced yield of **222** and formed more diol **224**. The *ortho*/*meta* product ratio was further improved to that shown above by slow addition of a more dilute solution of pinBH (details are given in the experimental section).

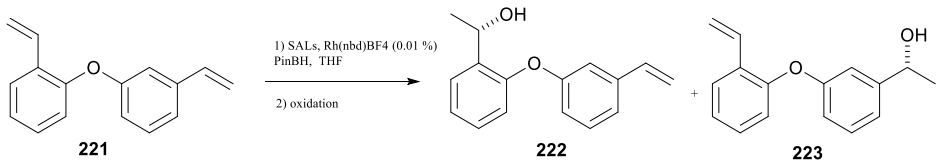


| *ortho* selective SAL (S13TAR15TA) | | | | | |
|---|---|---|---|---|---|
| PinBH | Yield (%) | | | | |
| eqvt | ST | *ortho* | *meta* | diol | ratio |
| 1.0 | 21.6 | 41.3 | 4.6 | 16.3 | 9.0 : 1 |
| 1.1 | 18.6 | 50.3 | 4.7 | 20.9 | 10.7 : 1 |
| 1.2 | 12.7 | 57.6 | 5.2 | 23.5 | 11.1 : 1 |
| 1.3 | 7.3 | 62.3 | 5.4 | 24 | 11.5 : 1 |
| 1.4 | 0 | 69 | 5.6 | 25.9 | 12.3 : 1 |
| 1.5 | 0 | 59.4 | 5 | 34.1 | 11.8 : 1 |

**Figure 31.** Influence of PinBH stoichiometry on site selectivity.

It has become common for researchers in the Takacs group to employ 1.0 - 2.0% catalyst loadings for hydroboration reactions. However, during the course of styrene asymmetric hydroboration study it was reported that a lower catalyst loading (0.8%) was as effective as 2.0%[73]. With current trend toward moving away from toxic and expensive metal catalysts and focus shifting to greener chemistry, the use of low

catalyst loading is much preferred. This is especially true for industry processes where TON and TOF are often emphasized more than in the academic environment. Therefore, in order to develop a competitive and attractive chemical process, it was my interest to investigate the possibility of lowering the catalyst loading with the hope of retaining the excellent site selectivity. It was interesting to discover that the "normal 1-2% catalyst conditions" did not afford the best site selectivity. The ratio of *ortho* to *meta* increased as catalyst loading was lowered; I found that the optimal catalyst loading is 0.01% (Figure 32). Lowering the catalyst load below this amount resulted in sluggish reaction and somewhat lower site selectivity under the conditions used due to the possibility of catalyst deactivation or decomposition. Even though the catalyst loading of 0.005% (i.e., 50 ppm) showed diminished site selectivity and reactivity, it still gave reasonable yields of hydroboration products overall. Compared to the normal 2% catalyst loading, this represents 400-fold increase in TON and shows that with further optimization this catalyst system may be practical.

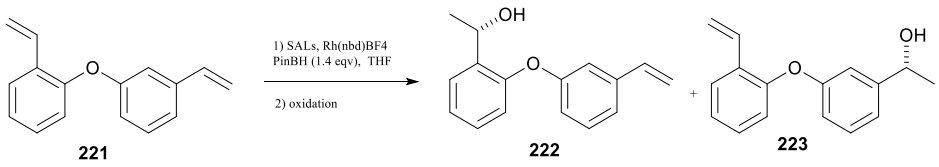


| cat load | *Ortho* selective SAL (S13TAR15TA) | | | |
|---|---|---|---|---|
| mol % | *ortho* | *meta* | diol | ratio |
| 1 | 58.7 | 5.5 | 29.6 | 10.7 : 1 |
| 0.05 | 69 | 5.6 | 24.2 | 12.3 : 1 |
| 0.04 | 69.8 | 5.3 | 23.8 | 13.2 : 1 |
| 0.03 | 70.3 | 4.7 | 23.3 | 15 : 1 |
| 0.02 | 72.2 | 4.5 | 21.4 | 16 : 1 |
| 0.01 | 74.8 | 4.1 | 20.4 | 18.2 : 1 |
| 0.005 | 59.7 | 3.5 | 11.9 | 17.1 : 1 |

**Figure 32.** Effect of amount of catalyst loading on site selectivity.

In the hope of further enhancing site selectivity, the influence of the reaction solvent was investigated. A selection of solvents (Figure 33), most of which had been employed rhodium-catalyzed reactions and/or other asymmetric hydroboration reactions developed by other groups, were investigated[118]. However, reactivity dropped significantly for all solvents other than THF. A recent computational study showed that an incorporation of THF molecule into asymmetric hydroboration mechanism facilitates faster reductive elimination step[71]. This data agrees with a report describing THF works as a facilitator of asymmetric hydroboration reaction[71].

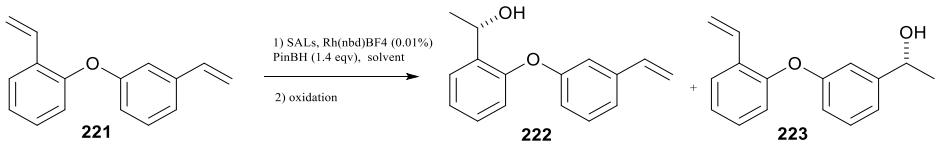

| | *Ortho* selective SAL (S13TAR15TA) | | | |
|---|---|---|---|---|
| Solvent | *ortho* | *meta* | diol | ratio |
| THF | 74.8 | 4.1 | 20.4 | 18.2 : 1 |
| DCM | 5.5 | 5.3 | 1.2 | 1 : 1 |
| EtOAc | 11.1 | 10.8 | 1.4 | 1 : 1 |
| Toluene | 5 | 4.9 | 0.8 | 1 : 1 |
| $CF_3$-toluene | 14.3 | 15.6 | 1.3 | 1 : 1.1 |
| DCE | 40.2 | 16.9 | 15.4 | 2.3 : 1 |
| ether | 32.1 | 25.1 | 20 | 1.3 : 1 |

**Figure 33.** Effect of commonly available solvents on site selectivity.

One of the things that group members in the Takacs group tend to underestimate is the effects of metal precursors on the catalytic reaction. Based on the past observations $Rh(nbd)_2BF_4$ has been the choice of Rh metal precursor for years. So it seemed important to revisit and test the other metal precursors for their possible influence on site selectivity. Several available catalyst precursors were investigated, including $Rh(nbd)_2OTf$, $Rh(cod)_2BF_4$, $Rh(cod)_2OTf$) and $[Rh(nbd)Cl]_2$ (Figure 34). It is a clear conclusion that most cationic Rh (I) complexes (i.e., those with readily dissociated counterions) are effective with only increment changes (either positive or negative). In contrast, the neutral Rh (I) precursor, $[Rh(nbd)Cl]_2$, while reasonably active was only slightly site selective. Due to the cost associated with preparing other Rh metal precursors, further optimization of metal precursors have not been done,

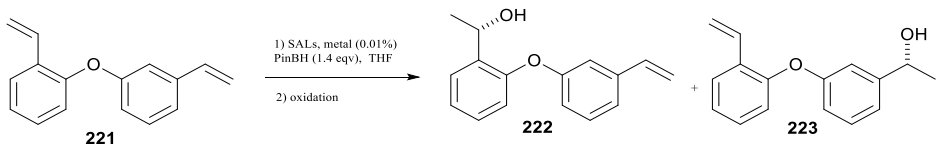


221 222 223

| metal precursor | *Ortho* selective SAL (S13TAR15TA) | | | |
|---|---|---|---|---|
| | *ortho* | *meta* | diol | ratio |
| $Rh(nbd)_2BF_4$ | 74.8 | 4.1 | 20.4 | 18.2 : 1 |
| $Rh(nbd)_2OTf$ | 71 | 5.3 | 22.3 | 13.4 : 1 |
| $Rh(cod)_2BF_4$ | 71.4 | 4.2 | 24 | 17 : 1 |
| $Rh(cod)_2OTf$ | 70.5 | 4.6 | 24.7 | 15.3 : 1 |
| $[Rh(nbd)Cl]_2$ | 52.7 | 31.5 | 15.4 | 1.7 : 1 |

**Figure 34.** Effect of metal precursor on site selectivity (neutral vs cationic Rh).

Having established the optimum reaction conditions for site selective hydroboration, I became interested in whether the SAL-derived supramolecular catalysts S13TAR15TA and S3pTAR7pTA could be further improved. In past studies SAL-derived catalysts were first systematically optimized with respect to the combination of scaffold-building tethers needed to achieve high regio- and enantioselectivity by changing tether structures one at a time.[78] Later, ligating group combinations were explored one at a time for a given scaffold, providing a path to further optimized catalysts structures.[73] The same protocol was applied to further search for better ligand combinations for site selective hydroboration. The objective of this experiment was to seek possible improvements which held the catalyst scaffold constant while changing one ligating group at a time. I had also hoped that I might gain some meaningful insight into how closely related TADDOL derivatives effect site selectivity. There are three TADDOL-based ligating groups that were used for CAHB in the Takacs group. The three differ by the number of methyl substituents on each of the four aryl substituents: zero

in the case of TADDOL, one in the case of pTADDOL; and two in the case of xTADDOL. Surprisingly, these rather subtle structural differences are found to have a rather substantial impact on both reactivity and selectivity in CAHB.[77]

Since each SAL contains two tethers subunits and each of the three TADDOL ligating groups can readily be appended to either tether or both as desired, there are total nine unique combinations of ligating groups to investigate. The results of modifying the S13TAR15TA catalyst are tabulated in Figure 35. Entry 1 shows the data for S13TAR15TA, which turned out to be the most selective catalyst among the nine variations tested. It is worth pointing out that catalysts containing at least one TADDOL-ligating group in all cases exhibited at least somewhat higher *ortho*-selectivity (entries 1, 2, 3, 5, and 6) compared to the combinations which do not include a TADDOL-ligating group (entries 4, 7, 8, and 9). Entries 10, 11, and 12 show the results obtained from using monomer ligands. None were selective. This further affirms the importance of the role of SAL scaffolds toward site selectivity.

It seems remarkable that the modest extra degree of steric bulk brought by inclusions of methyl groups has paramount effect on the site selectivity. This is presumed to be the result of changing the shape of the chiral pocket created by the SALs in such a way that the dimeric substrate does not fit into the space snugly enough to prefer *ortho* substituted alkene moiety. Unfortunately, our attempts to grow a crystal of a SAL-Rh complex suitable for x-ray analysis have thus far failed and any computational study of Rh complex with supramolecular ligand would be a major undertaking. Consequently, it is hard to assess the actual active catalyst structures.

However, it seems that it would be possible to further enhance the site-selectivity by exploring alternate classes of ligating groups, for example, BIPHEP, BINOL, or BINAP, The challenge to find the appropriate ligating groups requires finding the balance of both reactivity and selectivity. It needs to be highly reactive to deliver effective asymmetric hydroboration as well as highly site selective toward the substrates of interests.

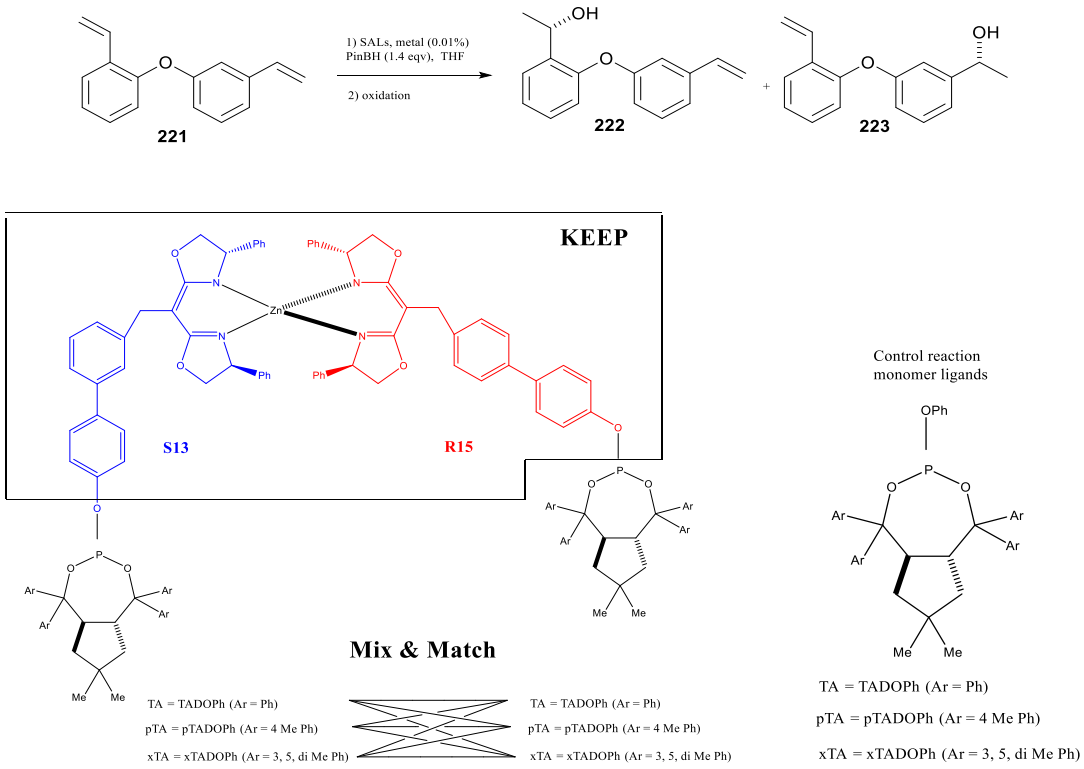


| entry | SAL S13 | SAL R15 | Yield of *ortho* (%) | Yield of *meta* (%) | Yield of diol (%) | ratio o:m |
|---|---|---|---|---|---|---|
| 1 | TA | TA | 74.8 | 4.1 | 20.4 | 18.2 : 1 |
| 2 | pTA | TA | 64.2 | 10.2 | 22.7 | 6.3 : 1 |
| 3 | TA | pTA | 69.7 | 6.6 | 22.4 | 10.6 : 1 |
| 4 | pTA | pTA | 36.7 | 33.4 | 21 | 1.1 : 1 |
| 5 | TA | xTA | 61.8 | 8.2 | 25.7 | 7.5 : 1 |
| 6 | xTA | TA | 58.7 | 8.6 | 28.4 | 6.8 : 1 |
| 7 | xTA | xTA | 35.2 | 22.1 | 18.4 | 1.6 : 1 |
| 8 | pTA | xTA | 36.9 | 20.7 | 29.8 | 1.8 : 1 |
| 9 | xTA | pTA | 42.1 | 29.8 | 25.8 | 1.4 : 1 |
| 10 | (TADDOL)POPh | | 40 | 41.3 | 18.5 | 1 : 1 |
| 11 | (pTADDOL)POPh | | 39.5 | 41.8 | 18 | 1 : 1.1 |
| 12 | (xTADDOL)POPh | | 34.2 | 36.1 | 15.7 | 1 : 1.1 |

**Figure 35.** Effect on changing ligating groups one at a time for on the *ortho*-selective while keeping the catalyst scaffold constant.

The same ligating group substitution protocol was applied to the *meta*-selective S3pTAR7pTA catalyst. Again, the SAL scaffold was kept constant. S3pTAR7pTA gave a ratio of *ortho*/*meta* products of 1 to 21.8 (Figure 36 entry 4). When TA was used in place of pTA on S3 tether (i.e., S3TAR7pTA), the site selectivity increased slightly to 1 : 23.4 (entry 3); this is the highest *meta* site selectivity obtained for this substrate. It is curious to note that in this case, any ligating combination that contains at least one pTADDOL ligating group (entries 2, 3, 4, 8, and 9) exhibited reasonably good *meta* selectivity. If the pTADDOL ligating group of R7 tether on the best SAL (entry 3) was switched to xTADDOL, the site-selectivity disappears (entry 5). A similar phenomenon was observed when the ligating R7 tether on the best SAL (entry 3) was switched to TA ligating group; the *ortho* : *meta* ratio became 1 : 1.7 (entry 1). The selectivity observed in entries 1 and 5 were essentially the same as those seen with monophosphite ligands (entries 10-12) which do not possess SAL backbone scaffolds. It is difficult to envision how the site selectivity is controlled but the presence of an extra methyl group (entries 3 and 5) or one fewer methyl group less (entries 3 and 1) on aryl of TADDOL has power to disrupt any meaningful selectivity.

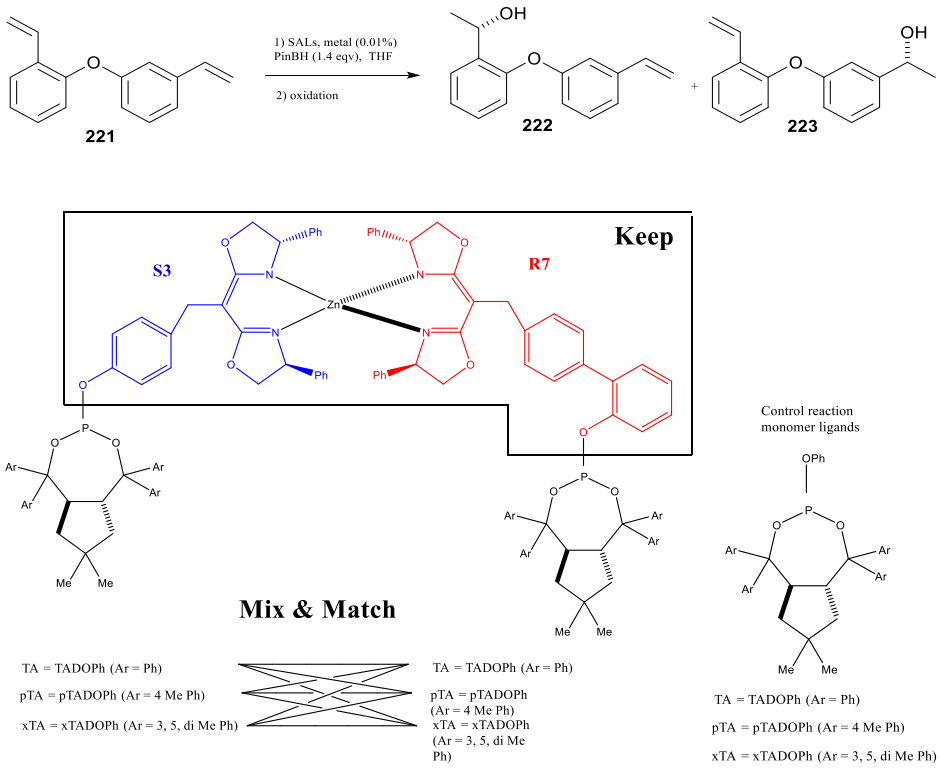


| entry | SAL | | Yield of *ortho* (%) | Yield of *meta* (%) | Yield of diol (%) | ratio o:m |
|---|---|---|---|---|---|---|
| | S3 | R7 | | | | |
| 1 | TA | TA | 22.4 | 39 | 23.1 | 1 : 1.7 |
| 2 | pTA | TA | 4.3 | 72.2 | 22.6 | 1 : 16.8 |
| 3 | TA | pTA | 3.4 | 79.5 | 17 | 1 : 23.4 |
| 4 | pTA | pTA | 3.6 | 78.6 | 17.3 | 1 : 21.8 |
| 5 | TA | xTA | 28.7 | 30 | 26.9 | 1 : 1 |
| 6 | xTA | TA | 16.9 | 44.5 | 24.1 | 1 : 2.6 |
| 7 | xTA | xTA | 24.6 | 27.8 | 30.1 | 1 : 1.1 |
| 8 | pTA | xTA | 6.5 | 70 | 23.4 | 1 : 10.8 |
| 9 | xTA | pTA | 5.1 | 73.4 | 21.2 | 1 : 14.4 |
| 10 | (TADDOL)POPh | | 40 | 41.3 | 18.5 | 1 : 1 |
| 11 | (pTADDOL)POPh | | 39.5 | 41.8 | 18 | 1 : 1.1 |
| 12 | (xTADDOL)POPh | | 34.2 | 36.1 | 15.7 | 1 : 1.1 |

**Figure 36.** Effect on changing ligating group on *meta* selective SAL

Having probed how changes in the combination of ligating groups impacted site selectivity for both *ortho* and *meta* site selective hydroboration, it was my intention to gain a similar understanding of the influence of scaffold-building tethers. Given the information obtained from the experiments above, it was expected that any significant change to SAL scaffolds would likely impact site selectivity. Using the identified optimal ligating groups, the investigation below focused of changing the position of the ligating group on the tether. The protocol employed evaluated SAL-derived catalysts in which the point of attached of the ligating group on aromatic ring on one tether is moved is systematically varying while the other tether subunit is unchanged.

The data for the *ortho*-selective S13TAR15TA catalyst is presented in Figure 37. First, the (*S*,*S*)-box linked scaffold-building tether (i.e., "S13TA", the "left tether and ligating group" pictured in Figure 37) and its (TADDOL)P ligating groups were kept constant and three SAL-derived catalysts in which (R,R)-box-linked tether (i.e., the "right tether") scaffold incorporated R15TA, R11TA, and R7TA. While all three catalysts efficiently promoted the hydroboration, repositioning of the ligating group had significant negative impact on site selectivity (Figure 37, compare entries 1, 2, and 3). Essentially the same results resulted from changing the location of the ligating group around (*S*, *S*)-box linked (i.e., left) tether (Figure 37, compare entries 1, 4, and 5). Repositioning the point of attachment of the TADDOL-ligating group led to marked diminished site selectivity. Compared to S13TAR15TA (18.2:1 *ortho*/*meta*-selectivity), none of the repositioned scaffolds gave better than 4.7:1 selectivity.

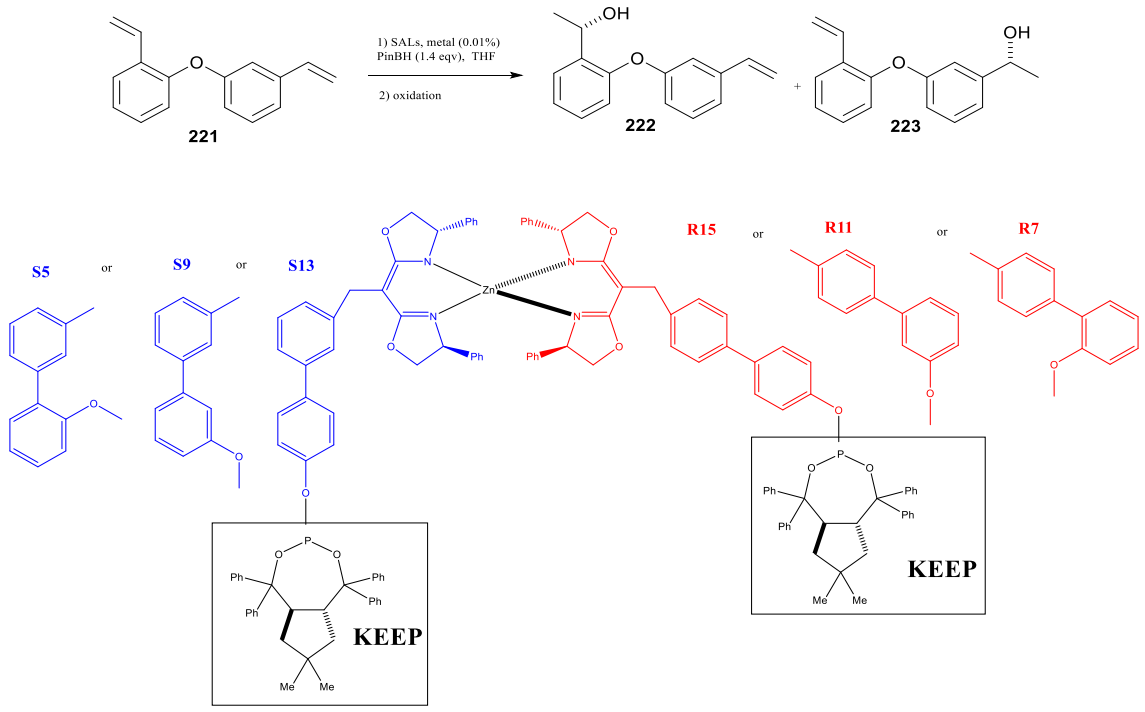


| entry | tether | | Yield of *ortho* (%) | Yield of *meta* (%) | Yield of diol (%) | ratio o:m |
|---|---|---|---|---|---|---|
| | S | R | | | | |
| 1 | 13TA | 15TA | 74.8 | 4.1 | 20.4 | 18.2 : 1 |
| 2 | 13TA | 11TA | 53.1 | 17.2 | 23.1 | 3.1 : 1 |
| 3 | 13TA | 7TA | 38.6 | 22.4 | 25.9 | 1.7 : 1 |
| 4 | 9TA | 15TA | 59.6 | 12.7 | 20 | 4.7 : 1 |
| 5 | 5TA | 15TA | 33.9 | 29.4 | 26.6 | 1.2 : 1 |

**Figure 37.** Investigation of the location of ligating attachment on *ortho* selectivity.

The same scaffold variations were explored for the *meta*-selective S3pTAR7pTA catalyst. One difference is that (*S*,*S*)-box linked tether has only one alternative tether besides S3, because a ligating group at *ortho* position in that monocyclic series of scaffold-building tethers is omitted from consideration due to unfavorable steric interactions. Nonetheless, repositioning the ligating group significantly disrupted *meta*-

selectivity. The results obtained both from these and previous experiments suggest that it is paramount to have the correct combination of tethers which allow the SAL-derived catalyst scaffold to create a suitable chiral pocket for site selectivity. In addition, changing the ligating structures by inserting one or more methyl groups on aryl of TADDOL can change site selectivity but this does not have as much effect as changing the location of ligating group on tethers.

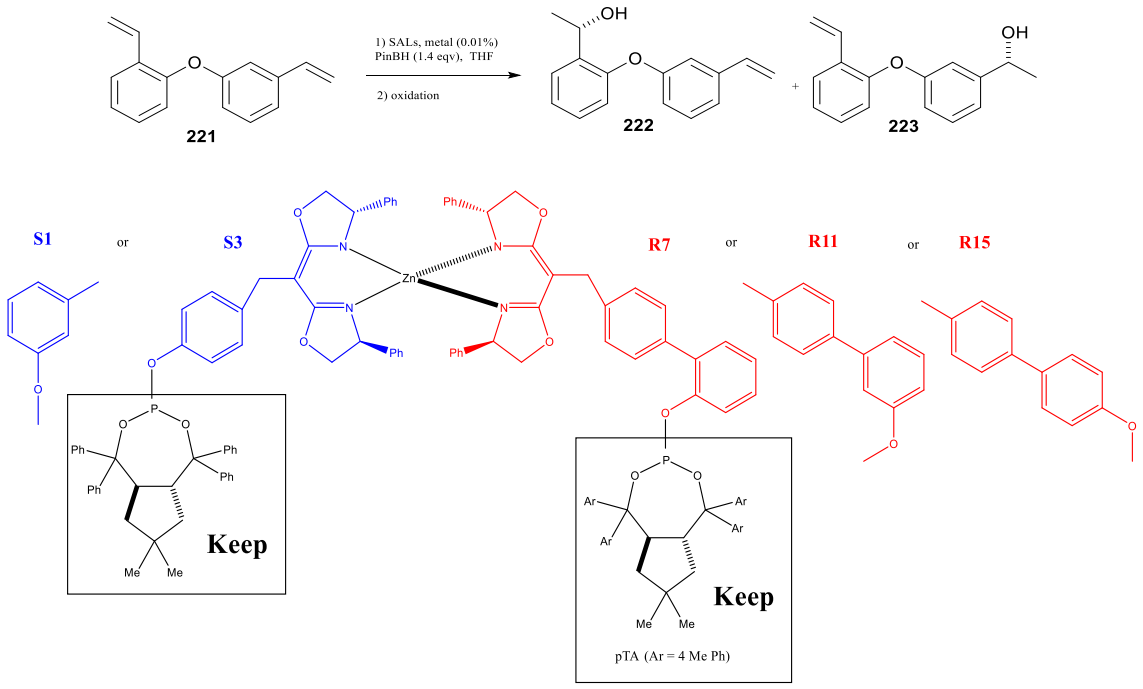


| entry | tether | | Yield of *ortho* (%) | Yield of *meta* (%) | Yield of diol (%) | ratio o:m |
|---|---|---|---|---|---|---|
| | S | R | | | | |
| 1 | 3TA | 7pTA | 3.4 | 79.5 | 17 | 1 : 23.4 |
| 2 | 3TA | 11pTA | 11.1 | 64.2 | 22.8 | 1 : 5.8 |
| 3 | 3TA | 15pTA | 26.8 | 33.1 | 24 | 1 : 1.2 |
| 4 | 1TA | 7pTA | 9.6 | 65 | 22.1 | 1 : 6.8 |

**Figure 38.** Investigation of effect of changing the location of ligating attachment for *meta* selective SAL.

Throughout the preceding studies, the S13TAR15TA and S3pTAR7pTA catalysts showed excellent site selectivity for *ortho* and *meta* substituents, respectively. What is remarkable is that the reactivity is catalyst controlled and one can direct reaction toward one site by picking the correct catalyst scaffold and ligating groups. Many of the examples of site-selective catalysis reported to date have reactivity issues (i.e., slow

reaction or very low conversion). However, the catalysts reported herein are highly reactive; only 0.01 % of catalyst loading is required to effect complete reaction within 2 hours at room temperature. Yet the reaction is highly selective and by just swapping the supramolecular catalysts the ratio of *ortho* to *meta* hydroborated products inverts from 18.2 : 1 to 1 : 23. 4 (*ortho* : *meta*). This work is distinguished from others in that most research until this point on site selective catalysts done utilizes peptide based or small molecule catalysts. It is hoped that our observations of site selective catalysts based upon self-assembled supramolecules will stimulate new direction of research in site-selective chemistry.

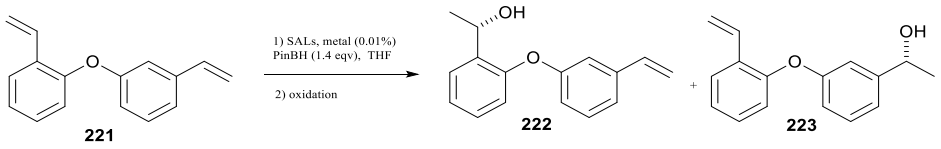


| | Yield of *ortho* (%) | Yield of *meta* (%) | Yield of diol (%) | ratio o:m |
|---|---|---|---|---|
| *Ortho* selective SAL (S13TAR15TA) | 74.8 | 4.1 | 20.4 | 18.2 : 1 |
| *Meta* selective SAL (S3TAR7pTA) | 3.4 | 79.5 | 17 | 1 : 23.4 |

**Figure 39.** Optimal site selective results for *ortho* and *meta* selective SALs.

## 2.14 Site selective hydroboration – single dimeric substrate study (*ortho* and *para* substituted alkene substrate & *meta* and *para* substituted alkene substrate)

Takacs's supramolecular SALs have demonstrated that effective site selective chemistry can be accomplished by catalyst controlled manner for asymmetric hydroboration reaction of the dimeric substrate **221** in which two alkene substituents were positioned *ortho* and *meta* to an oxygen substitutent. To further investigate the potential for site selective reaction, the dimeric substrates **225** and **229** were prepared. Each sets up a competition between *ortho*- and *para*-substituted (225) and *meta*- and *para*-substituted alkenes (**229**) in a single molecule. The question to be answered is if the *ortho* selective SAL identified previously is used on *ortho* and *para* dimeric substrate, will it show *ortho* site selectivity? Likewise, if *meta* selective SAL identified above is used on *meta* and *para* dimeric substrate, will it show *meta* site selectivity? What is more, we were curious as to whether a para selective SAL could override the inherently lower reactivity of *para* substituted styrenes observed in our earlier work.

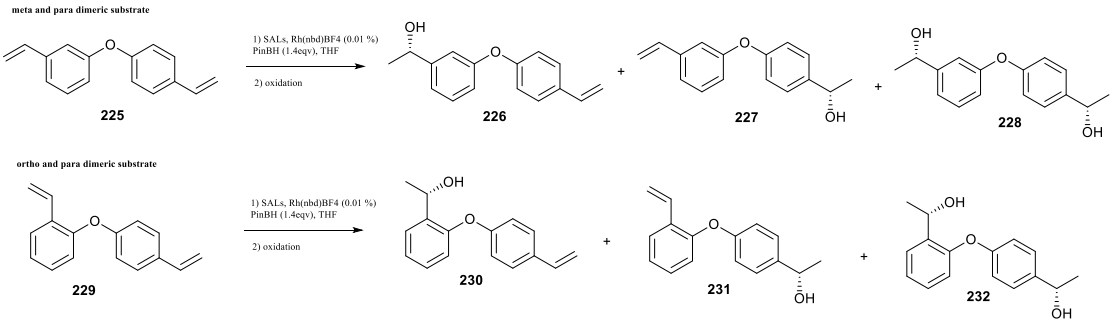


**Figure 40.** Newly synthesized dimeric substrates for site selective hydroboration.

Optimizing the catalysts for the new substrates was limited to varying the combination of ligating groups rather than varying tether combinations; the previous study showed that the latter approach invariably diminished the level of site selectivity. Therefore, our focus was on searching for ligating group combinations that allow SAL catalysts to selectively react on one site over the other. Control reactions (Figure 41, entries 10, 11, and 12) carried out using the chiral monophosphite ligands found that the inherent reactivity of *meta*-substituted alkenes is greater than that of *para*-substituted alkenes. This is in line with previous studies. The monophosphite ligands tend to react with the *meta*-substituted alkene 1.5 to 2.0 times faster with the *para*-substituted alkene. The formation of diol (i.e., **229 & 232**) was also found in about the same amount as previously observed with the *ortho*/*meta* dimeric substrate case.

Screening catalysts in which the ligating groups had been changed revealed that the catalyst previously associated with the best *meta*-selectivity (i.e., S3TAR7pTA) did not afford the best site selectivity with substrate **225** (Figure 41, entry 2 20 : 1 *meta*/*para*). The best *meta*-selectivity was obtained by the catalyst having pTADDOL-ligating groups on each tether; S3pTAR7pTA gave a 27 : 1 *meta*/*para* ratio of products (entry 1). It was noted above that catalysts containing at least one pTADDOL-ligating tended to preferentially react *meta*-substituted (entries 1, 2, 3, 4, and 5). Catalysts lacking at least one pTADDOL-ligating group showed moderate or low site selectivity (entries 6, 7, 8, and 9). It is again worth highlighting the fact that the presence of the SAL-derived catalysts scaffold structure increased *meta* site-selectivity drastically from

1.8 : 1 to 27 : 1 *meta*/*para* (comparing entries 1 and 11) demonstrating how effective and important of supramolecular assembled ligands are in site selective hydroboration.

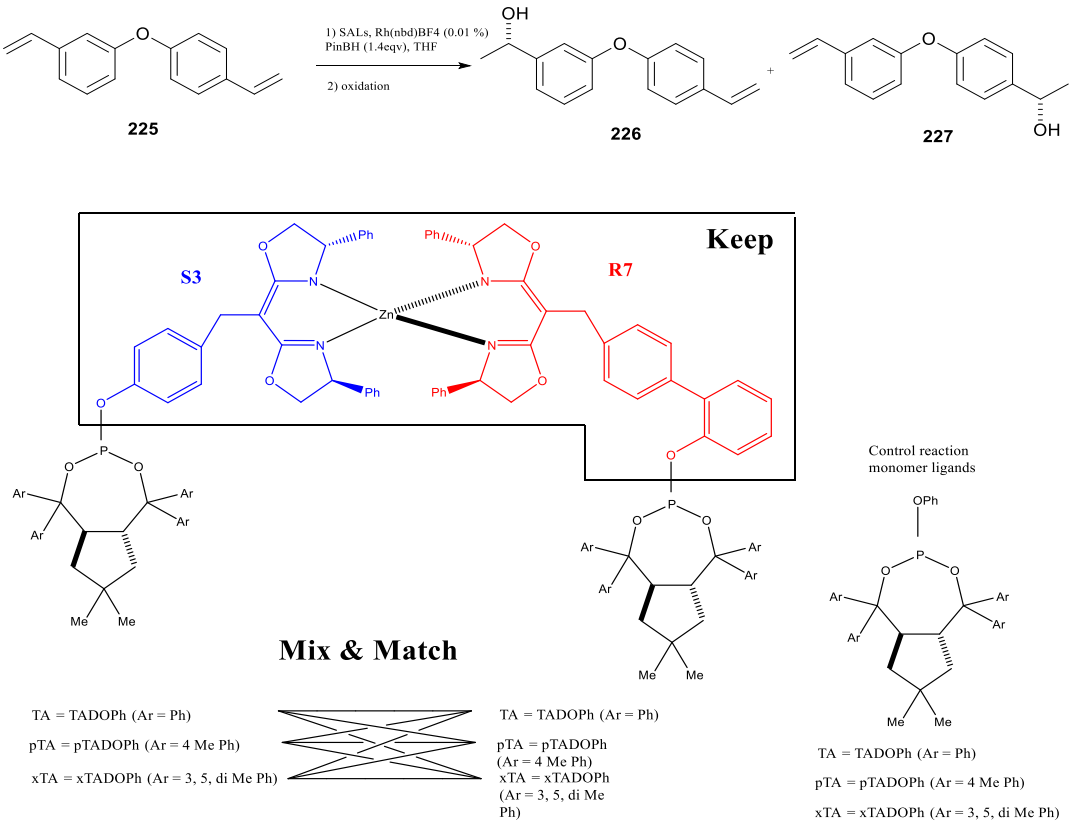


| entry | tether | | Yield (%) | | | ratio |
|---|---|---|---|---|---|---|
| | S3 | R7 | *meta* | *para* | diol | m : p |
| 1 | pTA | pTA | 69.8 | 2.6 | 25.4 | 27 : 1 |
| 2 | TA | pTA | 68.7 | 3.4 | 21 | 20 : 1 |
| 3 | xTA | pTA | 70.1 | 3.6 | 25.3 | 19 : 1 |
| 4 | pTA | TA | 71.4 | 2.7 | 24.1 | 26 : 1 |
| 5 | pTA | xTA | 65.9 | 3.2 | 22.8 | 21 : 1 |
| 6 | TA | TA | 65.4 | 4.8 | 24.8 | 14 : 1 |
| 7 | xTA | xTA | 61.3 | 4.6 | 24.9 | 13 : 1 |
| 8 | xTA | TA | 48.6 | 17.4 | 20 | 2.8 : 1 |
| 9 | TA | xTA | 42.2 | 19.7 | 15.9 | 2.1 : 1 |
| 10 | (TADDOL)POPh | | 41.1 | 28.8 | 24 | 1.4 : 1 |
| 11 | (pTADDOL)POPh | | 41.9 | 22.8 | 25.6 | 1.8 : 1 |
| 12 | (xTADDOL)POPh | | 42.8 | 23.1 | 24.8 | 1.9 : 1 |

**Figure 41.** Optimization of *meta* site selectivity on *meta* and *para* substituted dimeric substrate.

The analysis of previous data revealed S13pTAR15pTA as a possible *para* selective SAL-derived catalyst; recall that only the pTADDOL-ligating groups differentiate it from the *ortho*-selective S13TAR15TA catalyst. Therefore, catalysts of varying combinations of pTADDOL- and xTADDOL-ligating groups were compared. The control reactions using (pTADDOL)POPh and (xTADDOL)POPh revealed a slight *meta*-alkene preference; the observed *meta*/*para* ratio was 1.8-1.9 : 1 (Figure 42 entry 5 and 6). Given the inherent lower reactivity for the *para* substituted styrenes, any ratio that prefers reaction of the para- substituted isomer is an indication of improved *para* selectivity. Varying the ligating group combination revealed that a combination of pTA on left tether and xTA on right tether of the catalyst (entry 2) afforded 1 : 1 *meta*/*para*-product ratio and reflects about a 10% increase in the yield of **227** over that obtained with (pTADDOL)POPh or (xTADDOL)POPh. The change, while small, is in desired direction and suggested to us that *para*-selective catalysts could eventually be found.

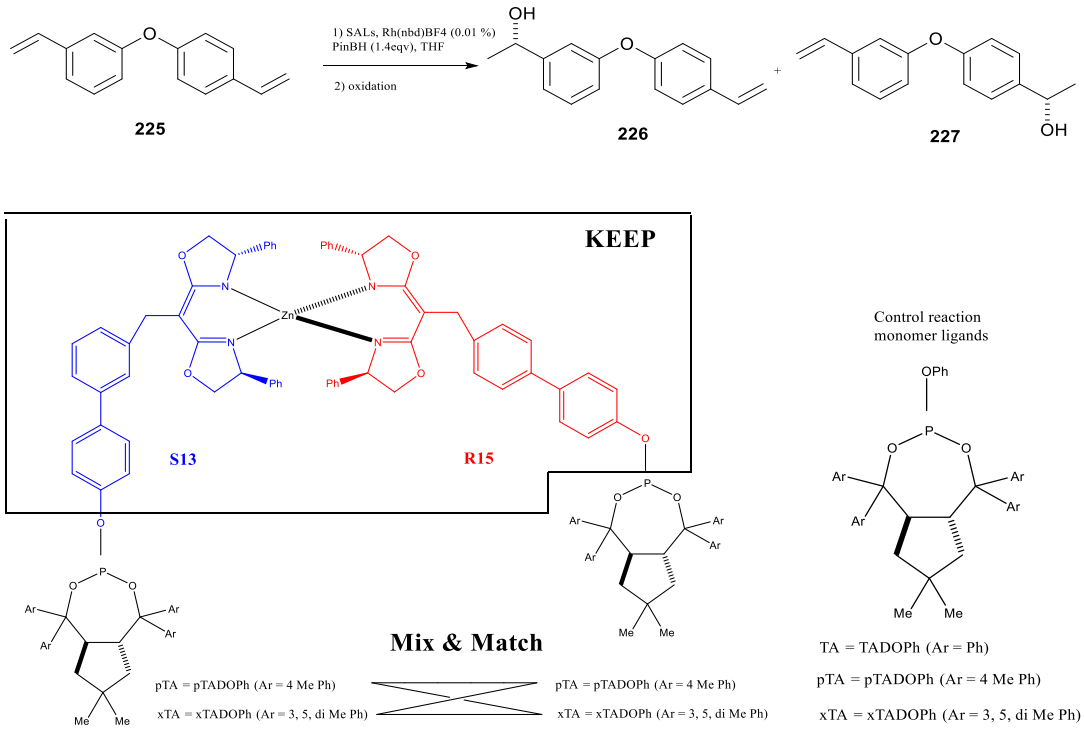


| entry | tether | | Yield (%) | | | ratio |
|---|---|---|---|---|---|---|
| | S13 | R15 | *meta* | *para* | diol | m : p |
| 1 | pTA | pTA | 38.4 | 32.3 | 21.9 | 1.2 : 1 |
| 2 | pTA | xTA | 31.8 | 33.7 | 26.7 | 1 : 1 |
| 3 | xTA | pTA | 39.7 | 27.9 | 22 | 1.4 : 1 |
| 4 | xTA | xTA | 39.9 | 30 | 20.7 | 1.3 : 1 |
| 5 | pTADOPh | | 41.9 | 22.8 | 25.6 | 1.8 : 1 |
| 6 | xTADOPh | | 42.8 | 23.1 | 24.8 | 1.9 : 1 |

**Figure 42.** Optimization of para site selectivity on *meta* and *para* substituted dimeric substrate.

Turning to the *ortho*/*para*-combination substrate **229**, the data discussed above suggests that it should be possible to target selective reaction of *ortho*-substituted alkenes; their inherently greater reactivity and the rather efficient *ortho*-selective S13TAR15TA catalyst should help boost the level of site-selectivity. The *ortho*-selective

S13TAR15TA and *para*-selective S13pTAR15xTA catalysts have the same SAL-derived scaffold; the results previous discussed above already showing how different ligating groups on the same supramolecular scaffolds can have a large effect on site selectivity. It is astonishing to compare the results obtained using SAL scaffolds and the monomer results. The best *ortho* selective SAL afforded a 35 : 1 *ortho* : *para* ratio, (entry 1) and the isolated yield of *ortho* hydroborated product was 73.8 % and that of *para* was 2.1 %. This high selectivity is in stark contrast to the results obtained using (TADDOL)POPh, (pTADDOL)POPh or (xTADDOL)POPh each of which promoted only a two-fold faster reaction at the *ortho* site in **229** (Figure 43, entries 10, 11, and 12). Given that the ligating groups used for entry 1 and entry 10 are the same, the reactivity toward the *ortho* site significantly improved due to the presence of the supramolecular SAL scaffold. The same SAL scaffold but with the combination of pTA on left and xTA on right side tether indirectly revealed modest *para*-selectivity (entry 9). Even though this change in ligating groups did not override the inherent reactivity difference between *ortho* and *para* sites of the dimeric substrate, the yield of the *para*-product increased from 2.1% with S13TAR15TA to 28.7% with S13pTAR15xTA. With regard to favoring *ortho*-selectivity, catalysts which contain at least one TA ligating group showed high *ortho* selectivity (entry 1, 2, 3, 4, and 5).

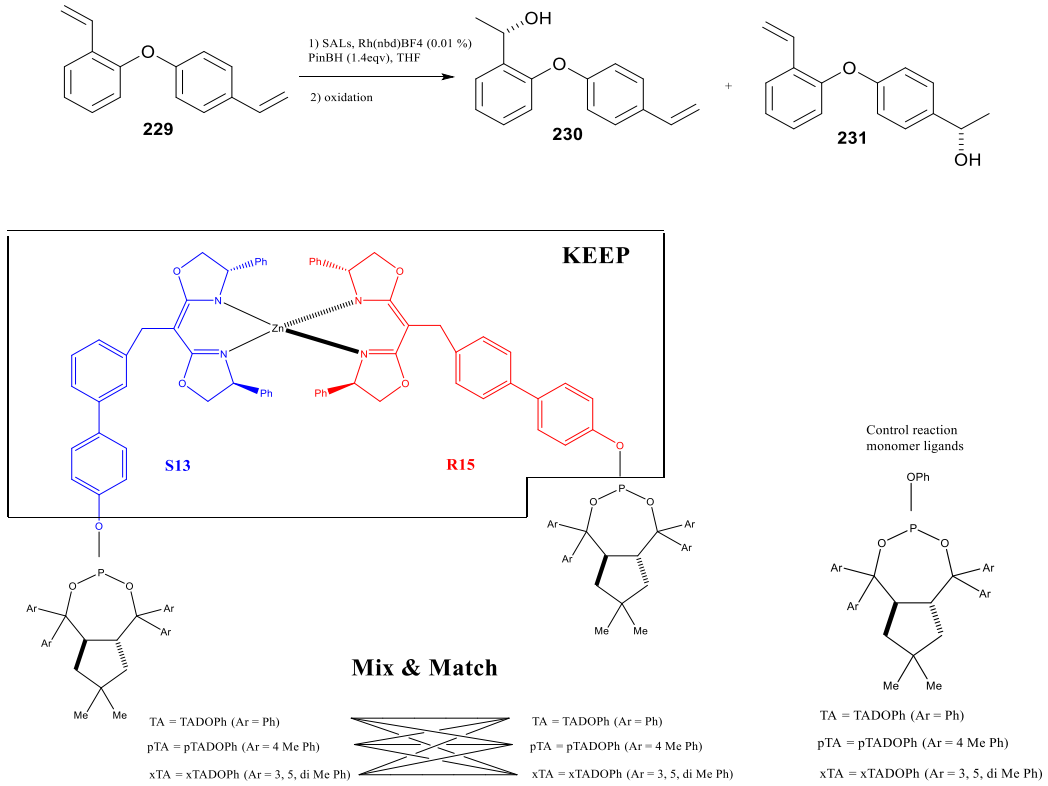


| entry | tether | | Yield (%) | | | ratio |
|---|---|---|---|---|---|---|
| | S13 | R15 | *ortho* | *para* | diol | o : p |
| 1 | TA | TA | 73.8 | 2.1 | 19.2 | 35 : 1 |
| 2 | pTA | TA | 72.8 | 2.5 | 17.4 | 29 : 1 |
| 3 | xTA | TA | 70.5 | 2.4 | 14.9 | 29 : 1 |
| 4 | TA | pTA | 72.4 | 2.8 | 17.8 | 26 : 1 |
| 5 | TA | xTA | 70.8 | 2.9 | 17 | 24 : 1 |
| 6 | pTA | pTA | 41.2 | 29.7 | 21.8 | 1.4 : 1 |
| 7 | xTA | xTA | 52 | 22.4 | 14.5 | 2.3 : 1 |
| 8 | xTA | pTA | 29.7 | 22.9 | 23.7 | 1.3 : 1 |
| 9 | pTA | xTA | 34.9 | 28.7 | 21.7 | 1.2 : 1 |
| 10 | (TADDOL)POPh | | 49.5 | 20.4 | 24.8 | 2.4 : 1 |
| 11 | (pTADDOL)POPh | | 45.1 | 25.6 | 20.4 | 1.8 : 1 |
| 12 | (xTADDOL)POPh | | 48.1 | 20.5 | 22.3 | 2.3 : 1 |

**Figure 43.** Optimization of *ortho* and *para* site selectivities on *ortho* and *para* substituted dimeric substrate.

**2.15 Site selective hydroboration –search for a structural basis for the site selectivity observed with supramolecular SALs**

Typical structure determination methods have not been successful with Takacs supramolecular SALs. The main reasons are the high molecular weights (ca 2 kD), which makes high level calculations difficult, and the relatively flexible nature of tethers and ligating groups, which makes it difficult to grow single crystals. Attempted characterization methods include crystallography, low-temperature NMR, DOSY-NMR spectroscopy, calculations, UV/VIS spec, high resolution mass spec, circular dichroism (CD), and gel permeation chromatography (GPC). Among these techniques, CD spectroscopy has provided the best evidence of significant structural difference between two successful site-selective catalyst complexes (i.e., S13TAR15TA and S3pTAR7pTA) discussed above.

Circular dichroism (CD) is a technique that employs circularly polarized light to study optically active chiral molecules for examples, often proteins. Researchers in biology field have used CD for investigation of the secondary structure of proteins[119] in solution. Any difference observed within samples means that there are differences in terms of the chiral environments in the vicinity of the chromophore. This information is potentially useful for my purpose, although exact interpretation of how the structures are arranged in space in solution is not an easy task. CD spectra of S13TAR15TA and S3pTAR7pTA were obtained in an effort to ascertain whether their chiral environments differed significantly. First, the *ortho*-selective S13TAR15TA scaffold and *meta*-selective S3pTAR7pTA scaffold in the absence of Rh (I) were recorded (Figure 44A). Above 300

nm the CD peaks for each are essentially identical. Below 300 nm range the shapes of two CD specs were essentially identical but slightly shifted. Overall, the two spectra are very similar suggesting that the structures of the two scaffolds are very similar in solution. However, the conclusion changes when S13TAR15TA and S3pTAR7pTA complex Rh (I); their CD spectra are shown in Figure 44B. The overall shapes of the two curves are very different, in particular there is a significant difference observed between 280 and 330 nm range. Although an interpretation of the observed spectral changes and differences between the two spectra lacking, it is reasonable to conclude that the S13TAR15TA- and S3pTAR7pTA-catalyst complexes have marked different structures in solution and by inference markedly different chiral environments that may account for their selectivities.

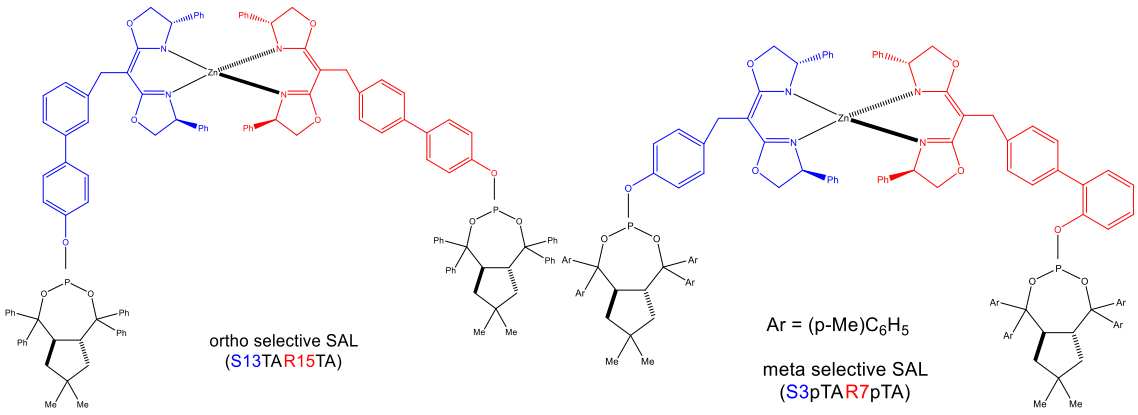

(a)

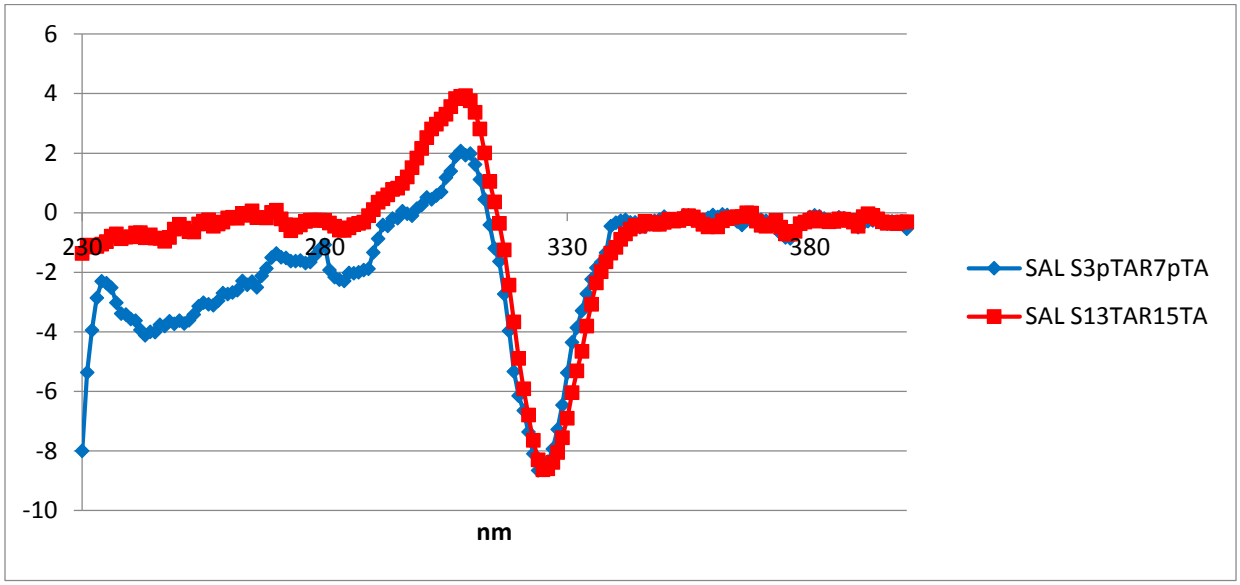


(b)

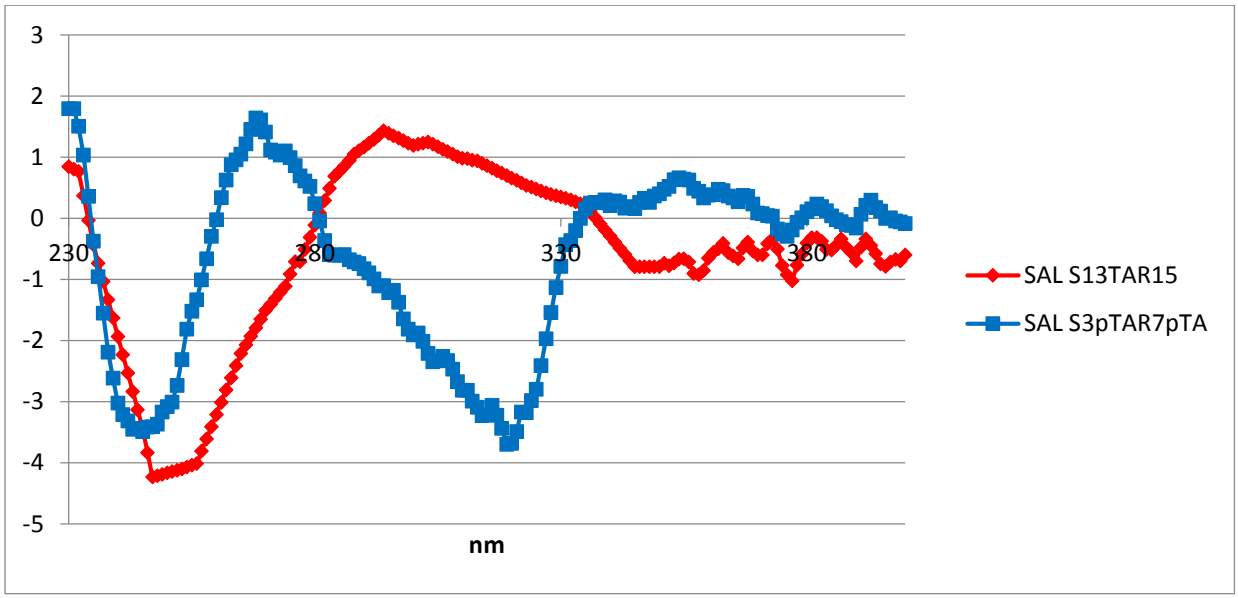


**Figure 44.** Investigation of catalysts structural differences using CD spec (a) CD spec without Rh. (b) CD spec with Rh.

**2.15 Site selective hydroboration – Structural proof of product stereochemistry based upon the Mosher ester method**

The absolute configuration of the hydroboration products was determined by Mosher ester method described in the literature.[120] Despite the effort toward figuring out all the proton assignments, the presence of benzene rings in both the Mosher ester and the substrates made it harder to assign each proton. Therefore, we focused on the secondary methyl group adjacent to the Mosher ester moiety. The chemical shift of methyl group for (*R*) and (*S*) MTPA ester was 1.641 ppm and 1.567 ppm, respectively. $\Delta\sigma^{SR}$ was -0.074 ppm. The greater shielding of the methyl group in the ester formed from the (S)- Mosher acid results from shielding by the Mosher acid phenyl group and suggests an (S) configuration of the alcohol. Based on these observations the absolute configuration of alcohol was determined to be (*S*). The rest of the Mosher esters were used to obtain the absolute configuration for each substrate, which collectively showed that all of the cases the alcohol had (*S*) configuration.

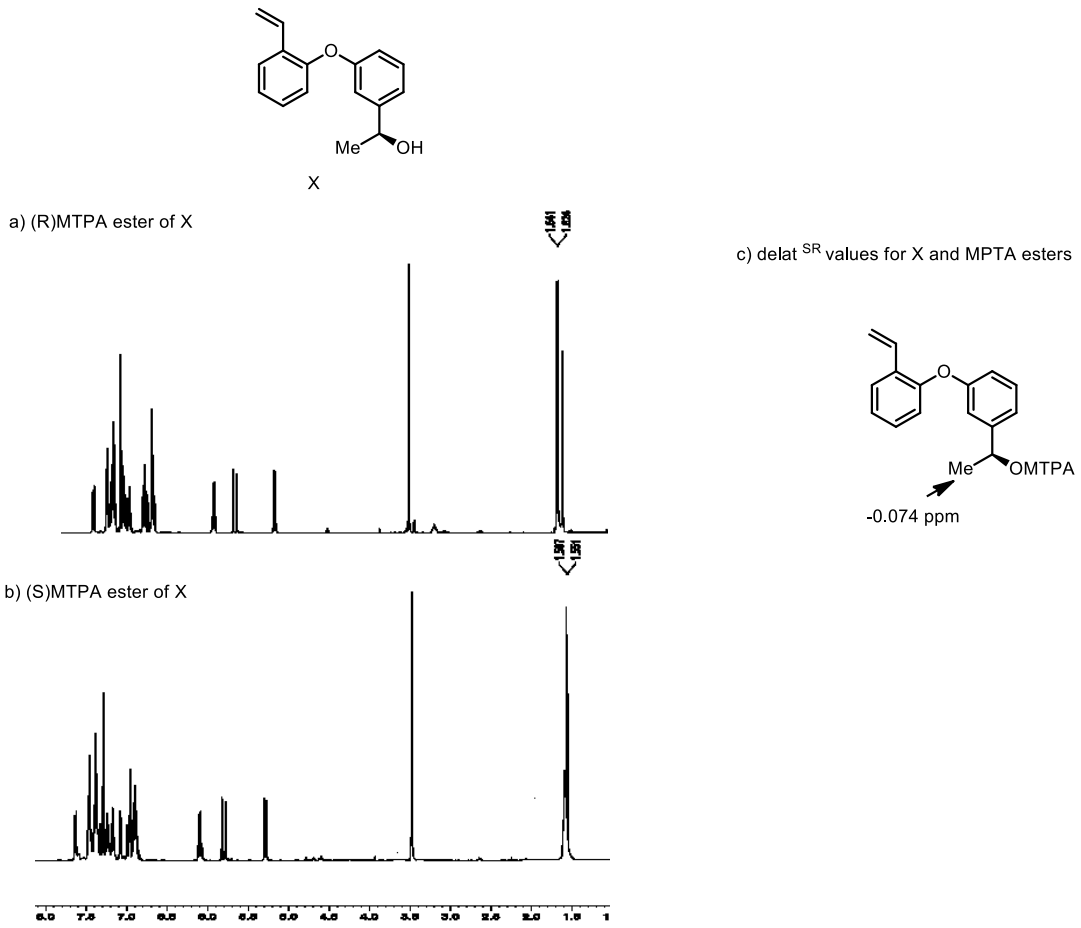


**Figure 45.** Structural proof of hydroborated product using Mosher ester method.

This project has mainly focused on site selectivity and accordingly optimization of SALs has resulted in greater site selectivity. Figure 46 lists the best enantioselectivity obtained with the optimum site selective SALs which have been identified from the optimization steps described above. *Ortho*- and *meta*- selective SALs not only displayed excellent site selectivity on all of the dimeric substrate (**221**, **222**, and **223**), but also exhibited reasonably high enantiomeric excess. For example, the *ortho*- selective SAL generated 91% ee and 87% ee for the *ortho*- and *meta*- dimeric substrate **221** and for the *ortho*- and *para*- dimeric substrate **229**, respectively. The *meta*- selective SAL

generated 93% ee and 91% ee for the *ortho*- and *meta*- dimeric substrate **221** and for the *meta*- and *para*- dimeric substrate **225**, respectively. Despite the successful performances of both the *ortho*- and *meta*- selective SALs, the level of enantioselectivity observed with the *para*- selective SAL was rather lower especially for the *meta*- and *para*- dimeric substrate **225** (hydroborated product **227**:78% ee).

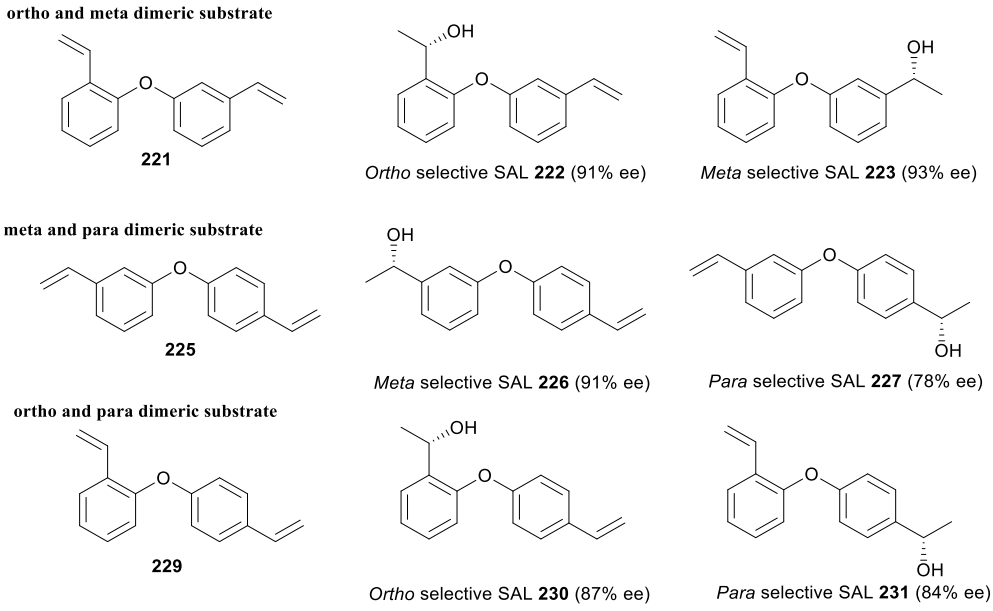


**Figure 46.** Best enantioselectivity observed for each substrate with site selective SALs.

**2.16. Conclusions**

Figure 47 lists the best selectivity obtained for each dimeric substrate and the component monophosphite ligands; the latter is taken as an indication of the inherent reactivity of the dimeric substrates. First of all, the *ortho* and *meta* dimeric substrate **221** affords the most interesting results. The inherent reactivity determined with monophosphite ligand (TADDOL)POPh showed that both alkenes react about the same rate under the hydroboration conditions. The reactivity of *ortho*- and *meta*-substituted alkenes can be tuned by just selecting one of the two SALs identified through the screening process. The *ortho*-selective catalyst S13TAR15TA provides better *ortho*-selectivity, up to 18.2: 1 selectivity, while the *meta*-selective catalyst S3TAR7pTA affords up to 23.4 : 1 *meta*-selectivity. Since the reaction conditions used for each screening process are the same, these significant differences reflect only the influence of the catalysts.

As for substrates **229** and **225**, which contain *para*-substituted alkenes in combination with *ortho* or *meta* isomers, a number of catalysts resulted in an increased percentage (ca 10-25%) of the product resulting from exclusive reaction of the *para*-substituted alkene, but in no case did this become the major product. In contrast, *meta*- and *ortho*-selective catalysts exhibited excellent site selectivity on these substituted alkene dimeric substrates. For the *meta* and *para* dimeric substrate **225**, the *meta*-selective catalyst S3TAR7pTA showed excellent *meta* selectivity up to 27 : 1 (*meta* : *para*). The *ortho*-selective catalyst S13TAR15TA exhibits 35 : 1 *ortho*:*para* selectivity in the reaction of **229**.

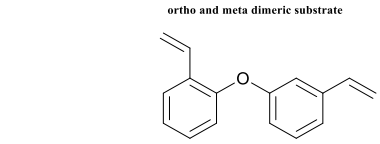


| | Yield (%) (ortho:meta) | ratio (ortho : meta) |
|---|---|---|
| Ortho selective SAL (S13TA R15TA) | 74.8 : 4.1 | 18.2 : 1 |
| Meta selective SAL (S3TA R7pTA) | 3.4 : 79.5 | 1 : 23.4 |
| (TADDOL)PO Ph | 40 : 41.3 | 1 : 1 |

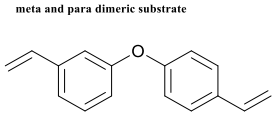


| | Yield (%) (ortho:meta) | ratio (meta : para) |
|---|---|---|
| Meta selective SAL (S3pTA R7pTA) | 69.8 : 2.3 | 27 : 1 |
| Para selective SAL (S13pTA R15xTA) | 31.8 : 33.7 | 1 : 1 |
| (pTADDOL)POPh | 41.9 : 22.8 | 1.8 : 1 |

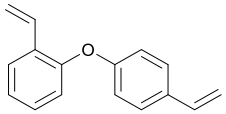


| | Yield (%) (ortho:meta) | ratio (ortho : para) |
|---|---|---|
| Ortho selective SAL (S13TA R15TA) | 73.8 : 2.1 | 35 : 1 |
| Para selective SAL (S13pTA R15xTA) | 34.9 : 28.7 | 1.2 : 1 |
| (xTADDOL)POPh | 48.1 : 20.5 | 2.3 : 1 |

**Figure 47.** Best site selectivities observed by supramolecular SALs on asymmetric hydroboration.

Throughout the preceding studies, the S13TAR15TA and S3pTAR7pTA catalysts showed excellent site selectivity for *ortho* and *meta*-substituents, respectively, during asymmetric hydroboration. What is remarkable is that the reactivity is catalyst controlled and one can direct reaction toward one site by picking the correct catalyst scaffold and ligating groups. Many of the examples of site-selective catalysis reported to date have reactivity issues (i.e., slow reaction or very low conversion). However, the catalysts reported herein are highly reactive; only 0.01 % of catalyst loading is required to effect complete reaction within 2 hours at room temperature. The catalysts are highly selective; swapping the supramolecular catalysts alter the ratio of *ortho* to *meta* hydroborated products from 18.2 : 1 (*ortho* : *meta*) to 1 : 23.4 (*ortho* : *meta*). Most research to date on site selective reactions relies upon peptide-based or small molecule catalysts. The current work using self-assembled supramolecular catalysts offers a distinctly different approach. From the observations that have made in the past[38], any

change that made to supramolecular SALs has some impacts in reactivity or selectivity, although there are some trends that can be drawn from the data. The trends are dependent on reaction conditions and despite the numerous hours of time devoted into understanding the structures of supramolecular SALs, unfortunately, at this point there is no successful formula that allows one to predict high reactivity and selectivity. Nonetheless, it is hoped that the development of supramolecular based site selective catalysts will stimulate the field of site-selective chemistry to gain a better understanding of the site-control factors.

**2.16 Experimental**

All reactions were carried out under an atmosphere of dry nitrogen. Dichloromethane, tetrahydrofuran (THF), and benzene were freshly distilled under the following conditions: benzene from sodium metal, THF from sodium/benzophenone and dichloromethane from calcium hydride. Pinacolborane was obtained from Aldrich Chemicals and distilled immediately prior to use. All other chemicals were used as received from the appropriate suppliers. NMR spectra were recorded on 300 or 400 MHz Bruker Avance NMR spectrometers using residue $CDCl_3$ ( = 7.26) for $^1H$ NMR and the central $CDCl_3$ resonance (δ 77.16 ppm) for $^{13}C$ NMR. $^1H$ NMR spectra are reported as follows (s = singlet, d = doublet, t = triplet, q = quartet, m = unresolved multiplet). Flash chromatography was carried out using EMD Silica Gel 60 Geduran®. Thin Layer Chromatography analyses were performed on Analtech Silica Gel HLF (0.25 mm) precoated analytical plates and visualized with use of handheld short wavelength UV light, iodine stain ($I_2$ and EMD Silica Gel 60 Geduran®) and/or vanillin stain (Ethanol, $H_2SO_4$, and vanillin). Data were recorded and analyzed with ChromPerfect chromatography software (version 5.1.0). Chiral capillary GC analysis was performed on a Shimadzu GC14APFSC with a J&W Scientific 30.0 m x 0.25 mm ID Cyclosil β column, column temperature program 120 $^oC$ (1 min hold) to 130 $^oC$ @ 1 $^oC$/min then 165$^oC$ @ 2 $^oC$/min). HRMS analyses were performed by the Nebraska Center for Mass Spectrometry. CD spectra were recorded on JASCO J-815 CD spectrometer.

**Preparation of SAL tethers**

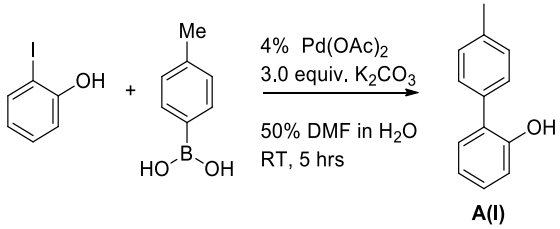


A(I)

***a*. Preparation of 4'methyl-[1,1'-biphenyl]-2ol (A(I)) (*adapted from the procedure of Cowart, et al.*)[1].** To a 500 mL round-bottom flask was added 2-iodophenol (11.0 g, 50.0 mmol), 4-toluyl boronic acid (7.48 g, 55.0 mmol), and palladium acetate (0.455 g, 2.03 mmol). The mixture was dissolved in DMF (150 mL) and stirred at room temperature. Potassium carbonate (20.7 g, 150 mmol) was dissolved in 150 mL of degassed water, added to the reaction over 10 min and the resulting mixture was stirred at room temperature (5 h). Tthe mixture was extracted with ethyl acetate (3 x 100 mL) and the combined organic layers dried ($MgSO_4$) and concentrated. The **A(I)** was purified by flash chromatography on silica (ca 150 g, 10:90 ethyl acetate: hexane) to give **A(I)** (8.30 g, 90 %) as clear oil: $^1$H NMR (400 MHz, $CDCl_3$) δ 7.40-7.38 (2H, m), 7.34-7.30 (2H, m), 7.28-7.25 (2H, m), 7.03-6.99 (2H, m), 2.45 ppm (3H, s); $^{13}$C NMR (100 MHz, $CDCl_3$) δ 152.7, 137.7, 134.3, 130.4, 130.1, 129.1, 129.1, 128.3, 121.0, 116.0, 21.3 ppm; HRMS (FAB, 3-NBA matrix) calcd. for $C_{13}H_{12}O$ ($M^+$), 184.0888; found, 184.0893 *m/z*.

4'methyl-[1,1'-biphenyl]-4ol **(B(I))** was prepared similarly from 4-toluyl boronic acid and 4-iodophenol

**B(I)** (8.90 g, 96 %) as clear oil: $^1$H NMR (400 MHz, $CDCl_3$) δ 7.44-7.35 (1H, m), 7.32-7.25 (5H, m), 7.05-7.00 (2H, m), 2.46 ppm (3H, s); 13C NMR (100 MHz, $CDCl_3$) δ 152.6, 139.1, 137.2, 130.3, 130.0, 129.9, 129.3, 129.1, 128.7, 126.2, 120.9, 115.9, 21.6

[1] M. Cowart, R. Faghih, M. P. Curtis, G. A. Gfesser, Y. L. Bennani, L. A. Black, L. Pan, K. C. Marsh, J. P. Sullivan, T. A. Esbenshade, G. B. Fox, A. A. Hancock , *J. Med. Chem.* **2005**, *48*, 38-55.

ppm; HRMS (FAB, 3-NBA matrix) calcd. for $C_{13}H_{12}O$ ($M^+$), 184.0888; found, 184.0886 *m/z*.

**General scheme for the synthesis of SALs and Rh-active catalyst.**[2]

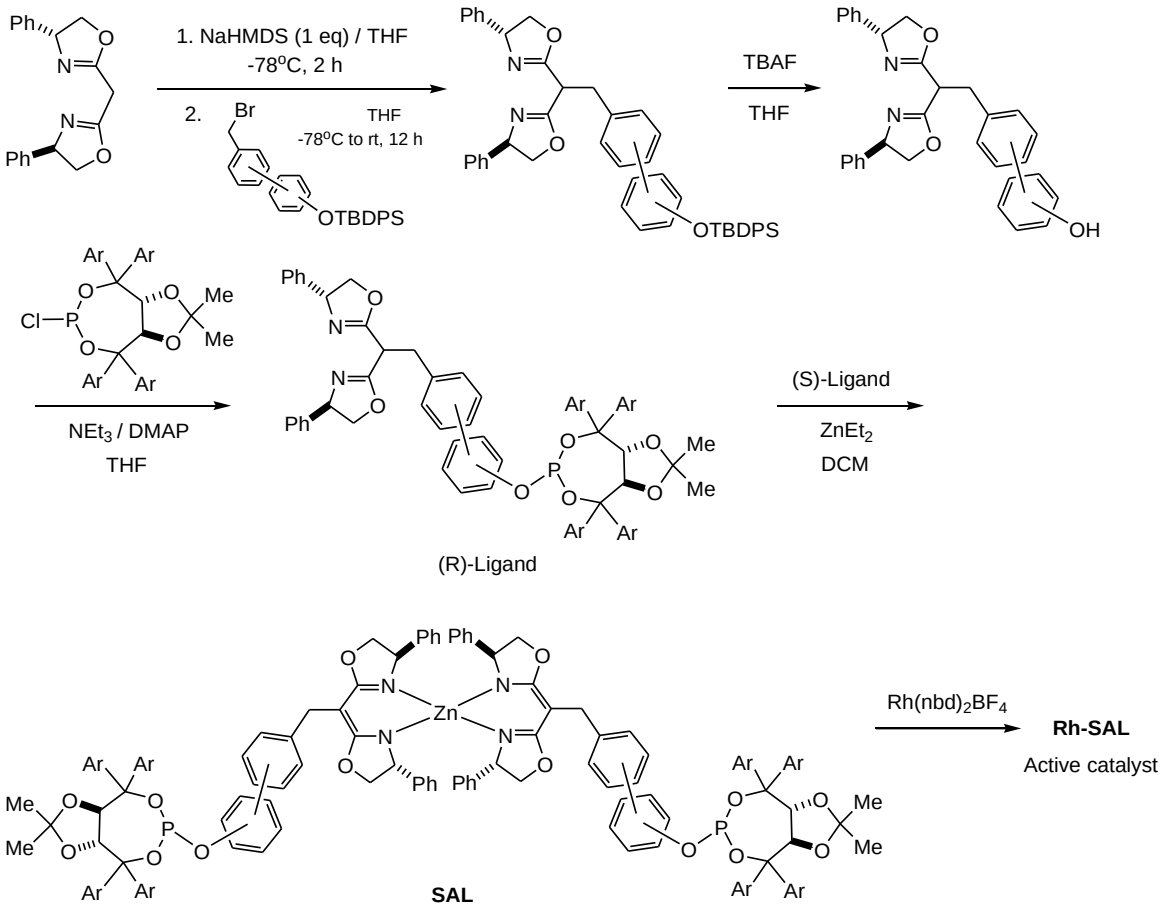


General procedure for the preparation of tether C-alkylated BOX derivatives.

Tethers 7OTBDPS, 15OTBDPS, 3OTBDPS, and 13OTBDPS were synthesized according to the literature procedures.[2,3,4]

[2] Moteki S. A., Takacs J. M. *Angew. Chem. Int Ed*., **2008**, 47(5), 894-897.
[3] Davies J. S., Higginbotham C. L., Tremeer E. J., Brown C., Treadgold R. C. *J. Chem. Soc. Perkin Trans 1*., **1992**, 22, 3043-3048.
[4] Moteki S. A., Toyama K., Liu Z., Ma J., Holmes A. E., Takacs J. M. *Chem. Commun*, **2012**, 48(2), 263-265.

(R)7OTBDPS was characterized in the previous work following the general procedure of BOX alkylation.[4]

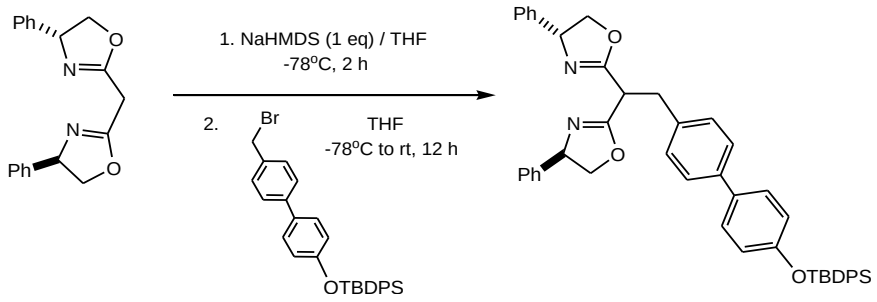


**(R)BOX** **R15OTBDPS** **(R)15OTBDPS**

**(R)15OTBDPS:** (8.51 g, 89 %) as a white solid: TLC analysis $R_f$ 0.30 (10:90 methanol:dichloromethane); mp 91-92 °C; [α]D $^{25}$ = +20.2 (c = 1.8, $CH_2Cl_2$); $^1$H NMR (400 MHz, $CDCl_3$) δ 7.80-7.73 (5H, m), 7.49-7.18 (19H, m), 7.17-7.08 (2H, m), 7.05-6.96 (2H, m), 6.69 (1H, d, *J* = 8.4 Hz), 5.26-5.15 (2H, m), 4.69 and 4.61 (2H, overlapping dd, *J*= 10.0, 10.3 Hz), 4.19-4.12 (1H, dd, *J* = 7.9, 7.9 Hz), 4.10-4.03 (2H, m), 3.53-3.40 (2H, m), 1.16 (s, 9H) ppm; $^{13}$C NMR (100 MHz, $CDCl_3$) δ 165.5 (2C), 155.3, 142.13, 142.05, 141.1, 138.5, 135.6, 133.9, 133.0, 130.1, 129.0, 128.9, 128.8, 128.7, 128.0, 127.9, 127.7, 127.65, 127.63, 127.5, 126.74, 126.72, 120.1, 202 75.5, 75.2, 69.73, 69.68, 41.5, 36.1, 26.7, 19.6 ppm; IR (neat) 3521, 2978, 2930 (C-H stretch), 1398, 1245, 1014 (C-H bend), 898 cm$^{-1}$; HRMS (FAB, 3-NBA matrix) calcd. for $C_{48}H_{47}N_2O_3Si$ [$(M+H)^+$], 727.3356; found, 727.3361 *m/z*.

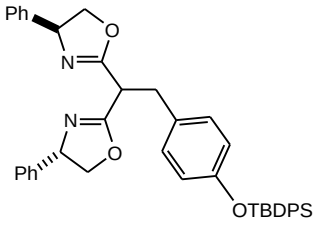


**(S)3OTBDPS:** (7.15 g, 84 %) as a white solid: TLC analysis $R_f$ 0.29 (10:90 methanol:dichloromethane); mp 76-77 °C; [α]D $^{25}$ = -16.4 (c = 0.2, $CH_2Cl_2$); $^1$H NMR (400 MHz, $CDCl_3$) δ7.76-7.73 (4H, m), 7.44-7.20 (17H, m), 7.06-7.05 (3H, m), 6.76-6.74 (1H, d, *J* = 6.4 Hz), 5.23-5.15 (2H, m), 4.66-4.59 (2H, m), 4.15-4.11 (1H, t, 8.4 Hz), 4.08-4.04 (1H,

t, 8.4 Hz), 3.98-3.93 (1H, t, 8.0 Hz), 3.36-3.25 (2H, m), 1.14 (9H, s) ppm; $^{13}$C NMR (100 MHz, $CDCl_3$) δ 165.6, 165.5, 154.4, 142.1, 142.0, 135.6, 133.0, 130.4, 129.9, 129.8, 128.7, 128.6, 127.8, 127.6, 127.5, 126.7, 126.6, 119.7, 75.3, 75.1, 69.6, 41.6, 35.2, 26.6, 19.5 ppm; IR (neat) 3523, 2983, 2937 (C-H stretch), 1398, 1245, 1016 (C-H bend), 887 $cm^{-1}$ ; HRMS (ESI) calcd. for $C_{42}H_{42}N_2O_3Si$ [(M+Na)], 673.2862; found, 673.2876 *m/z*.

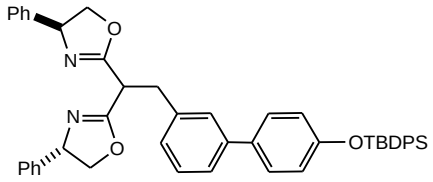


**(S)13OTBDPS:** (8.18 g, 86 %) as a white solid: TLC analysis $R_f$ 0.29 (10:90 methanol:dichloromethane); mp 82-83 °C; [α]D $^{25}$ = -42.3 (c = 0.3, $CH_2Cl_2$); $^1$H NMR (400 MHz, $CDCl_3$) δ 7.81-7.75 (4H, m), 7.48-7.22 (19H, m), 7.15-7.06 (2H, m), 7.01-6.95 (2H, m), 6.77-6.74 (1H, dd, *J* = 7.9 Hz, 7.9 Hz), 5.26-5.20 (2H, m), 4.67 and 4.64 (2H, overlapping dd, *J*= 10.2, 10.2 Hz), 4.20-4.15 (1H, dd, *J* = 8.3, 8.3 Hz), 4.08-4.00 (2H, m), 3.51-3.38 (2H, m), 1.15 (s, 9H) ppm; $^{13}$C NMR (100 MHz, $CDCl_3$) δ 165.51, 165.47, 156.0, 142.2, 142.1, 141.2, 138.5, 135.7, 135.7, 133.0, 130.1, 129.6, 129.5, 129.0, 128.9, 128.8, 128.7, 128.2, 128.0, 127.7, 127.6, 126.8, 126.5, 125.5, 120.0, 118.7, 75.5, 75.2, 69.8, 69.7, 41.6, 36.0, 26.7, 19.6 ppm; IR (neat) 3520, 2987, 2935 (C-H stretch), 1396, 1241, 1011 (C-H bend), 888 $cm^{-1}$; HRMS (FAB, 3-NBA matrix) calcd. for $C_{48}H_{47}N_2O_3Si$ [$(M+H)^+$], 727.3356; found, 727.3349 *m/z*.

**General procedure for the preparation of tether C-alkylated BOX hydroxyl derivatives.**

BOX hydroxyl derivatives (R)15OH, (S)3OH and (S)13OH were obtained according to literature[Error! Bookmark not defined.] via deprotection of silyl derivatives (R)15OTBDPS, (S)3OTBDPS, and (S)13OTBDPS by tetrabutylammonium fluoride (TBAF).

(R)7OH was characterized in the previous work.[4]

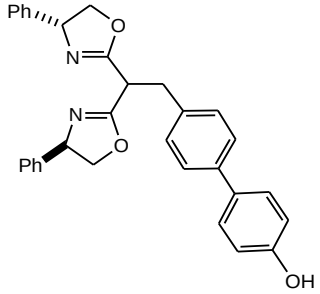


**(R)15OH:** (4.88 g, 91 %) as a white solid: TLC analysis $R_f$ 0.25 (10:90 methanol:dichloromethane); mp 110-111 $^{o}$C; [α]D $^{25}$ = 29.8 (c = 0.7, $CH_2Cl_2$); $^{1}$H NMR (400 MHz,$CDCl_3$) δ 7.45-7.43 (2H, m), 7.37-7.20 (13H, m), 6.99-6.96 (2H, m), 6.65 (2H, dd, *J* = 8.4, 8.4 Hz), 5.27-5.22 (2H, m), 4.75-4.69 (2H, m), 4.24 and 4.20 (2H, overlapping dd, *J* = 8.2, 7.8 Hz), 4.15-4.11 (1H, dd, *J* = 8.5, 8.5 Hz), 3.54-3.47 (2H, m) ppm; $^{13}$C NMR (100 MHz, $CDCl_3$) δ 166.2, 166.1, 156.7, 141.7, 141.5, 141.4, 137.9, 132.1, 129.0, 128.9, 128.8, 128.1, 127.9, 127.8, 127.3, 127.2, 126.8, 126.7, 125.3, 115.9, 75.6, 75.5, 69.3, 69.2, 41.4, 35.9 ppm; IR (neat) 3680, 2977 (C-H stretch), 2360, 1401, 1255, 1022 (C-H bend), 893 cm$^{-1}$; HRMS (FAB, 3-NBA matrix) calcd. for $C_{32}H_{29}N_2O_3$ [$(M+H)^+$], 489.2178; found, 489.2176 *m/z*.

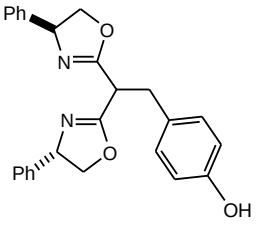


**(S)3OH:** (3.86 g, 85 %) as a white solid: TLC analysis $R_f$ 0.27 (10:90 methanol:dichloromethane); mp 84-85 $^{o}$C; [α]D $^{25}$ = -41.3 (c = 0.2, $CH_2Cl_2$); $^{1}$H NMR (400 MHz,$CDCl_3$) δ 7.31-7.25 (10H, m), 7.00-6.92 (4H, m), 6.30-6.28 (2H, d, *J* = 8.4 Hz), 5.25-

5.21 (2H, t, *J* = 8.8 Hz), 4.75-7.70 (2H, t, *J* = 9.2 Hz), 4.27-4.23 (1H, t, *J* = 8.0 Hz), 4.17-4.13 (2H, t, *J* = 8.0 Hz), 3.39-3.23 (2H, m) ppm; $^{13}$C NMR (100 MHz, $CDCl_3$) δ 166.1, 155.9, 141.7, 141.4, 129.8, 128.8, 127.9, 127.8, 127.7, 127.0, 126.6, 115.6, 75.7, 75.4, 69.3, 69.1, 41.8, 34.9 ppm; IR (neat) 3728, 2983, 2936 (C-H stretch), 1398, 1245, 1061 (C-H bend), 921 $cm^{-1}$; HRMS (ESI) calcd. for $C_{26}H_{24}N_2O_3$ [$(M+Na)^+$], 435.1685; found, 435.1679 *m/z*.

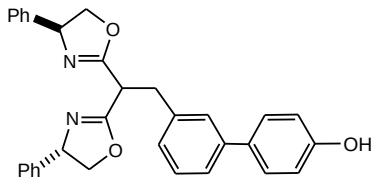


**(S)13OH:** (5.00 g, 93 %) as a white solid: TLC analysis $R_f$ 0.25 (10:90 methanol:dichloromethane); mp 113-114 $^0$C; [α]D $^{25}$ = -41.3 (c = 0.2, $CH_2Cl_2$); $^1$H NMR (400 MHz,$CDCl_3$) δ 7.53 (1H, s), 7.45 (1H, d, *J* = 7.6 Hz), 7.36-7.10 (12H, m), 7.05-7.02 (2H, m), 6.97-6.94 (2H, m), 6.68-6.65(1H, dd, *J* = 8.7, 8.1 Hz), 5.25-5.20 (2H, m), 4.72-4.67 (2H, m), 4.23-4.16 (2H, m), 4.10-4.07 (1H, dd, *J* = 8.3, 8.3 Hz), 3.56-3.43 (2H, m) ppm; $^{13}$C NMR (100 MHz, $CDCl_3$) δ 166.09, 166.07, 157.4, 142.3, 141.7, 141.6, 141.5, 137.9, 129.6, 129.0, 128.9, 128.8, 128.0, 127.8, 127.7, 126.73, 126.69, 126.4, 125.8, 118.5, 114.64, 114.59, 75.7, 75.4, 69.32, 69.25, 41.4, 35.8 ppm; IR (neat) 3689, 2987 (C-H stretch), 2362, 1405, 1250, 1028 (C-H bend), 895 $cm^{-1}$; HRMS (FAB, 3-NBA matrix) calcd. for $C_{32}H_{29}N_2O_3$ [$(M+H)^+$], 489.2178; found, 489.2171 *m/z*.

**General procedure for the synthesis of BOX derived TADDOL phosphites (*adapted from the procedure of Kranich et al.*).**[5]

(*R*,*R*)-(TADDOL)PCl and BOX derived TADDOL phosphites (R)15TA, (S)3pTA and (S)13TA were prepared according to the published procedure.[6]

Synthons and characterizations for (R)7pTA, (R)7xTA, (R)7TA were described in the previous work.[4]

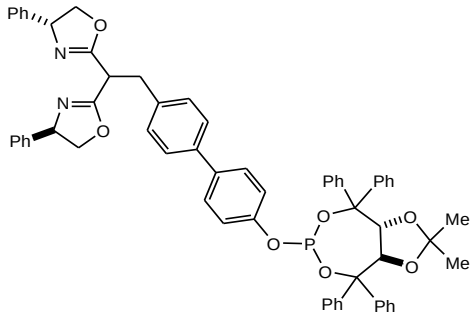


**(R)15TA:** (500 mg, 83 %) as a white solid: TLC analysis $R_f$ 0.18 (5:95 methanol:dichloromethane); mp 134-135 $^{o}$C; [α]D $^{25}$ = -98.5 (c = 0.4, $CH_2Cl_2$); $^{1}$H NMR (400 MHz, $CDCl_3$) δ 7.66-7.63 (2H, m), 7.59-7.52 (7H, m), 7.46-7.22 (24H, m), 7.04-7.02 (2H, m), 6.59 (2H, d, *J* = 7.9 Hz), 5.65 (1H, d, *J* = 8.2 Hz), 5.28 (2H, m), 5.15 (1H, d, *J* = 8.3 Hz), 4.73-4.68 (2H, m), 4.22-4.17 (1H, dd, *J* = 8.2, 8.2 Hz), 4.16-4.09 (2H, m), 3.59-3.46 (2H, m), 0.85 (3H, s), 0.70 (3H, s) ppm; $^{13}$C NMR (100 MHz, $CDCl_3$) δ 165.5 (2C), 151.7 (d, $J_{CP}$ = 5.6 Hz), 145.97, 145.93, 142.0, 141.97, 141.3, 140.9, 138.5, 136.0, 129.2, 129.0, 128.95, 128.8, 128.7, 128.67, 128.2, 128.1, 128.0, 127.8, 127.7, 127.6, 127.5, 127.4, 127.3, 127.2, 127.19, 127.17, 126.7, 126.67, 126.64, 126.4, 125.3, 120.1, 120.06, 113.1, 86.8 (d, $J_{CP}$ = 11.7 Hz), 85.2 (d, $J_{CP}$ = 6.9 Hz), 82.3 (d, $J_{CP}$ = 9.9 Hz), 80.2 (d, $J_{CP}$ = 5.2 Hz), 75.5, 75.2, 69.7, 69.6, 41.4, 36.0, 26.7, 26.4 ppm; $^{31}$P NMR (162 MHz, $CDCl_3$) δ 126.4 ppm; IR (neat) 3674, 2972, 2929(C-H stretch), 1399, 1251, 1059 (C-H bend), 895 cm$^{-1}$; HRMS (FAB, 3-NBA matrix) calcd. for $C_{63}H_{56}N_2O_7P$ [$(M+H)^+$], 983.3825; found, 983.3789 *m/z*.

[5] Kranich R., Eis K., Geis O., Muhle S., Bats J. W., Schmalz H. *Chem Eur J*., **2000**, 6(15), 2874-2894.
[6] Sakaki J., Schweizer W. B., Seebach D. *Helv Chim Acta*, **1993**, 76(7), 2654-2665.

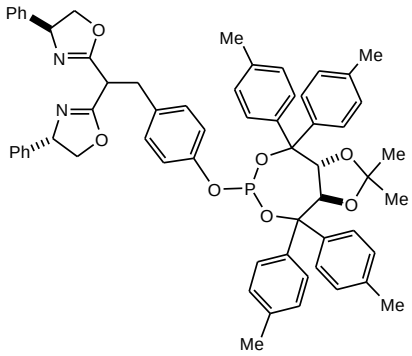

**(S)3pTA:** (487 mg, 83 %) as a white solid: TLC analysis $R_f$ 0.19 (5:95 methanol:dichloromethane); mp 116-118 $^{o}$C; [α]D $^{25}$ = -58.9 (c = 0.4, $CH_2Cl_2$); $^{1}$H NMR (400 MHz, $CDCl_3$) δ 7.49-7.17 (18H, m), 7.11-6.98 (10H, m), 6.59 (2H, d, *J* = 8.0 Hz), 5.48 (1H, d, *J* = 7.6 Hz), 5.25-5.19 (2H, m), 5.10 (1H, d, *J* = 8.4 Hz), 4.69-4.63 (2H, m), 4.18 (1H, t, *J* = 8.4 Hz), 4.06 (1H, t, *J* = 8.0 Hz), 4.00 (1H, t, *J* = 8.0 Hz), 3.34-3.33 (2H, m), 2.37-2.28 (12H, m), 0.79 (3H, s), 0.74 (3H, s) ppm; $^{13}$C NMR (100 MHz, $CDCl_3$) δ 165.5, 151.7, 151.6, 146.0, 145.9, 142.03, 141.97, 141.3, 140.9, 138.5, 136.0, 129.2, 129.01, 128.95, 128.72, 128.67, 128.2, 128.1, 128.0, 127.81, 127.7, 127.6, 127.5, 127.4, 127.3, 127.22, 127.19, 127.17, 126.72, 126.67, 126.64, 125.4, 120.2, 120.1, 113.1, 86.8, 86.7, 85.2, 85.1, 82.3, 80.23, 80.16, 77.4, 77.1, 76.8, 75.5, 75.2, 69.7, 69.6, 41.4, 36.0, 26.7, 26.4 ppm; $^{31}$P NMR (162 MHz, $CDCl_3$) δ 126.35 ppm; IR (neat) 3449, 3011, 2896 (C-H stretch), 1398, 1237, 1080 (C-H bend), 890 $cm^{-1}$; HRMS (ESI) calcd. for $C_{61}H_{59}N_2O_7P$ [$(M+Na)^+$], 985.3958; found, 985.3964 *m/z*.

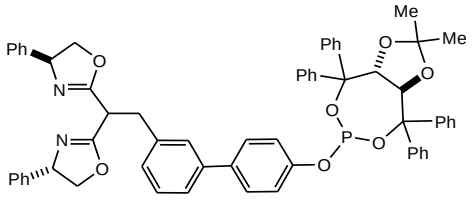

**(S)13TA:** (540 mg, 90 %) as a white solid: TLC analysis $R_f$ 0.19 (5:95 methanol:dichloromethane); mp 123-124 $^{o}$C; [α]D $^{25}$ = -53.9 (c = 0.6, $CH_2Cl_2$); $^{1}$H NMR (400 MHz, $CDCl_3$) δ 7.64-7.62 (2H, m), 7.57-7.51 (7H,m), 7.47 (1H, s), 7.41-7.16 (24H, m), 7.05-7.03 (2H, m), 6.72 (1H, s), 6.57-6.55 (1H, dd, *J* = 7.8, 1.2 Hz), 5.67 (1H, d, *J* = 8.3 Hz), 5.27 and 5.23 (2H, overlapping dd, *J* = 8.2, 8.2 Hz), 5.14 (1H, d, *J* = 8.3 Hz), 4.71 and 4.66

(2H, overlapping dd, *J* = 9.9, 9.6 Hz), 4.22-4.19 (1H, dd, *J* = 8.2, 5.6 Hz), 4.17-4.08 (2H, m), 3.59-3.48 (2H, m), 0.86 (3H, s), 0.65 (3H, s) ppm; $^{13}$C NMR (100 MHz, $CDCl_3$) δ 165.44, 165.39, 152.5 (d, $J_{CP}$ = 6.6 Hz), 146.0, 142.1, 142.04, 141.96, 141.4, 141.3, 140.7, 138.5, 129.5, 129.3, 129.1, 128.9, 128.7, 128.69, 128.65, 128.2, 128.1, 127.9, 127.7, 127.6, 127.5, 127.4, 127.3, 127.2, 127.1, 126.7. 126.6, 126.4, 125.6, 122.1, 121.9, 118.6, 118.5, 118.5, 118.4, 113.0, 86.6 (d, $J_{CP}$ = 11.5 Hz), 85.2 (d, $J_{CP}$ = 7.9 Hz), 82.3 (d, $J_{CP}$ = 10.1 Hz), 80.2 (d, $J_{CP}$ = 4.5 Hz), 75.4, 75.2, 69.7, 69.6, 41.5, 36.0 26.7, 26.4 ppm; $^{31}$P NMR (162 MHz, $CDCl_3$) δ 126.35 ppm; IR (neat) 3680, 2982, 2924 (C-H stretch), 1398, 1244, 1062 (C-H bend), 896 $cm^{-1}$; HRMS (FAB, 3-NBA matrix) calcd. for $C_{63}H_{56}N_2O_7P$ [$(M+H)^+$], 983.3825; found, 983.3833 *m/z*.

**General procedure for the preparation of heterodimeric BOX SALs.**

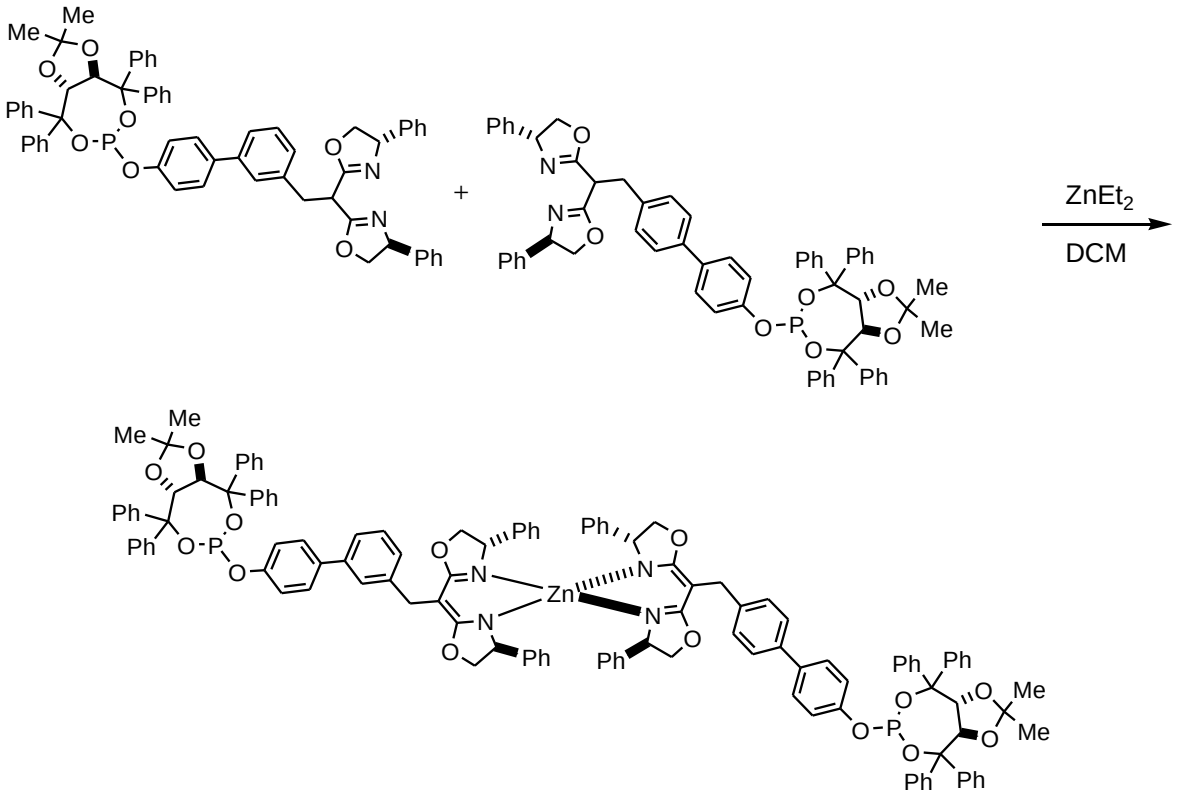


**Zn(R15TA, S13TA)**

**Zn(R15TA, S13TA):** Solutions of (**R)15TA** (200 mg, 0.20 mmol) in DCM and (**S)13TA** (200 mg, 0.20 mmol) in DCM were mixed and a solution of $ZnEt_2$ (25.9 mg, 0.20 mmol) in DCM was added. After the solution was stirred at room temperature (ca 5 mins), the solvent was evaporated and residue dried under vacuum (< 1 torr) to give **Zn(R15TA, S13TA)** (398 mg, 99 %) as a white solid: mp 187-188 $^0$C; [α]D $^{25}$ = -90.5 (c = 0.1, $CH_2Cl_2$); $^1$H NMR (400 MHz, $CDCl_3$) δ 7.47-7.42 (16H, m), 7.34-7.12 (52H, m), 7.03-6.98, (8H, m), 5.06 (4H, s), 4.02-3.98, (4H, m), 3.86-3.80 (4H, m), 3.76 (4H, s), 3.37-3.33 (4H, m), 0.99 (6H, s), 0.37 (3H, s), 0.35 (3H, s) ppm; $^{13}$C NMR (100 MHz, $CDCl_3$) δ 169.9, 149.0, 148.9, 145.7, 145.6, 145.3, 144.1, 143.7, 141.50, 141.45, 140.8, 140.7, 135.14, 135.05, 135.0, 134.9, 130.8, 129.3, 129.1, 128.81, 128.76, 128.4, 128.3, 127.8, 127.7, 127.6, 127.43, 127.39, 127.4, 127.3, 127.2, 127.1,, 127.0, 125.0, 124.2, 122.4, 122.2, 113.24, 113.1, 85.8, 85.7, 83.1, 83.0, 82.3, 82.1, 80.9, 80.8, 72.9, 65.6, 64.4, 64.3, 53.5, 31.1, 27.2,

25.79, 25.75; $^{31}$P NMR (162 MHz, $CDCl_3$) δ 133.7, ppm; HRMS (FAB) calcd for $C_{126}H_{108}N_4O_{14}P_2Zn$ [$(M+H)^+$], 2027.6709; found: 2027.6664 *m/z*.

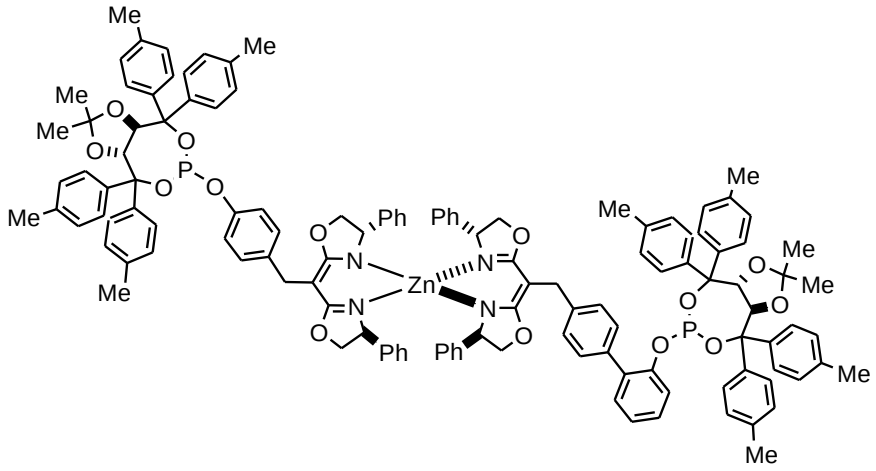


**Zn(R7pTA, S3pTA):** (407 mg, 99 %) as a white solid: mp 172-173 $^0$C; [α]D $^{25}$ = -57.5 (c = 0.3, $CH_2Cl_2$); $^1$H NMR (400 MHz, $CDCl_3$) δ 7.54-7.00 (62H, m), 6.72 (2H, d, *J* = 10.8 Hz), 5.43 (1H, d, *J* = 11.2 Hz), 5.32 (2H, s), 5.14 (1H, d, *J* = 10.8 Hz), 5.02-4.99 (2H, m), 4.07-4.00 (4H, m), 3.89-3.82 (4H, m), 3.77 (2H, s), 3.59 (2H, s), 3.38-3.34 (3H, m), 2.35-2.29 (24H, m), 1.07 (3H, s), 0.87 (3H, s), 0.69 (3H, s), 0.36 (3H, s) ppm; $^{13}$C NMR (100 MHz, $CDCl_3$) δ 169.91, 169.81, 149.03, 144.17, 144.12, 143.69, 143.54, 143.30, 143.13, 142.64, 140.08, 138.66, 138.58, 138.15, 137.19, 137.07, 136.80, 136.74, 136.58, 136.47, 135.11, 134.94, 130.75, 129.30, 128.87, 128.82, 128.69, 128.43, 128.30, 128.01, 127.94, 127.85, 127.76, 127.49, 127.23, 127.14, 127.07, 126.86, 124.16, 119.77, 119.67, 112.78, 112.72, 85.81, 85.68, 85.23, 85.13, 84.38, 82.96, 82.54, 82.38, 82.21, 81.21, 80.79, 72.93, 65.65, 65.03, 64.70, 53.44, 27.33, 26.87, 26.41, 25.75, 21.15, 21.03, 21.01 ppm; $^{31}$P NMR (162 MHz, $CDCl_3$) δ 134.92, 131.08 ppm; HRMS (ESI) calcd for $C_{124}H_{113}N_4O_{14}P_2Zn$ [$(M+Li)^+$], 2065.7570; found: 2065.8459 *m/z*.

**General procedure for the synthesis of vinylphenoxystyrenes.**

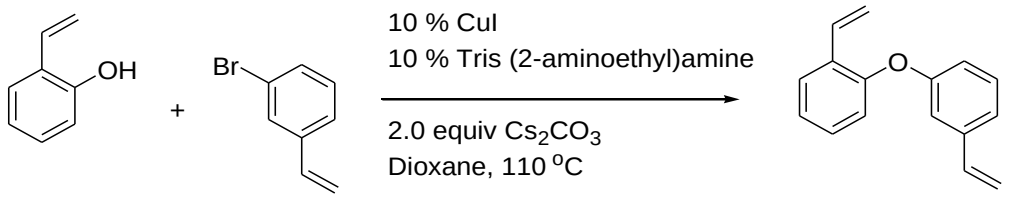


**2-(3-Vinylphenoxy)styrene:** (***adapted from the procedure of N. R. Jogdand et al.***).[7] Into a 50 mL round bottom flask dioxane (3 mL), tris (2-aminoethyl)amine (0.085 mmol), CuI (0.085 mmol), 3-bromostyrene (0.85 mmol), 2-hydroxylstyrene (1.02 mmol), and $Cs_2CO_3$ (2.04 mmol) were added. The reaction mixture was stirred at RT for 30 min and heated to 110 $^oC$ for 24 h. The reaction mixture was cooled to room temperature and water (~15 mL) was added. The crude mixture was extracted with ethyl acetate and the organic layer was dried ($MgSO_4$) and concentrated. Chromatography on silica gel (10:90 ethyl acetate:hexane) gave the product as a clear oil (1.06 g, 56 %): TLC analysis $R_f$ = 0.95 (10:90 ethyl acetate:hexane); $^1H$ NMR (400 MHz, $CDCl_3$) δ 7.68-7.66 (1H, dd, *J* = 7.6, 1.6 Hz), 7.32-7.26 (2H, m), 7.21-7.16 (2H, m), 7.10-7.02 (2H, m), 6.98-6.96 (1H, dd, *J* = 8.4, 1.2 Hz), 6.88-6.85 (1H, ddd, *J* = 8.4, 2.4, 0.8 Hz), 6.75-6.71 (1H, dd, *J* = 17.6, 10.8 Hz), 5.88-5.83 (1H, dd, *J* = 17.6, 0.9 Hz), 5.79-5.74 (1H, dd, *J* = 17.6, 0.8 Hz), 5.35-5.32 (1H, dd, *J* = 10.8, 1.2 Hz), 5.31-5.29 (1H, dd, *J* = 10.8, 0.8 Hz) ppm; $^{13}C$ NMR (100 MHz, $CDCl_3$) δ 158.2, 153.6, 139.5, 136.4, 131.0, 129.8, 129.1, 126.7, 124.1, 120.86, 120.1, 117.2, 115.5, 115.5, 114.7 ppm; IR (neat) 3062, 3031 (aromatic C-H stretch), 1830, 1627, 1570, 1481, 1450 (C=ring stretch), 1248 (C-O-C stretch), 911, 794, 763 $cm^{-1}$ (out of plane C-H bend); HRMS (ESI) calcd for $C_{16}H_{14}O$ [$(M+Na)^+$], 245.0942; found: 245.0954 *m/z*.

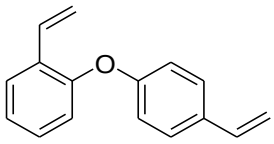


**2-(4-Vinylphenoxy)styrene:** Yield (61%) as a clear oil: TLC analysis $R_f$ = 0.95 (10:90 ethyl acetate:hexane); $^1H$ NMR (400 MHz, $CDCl_3$) δ 7.68-7.66 (1H, dd, *J* = 8.0, 2.0 Hz), 7.33-

[7] Jogdand N. R., Shingate B. B., Shingare M. S. *Tetrahedron Lett*, **2009**, 50(28), 4019-4021.

7.26 (2H, m), 7.21-7.16 (2H, m), 7.10-7.02 (2H, m), 6.98-6.96 (1H, dd, *J* = 8.4, 0.6 Hz), 6.88-6.85 (1H, ddd, *J* = 8.4, 2.4, 0.8 Hz), 6.75-6.68 (1H, dd, *J* = 17.6, 10.8 Hz), 5.88-5.83 (1H, dd, *J* = 17.6, 1.2 Hz), 5.79-5.74 (1H, dd, *J* = 17.6, 0.8 Hz), 5.35-5.32 (1H, dd, *J* = 10.8, 1.6 Hz), 5.31-5.29 (1H, dd, *J* = 10.8, 0.8 Hz) ppm; $^{13}$C NMR (100 MHz, $CDCl_3$) δ 158.2, 153.6, 139.5, 136.4, 131.0, 129.8, 129.1, 126.7, 124.1, 120.9, 120.1, 117.2, 115.52, 115.48, 114.6 ppm; IR (neat) 3091, 3046, 3031 (C-H stretch), 1594, 1581, 1523, 1498 (C=C ring stretch), 1236, 1231 (C-O-C stretch), 1027, 1047, 932 (alkene), 859, 791 (C-H bend), 739, 718 (C=C bend); HRMS (EI) calcd for $C_{16}H_{14}O$ [$M^+$], 222.1045; found: 222.1040 *m/z*.

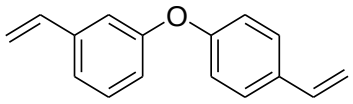


**3-(4-Vinylphenoxy)styrene:** Yield (60%) as a clear oil: TLC analysis $R_f$ = 0.95 (10:90 ethyl acetate:hexane); $^1$H NMR (400 MHz, $CDCl_3$) δ 7.50-7.46 (2H, m), 7.39 (1H, t, *J* = 8 Hz), 7.28-7.26 (1H, m), 7.22 (1H, t, *J* = 2.0 Hz), 7.11-7.08 (2H, m), 6.82 (1H, t, *J* = 10.4 Hz), 6.77 (1H, t, *J* = 10.4 Hz), 5.84 (1H, dd, *J* = 17.6, 0.8 Hz), 5.79 (1H, dd, *J* = 17.6, 0.8 Hz), 5.37 (1H, dd, *J* = 6.8, 0.4 Hz), 5.31 (1H, dd, *J* = 10.8, 0.8 Hz) ppm; $^{13}$C NMR (100 MHz, $CDCl_3$) δ 157.50, 157.07, 139.66, 136.38, 136.15, 132.98, 129.95, 1297.74, 123.36, 121.58, 118.94, 118.46, 116.68, 114.81, 114.74, 113.00 ppm; IR (neat) 3087, 3056, 3044 (C-H stretch), 1598, 1574, 1503, 1486 (C=C ring stretch), 1232, 1215 (C-O-C stretch), 1024, 1011, 905 (alkene), 837, 788 (C-H bend), 733, 712 (C=C bend); HRMS (EI) calcd for $C_{16}H_{14}O$ [$M^+$], 222.1045; found: 222.1042 *m/z*.

**General procedure employed for the preparative scales reactions**

A solution of **(*R*)SAL1** (19.6 x $10^{-3}$ mmol) and (*S*)**SAL2** (19.6 x $10^{-3}$ mmol) in DCM (6 mL) was combined with a solution of $ZnEt_2$ (1.28 mg, 19.6 x $10^{-3}$ mmol) in DCM (3 mL) and stirred at ambient temperature (RT, ca. 5 min.) and then a solution of $Rh(nbd)_2BF_4$ (7.4 mg, 19.6 x $10^{-3}$ mmol) in DCM (2 mL) was added. The resulting mixture was stirred at room temperature (0.5 h) after which the volatile solvent was removed under vacuum. The residue was dissolved in THF (6 mL), stirred (0.5 h) and then 0.3mL aliquot of the solution was transferred into a 50 mL round bottom flask. The substrate (132 mg, 0.98mmol) in THF (2.0 mL) was added. The resulting mixture was cooled (0 $^oC$) and a solution of pinacolborane (150.5 mg, 1.18 mmol) in THF (3.0 mL) added by syringe pump. The reaction mixture was gradually warmed to RT and stirred (12 h). The mixture was quenched by the addition of MeOH (10 mL), aq. NaOH (3.0 *M*, 15 mL), and aq. $H_2O_2$ (1 mL of a 30% solution) and stirred (1 h, RT). The solution was extracted with ethyl acetate (3 x 15 mL) and the combined organics were dried ($MgSO_4$), filtered and concentrated *in vacuo*. The crude product was purified by chromatography on silica (10:90 ethyl acetate:hexane) to give three products:

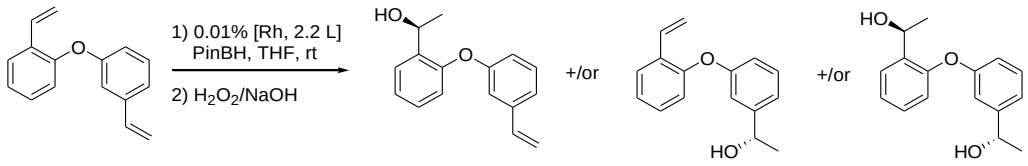


**(*S*)-Mono HB (ortho)** as a clear oil: TLC analysis $R_f$ = 0.37 (10:90 ethyl acetate:hexane); [α]D $^{25}$ = -57.5 (c = 0.3, $CH_2Cl_2$); $^1$H NMR (400 MHz, $CDCl_3$) δ 7.68-7.65 (1H, dd, *J* = 7.6, 2.0 Hz), 7.34-7.15 (5H, m), 6.95-6.92 (2H, m), 6.77-6.69 (1H, dd, *J* = 17.6, 11.2 Hz), 5.82-5.78 (1H, dd, *J* = 17.6, 0.4 Hz), 5.34-5.26 (2H, m), 3.38 (1H, *J* = 4.4 Hz), 1.58 (3H, d, *J* = 6.8 Hz) ppm; $^{13}$C NMR (100 MHz, $CDCl_3$) δ 157.8, 153.4, 139.7, 137.2, 136.4, 130.0, 128.4, 126.8, 124.2, 121.3, 118.9, 117.7, 116.1, 114.9, 65.1, 31.7 ppm; IR (neat) 3339 (O-H stretch), 2972, 2894 (C-H stretch), 1573, 1480, 1448 (C=ring stretch), 1238 (C-O-C stretch), 1067, 762 (out of plane C-H bend), 698 $cm^{-1}$ (out of plane ring C=C bend); HRMS (ESI) calcd for $C_{16}H_{16}O_2$ [$(M+Na)^+$], 263.1048; found: 263.1049 *m/z*.

**(*S*)-Mono HB (meta)** as a clear oil: TLC analysis $R_f$ = 0.33 (10:90 ethyl acetate:hexane); [α]D $^{25}$ = -57.5 (c = 0.3, $CH_2Cl_2$), Chiral HPLC analysis: Chiralcel-OD, isopropanol:hexanes=10:90, flow rate 0.9= mL/min; showed peaks at 22.4 minutes ( 93% (*S*)) and 30.2 minutes (7% (*R*)), $^1$H NMR (400 MHz, $CDCl_3$) δ 7.66-7.63 (1H, dd, *J* = 7.6, 1.6 Hz), 7.32-7.24 (2H, m), 7.19-7.15 (1H, dt, *J* = 7.6, 0.8 Hz), 7.11-6.93 (4H, m), 6.85-6.84 (1H, ddd, *J* = 8.0, 2.4, 0.8 Hz), 5.85-5.79 (1H, dd, *J* = 17.6, 1.2 Hz), 5.32-5.29 (1H, dd, *J* = 11.2, 1.2 Hz), 1.91 (1H, d, *J* = 3.6 Hz), 1.49 (3H, d, *J* = 6.4 Hz) ppm; $^{13}$C NMR (100 MHz, $CDCl_3$) δ 158.1, 153.5, 147.9, 131.0, 129.8, , 129.1, 126.7, 124.2, 120.1, 119.6, 116.6, 115.4, 114.8, 70.1, 25.2 ppm; IR (neat) 3337 (O-H stretch), 2966, 2881 (C-H stretch), 1563, 1485, 1444 (C=ring stretch), 1231 (C-O-C stretch), 1059, 760 (out of plane C-H bend), 696 cm$^{-1}$ (out of plane ring C=C bend); HRMS (ESI) calcd for $C_{16}H_{16}O_2$ [$(M+Na)^+$], 263.1048; found: 263.1049 *m/z*.

**(*S,S*)-o,m-Diol** as a clear oil: TLC analysis $R_f$ = 0.12 (10:90 ethyl acetate:hexane); [α]D $^{25}$ = -57.5 (c = 0.3, $CH_2Cl_2$), $^1$H NMR (400 MHz, $CDCl_3$) δ 7.54-7.52 (1H, dd, *J* = 7.6, 1.6 Hz), 7.31-7.27 (1H, t, *J* = 7.6 Hz), 7.24-7.19 (1H, tt, *J* = 7.6, 1.2 Hz), 7.17-7.13 (1H, t, *J* = 7.2 Hz), 7.09-7.05 (1H, t, *J* = 7.2 Hz), 7.01-6.99 (1H, q, *J* = 2.0 Hz), 6.88-6.84 (2H, m), 5.19-5.13 (1H, m), 4.83-4.78 (1H, m), 2.84-2.77 (1H, dd, *J* = 21.6, 4.4 Hz), 2.69-2.65 (1H, dd, *J* = 14.4, 3.2 Hz), 1.50-1.48 (3H, dd, *J* = 6.4, 2.0 Hz), 1.46-1.43 (3H, dd, *J* = 6.4, 5.6 Hz) ppm; $^{13}$C NMR (100 MHz, $CDCl_3$) δ 157.55 (d, *J* = 3.6 Hz), 153.35 (d, *J* = 3.6 Hz), 148.2, 136.8 (d, *J* = 4.0 Hz), 129.83 (d, *J* = 0.8 Hz), 128.42, 126.70, 124.80 (d, *J* = 2.4 Hz), 120.15 (d, *J* = 3.2 Hz), 119.96 (d, *J* = 3.6 Hz), 116.98, 115.18 (d, *J* = 11.2 Hz), 69.89 (d, *J* = 2.4 Hz), 65.36 (d, *J* = 3.2 Hz), 25.17 (d, *J* = 2.4 Hz), 23.8 ppm; IR (neat) 3323 (O-H stretch), 2970, 2927 (C-H stretch), 1578, 1481, 1445 (C=ring stretch), 1236 (C-O-C stretch), 1069, 861, 753 (out of plane C-H bend), 697 cm$^{-1}$ (out of plane ring C=C bend) ; HRMS (ESI) calcd for $C_{16}H_{18}O_3$ [$(M+Na)^+$], 281.1154; found: 281.1158 *m/z*.

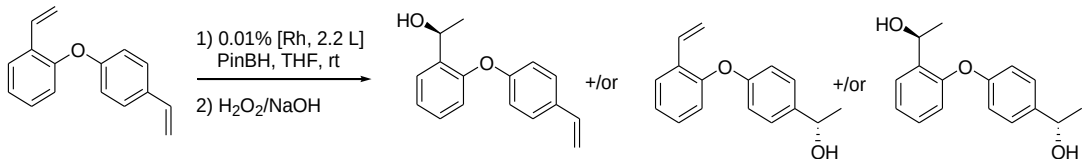


**(*S*)-Mono HB (ortho)** as a clear oil: TLC analysis $R_f$ = 0.37 (10:90 ethyl acetate:hexane); [α]D $^{25}$ = -150 (c = 0.2, $CH_2Cl_2$), $^1$H NMR (400 MHz, $CDCl_3$) δ 7.60 (1H, dd, *J* = 6.0, 1.6 Hz), 7.42-7.40 (2H, m), 7.28-7.23 (1H, m), 7.21-7.17 (1H, m), 6.99-6.96 (2H, m), 6.91 (1H, dd, *J* = 8.0, 1.2 Hz), 6.74 (1H, dd, *J* = 17.6, 10.8 Hz), 5.72 (1H, dd, *J* = 17.2, 0.8 Hz), 5.27-5.21 (2H, m), 2.76 (1H, d, *J* = 3.6 Hz), 1.54 (3H, d, *J* = 6.4 Hz) ppm; $^{13}$C NMR (100 MHz, $CDCl_3$) δ 157.13, 153.39, 136.92, 136.01, 132.83, 128.42, 127.71, 126.73, 124.17, 118.99, 118.27, 112.97, 65.35, 23.94 ppm; IR (neat) 3346 (O-H stretch), 2972, 2900 (C-H methylene stretch), 1629, 1601, 1584, 1504, 1483, 1449 (C=C ring stretch), 1246, 1179, (C-O-C stretch), 1165, 1111, 1074 (alkene), 873, 838, 750 (C-H aromatic bend), 692 (C=C aromatic bend); HRMS (EI) calcd for $C_{16}H_{16}O_2$ [$M^+$], 240.1150; found: 240.1150 *m/z*.

**(*S*)-Mono HB (para)** as a clear oil: TLC analysis $R_f$ = 0.33 (10:90 ethyl acetate:hexane); [α]D $^{25}$ = -135.9 (c = 0.2, $CH_2Cl_2$), $^1$H NMR (400 MHz, $CDCl_3$) δ 7.66 (1H, dd, *J* = 8.0, 1.6 Hz), 7.35-7.33 (2H, m), 7.26 (1H, dt, *J* = 8.0, 1.6 Hz), 7.20-7.18 (1H, m), 7.04 (1H, dd, *J* = 28.8, 6.4 Hz), 6.97-6.93 (3H, m), 5.84 (1H, dd, *J* = 17.6, 1.2 Hz), 5.32 (1H, dd, *J* = 11.2, 1.2 Hz), 4.91-4.85 (1H, m), 2.32 (1H, d, *J* = 3.6 Hz), 1.51 (3H, d, *J* = 6.8 Hz) ppm; $^{13}$C NMR (100 MHz, $CDCl_3$) δ 157.24, 153.65, 140.19, 130.96, 129.81, 129.07, 126.94, 126.69, 124.17, 120.10, 117.72, 115.49, 69.87, 25.16 ppm; IR (neat) 3317 (O-H stretch), 2977, 2936 (C-H methylene stretch), 1636, 1589, 1511, 1487 (C=C ring stretch), 1246, 1218 (C-O-C stretch), 1110, 1089 (alkene), 841, 781 (C-H aromatic bend), 657 (C=C aromatic bend); HRMS (EI) calcd for $C_{16}H_{16}O_2$ [$M^+$], 240.1150; found: 240.1231 *m/z*.

**(*S,S*)-o,p-Diol** as a clear oil: TLC analysis $R_f$ = 0.12 (10:90 ethyl acetate:hexane); [α]D $^{25}$ = -50.0 (c = 0.2, $CH_2Cl_2$), $^1$H NMR (400 MHz, $CDCl_3$) δ 7.55 (1H, dd, *J* = 7.2, 1.6 Hz), 7.36-7.34 (2H, m), 7.25-7.21 (1H, m), 7.18-7.14 (1H, m), 6.98-6.95 (2H, m), 6.85 (1H, dd, *J* =

8.0, 1.2 Hz), 5.20 (1H, q, *J* = 6.4 Hz), 4.90 (1H, q, *J* = 6.4 Hz), 2.41 (1H, s), 2.08 (1H, s), 1.54-1.50 (6H, m) ppm; $^{13}$C NMR (100 MHz, $CDCl_3$) δ 156.55, 153.67, 140.72, 136.57, 128.42, 126.98, 126.65, 123.96, 118.76, 118.29, 69.85, 65.62, 25.19, 23.75 ppm; IR (neat) 3317 (O-H stretch), 2974 (C-H methylene stretch), 1603, 1506, 1484 (C=C ring stretch), 1234, 1216, 1180 (C-O-C stretch), 1075 (C-O stretch), 899, 873 (C-C aromatic stretch), 699 (C=C bend); HRMS (EI) calcd for $C_{16}H_{18}O_3$ [$M^+$], 258.1256; found: 258.1289 *m/z*.

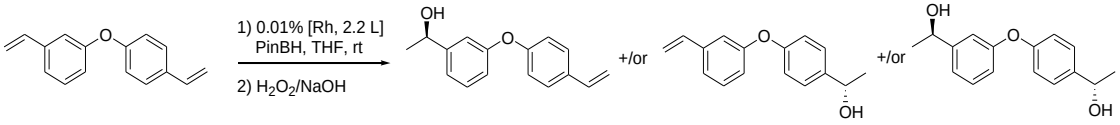


**(*S*)-Mono HB (meta)** as a clear oil: TLC analysis $R_f$ = 0.33 (10:90 ethyl acetate:hexane); [α]D $^{25}$ = -31.2 (c = 0.4, $CH_2Cl_2$);$^1$H NMR (400 MHz, $CDCl_3$) δ 7.41 (2H, d, *J* = 8.8 Hz), 7.33 (1H, t, *J* = 8.0 Hz), 7.13 (1H, d, *J* = 7.6 Hz), 7.08-7.07 (1H, m), 7.01-6.99 (2H, m), 6.94 (1H, dd, *J* = 8.0, 2.4 Hz), 6.73 (1H, dd, *J* = 18.0, 11.2 Hz), 5.70 (1H, d, *J* = 17.6 Hz), 5.24 (1H, d, *J* = 11.2 Hz), 4.90-4.84 (1H, m), 2.27 (1H, d, *J* = 3.6 Hz), 1.49 (3H, d, *J* = 6.4 Hz) ppm; $^{13}$C NMR (100 MHz, $CDCl_3$) δ 157.34, 156.86, 136.04, 132.94, 129.84, 127.64, 120.31, 118.94, 117.71, 115.90, 112.95, 70.02, 25.23 ppm; IR (neat) 3343 (O-H stretch), 2970, 2907 (C-H methylene stretch), 1631, 1600, 1587, 1508, 1491, 1438 (C=C ring stretch), 1245, 1174, (C-O-C stretch), 1171, 1107, 1071 (alkene), 876, 839, 755 (C-H aromatic bend), 698 (C=C aromatic bend); HRMS (EI) calcd for $C_{16}H_{16}O_2$ [$M^+$], 240.1150; found: 240.1143 *m/z*.

**(*S*)-Mono HB (para)** as a clear oil: TLC analysis $R_f$ = 0.30 (10:90 ethyl acetate:hexane); [α]D $^{25}$ = -21.6 (c = 0.4, $CH_2Cl_2$), $^1$H NMR (400 MHz, $CDCl_3$) δ 7.38-7.35 (2H, m), 7.31 (1H, t, *J* = 4.0 Hz), 7.18 (1H, d, *J* = 7.6 Hz), 7.10 (1H, t, *J* = 2.0 Hz), 7.03-7.00 (2H, m), 6.94-6.91 (1H, m), 6.70 (1H, d, *J* = 17.6, 11.2 Hz), 5.75 (1H, d, *J* = 17.2 Hz), 5.29 (1H, d, *J* = 10.8 Hz), 4.92 (1H, t, *J* = 6.4 Hz), 1.91 (1H, s), 1.53 (3H, d, *J* = 6.4 Hz) ppm; $^{13}$C NMR (100 MHz,

$CDCl_3$) δ 157.48, 156.53, 140.69, 139.52, 136.28, 129.81, 126.92, 121.38, 118.81, 118.26, 116.49, 114.68, 69.96, 25.18 ppm; IR (neat) 3327 (O-H stretch), 2967, 2929 (C-H methylene stretch), 1601, 1576, 1505, 1485 (C=C ring stretch), 1245, 1215 (C-O-C stretch), 1112, 1086 (alkene), 835, 788 (C-H aromatic bend), 697 (C=C aromatic bend); HRMS (EI) calcd for $C_{16}H_{16}O_2$ [$M^+$], 240.1150; found: 240.1160 *m/z*.

**(*S,S*)-m,p-Diol** as a clear oil: TLC analysis $R_f$ = 0.12 (10:90 ethyl acetate:hexane); [α]D $^{25}$ = -20.5 (c = 0.4, $CH_2Cl_2$); $^1$H NMR (400 MHz, $CDCl_3$) δ 7.29-7.24 (3H, m), 7.07 (1H, d, *J* = 7.6 Hz), 7.02-7.01 (1H, m), 6.96-6.93 (2H, m), 6.86 (1H, dd, *J* = 8.0, 2.4 Hz), 4.84-4.77 (2H, m), 2.90 (1H, s), 2.82 (1H, s), 1.45 (3H, d, *J* = 6.4 Hz), 1.43 (3H, d, *J* = 6.4 Hz) ppm; $^{13}$C NMR (100 MHz, $CDCl_3$) δ 157.40, 156.29, 148.21, 140.83, 129.72, 126.93, 120.21, 118.80, 117.46, 115.81, 69.83, 69.71, 25.18, 25.12 ppm; IR (neat) 3337 (O-H stretch), 2985, 2921 (C-H methylene stretch), 1621, 1504, 1492 (C=C ring stretch), 1228, 1208 (C-O-C stretch), 1074 (C-O stretch), 888 (C-C aromatic stretch), 696 (C=C bend); HRMS (EI) calcd for $C_{16}H_{18}O_3$ [$M^+$], 258.1256; found: 258.1247 *m/z*.

**General procedure employed for the preparation of Mosher ester for the determination of absolute configuration.**

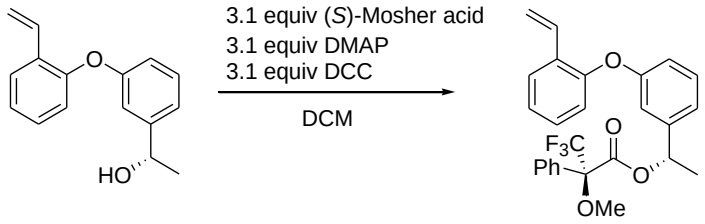


**(*S*)-Mosher ester:** Into a 25 mL round bottom flask dichloromethane (1.3 mL), DCC (53 mg, 0.25 mmol), DMAP (32 mg, 0.25 mmol), the alcohol (20 mg, 0.083 mmol), and (S)-Mosher acid (60.4 mg, 0.25 mmol) were added. The reaction mixture was stirred at RT overnight. The white precipitate was filtered through a cotton plug. Volatile solvent was removed under reduced pressure. Chromatography on silica gel (10:90 ethyl acetate:hexane) gave the target product (27 mg, 72 %) as a clear oil: TLC analysis $R_f$ = 0.63 (20:80 ethyl acetate:hexane); [α]D $^{25}$ = -3.5 (c = 0.2, $CH_2Cl_2$); $^1$H NMR (400 MHz, $CDCl_3$) δ 7.64-7.62 (1H, dd, *J* = 7.6, 1.6 Hz), 7.48-7.6.88 (15H, m), 6.12-6.07 (1H, q, *J* = 6.4 Hz), 5.82-5.78 (1H, d, *J* = 17.6 Hz), 5.30-5.27 (1H, d, *J* = 10.8 Hz), 3.47 (1H, s), 1.57-1.55 (1H, d, *J* = 6.4 Hz) ppm; $^{13}$C NMR (100 MHz, $CDCl_3$) δ 165.78, 158.21, 153.19, 142.16, 139.85, 132.29, 130.80, 129.96, 129.55, 129.07, 128.37, 127.34, 126.72, 124.38, 120.53, 120.17, 117.45, 115.55, 115.42, 74.48, 55.77, 55.42, 34.94, 25.47, 24.71, 21.81 ppm; $^{19}$F NMR (376.5 MHz, $CDCl_3$) δ -71.42 ppm; IR (neat) 2930, 2854, 2116, 1748, 1505, 1488, 1450 (C=ring stretch), 1248 (C-O-C stretch), 1123 cm$^{-1}$; HRMS (HR-EI) calcd for $C_{26}H_{23}F_3O_4$ [M$^+$], 456.1548; found: 456.1554 *m/z*.

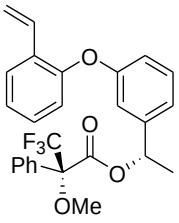


**(*R*)-Mosher ester** was prepared the same way described in preparation of Mosher ester. Yield (70%) as a clear oil: TLC analysis $R_f$ = 0.63 (20:80 ethyl acetate:hexane); [α]D $^{25}$ =

3.0 (c = 0.2 $CH_2Cl_2$); $^1$H NMR (400 MHz, $CDCl_3$) δ 7.64-7.62 (1H, dd, *J* = 7.6, 1.6 Hz), 7.46-7.34 (5H, m), 7.28-7.21 (2H, m), 7.18-7.14 (1H, td, *J* = 7.2, 0.8 Hz), 6.99-6.93 (2H,m), 6.88-6.84 (3H, m), 6.10-6.05 (1H, q, *J* = 6.4 Hz), 5.82-5.78 (1H, dd, *J* = 17.6, 1.2 Hz), 5.31-5.28 (1H, dd, *J* = 10.8, 1.2 Hz), 3.36-3.35 (3H, d, *J* = 1.2 Hz), 1.64-1.62 (3H, d, *J* = 6.8 Hz) ppm; $^{13}$C NMR (100 MHz, $CDCl_3$) δ 165.60, 158.03, 153.27, 142.21, 134.16, 130.85, 129.83, 129.56, 129.05, 128.33, 127.31, 126.68, 124.25, 120.38, 120.01, 117.37, 115.48, 115.41, 74.50, 55.77, 55.48, 34.94, 25.47, 24.71, 22.13 ppm; $^{19}$F NMR (376.5 MHz, $CDCl_3$) δ -71.65 ppm; IR (neat) 2931, 2855, 2114, 1744, 1500, 1488, 1451 (C=ring stretch), 1247 (C-O-C stretch), 1120 $cm^{-1}$; HRMS (HR-EI) calcd for $C_{26}H_{23}F_3O_4$ [$M^+$], 456.1548; found: 456.1558 *m/z*.

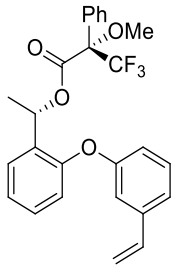


**(*R*)-Mosher ester** was prepared the same way described in preparation of Mosher ester. Yield (74%) as a clear oil: TLC analysis $R_f$ = 0.63 (20:80 ethyl acetate:hexane); [α]D $^{25}$ = 4.9 (c = 0.2, $CH_2Cl_2$); $^1$H NMR (400 MHz, $CDCl_3$) δ 7.53-7.51 (2H, d, *J* = 7.1 Hz), 7.46-7.37 (4H, m), 7.26-7.18 (3H, m), 7.10-7.09 (1H, t, *J* = 2.0 Hz), 7.07-7.03 (1H, td, *J* = 7.5, 0.9 Hz), 6.91-6.89 (1H, dd, *J* = 8.1, 1.6 Hz), 6.86-6.84 (1H, m), 6.73-6.66 (1H, dd, *J* = 17.6, 10.9 Hz), 6.55-6.50 (1H, q, *J* = 6.5 Hz), 5.78-5.73 (1H, d, *J* = 17.6 Hz), 5.30-5.28 (1H, d, *J* = 10.9 Hz), 3.59 (3H, d, *J* = 0.9 Hz), 1.68-1.66 (3H, d, *J* = 6.6 Hz) ppm; $^{13}$C NMR (100 MHz, $CDCl_3$) δ 165.42, 157.20, 153.83, 139.59, 136.21, 131.51, 129.87, 129.53, 129.18, 128.32, 127.40, 126.64, 123.49, 121.63, 118.31, 118.16, 116.66, 114.77, 69.98, 55.77, 55.50, 34.94, 25.47, 24.71, 21.40 ppm; $^{19}$F NMR (376.5 MHz, $CDCl_3$) δ -71.50 ppm; IR (neat) 2935, 2857, 2111, 1740, 1507, 1489, 1450 (C=ring stretch), 1249 (C-O-C stretch), 1128 $cm^{-1}$; HRMS (HR-EI) calcd for $C_{26}H_{23}F_3O_4$ [$M^+$], 456.1548; found: 456.1551 *m/z*.

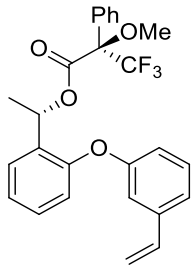


**(*S*)-Mosher ester** was prepared the same way described in preparation of Mosher ester. Yield (74%) as a clear oil: TLC analysis $R_f$ = 0.63 (20:80 ethyl acetate:hexane); [α]D $^{25}$ = -7.5 (c = 0.2, $CH_2Cl_2$); $^1$H NMR (400 MHz, $CDCl_3$) δ 7.53-7.51 (2H, d, *J* = 6.8 Hz), 7.47-7.35 (5H, m), 7.32-7.30 (1H, d, *J* = 7.8 Hz), 7.26-7.23 (1H, m), 7.19-7.08 (2H, m), 6.91-6.85 (2H, m), 6.72-6.65 (1H, dd, *J* = 17.6, 10.9 Hz), 6.58-6.53 (1H, m), 5.76-5.71 (1H, dd, *J* = 17.6, 0.7 Hz), 5.29-5.27 (1H, d, *J* = 10.8 Hz), 3.54 (3H, d, *J* = 1.2 Hz), 1.61-1.60 (3H, d, *J* = 6.5 Hz) ppm; $^{13}$C NMR (100 MHz, $CDCl_3$) δ 165.59, 157.15, 153.79, 139.83, 136.19, 132.32, 131.34, 129.88, 129.52, 129.31, 128.35, 127.53, 126.99, 123.60, 121.63, 118.26, 118.20, 116.52, 114.78, 69.82, 55.76, 55.38, 34.93, 25.47, 24.70, 21.05 ppm; $^{19}$F NMR (376.5 MHz, $CDCl_3$) δ -71.46 ppm IR (neat) 2931, 2859, 2117, 1741, 1507, 1488, 1450 (C=ring stretch), 1248 (C-O-C stretch), 1120 cm$^{-1}$; HRMS (HR-EI) calcd for $C_{26}H_{23}F_3O_4$ [$M^+$], 456.1548; found: 456.1553 *m/z*.

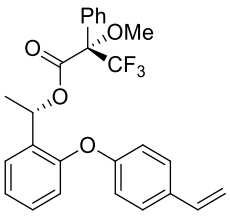


**(*R*)-Mosher ester** was prepared the same way described in preparation of Mosher ester. Yield (72%) as a clear oil: TLC analysis $R_f$ = 0.63 (20:80 ethyl acetate:hexane); [α]D $^{25}$ = 5.2 (c = 0.2, $CH_2Cl_2$); $^1$H NMR (400 MHz, $CDCl_3$) δ 7.59-7.58 (1H, m), 7.52-7.50 (2H, m), 7.46-7.38 (5H, m), 7.26-7.24 (1H, m), 7.19-7.17 (1H, d, *J* = 8.5 Hz), 7.07-7.03 (1H, t, *J* = 8.0 Hz), 6.98-6.96 (2H, m) 6.75-6.71 (1H, dd, *J* = 17.6, 10.8 Hz), 6.86-6.80 (1H, dd, *J* = 16.0, 16.0 Hz), 6.75-6.68 (1H, dd, *J* = 17.6, 10.9 Hz), 6.54-6.47 (1H, dd, *J* = 14.8, 6.6 Hz), 5.71-5.67 (1H, d, *J* = 17.6 Hz), 5.24-5.21 (1H, d, *J* = 10.9 Hz), 3.59 (3H, s), 1.67-1.65 (3H, d,

*J* = 6.5 Hz) ppm; $^{13}$C NMR (100 MHz, $CDCl_3$) δ 165.41, 156.72, 153.70, 135.98, 133.09, 132.31, 131.64, 129.53, 129.18, 128.75, 128.31, 127.65, 127.40, 126.65, 123.62, 119.09, 118.88, 118.38, 113.01, 69.96, 55.77, 55.50, 34.94, 25.47, 24.71, 21.41 ppm; $^{19}$F NMR (376.5 MHz, $CDCl_3$) δ -71.49 ppm; IR (neat) 2939 2858, 2114, 1740, 1508, 1484, 1451 (C=ring stretch), 1249 (C-O-C stretch), 1125 $cm^{-1;}$ HRMS (HR-EI) calcd for $C_{26}H_{23}F_3O_4$ [$M^+$], 456.1548; found: 456.1571 *m/z*.

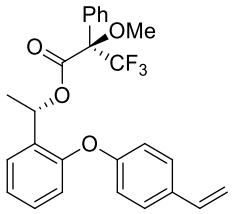


**(*S*)-Mosher ester** was prepared the same way described in preparation of Mosher ester. Yield (70%) as a clear oil: TLC analysis $R_f$ = 0.63 (20:80 ethyl acetate:hexane); [α]D $^{25}$ = -22.7 (c = 0.2, $CH_2Cl_2$); $^1$H NMR (400 MHz, $CDCl_3$) δ 7.53-7.52 (1H, m), 7.47-7.37 (5H, m), 7.27-7.17 (2H, m), 7.15-7.09 (1H, q, *J* = 7.8 Hz), 6.99-6.94 (2H, m), 6.90-6.84 (1H, dd, *J* = 15.8, 8.2 Hz), 6.75-6.68 (1H, dd, *J* = 17.6, 10.9 Hz), 6.59-6.54 (1H, dd, *J* = 13.9, 7.1 Hz), 5.71-5.67 (1H, d, *J* = 17.6 Hz), 5.24-5.21 (1H, d, *J* = 10.9 Hz), 3.55 (3H, s), 1.61-1.59 (3H, d, *J* = 6.4 Hz) ppm; $^{13}$C NMR (100 MHz, $CDCl_3$) δ 165.41, 156.72, 153.70, 135.98, 133.09, 132.31, 131.64, 129.53, 129.18, 128.75, 128.31, 127.65, 127.40, 126.65, 123.62, 119.09, 118.88, 118.38, 113.01, 69.96, 55.77, 55.50, 34.94, 25.47, 24.71, 21.41 ppm; $^{19}$F NMR (376.5 MHz, $CDCl_3$) δ -71.43 ppm; IR (neat) 2938, 2851, 2117, 1745, 1507, 1489, 1459 (C=ring stretch), 1247 (C-O-C stretch), 1121 $cm^{-1;}$ HRMS (HR-EI) calcd for $C_{26}H_{23}F_3O_4$ [$M^+$], 456.1548; found: 456.1543 *m/z*.

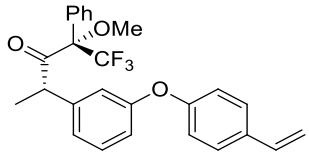


**(*R*)-Mosher ester** was prepared the same way described in preparation of Mosher ester. Yield (70%) as a clear oil: TLC analysis $R_f$ = 0.63 (20:80 ethyl acetate:hexane); [α]D $^{25}$ = 7.6 (c = 0.2, $CH_2Cl_2$); $^1$H NMR (400 MHz, $CDCl_3$) δ 7.65-7.63 (1H, dd, *J* = 7.7, 1.4 Hz), 7.46-

7.32 (7H, m), 7.27-7.16 (3H, m), 7.01-6.86 (3H, m), 6.12-6.07 (1H, q, *J* = 6.6 Hz), 5.84-5.79 (1H, dd, *J* = 17.7, 1.1 Hz), 5.32-5.29 (1H, dd, *J* = 11.1, 1.1 Hz), 3.58-3.57 (3H, d, *J* = 0.9 Hz), 1.66-1.64 (3H, d, *J* = 6.6 Hz) ppm; $^{13}$C NMR (100 MHz, $CDCl_3$) δ 165.64, 157.94, 153.22, 134.26, 132.23, 130.81, 129.50, 129.07, 128.76, 128.38, 128.28, 127.89, 127.63, 127.30, 126.70, 124.41, 120.33, 117.42, 115.56, 74.59, 55.77, 55.50, 34.94, 25.47, 24.71, 21.97 ppm; $^{19}$F NMR (376.5 MHz, $CDCl_3$) δ -71.65 ppm; IR (neat) 2932, 2855, 2116, 1744, 1501, 1493, 1451 (C=ring stretch), 1245 (C-O-C stretch), 1124 $cm^{-1;}$ HRMS (HR-EI) calcd for $C_{26}H_{23}F_3O_4$ [$M^+$], 456.1548; found: 456.1549 *m/z*.

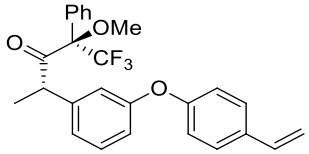


**(*S*)-Mosher ester** was prepared the same way described in preparation of Mosher ester. Yield (71%) as a clear oil: TLC analysis $R_f$ = 0.63 (20:80 ethyl acetate:hexane); [α]D $^{25}$ = -13.6 (c = 0.2, $CH_2Cl_2$); $^1$H NMR (400 MHz, $CDCl_3$) δ 7.65-7.64 (1H, dd, *J* = 7.7, 1.6 Hz), 7.46-7.44 (2H, m), 7.40-7.32 (5H, m), 7.27-7.24 (1H, dd, *J* = 7.6, 1.3 Hz), 7.21-7.16 (1H, m), 7.01-6.89 (4H, m), 6.15-6.10 (1H, q, *J* = 6.6 Hz), 5.83-5.79 (1H, dd, *J* = 17.7, 1.1 Hz), 5.31-5.28 (1H, dd, *J* = 11.1, 1.2 Hz), 3.49-3.49 (3H, d, *J* = 0.9 Hz), 1.60-1.58 (3H, d, *J* = 6.6 Hz) ppm; $^{13}$C NMR (100 MHz, $CDCl_3$) δ 165.84, 158.10, 153.15, 139.83, 130.79, 129.99, 129.52, 129.08, 128.34, 128.09, 127.65, 127.39, 127.30, 126.71, 124.47, 120.41, 117.49, 115.57, 74.52, 55.76, 55.35, 34.94, 25.47, 24.70, 21.59 ppm; $^{19}$F NMR (376.5 MHz, $CDCl_3$) δ -71.44 ppm; IR (neat) 2931, 2850, 2117, 1744, 1507, 1488, 1455 (C=ring stretch), 1249 (C-O-C stretch), 1120 $cm^{-1;}$ HRMS (HR-EI) calcd for $C_{26}H_{23}F_3O_4$ [$M^+$], 456.1548; found: 456.1547 *m/z*.

**2.17 References:**


1. S. S. Gujral, S. Khatri, P. Riyal, V. Gahlot. "Suzuki Cross Coupling Reaction- A Review". *Indo Global Journal of Pharmaceutical Science*, **2012**, 2, 351
2. H. C. Brown, P. V. Ramachandran. "Recent advances in the boron route to asymmetric synthesis", *Pure & Appl. Chem*. **1994**, 66, 201
3. T. Hayashi, "*Comprehensive Asymmetric Catalysis*", Springer, New York, **1999**, 1, 349
4. a) D. S. Matteson, K. M. Sadhu and M. L. Peterson, "99% Chirally Selective synthesis via pinanediol boronic esters: insect pheromones, diols, and an amino alcohol". *J. Am. Chem. Soc*., **1986**, 108, 810; b) E. Hupe, M. I. Calaza and P. Knochel, "Highly Diastereoselective [3+2] Cycloadditions between Nonracemic p-Tolylsulfinimines and Iminoesters: An Efficient Entry to Enantiopure Imidazolidines and Vicinal Diaminoalcohols". *Chem.–Eur. J.,* **2003**, 9, 2789; c) D. Imao, B. W. Glasspoole, V. S. Laberge and C. M. Crudden, "Cross Coupling Reactions of Chiral Secondary Organoboronic Esters With Retention of Configuration". *J. Am. Chem. Soc*., **2009**, 131, 5024–5025; d) D. L. Sandrock, L. JeanGérard, C.-y. Chen, S. D. Dreher and G. A. Molander, "Stereospecific Cross-Coupling of Secondary Alkyl β-Trifluoroboratoamides". *J. Am. Chem. Soc.,* **2010**, 132, 17108–17110; e) T. Ohmura, T. Awano and M. Suginome, "Stereospecific Suzuki-Miyaura Coupling of Chiral α-(Acylamino) benzylboronic Esters with Inversion of Configuration". *J. Am. Chem. Soc.*, **2010**, 132, 13191–13192.
5. R. Wilczynski, L. G. Sneddon, "Transition metal catalyzed reactions of alkynes and boron hydrides: synthesis of 2-(cis-2-butenyl)pentaborane(9) and its conversion into monocarbon carboranes". *J. Am. Chem. Soc*. **1980**, 102, 2857
6. D. Manning, H. Noth, *Angew. Chem. Int. Ed. Engl*. **1985**, 24, 878
7. T. Hayashi, Y. Matsumoto, Y. Ito, "Catalytic asymmetric hydroboration of styrenes". *J. Am. Chem. Soc*. **1989**, 111, 3426

8. F. C. Fu, D. A. Evans, A. R. Muci. “Metal-Catalyzed Hydroboration Reactions”, Advances in Catalytic Processes, **1995**, Doyle, M. P. Ed.; JAI Press, Inc.: Greenwich, CT; pp. 95-121
9. D. A. Evans, A. R. Muci, R. Sturmer, “Samarium(III)-Catalyzed Hydroboration of Olefins with Catecholborane. A General Approach to the Synthesis of Boronate Esters”. *J. Org. Chem.*, **1993**, *58*, 5307-5309
10. D. A. Evans, G. C. Fu, A. H. Hoveyda, “Rhodium(I)- and Iridium(I)-Catalyzed Hydroboration Reactions: Scope and Synthetic Applications”. *J. Am. Chem. Soc.*, **1992**, *14*, 6671-6679
11. D. A. Evans, G. C. Fu, B. A. Anderson, “Mechanistic Study of the Rhodium(I)-Catalyzed Hydroboration Reaction”. *J. Am. Chem. Soc.*, **1992**, *114*, 6679-6685
12. D. A. Evans, G. C. Fu, “Amide-Directed, Iridium-Catalyzed Hydroboration of Olefins: The Documentation of Regio- and Stereochemical Control in Cyclic and Acyclic Systems”. *J. Am. Chem. Soc.*, **1991**, *113*, 4042-4043
13. D. A. Evans, G. C. Fu, “The Rhodium-Catalyzed Hydroboration of Olefins: A Mechanistic Investigation”. *J. Org. Chem.*, **1990**, *55*, 2280-2282
14. D. A. Evans, G. C. Fu, A. H. hoveyda, “Rhodium(I)-Catalyzed Hydroboration of Olefins. The Documentation of Regio- and Stereochemical Control in Cyclic and Acyclic Systems”. *J. Am. Chem. Soc.*, **1988**, *110*, 6917-6918
15. D. A. Evans, J. Bartroli, T. Godel, “Acyclic Diastereoselection in the Hydroboration Process. Documented Cases of 1,3-Asymmetric Induction”. *Tetrahedron Lett.*, **1982**, *23*, 4577-4580
16. K. Burgess, W. A. van der Donk, “On Titanium-Promoted Hydroborations of Alkenes by Borohydride and by Catecholborane”, *Oganometallics*, **1994**, 13, 3616
17. K. Burgess, W. A. van der Donk, “The importance of phosphine-to-rhodium ratios in enantioselective hydroboration”, *Inorganica Chimica Acta*, **1994**, 220, 93
18. K. Burgess, W. A. van der Donk, “Hydroborations of alkenes catalyzed by titanium complexes”, *Tetrahedron Letters*, **1993**, 34, 6817

19. K. Burgess, M. Jaspars, “Hydroboration reactions mediated by bis(mesityl)niobium: beware of the Trojan horse”, *Tetrahedron Letters*, **1993**, 34, 6813
20. K. Burgess, M. Jaspars, “Ruthenium-catalyzed hydroboration of alkenes”, *Organometallics*, **1993**, 12, 4197
21. K. Burgess, W. A. Van der Donk, M. J. Ohlmeyer, “Enantioselective hydroboration catalyzed by rhodium (1+) complexes”, **1991**, 2, 613
22. K. Burgess, M. J. Ohlmeyer, “Transition-metal promoted hydroboration of alkenes, emerging methodology for organic transformations”, *Chem. Rev*. **1991**, 91, 1179
23. K. Burgess, W. A. Van der Donk, M. B. Jarstfer, M. J. Ohmeyer, “Further evidence for the role of dn-pn bonding in rhodium-mediated hydroboration”, *J. Am. Chem. Soc*, **1991**, 113, 6139
24. K. Burgess, W. A. Van der Donk, A. M. Kook, “On deuterium-labeling studies for probing rhodium-catalyzed hydroboration reactions”, *J. Org. Chem*, **1991**, 56, 2949
25. K. Burgess, J. Cassidy, M. J. Ohlmeyer, “Substrate-controlled diastereoselectivities in catalyzed and uncatalyzed hydroboration of acyclic allylic alcohol derivatives: secondary orbital effects involving dn-pn interactions”, *J. Org. Chem*. **1991**, 56, 1020
26. K. Burgess, M. J. Ohlmeyer, “Manipulation of substrate-controlled diastereoselectivities in hydroboration of acyclic allylamine derivatives”, *J. Org. Chem*. **1991**, 56, 1027
27. K. Burgess, M. J. Ohlmeyer, “Substrate-controlled diastereoselectivities in catalyzed and uncatalyzed hydroboration of allylic amine derivatives”, *Tetrahedron Letters*, **1989**, 30, 5857
28. K. Burgess, M. J. Ohlmeyer, “On catalyzed and uncatalyzed hydroboration of chiral allylic alcohols and amines”, *Tetrahedron Letters*, **1989**, 30, 5861

29. K. Burgess, M. J. Ohlmeyer, “Diastereocontrol in rhodium-catalyzed hydroboration of chiral acyclic allylic alcohol derivatives”, *Tetrahedron Letters*, **1989**, 30, 395
30. K. Burgess, M. J. Ohlmeyer, “Enantioselective hydroboration mediated by homochiral rhodium catalysts”, *J. Org. Chem*. **1988**, 53, 5178
31. A. C. Maxwell, S.P. Flanagan, R. Goddard, P. J. Guiry, “Rhodium-catalysed hydroboration employing new quinazolinap ligands; an investigation into electronic effects”, *Tetrahedron: Asymmetry*, **2010**, 21, 1458
32. A. M. Carroll, T. P. O’Sullivan, P. J. Guiry, “The development of enantioselective Rhodium-catalyzed hydroboration of olegins”, Advanced Synthesis & Catalysis, **2005**, 347, 609
33. D. J. Connolly, P. M. Lacey, M. McCarthy, C. P. Saunders, A. M. Carroll, R. Goddard, P. J. Guiry, “Preparation and Resolution of a Modular Class of Axially Chiral Quinazoline-Containing Ligands and their Application in Asymmetric Rhodium-Catalyzed Olefin Hydroboration”, *J. Org. Chem*, **2004**, 69, 6572
34. M. MacCarthy, P. J. Guiry, M. W. “Hooper, Enantioselective hydroboration of olefins catalyzed by cationic rhodium complexes of 2-phenylquinazolin-4-yl-2-(diphenylphosphino)naphthalene”, *Chem. Commun*, **2000**, 14, 1333
35. R. Corberan, N. W. Mszar, A. H. Hoveyda, “NHC-Cu-Catalyzed Enantioselective Hydroboration of Acyclic and Exocyclic 1,1-Disubstituted Aryl Alkenes”, *Angew. Chem. Int. Ed*. **2011**, 50, 7079
36. H. Jang, A. R. Zhugralin, Y. Lee, A. H. Hoveyda, “Highly Selective Methods for Synthesis of Internal (α-) Vinylboronates through Efficient NHC-Cu-Catalyzed Hydroboration of Terminal Alkynes. Utility in Chemical Synthesis and Mechanistic Basis for Selectivity”, *J. Am. Chem. Soc*. **2011**, 133, 7859
37. Y. Lee, A. H. Hoveyda, “Efficient Boron-Copper Additions to Aryl-Substituted Alkenes Promoted by NHC-Based Catalysts. Enantioselective Cu-Catalyzed Hydroboration Reactions”, *J. Am. Chem. Soc*. **2009**, 131, 3160

38. C. J. Lata, C.M. Crudden, “Hydroboration revisited: The dramatic effect of Lewis acids and counterions on the outcome of transition-metal catalyzed hydroboration”, *J. Am. Chem. Soc*, **2010**, 132, 131-137.
39. D. R. Edwards, Y. B. Hleba, C. Lata, L. Calhoun, C. M. Crudden, “Regioselectivity of the Rhodium Catalyzed Hydroboration of Vinyl Arenes: Electronic Twists and Mechanic Shifts”, *Angew. Chem. Int. Ed*, **2007**, 46, 7799-7802.
40. C.M. Crudden, Y.B. Hleba, A.C. Chen, “Regio and Enantiocontrol in the Room Temperature Hydroboration of Vinyl Arenes”, *J. Am. Chem. Soc*, **2004**, 126, 9200-9201.
41. C.M. Crudden and D. Edwards “Catalytic Asymmetric Hydroboration: Recent Advances and Applications in Carbon-Carbon Bond Forming Reactions”, *Eur. J. Org. Chem*. **2003**, 4695-4712.
42. M. Fairgrieve, C.M. Crudden, “Asymmetric Hydroboration-Homologation: Towards the Synthesis of Gliflumide”, *In Catalysis of Organic Reactions*, **2003**, 40, 509.
43. A.C. Chen, L. Ren and C.M. Crudden, “Catalytic Asymmetric Carbon-Carbon Bond Forming Reactions. 1. Preparation of Optically Enriched 2-Aryl Propionic Acids by a Catalytic Asymmetric Hydroboration/Homologation Sequence”, *Chem. Commun*, **1999**, 611-612.
44. S. J. Geier, S. A. Westcott, “Dehydrogenative borylation: the dark horse in metal-catalyzed hydroboration and diborations?”, *Reviews in Inorganic Chemistry*, **2015**, 35(2), 69-79
45. R. J. Burford, M. J. Geier, C. M. Vogels, A, Decken, S. A. Westcott, “Addition of boranes to iminophosphines: Synthesis and reactivity of a new bulky hydroboration reagent”, *Journal of Organometallic Chemistry,* **2013**, 731, 1-9
46. M. J. Geier, S. J. Geier, N. R. Halcovitch, C. M. Vogels, A. Decken, S. A. Westcott, “Rhodium complexes containing arylspiroboranes derived from 3,5-ditert-butylcatechol and their use in catalyzed hydroboration”, *Polyhedron*, **2013**, 52, 1181

47. G. M. Lee, C. M. Vogels, A. Decken. S. A. Westcott, “Iridium phosphane complexes containing arylspiroboronate esters for the hydroboration of alkenes”, *Eur. J. Inorg. Chem*. **2011**, 15, 2433
48. J. A. Melanson, C. M. Vogels, A. Decken, S. A. Westcott, “Catalytic hydroboration of vinylarenes using a zwitterionic arylspiroboronate ester iridium complex”, *Inorganic Chemistry Communications*, **2010**, 13, 1396
49. M. J. Geier, C. M. Vogels, A. Decken, S. A. Westcott, “The transition metal catalyzed hydroboration of enamines”, *Journal of Organometallic Chemistry*, **2009**, 694, 3154
50. M. J. Geier, S. J. Geier, C. M. Vogels, F. Beland, S. A. Westcott, “Hydroboration of vinyl arenes using SiO2-supported rhodium catalysts”, *Synlett*, **2009**, 3, 477
51. C. N. Garon, D. I. McIsaac, C. M. Vogels, A. Decken, I. D. Willias, C. Kleeberg, T. B. Marder, S. A. Westcott, “Synthesis and structure of indenyl rhodium (I) complexes containing unsaturated phosphines: catalyst precursors for alkene hydroboration”, *Dalton Transactions*, **2009**, 9, 1624
52. J. D. Webb, D. J. Harrison, D. W. Norman, J. M. Johanna, C. M. Vogels, A. Decken, G. G. Baite, D. Venkataraman, T. R. Baker, S. A. Westcott, “Metal catalyzed hydroboration of vinyl sulfides, sulfoxides, sulfonates, and sulfonates”, *Journal of Molecular Catalysis A: Chemical*, **2007**, 275, 91
53. J. Cipot, C. M. Vogels, R. McDonald, S. A. Westcott, “Catalytic Alkene Hydroboration Mediated by Cationic and Formally Zwitterionic Rhodium (I) and Iridium (I) Derivatives of a P, N-Substituted Indene”, *Organometallics*, **2006**, 25, 5965
54. C. M. Vogels, A. Decken, S. A. Westcott, “Rhodium (I) acetylacetonate complexes containing phosphinoalkynes as catalysts for the hydroboration of vinylarenes”, *Canadian journal of Chemistry*, **2006**, 84, 146
55. C. M. Vogels, A. Decken, S. A. Westcott, “Catalyzed hydroboration of nitrostyrenes and 4-vinylaniline: a mild and selective route to aniline derivatives containing boronate esters”, *Tetrahedron Letters*, **2006**, 47, 2419

56. N. A. Wnberg, L. J. Leger, M. L. Maren, C. M. Vogels, A. Decken, S. J. Duffy, S. A. Westcott, “Synthesis and catalyzed hydroboration of styryl sulfonamides”, *Canadian Journal of Chemistry*, **2005**, 83, 661
57. C. M. Vogels, S. A. Westcott, “Recent advances in organic synthesis using transition metal-catalyzed hydroboration”, *Current Organic Chemistry*, **2005**, 9, 687
58. M. G. Hamilton, C. E. Hughes, A. M. Irving, C. M. Vogels, S. A. Westcott, “Catalyzed hydroboration of alkyl sulfonamides”, *Journal of Organometallic Chemistry*, **2003**, 680, 143
59. C. M. Vogels, P. E. O’Connor, T. E. Philips, K. J. Watson, M. P. Shaver, P. G. Hayes, S. A. Westcott, “Rhodium-catalyzed hydroboration of allylamine and allylimines”, *Canadian journal of Chemistry*, **2001**, 79, 1898
60. C. A. G. Carter, C. M. Vogels, D. J. Harrison, K. J. Gagnon, D. W. Norman, R. F. Langler, S. A. Westcott, “Metal-Catalyzed Hydroration and Diboration of Thiocarbonyls and Vinyl Sulfides”, *Organometallics*, **2001**, 20, 2130
61. R. T. Baker, J. C. Calabrese, S. A. Westcott, T. B. Marder, “Reactions of Organoruthenium Phosphine Complexes with Hydroborating Reagents”, *Journal of American Chemical Society*, **1995**, 117, 8777
62. R. T. Baker, J. C. Calabrese, S. A. Westcott, “Coinage metal-catalyzed hydroboration of imines”, *Journal of Organometallic Chemistry*, **1995**, 498, 109
63. S. A. Westcott, T. B. Marder, R. T. Baker, “Transition Metal-Catalyzed addition of catecholborane to α-substituted vinylarenes: hydroboration vs dehydrogenative borylation”, *Oganometallics,* **1993**, 12, 975
64. K. Burgess, W. A. Van Der Donk, S. A. Westcott, T. B. Marder, R. T. Baker, J. C. Calabrese, “Reactions of catecholborane with Wilkinson’s catalyst: implications for transition metal-catalyzed hydroboration of alenes”, *J. Am. Chem. Soc*, **1992**, 114, 9350

65. S. A. Westcott, H. P. Blom, T. B. Marder, R. T. Baker, “New homogeneous rhodium catalysts for the regioselective hydroboration of alkenes”, *J. Am. Chem. Soc*, **1992**, 114, 8863
66. G. A. Molander, N. M. Ellis, “Highly Stereoselective Synthesis of Cis-Alkenyl Pinacolboronates and Potassium cis-Alkenyltrifluoroboranes via a Hydroboration/Protodeboronation Approach”*, J. Org. Chem*, **2008,** 73, 6841
67. G. A. Molander, K. L. Bobbitt, “Hydroboration/Intramolecular Reduction of Allyl Ketones with (Diisopinocamphenyl)borane: A Convenient Synthesis of Enantiomerically Enriched 1,4-Diols”, *J. Org. Chem*. **1994**, 59, 2676
68. V. M. Shoba, N. C. Thacker, A. J. Bochat, J. M. Takacs, “Synthesis of Chiral Tertiary Boronic Esters by Oxime-Directed Catalytic Asymmetric Hydroboration”, *Angew. Chem. Int. Ed*. **2016**, 55, 1465
69. G. L. Hoang, Z. Yang, S. M. Smith, R. Pal, J. L. Miska, D. E. Perez, L. S. W. Pelter, X. C. Zeng, J. M. Takacs, “Enantioselective Desymmetrization via Carbonyl-Directed Catalytic Asymmetric Hydroboration and Suzuki-Miyaura Cross-Coupling”, *Org. Lett*, **2015**, 17, 940
70. N. C. Thacker, V. M. Shoba, A. E. Geis, J. M. Takacs, “Surprisingly facile C-H activation in the course of oxime-directed catalytic asymmetric hydroboration”, *Tetrahedron Letters*, **2015**, 56, 3306
71. Z. Yang, R. Pal, G. L. Hoang, X. C. Zeng, J. M. Takacs, “Mechanistic Insights into Carbonyl-Directed Rhodium-Catalyzed Hydroboration: ab Initio Study of a Cyclic γ,δ- Unsaturated Amide”, *ACS Catal*, **2014**, 4, 763
72. S. M. Smith, G. L. Hoang, R. Pal, M. O. Khaled, L. S. W. Pelter, X. C. Zeng, J. M. Takacs, “γ-Selective directed catalytic asymmetric hydroboration of 1,1-disubstituted alkenes”, *Chem. Commun*, **2012**, 48, 12180
73. S. A> Moteki, K. Toyama, Z. Liu, J. Ma, A. Holmes, J. M. Takacs, “Two-stage optimization of a supramolecular catalyst for catalytic asymmetric hydroboration”, *Chem. Commun*, **2012**, 48, 263

74. S. M. Smith, M. Ulteuliyev, J. M. Takacs, “Catalytic asymmetric hydroboration of β, γ-unsaturated Weinreb amides: striking influence of the borane”, *Chem. Commun*, **2011**, 47, 7812
75. S. M. Smith, J. M. Takacs, “Remarkable Levels of Enantioswitching in Catalytic Asymmetric Hydroboration”, *Org. Lett*, **2010**, 12, 4612
76. S. M. Smith, J. M. Takacs, “Amide-Directed Catalytic Asymmetric Hydroboration of Trisubstituted Alkenes”, *J. Am. Chem. Soc*, **2010**, 132, 1740
77. S. M. Smith, N. C. Thacker, J. M. Takacs, “Efficient amide-directed catalytic asymmetric hydroboration”, *J. Am. Chem. Soc*, **2008**, 130, 3734
78. S. A. Moteki, J. M. Takacs, “Exploiting self-assembly for ligand-scaffold optimization: substrate-tailored ligands for efficient catalytic asymmetric hydroboration”, *Angew. Chem. Int. Ed*, **2008**, 47, 894
79. S. A. Moteki, D. Wu, K. L. Chandra, D. S. Reddy, J. M. Takacs, “TADDOL-derived phosphites and Phosphoraidites for Efficient Rhodium-Catalyzed Asymmetric Hydroboration”, *Org. Lett*, **2006**, 8, 3097
80. SciFinder key work search was used to obtain the necessary information
81. H. Kono, K. Ito, Y. Nagai, “Oxidative addition of 4, 4, 6-trimethyl-1, 3, 2-dioxaborinane and benzo[1, 3, 2]diaoxaborole to tris(triphenylphosphine) halorhodium”. *Chem. Lett*. **1975**,1095
82. S. A. Wescott, N. J. Taylor, T. B. Marder, R.T. Baker, N. J. Jones, J. C. Calabrese, “Reactions of catecholatoborane with phosphinorhodium complexes: molecular structures of [RhHCl(Bcat)($PPr^i_3$)$_2$] and [{($Pr^i_2PCH_2$)$_2$}Rh{($\eta^6$-cat)Bcat}](cat = 1,2-$O_2C_6H_4$)”. *Chem. Commun*. **1991**, 304
83. D. A. Evans, G. C. Fu, B. A. Anderson, “Mechanistic study of the rhodium(I)-catalyzed hydroboration reaction”. *J. Am. Chem. Soc*. **1992**, 114, 6679
84. K. Burgess, W. A. van der Donk, S. A. Westcott, T. B. Marder, R. T. Baker, J. C. Calabrese, “Reactions of catecholborane with Wilkinson's catalyst: implications for transition metal-catalyzed hydroboration of alkenes”. *J. Am. Chem. Soc*. **1992**, 114, 9350

85. A. E. Dorigo, P. von Rague Schleyer, “New Fluorescent Model Compounds for the Study of Photoinduced Electron Transfer: The Influence of a Molecular Electric Field in the Excited State”. *Angew. Chem. Int. Ed. Engl.* **1995**, 34, 115
86. D. G. Musaev, A. M. Mebel, K. Morokuma, “An ab initio molecular orbital study of the mechanism of the rhodium(I)-catalyzed olefin hydroboration reaction”. *J. Am. Chem. Soc*. **1994**, 116, 10693
87. C. Widauer, H. Grutzmacher, T. Ziegler, ”Comparative Density Functional Study of Associative and Dissociative Mechanisms in the Rhodium(I)-Catalyzed Olefin Hydroboration Reactions”, *Organometallics*. **2000**, 19, 2097
88. D. G. Musaev, A. M. Mebel, K. Morokuma, “An ab initio molecular orbital study of the mechanism of the rhodium(I)-catalyzed olefin hydroboration reaction”, *J. Am. Chem. Soc*, **1994**, 116, 10693
89. J. M. Brown, G. C. Lloyd-Hones, “Vinylborane Formation in Rhodium-Catalyzed Hydroboration of Vinylarenes. Mechanism versus Borane Structure and Relationship to Silation”, *J. Am. Chem. Soc*, **1994**, 116, 866
90. H. Renata, Jane. Z. Wang, F. H. Anold, “Expanding the Enzyme Universe: Accessing Non-Natural Reactions by Mechanism-Guided Directed Evolution”. *Angew. Chem. Int. Ed*. **2015**, 54, 3351
91. L. Y. P. Luk, E. J. Loveridge, R. K. Allemann, “Chemical Ligation and Isotope Labeling to Locate Dynamic Effects during Catalysis by Dihydrofolate Reductase”. *Phys. Chem. Chem. Phys*. **2015**, advance aiticle **DOI:** 10.1039/C5CP00794A
92. M. W. Giuliano, S. J. Miller, “Site-Selective Reactions with Peptide-Based Catalysts”, *Top. Curr. Chem*. **2016**, 372, 157
93. J. N. H. Reek, “New supramolecular approaches in transition metal catalysis; template-ligand assisted catalyst encapsulation, self-assembled ligands and supramolecular catalyst immobilization”, *Supramolecular Catalysis*, **2008**, 199
94. J. M. Takacs, D. S. Reddy, S. A. Moteki, D. Wu, H. Palencia, “Asymmetric Catalysis Using Self-Assembled Chiral Bidentate *P,P*-Ligands”. *J. Am. Chem. Soc*. **2004**, 126, 4494

95. D. Seebach, A. K. Beck, A. Heckel, “TADDOLs. Their derivatives, and TADDOL analogs: versatile chiral auxiliaries”, *Angew. Chem. Int. Ed*, **2001**, 40, 92

96. H. Doucet, E. Fernandez, T.P. Layzell, and J.M. Brown, “The scope of catalytic asymmetric hydroboration/oxidation with rhodium complexes of 1, 1’-(2-diarylphosphino-1-naphthyl)isoquinolines”. *Chem. Eur. J.* **1999**, 5, 1320

97. S. D. Dipl, F. Volant, P. Knochel, “Functionalized main-group organometallics for organic synthesis”. Angew. Chem., Int. Ed. **2001**, 40, 1235

98. S. A. Moteki, “Developing a supramolecular catalyst for asymmetric hydroboration”, PhD thesis (January 1, 2008)

99. J. Zhang, B. Lou, G. Guo, L. Dai, “Reversed Regiochemistry in the Hydroboration of Vinylarenes Catalyzed by Neutral Rhodium Complexes and the Related Asymmetric Version”, *J. Org. Chem*. **1991**, 56, 1670

100. M. Segarra, E. D. Oller, C. Claver, J. M. Poblet, C. Bo, E. Fernandez, “In Quest of Factors That Control the Enantioselective Catalytic Markovnikov Hydroboration/Oxidation of Vinylarenes”, *Chem. Eur. J*. **2004**, 10, 6456

101. When *ortho*-, *meta*-, and *para*-methoxy styrenes are mixed, the corresponding products can’t be separated. Thus, directly comparing three substrates in the same reaction mixture to measure inherent reactivities has not been done.

102. E. Fogassy, M. Nogradi, D. Kozma, G. Egri, E. Palovics, V. Kiss, “Optical resolution methods”, *Organic & Biomolecular Chemistry*, **2006**, 4, 3011

103. J. Mahatthananchai, A. M. umas J. W. Bode, “Catalytic selective Synthesis”, *Angew. Chem. Int. Ed*. **2012**, 51, 10954

104. A. Lewis, S. J. Miller, “Site-Selective Derivatization and Remodeling of Erythromycin A by Using Simple Peptide-Based Chiral Catalysts”, *Angew. Chem. Int. Ed*. **2006**, 45, 5616

105. J. Szychowski, J. F. Truchon, Y. L. Bennani, “Natural Products in Medicine: Transformational Outcome of Synthetic Chemistry”. *J. Med. Chem*. **2014**, 57, 9292

106. M. A. Fischbach, C. T. Walsh, “Antibiotics for emerging pathogens”. *Science*, **2009**, 325, 1089

107. R. C. James, J. G. Pierce, A. Okano, J Xie, D. L. Boger, “Redesign of glycopeptide antibiotics: back to the future”. *ACS Chem. Biol*. **2012**, 7, 797

108. Robles, D. Romo, “Chemo- and site-selective derivatizations of natural products enabling biological studies”. *Nat. Prod. Rep*. **2014**, 31, 318

109. Sculimbrene, B. R.; Miller, “Discovery of a Catalytic Asymmetric Phosphorylation through Selection of a Minimal Kinase Mimic: A Concise Total Synthesis of D-*myo*-Inositol-1-Phosphate”. S. J. *Am. Chem. Soc.* **2001**, *123*, 10125-10126.

110. Sculimbrene, B. R.; Xu, Y.; Miller, S. J. « Asymmetric Syntheses of Phosphatidylinositol-3-Phosphates with Saturated and Unsaturated Side Chains through Catalytic Asymmetric Phosphorylation”. *J. Am. Chem. Soc.* **2004**, *126*, 13182-13183.

111. J. M. McGuire, R. L. Bunch, R. C. Anderson, H. E. Boaz, E. H. Flynn, H. M. Powell, J. W. Smith, Ilotycin, a new antibiotic. *Antibiot. Chemother*. **1952**, 2, 281

112. Lewis, C. A.; Miller, S. J. “Site-Selective Derivatization and Remodeling of Erythromycin A by Using Simple Peptide-Based Chiral Catalysts”. *Angew. Chem. Int. Ed.* **2006**, *45*, 5616-5619.

113. P. A. Lichtor, S. J. Miller. “Combinatorial evolution of site- and enantioselective catalysts for polyene epoxidation”. *Nature chemistry*, **2012**, 4, 990

114. P. E. Gormisky, M. C. White. “Catalyst-Controlled Aliphatic C–H Oxidations with a Predictive Model for Site-Selectivity”. *J. Am. Chem. Soc***. 2013**, 135, 14052

115. A. Bastian, A. Marcozzi, A. Herrmann. “Selective transformations of complex molecules are enabled by aptameric protective groups”. *Nature chemistry*, **2012**, 4, 789

116. Y. Ueda, K. Mishiro, K. Yoshida, F. Furuta, T. Kawabata*, "*Regioselective Diversification of a Cardiac Glycoside, Lanatoside C, by Organocatalysis". *J. Org. Chem*. **2012**, 77, 7850

117. V. Rautenstrauch, *Bull. Soc. Chim. Fr*. **1994**, 131, 515

118. Y. Lee, A. H. Hoveyda. "Efficient Boron−Copper Additions to Aryl-Substituted Alkenes Promoted by NHC−Based Catalysts. Enantioselective Cu-Catalyzed Hydroboration Reactions". *J. Am. Chem. Soc*. **2009**, 131, 3160

119. K. Nakanishi, N. Berova, R. Woody, Circular dichroism: principles and applications. VCH. P 473 **1994**

120. Hoye T. R., Jeffrey C.S., Shao F. "Mosher ester analysis for determination of absolute configuration of stereogenic (chiral) carbinol carbons". *Nat Protoc*., **2007**, 2(10), 2451-2458.

# Chapter 3. Application site selective hydroboration

## 3.1 Application of site selective hydroboration - introduction

After observing the striking site selectivity displayed by supramolecular SALs system on catalytic symmetric hydroboration on dimeric substrates, it was my desire to demonstrate the synthetic potential of the methodology. Given that high site selectivity was observed only for *ortho* and *meta* substituted aryl alkenes, the search for suitable natural products was not a trivial task. After reviewing more than 20,000 structures which were showed up by SciFinder structure search, one candidate natural product was identified. This particular natural product shows excellent anti-fungal properties and is used for the prevention of mold growth in livestock food. It is shown to be non-toxic to the animals and yet keeps the animal food safe[1]. Despite the user friendliness of the natural product, there has been no total synthesis reported to date. The molecule itself has two stereocenters (Figure 1). In recent years pharmaceutical companies have been interested in isolating pure enantiomers of existing or newly developed drugs[2]. In addition, for some drugs, only one enantiomer is effective toward treatment of diseases, the other may simply be innocuous or give rise to detrimental side effects[3]. In either case, the pure enantiomer of the effective form in theory can be active at only half of the dosage of a racemic mixture. Therefore, from the view of the pharmaceutical company this presents significant cost savings[4]. Our site selective asymmetric hydroboration offered an attractive strategy for synthesis of this target since it may be possible to use that chemistry it to control one or both of the

stereocenters in constructing the molecule and thereby gain a better understanding of the structure/activity relationship to the observed antifungal properties.

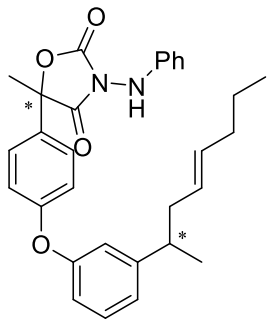


**Figure 1.** Anti-fungi natural product; * denotes the stereocenters.

My initial retrosynthetic analysis is shown in figure 2. There is a precedent to synthesize the final oxazolidinedione ring system via a one pot reaction proceeding in good yield (70 %) [5]. Based on Scifinder search, it should be possible to convert compound **304** into compound **305** as shown[5] by generation of ethyl trichloroacetate organometallic compound, which adds to ketone group to afford the compound **305**. Converting compound **303** into compound **304** can be achieved by regular hydroboration followed by oxidation. C-C Bond formation can be easily achieved by well-established Suzuki coupling of **302a** and **302b**. Compound **302a** can be prepared by highly *meta* selective asymmetric hydroboration described earlier in this in this thesis. Despite the fairly straightforward total synthesis route devised, it turned out during attempted execution of the route that many of the seemingly well-established methodologies did not work as intended. This chapter is intended to show a successful total synthesis of a chiral mixture of diastereomers of this anti-fungi natural product as a

real world application of site selective chemistry. It also documents the series of chemical obstacles that were overcome to achieve the efficient total synthesis.

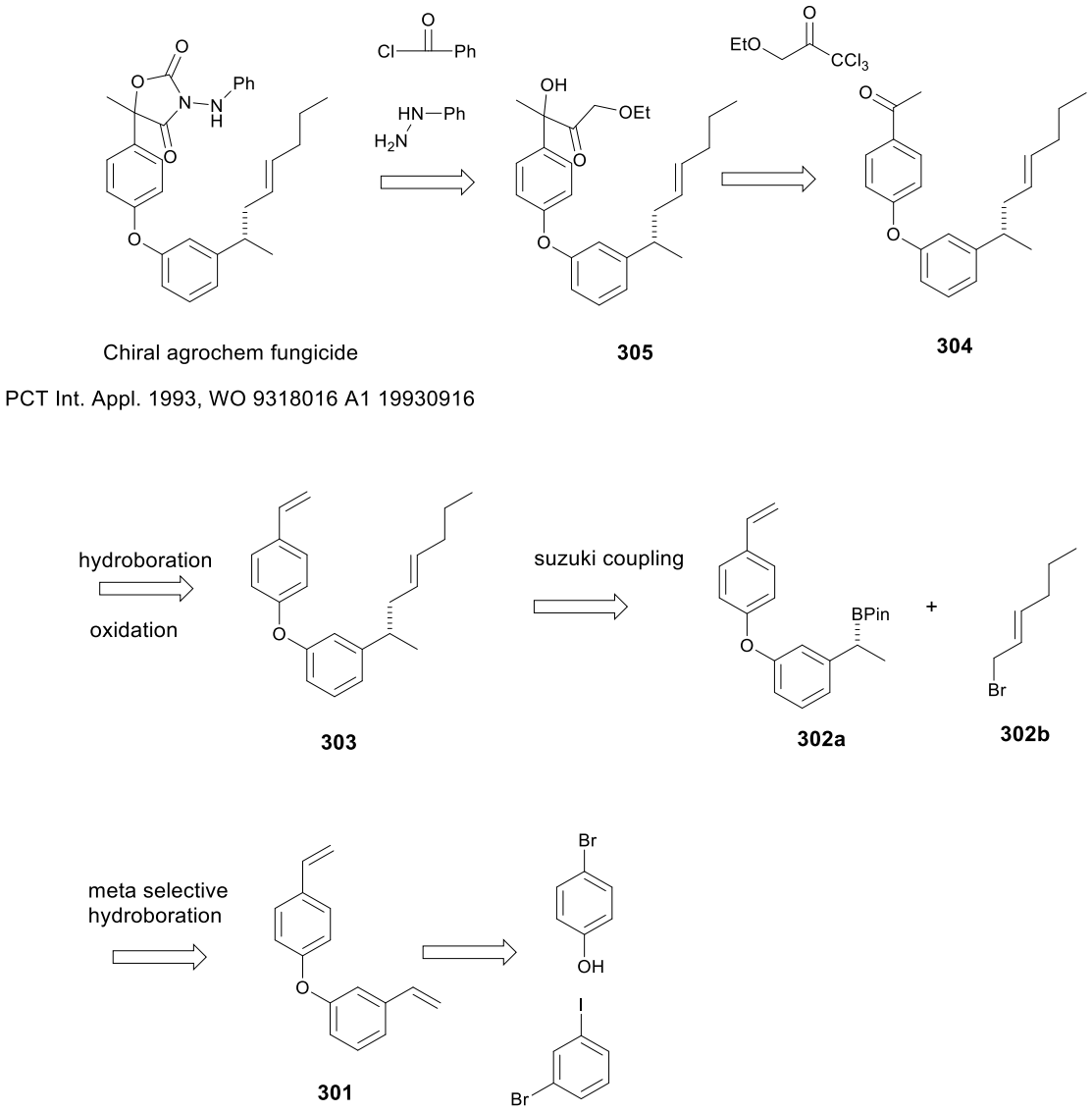


**Figure 2.** Initial retrosynthetic analysis of anti-fungi compound.

**3.2 Application of site selective hydroboration – overall description of the completed synthesis**

As pointed out earlier, although my retrosynthesis seemed relatively straightforward, some of the initial attempts failed due to low reactivity of the substrates or incompatibility of reaction conditions to the substrates. The final total synthesis consisted of 14 steps and an overall yield of 6.4%. Most of the steps proceeded in yields above 70%, and I was able to combine two or more transformations into a one pot sequence for efficiency. Only two of the 14 steps in the synthesis, the site-selective hydroboration and regular hydroboration/PDC oxidation, need expensive or toxic metals such as Rh. Low catalyst loading (0.01%) for the hydroboration contributes to keep the catalyst total cost low. Other steps utilize relatively cheaper and more abundant metals for examples, copper, zinc, magnesium, and so on. This is a very important factor when a pharmaceutical company decides to invest money into development of synthesis of enantiopure compounds.

The initial synthetic route to compound **301** consisted of installation of a vinyl group via Stille coupling followed by ether synthesis. However, the synthesis of **301** proved relatively difficult under the initial conditions used; the yield of ether fluctuated from reaction to reaction depending on how well the mixture was stirred (it forms a thick hard solid) and how uniformly heat was applied. Also the reaction time was less than ideal In order to obtain even moderate yield (40%) the reaction mixture needed at least 2 days of reflux time. Moreover, vinyl groups have been introduced by Stille coupling with good yield (70% range) with great repeatability but the difficulty of

removing tin by-product and toxicity of tin were not attractive feature of the synthesis. The procedure was improved by changing the sequence of reactions where first ether synthesis was performed using picolinic acid as a ligand for copper catalyzed ether synthesis between 4-bromobenzealdehyde and 3-hydroxybenzaldehyde and then Wittig reaction was used to overcome toxic by-product issues to install a vinyl group on the molecule. Overall two-step yield of preparing the dimeric substrate went from 20 % to over 70 %.

Conversion of the dimeric substrate **301** to hydroborated product **302a** went as expected with good isolated yield with 68% using the S3pTAR7pTA supramolecular catalyst described in Chapter 2 of this thesis. The hydroboration proceeded with excellent *meta*- site selectivity and produced a minimum of byproducts. In addition, the enantioselectivity was reasonably high (91% ee). The conversion of **302a** to **303** via C-C bond formation step was the most problematic step encountered in the synthesis. Despite the fact that Suzuki coupling is reported to work well with allylic halides or borane and aryl halides[6 - 8], none of the numerous combinations of metal precursors and ligands attempted afforded the desired cross-coupling product **303**. Finally, Negishi coupling with the acid chloride based on Knochel's zinc reagent procedure[32] were found to work the best, which necessitated the removal of oxygen. One of the downside of the step is the need for 20 equivalents diisopropylzinc relative to the substrate, which increases the overall synthetic cost. Knochel also observed the even more need to use excess amount of diisopropylzinc to conduct Negishi coupling[9]. The need to employ a more reactive acid chloride for the coupling introduces a ketone C=O moiety, which is

not in the final anti-fungi compound. Therefore, even though Negishi coupling successfully afforded the coupled product with good yield (67%), it introduced the need for an extra synthetic step. There were several options to remove oxygen atom from the molecule to obtain the compound **303** including radical deoxygenation of **339** and Wolff-Kishner reduction of **339**. First, radical deoxygenation was investigated to convert **339** into **303** since all of the reagents are easily available and cheap. The typical radical deoxygenation condition afforded the product **303** with about 13% yield over 2 steps. This is not the most appealing level of yields since especially this is in the middle of total synthesis, which would impact overall yield drastically. The presence of α, β alkene moiety is most likely the reason why the observed yield was disappointing. Because of the low yields of radical deoxygenation further reaction conditions were searched. Wolff-Kishner reduction presents advantages over radical deoxygenation because it does not involve radical[10 - 11] where possible side reaction could occur between the alkenes of the dimeric substrate. Simple Wolff-Kishner reduction using hydrazine hydrate showed promising result with the yield of 20% for the first trial, which was further improved with Myers modification[12] to Wolff-Kishner reduction. Myers modification allows one to perform deoxygenation with mild condition at room temperature whereas the typical deoxygenation condition requires the usage of high molarity of a base solution with extended reaction time at high temperatures. This is an important factor because compound **339** contains not only a ketone functional group, but also an internal alkene moiety which easily undergoes reduction or undesired

reactions. The final deoxygenation step from the molecule **302a** to deoxygenated product **303** was achieved with 75% yield.

Returning to the original route (Figure 3), compound **303** was subjected to another hydroboration followed by oxidation with PCC to form the ketone **304**. Although a chiral SAL ligand was used to maximize chemoselectivity, the stereocenter introduced in this reaction is irrelevant as it is destroyed in the subsequent step due to the necessity to convert the molecule to antifungal product. Conversion of the compound **304** to the compound **305** was straightforward and the optimization of reaction conditions were not necessary, since the obtained yields were close to 80 % for each step. The compound **304** was subjected into homologation condition where Willgerodt-Kindler reaction condition was used followed by the treatment of morphine phenylethane thione with base to afford the homologated carboxylic acid[43]. The resulting carboxylic acid was converted into the ester **306** using PTSA as a catalyst. The total yield over the three steps from the compound **304** to **306** was 79%. The ester **306** was subjected to α-methylation to afford the compound **307** with 76% yield. This is further modified by α-hydroxylation using $MoO_5$ pyridine reagent[44] to afford the compound **305** with 79% yield. The final ring closure of the total synthesis condition from **305** to the targeted anti-fungal compound is described by Infante *et al*.[11] This patent is assigned to Du Pont for the use of the fungicidal intermediate for plant diseases[14]. This is one pot high yielding reaction and gave the desired product with 68% yield. The following sections of the chapter describes the detailed explanations of individual synthetic step toward the final antifungal natural product. The following

sections of the chapter focuses and describes some of the challenges that I faced with in order to successfully complete efficient total synthesis of the anti-fungal compound. Specifically, the detailed discussion of syntheses of compound **301** from **321** and **317**, compound **339** from **302a**, and compound **303** from **339** will be given in the following section of chapter 3.

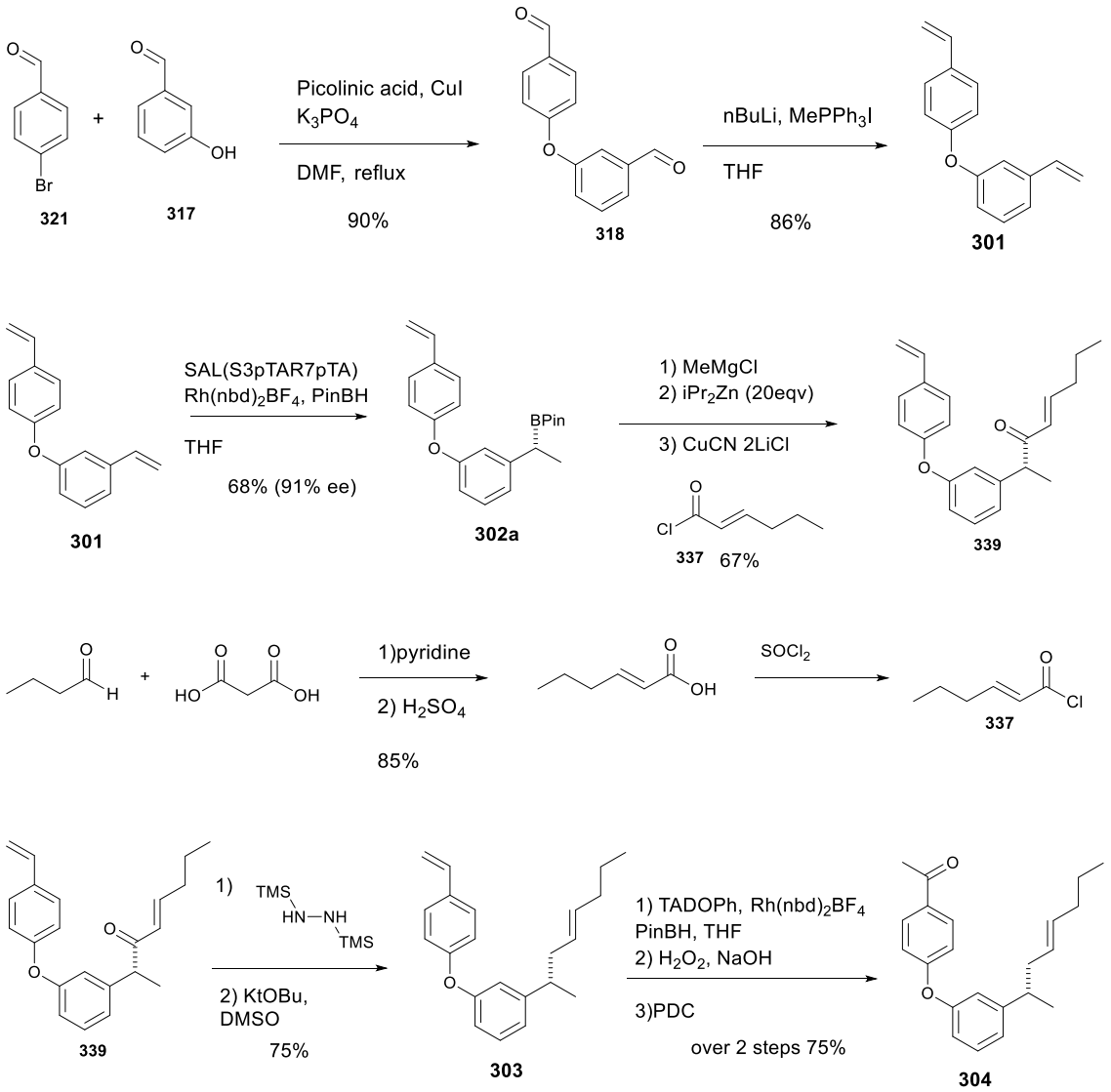

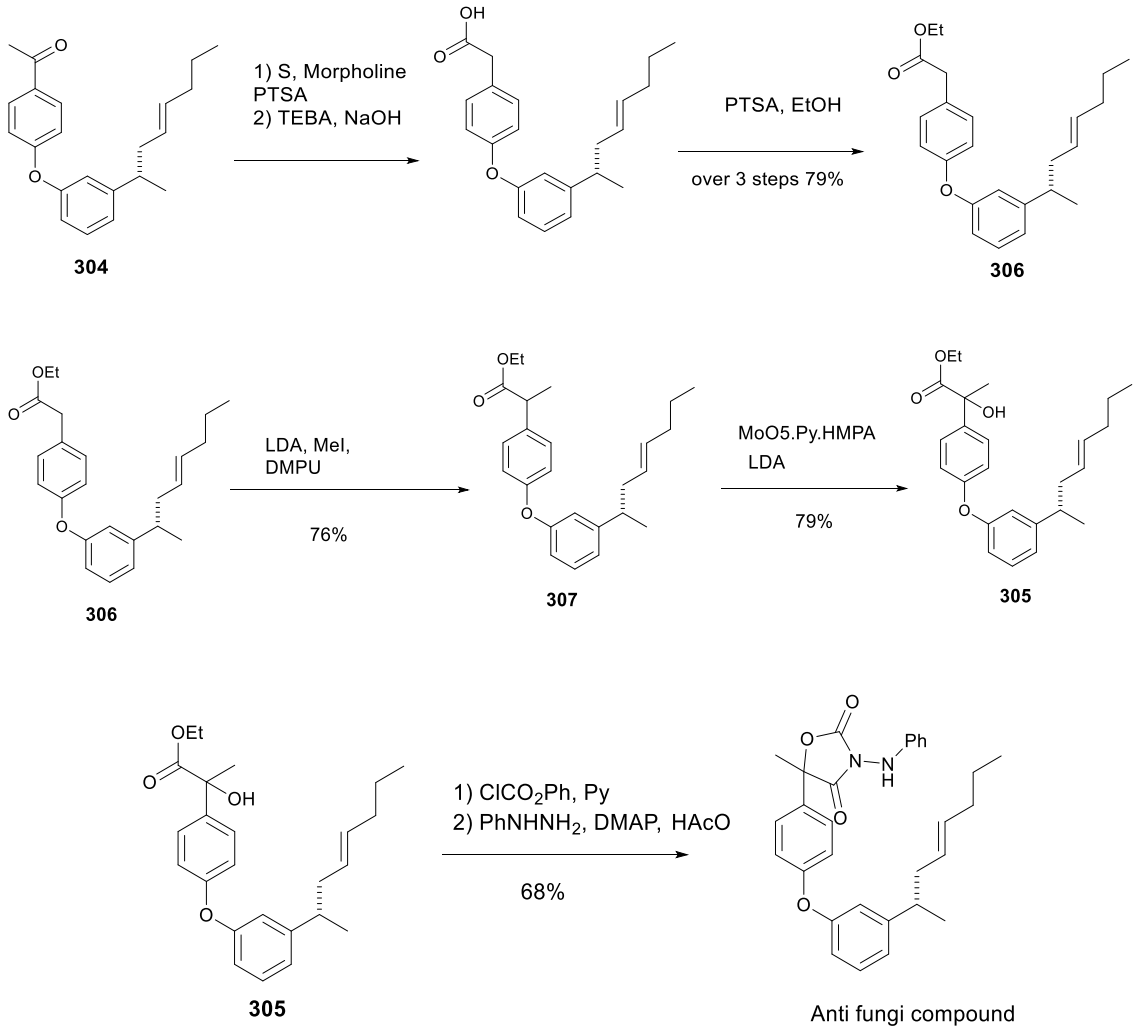


**Figure 3.** Completed total synthesis of antifungal compound (total yield 6.4% over 14 steps).

**3.3 Application of site selective hydroboration – Synthesis of the dimeric substrate**

The real world impact of a synthesis is related to the overall yield. The synthetic routes initially used to prepare the dimeric substrate had suffered from low yields and long reaction times. The dimeric synthesis started with preparation of a vinyltin compound with vinyl magnesium bromide (Figure 4, step 1). The tin compound was used in subsequent Stille coupling[15] with aryl iodides **308** and **310** to yield the corresponding bromo vinyl benzene **309** and hydroxyl vinyl benzene **311**. The Stille coupling needed the aryl iodides to obtain good yields. The corresponding bromide was not sufficient under the same reaction condition explored. However, the iodo compounds are usually expensive to purchase, and in this case, are not easily prepared. Purchasing them from commercial sources in a large amount was discouraged due to the cost issue. Also tin is known to have health issues and refraining from the use of tin compound is recommended[16] when there are other alternatives to achieve the same transformations. In addition, the purification step can be troublesome, because tributyltin hydride is present in equimolar amount. It is not easy to remove from the reaction mixture. Effective procedure[17] for removal of byproduct tri-*n*-butyltin halides from the reaction mixture has been reported but it is best not to deal with tin compounds due to the toxicity.

A more serious problem was the irreproducibility of the procedure for formation of the diaryl ether proved unreliable (Figure 4, Step 3). Refluxing for 2 days gave an only moderate yield of product **301**, typically 20 to 50% depending on how well the reaction mixture was stirred and how uniformly the heat was applied. On the positive side,

unreacted starting materials could be easily recycled and re-subjected to the coupling step to afford an enhanced yield of the desired product. Nonetheless, it typically took a total of 4 days to get about 50 % of the desired product and that coupled with the prohibitive cost of the starting aryl iodides on a large scale necessitated the search for the better synthetic route.

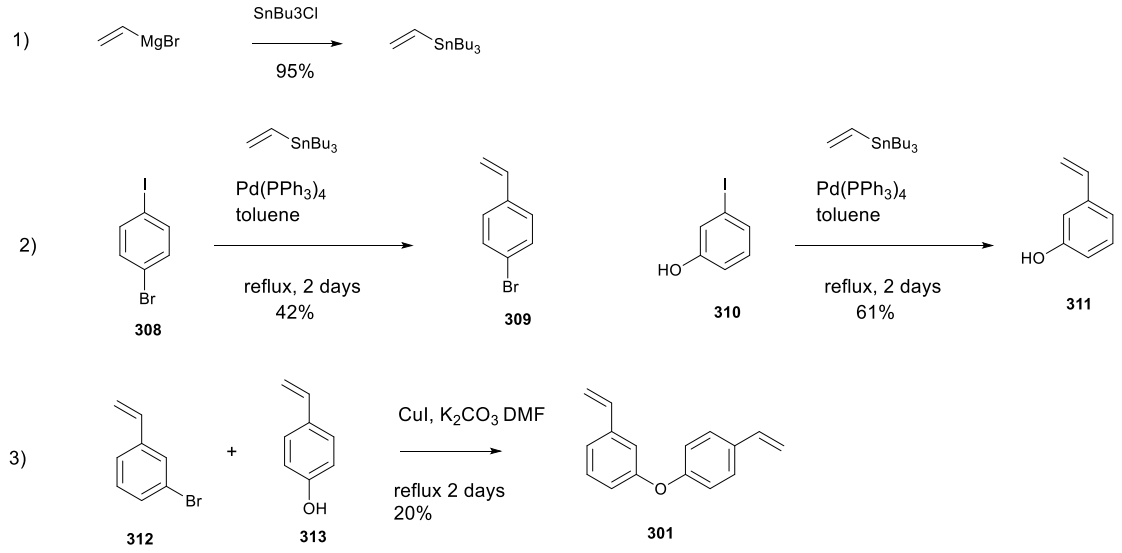


**Figure 4.** Initial synthetic route for the dimeric substrate **301**.

Figure 5 shows several alternative routes that were attempted. Figure 5A is the previously described Ullmann type reaction that was used to prepare the dimeric substrate. An alternative is nucleophilic aromatic substitution of 4-fluorobenzaldehyde (**316**) by 3-hydroxybenzaldehyde (**317**). Examples in the literature in which only one of the components contained aldehyde functionality were reported to be high yielding (ca 75%) under the conditions employed[19]. In the case at hand, two aldehyde moieties are

needed for later Wittig reaction to install vinyl moieties for the synthesis. The coupling of the required substrates proceeded in poor yield of **318** (20 to 50%) (Figure 5B). Buchwald published a procedure describing C-O bond formation by palladium-catalyzed coupling of 3-bromobenzaldehyde (**319**) with *o*-cresol (54% yield[) 20. This promoted me to try his conditions because they already had aldehyde moiety on one of the starting materials. 3-bromobenzaldehyde (**319**) was used with 4- hydroxyl benzaldehyde (**320**) under the reaction condition that Buchwald group successfully used. Unfortunately, this did not yield the desired product (**321**) at all (Figure 5C).

Going back to the Ullman-type conditions, we identified improved reaction conditions based on use of picolinic acid as a ligand in the copper-catalyzed ether synthesis. This methodology was developed by the Buchwald group[21]. The reported examples included the reaction between 3-bromo benzaldehyde and o-cresol which afforded the desired product 85% yield. The paper describes the method as tolerating a variety of functional groups and offering significant improvements over other procedures, particularly for the synthesis hindered diaryl ethers. This method proved to be very efficient for coupling 4-bromobenzaldehyde (**321**) and 3-hydroxybenzaldehyde (**317**) affording the desired product (**318**) in 90% yield (Figure 5D). This approach uses relatively cheap starting materials with no need for expensive iodo compounds. In addition, the reaction time is convenient, overnight rather than days.

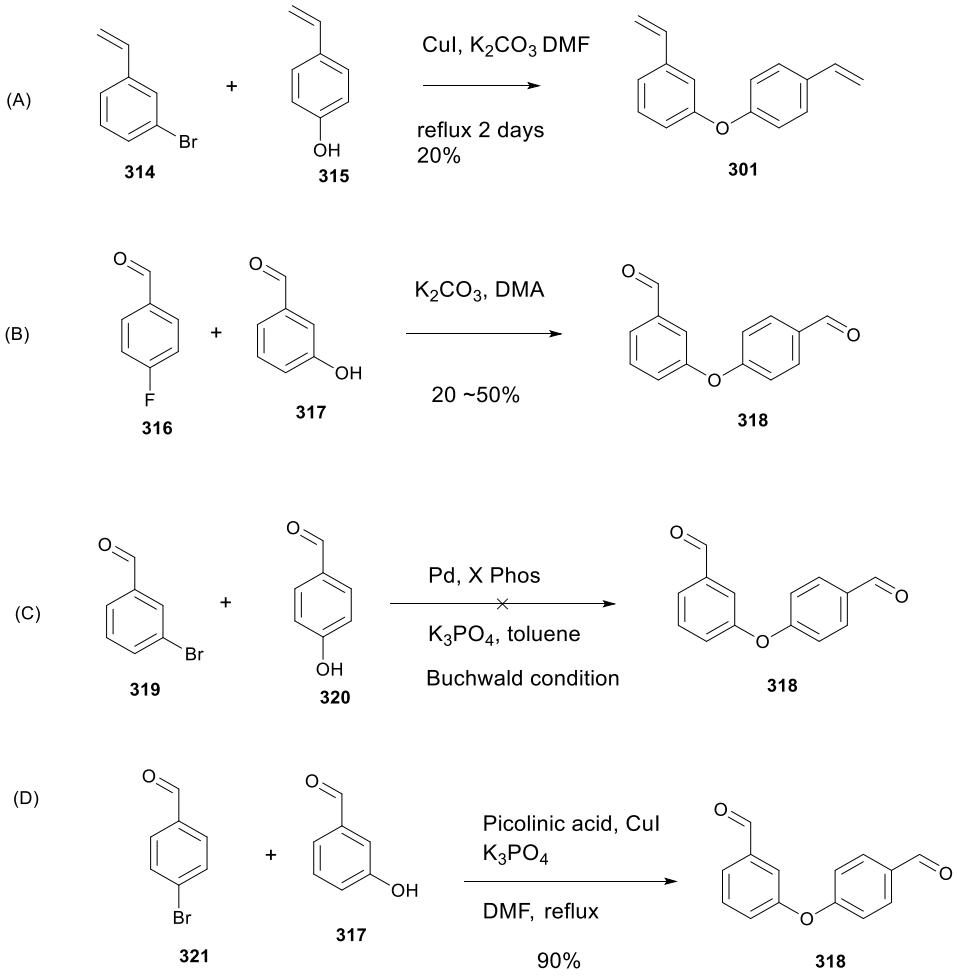


**Figure 5.** Ether synthesis to form the diary ether substrate **318** under several reaction conditions.

The conversion of the dialdehyde (**318**) to the diene (**301**) was accomplished in high yield by Wittig olefination under standard conditions.[18] Recall that the attempted installation of the required alkene moieties by a previous method (figure 4, steps 1-2) used toxic tin reagents and the purification was troublesome. The dialdehyde/Wittig

approach solved the both toxicity and purification issues at once. The overall yield was improved from 10% to about 80% over two steps.

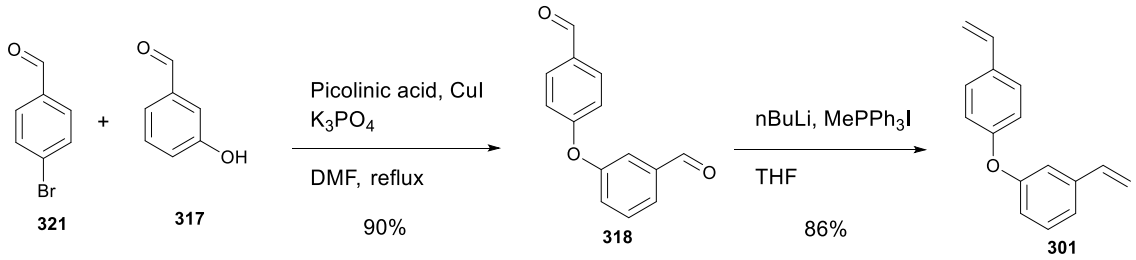


**Figure 6.** Optimized *meta*- and *para*-substituted diaryl ether substrate **301**.

**3.4 Application of site selective hydroboration – troubleshooting for C-C bond formation step**

In this segment of the chapter my intention is to describe approaches and data leading the optimized route and conditions for the key C-C coupling of the chiral boronic ester for the total synthesis of the targeted anti-fungal natural product. The Suzuki coupling reaction has attracted much attention and Suzuki shared in the 2010 Nobel Prize. While the coupling reaction represents a great advancement in the field of organic chemistry, the majority of applications have involved Csp2 – $Csp^2$ bond formation[25]. More recently, the development of $Csp^2$ – $Csp^3$ bond formation has attracted more attention[26]. In comparison, there have been relatively few examples of $Csp^3$ – $Csp^3$ bond formation reported. When successful, the latter usually involve activated $Csp^3$ systems such as allylic halides[27-28]. Nonetheless, considering the extensive literature on Suzuki coupling[22-23] and the development of asymmetric hydroboration in this thesis, it seemed natural to use Suzuki coupling to show the usefulness of our chiral boronic esters. However, contrary to expectation, C-C bond formation was the most troublesome step in the total synthesis step. From the initial retrosynthetic analysis the idea was to couple the boronic ester (**302a**) with an allyl bromide (**302b**) in one step via Suzuki coupling to afford the compound **303** (Figure 7A). However, the only high-yielding C-C bond formation we could identify required converting the boronic ester (**302a**) into the zinc species, which then coupled with an acid chloride in presence of copper to afford the coupled product (Figure 7B). This necessitates a subsequent deoxygenation, which ultimately added extra steps. This simple yet challenging step not only taught me how

difficult total syntheses are to accomplish in an efficient time and cost fashion, but how a small change in substrate or reaction conditions can drastically change reactivity in a complex molecule setting. It also taught me how rewarding one feels when he or she completes the total synthesis.

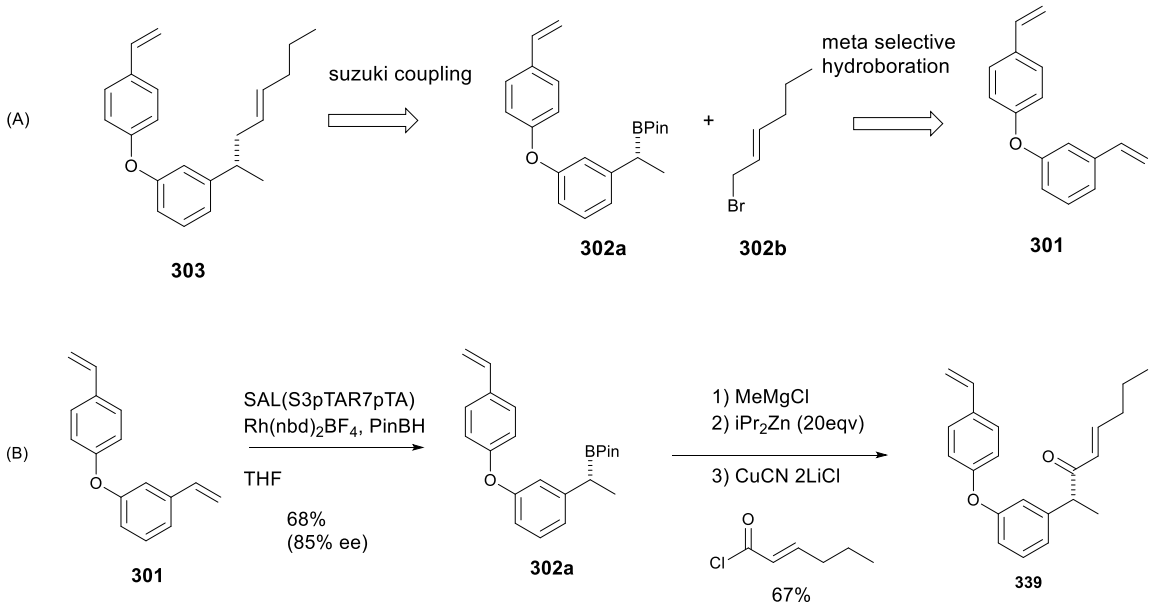


**Figure 7.** (A) Initial synthetic plan. (B) Optimized step for C-C bond formation.

I first prepared a model substrate in which a phenoxy substituent replaced the required aryl derivative. I tested the model compound under a variety of various reaction conditions for Suzuki coupling. The potassium trifluoroborate salt (**319**) of the model compound was prepared from known procedures, as trifluoroborates generally reacts faster than the boronic acids[24-26]. Ligands that the Buchwald group has developed are also known to be very effective in Suzuki coupling; [27] several of these ligands and metal precursors were screened (Figure 8). Most of the combinations failed

to give the desired product (**320**) in appreciable amounts, but it was obtained in 30% yield using $Pd(OAc)_2$ in combination with Ru PHOS[27] (Figure 8 entry 8). Substituting the allylic bromide with the corresponding iodo compound did not improve the yield (data not shown).

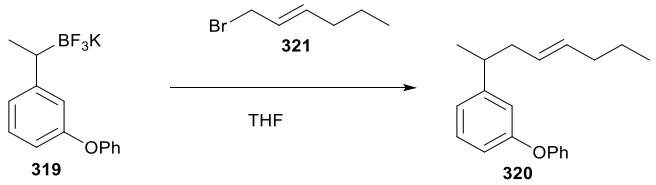


| entry | metal | ligand | base | Yield (%) |
|---|---|---|---|---|
| 1 | $Pd(PPh_3)_4$ | NA | $K_2CO_3$ | 0 |
| 2 | $Pd_2(dba)_3$ | $PPh_3$ | base | 0 |
| 3 | $Pd_2(dba)_3$ | $PCy_3$ | $K_2CO_3$ | 0 |
| 4 | $Pd_2(dba)_3$ | x PHOS | $Cs_2CO_3$ | 0 |
| 5 | $Pd_2(dba)_3$ | John PHOS | $Cs_2CO_3$ | 0 |
| 6 | $Pd_2(dba)_3$ | Ph Dave PHOS | $Cs_2CO_3$ | 0 |
| 7 | $Pd(OAc)_2$ | NA | $K_2CO_3$ | 10 |
| 8 | $Pd(OAc)_2$ | Ru PHOS | $Cs_2CO_3$ | 30 |
| 9 | $Pd(OAc)_2$ | $(t\text{-}Bu)_2MeP$ | $K_2CO_3$ | 25 |
| 10 | $Pd(OAc)_2$ | $PCy_3$ | $K_2CO_3$ | 8 |

**Figure 8.** Attempted Suzuki coupling of potassium trifluoroborate salt **319** with allyl bromide **321** under various reaction conditions.

While the initial result described above was encouraging, the required synthesis of potassium trifluoroborate salt adds one extra step and the yield of its preparation is

not ideal[28]. I therefore returned to examine the reactions of boronic ester **322**. While a number of conditions failed, I was delighted to find that one reaction condition (Figure 9. entry 3) gave the desired product (**320**) in 37% yield. For this reaction to be successful, the allylic iodide coupling partner (**323**) was required. It is furthermore worth pointing out that a suitable base and solvent mixture is yet another key to the reaction (Figure 9, compare entries 1, 2, and 3). For the coupling between boronic ester and iodo coupling partner, the best catalyst precursor was $Pd_2(dba)_3$ (Figure 9. entries 4, 5, 6, and 7).

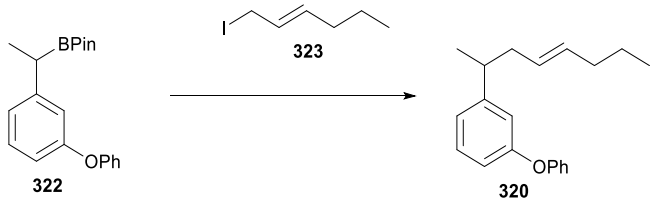


| entry | metal | ligand | base | solvent | Yield (%) |
|---|---|---|---|---|---|
| 1 | $Pd_2(dba)_3$ | $PPh_3$ | $K_2CO_3$ | DMF/$H_2O$ | 0 |
| 2 | $Pd_2(dba)_3$ | $PPh_3$ | $Ag_2O$ | DMF/$H_2O$ | 0 |
| 3 | $Pd_2(dba)_3$ | $PPh_3$ | $Ag_2O$ | tol/$H_2O$ | 37 |
| 4 | $Pd(PPh_3)_4$ | NA | $Ag_2CO_3$ | THF | 0 |
| 5 | $Pd(PPh_3)_4$ | NA | $K_2CO_3$ | THF | 0 |
| 6 | $Pd(OAc)_2$ | $PCy_3$ | $K_2CO_3$ | THF | 0 |
| 7 | $Pd(OAc)_2$ | NA | $K_2CO_3$ | THF | 0 |

**Figure 9.** Attempted Suzuki coupling of pinacol boronic ester (**322**) with allyl iodido (**323**) under various reaction conditions.

The same Suzuki coupling was attempted with the diaryl ether derived pinacol boronic ester **302a**. Unfortunately, despite the successful coupling of the model compound described above, the desired product was not formed with **323**, even after 2 days at reflux (Figure 10). There is no obvious reason why this should not work and the only difference between the model compound and the dimeric substrate is the presence of vinyl group on the other aryl. An extensive screening of reaction conditions, including various metal precursors, bases, ligands, and solvents, was conducted; a small subset of the conditions investigated is shown in shown in Figure 10. Unfortunately, I was not able to find conditions which gave the desired product (**303**).

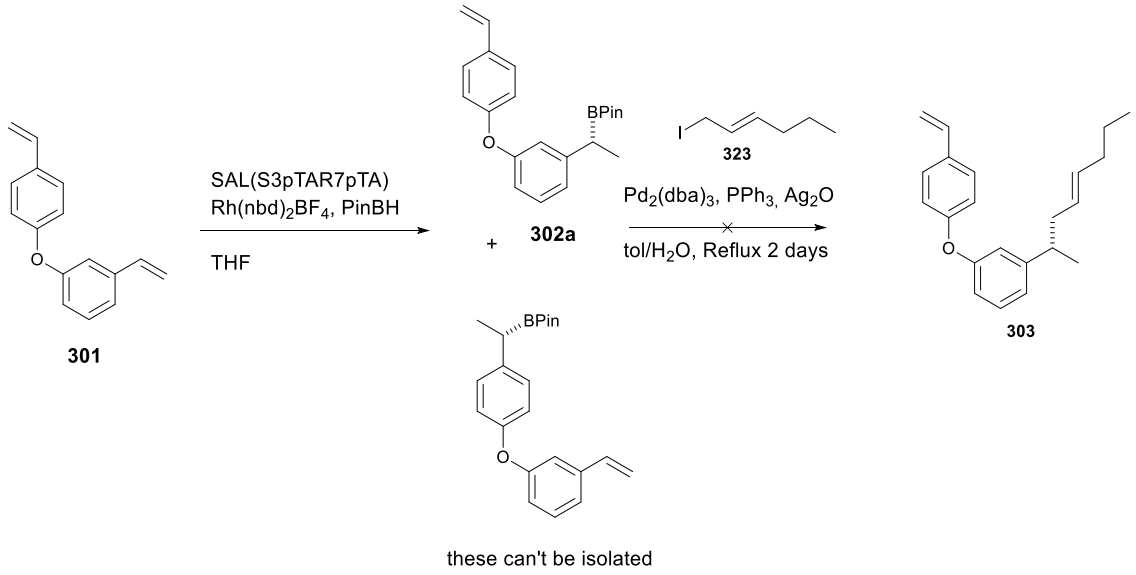


| entry | ligand | base | Yield (%) |
|---|---|---|---|
| 1 | $PPh_3$ | $Ag_2O$ | 0 |
| 2 | S PHOS | $Ag_2O$ | 0 |
| 3 | x PHOS | $Ag_2O$ | 0 |
| 4 | $PPh_3$ | $Ag_2CO_3$ | 0 |
| 5 | S PHOS | $Ag_2CO_3$ | 0 |
| 6 | x PHOS | $Ag_2CO_3$ | 0 |
| 7 | $PPh_3$ | $K_2CO_3$ | 0 |
| 8 | S PHOS | $K_2CO_3$ | 0 |
| 9 | x PHOS | $K_2CO_3$ | 0 |

**Figure 10.** The diaryl ether boronic ester (**302a**) did not did not afford the desired product (**303**) under conditions that were successful with the model compound.

Switching halide and boron functionalities for Suzuki coupling did not lead the formation of the desired product (**320**) shown in Figure 11. Allyl boronic ester (**324**), trifluoroborane potassium salt (**325**), and boronic acid (**326**) failed to undergo Suzuki coupling with the bromobenzaldehyde (**327**) to yield the coupled product. Although an

exhaustive screening of reaction conditions including various metal precursors, bases, ligands, and solvents was carried out, none of them produced any coupling product (**320**).

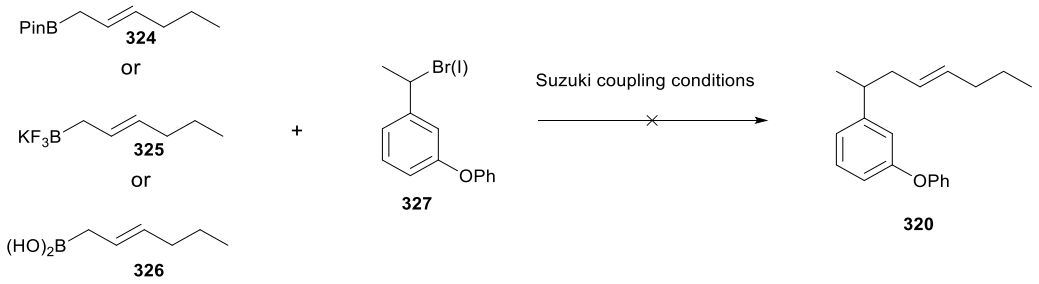


**Figure 11.** Transposition of the halide and boron-containing functionalities for Suzuki coupling did not lead the formation of the desired product.

Negishi coupling, a reaction for which more examples involving $Csp^2 – Csp^3$ and $Csp^3 – Csp^3$ have been documented[29-31] was explored as an alternative to Suzuki coupling. The use of organozinc compounds allows for a high degree of functional group tolerance and in contrast to Suzuki coupling, which requires base to enhance the reactivity, does not require the use of additives[32]. The main reason why I did not choose Negishi coupling as the first choice for the coupling reaction was that it requires a conversion of the boronic ester **302a** into the corresponding bromide reagent (**329**). To test the effectiveness of the Negishi approach, the zinc reagent was prepared from the allylic iodide **328** and used in attempted palladium- and nickel-catalyzed coupling (Figure 12). Neither led to the desired coupling product (**303**).

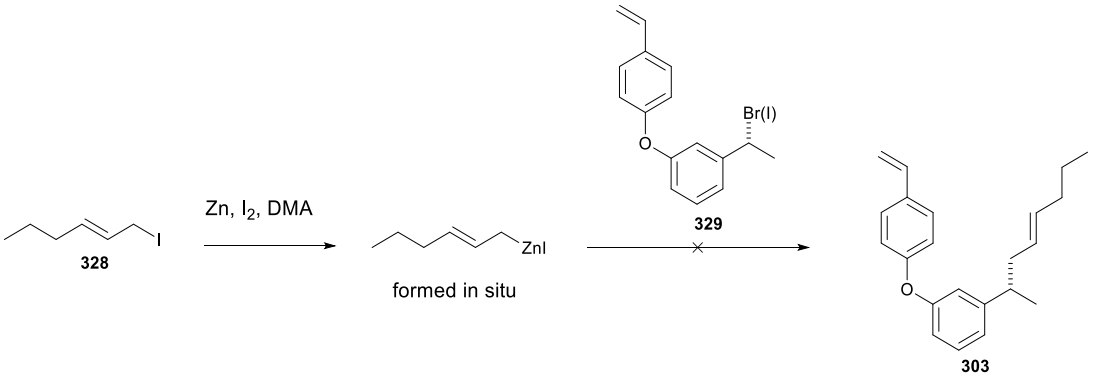


| entry | metal | ligand | Yield (%) |
|---|---|---|---|
| 1 | $Ni(PPh_3)_2Cl_2$ | $PPh_3$ | 0 |
| 2 | $Pd_2(dba)_3$ | $PPh_3$ | 0 |

**Figure 12.** Typical Negishi coupling condition with Pd and Ni.

Since there are several methods for preparing zinc reagents in-situ, other methods besides direct zinc exchange were explored. The benzylic zinc reagent **330** was generated and used in attempted coupling to the allylic bromide (**332**) and iodide (**331**) as shown in Figure 13. Surprisingly, none of the successful reaction condition identified by other groups[33-34] afforded the desired product (**303**). Instead, β-hydride elimination occurred (80% yield) to give **301** (Figure 13 entry 1). Although the end result was not what was expected, it does provide confirmation that the zinc reagent **330** was formed. This reaction was modeled using traditional (Zn, TMSCl) conditions for organozinc formation even though these result in formation of a racemic mix of stereoisomers.

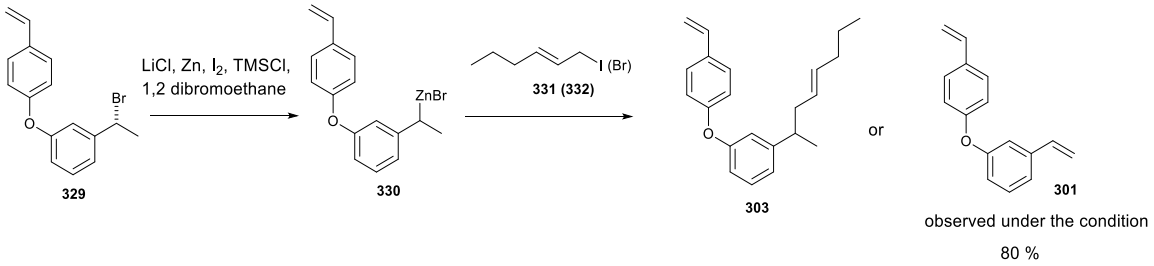


| entry | metal | ligand | additive | solvent | Yield (%) |
|---|---|---|---|---|---|
| 1 | $Pd_2(dba)_3$ | $PPh_3$ | NA | THF | 0 (80% of **1**) |
| 2 | $Pd(PPh_3)_4$ | NA | NA | THF | 0 |
| 3 | $Pd_2(dba)_3$ | $PCy_3$ | NA | THF | 0 |
| 4 | $Ni(PPh_3)_2Cl_2$ | $PPh_3$ | NA | THF | 0 |
| 5 | $Pd_2(dba)_3$ | X PHOS | NMI | THF/NMP | 0 |
| 6 | $Pd_2(dba)_3$ | XANPHOS | NMI | THF/NMP | 0 |
| 7 | $Pd_2(dba)_3$ | Ru PHOS | NMI | THF/NMP | 0 |

**Figure 13.** Negishi coupling with zinc preparation from activated zinc proceeded β-hydride elimination.

While exploring methods of preparing zinc reagent, it was found out that transmetallation of the Grignard reagent derived from the corresponding bromide (**327**) gave the zinc reagent. S PHOS identified by Knochel to be the best ligand in his study of cross-coupling reactions[33]. Unfortunately, in this case shown below, palladium-catalyzed cross-coupling did not give the desired coupling product (**320**). Instead, it afforded the $S_N2'$ reaction product (**333**) in moderate yield (62%). This reactions was observed only in presence of $Pd_2(dba)_3$ and S PHOS (Figure 14, compare entries 1, 2, 3, 4, 5, and 6). This reaction was also modeled with traditional conditions for Grignard formation even though these result in formation of a racemic mix of stereoisomers.

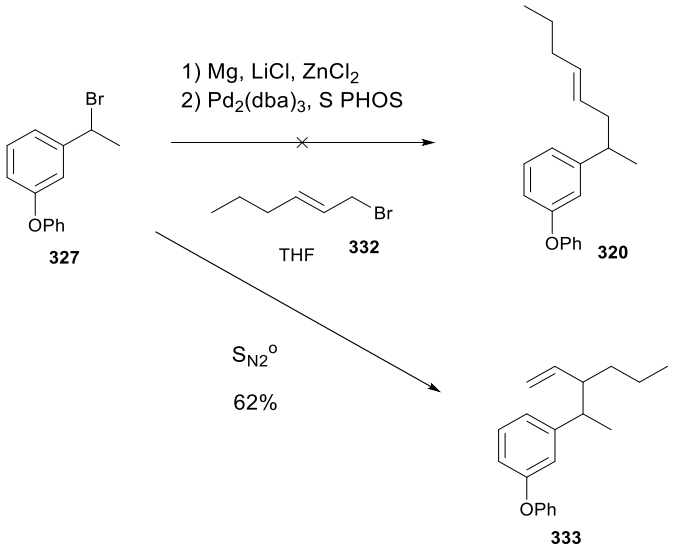


| entry | metal | ligand | Yield (%) |
|---|---|---|---|
| 1 | NA | NA | 0 |
| 2 | CuCN 2LiCl | NA | 0 |
| 3 | $Pd(OAc)_2$ | $PCy_3$ | 0 |
| 4 | $Pd_2(dba)_3$ | $PPh_3$ | 0 |
| 5 | $Pd_2(dba)_3$ | $PCy_3$ | 0 |
| 6 | $Pd(PPh_3)_4$ | NA | 0 |

**Figure 14.** S PHOS promoted Negishi coupling via $S_N2'$.

With the encouraging $S_N2'$results in hand, the allylic mesylate **334** was prepared with the expectation that the same mode of attack would yield the desired coupling product (**320**) from the model substrate (**327**). Indeed, Negishi coupling using the following conditions described below in Figure 15 proceeded in moderately good yield

(64%) (Figure 15, entry 1). $Pd(OAc)_2$ also worked but in lower yield (49%) (Figure 15. entry 2).

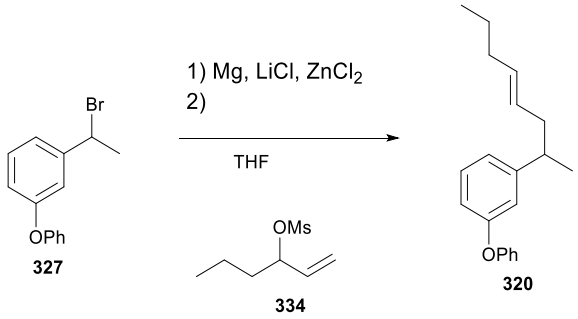


| entry | metal | ligand | Yield (%) |
|---|---|---|---|
| 1 | $Pd_2(dba)_3$ | S PHOS | 64 |
| 2 | $Pd(OAc)_2$ | S PHOS | 49 |
| 3 | $Pd_2(dba)_3$ | x PHOS | 0 |
| 4 | $Pd_2(dba)_3$ | John PHOS | 0 |
| 5 | $Pd_2(dba)_3$ | Ph Dave PHOS | 0 |
| 6 | $Pd_2(dba)_3$ | Ru PHOS | 0 |

**Figure 15.** Successful Negishi coupling with a model substrate to afford the desired product.

Knochel published two procedures for preparing zinc reagents in situ from boronic esters[33]. Both of them lead to the equally active zinc species and, in contrast to our model syntheses of organozincs based upon reduction, were expected to retain the stereochemistry of the organoboronate in the newly formed organozinc. Therefore, the **302a** was prepared via *meta* selective asymmetric hydroboration and converted to the zinc reagent followed by Negishi couplings. After numerous attempts to optimize the

reaction conditions, including various coupling partners, ligands, solvents, and temperatures, it was found that only up to 20% of the desired product **303** could be obtained under carefully optimized conditions with allylic tosylate **335**. Unfortunately, this was not a practical yield to continue the total synthesis. Therefore, my attention turned to different type of coupling partners which had been developed by Knochel[33].

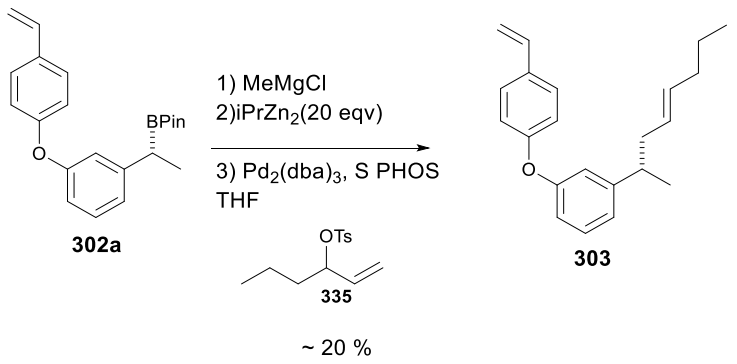


**Figure 16.** Boron to Zinc exchange followed by Negishi coupling did not afford the desired coupling product in satisfactory yield.

Knochel reported that zinc reagents couple well with acid chlorides under Negishi coupling conditions[33]. Acid chlorides (**337**) are easily prepared from the corresponding acid and Knochel even showed that the same acid chlorides (**337**) underwent coupling with copper catalysts (cheaper than palladium) in yields above 80%. These precedents encouraged me to try this method, even though the resulting product (**338**) contains a carbonyl which will need to be removed. Nonetheless, high yielding C-C bond formation to construct the target molecule to advance the progress of the synthesis was a top priority. As usual, the model substrate (**336**) was used to make sure that the coupling reaction works as it was reported (Figure 17A). Happily, the pinacol

boronic ester **302a** also underwent Negishi coupling without any issues in good yield (67%) (Figure 17B). The same reaction condition was applied to the hydroborated substrate **302a** with the acid chloride (**337**) resulting in successful formation of the desired coupling product (**339**).

(A)

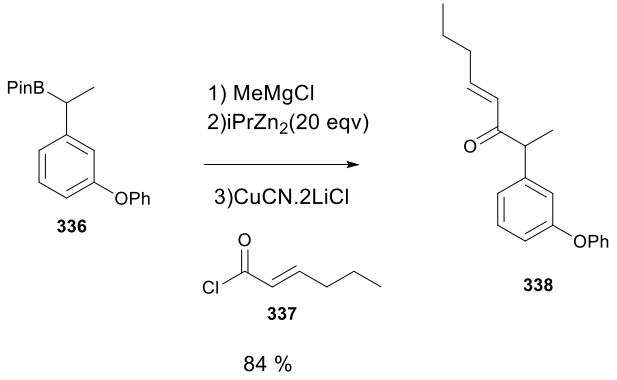


(B)

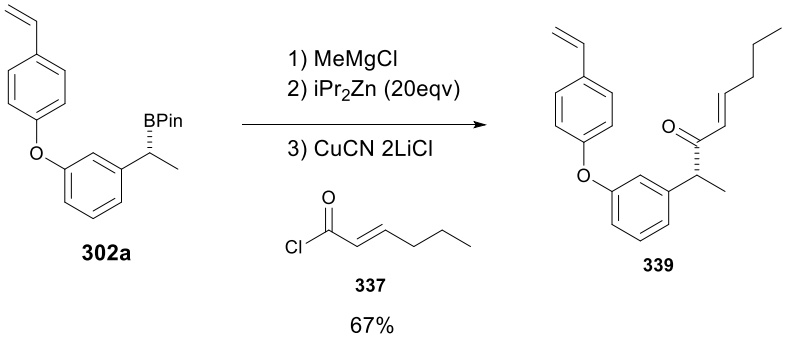


**Figure 17.** A: Negishi coupling of the model substrate. B: the dimeric substrate was successfully converted into the desired coupled product with good yield.

As a conclusion of this section of the chapter, the challenging aspect of this particular C-C bond formation was the limited methodology available for catalyzed $Csp^3$ – $Csp^3$ bond formation. Most of the Suzuki coupling literature were devoted into $Csp^2$ –

$Csp^2$ bond formation and only in the past decade research on $Csp^3$ – $Csp^3$ has started to pick up. However, most reports deal with activated $Csp^3$ center such as benzylic or allylic carbons, which initially seemed encouraging but ultimately proved difficult. Negishi coupling proved a better choice for $Csp^3$ – $Csp^3$ bond formation. This is especially true using to Knochel's[33, 39] $(RO)_2B/Zn$ in situ exchange permits a one pot coupling reaction.

### 3.5 Application of site selective hydroboration – Deoxygenation step

A reductive deoxygenation, while not part of our original retrosynthesis, became necessary upon the use of an acid chloride as an electrophile for C-C bond formation (see above). The challenge here is that the reduction/deoxygenation should be high yielding, take place in one step, and be compatible with the alkenes present in the substate. Because of the requirements my initial thought was to skip Barton – McCombie radical deoxygenation[34] as it might react with alkene groups which are present in the molecule. However, several total synthesis papers including Danishefsky[40] have used the radical deoxygenation for the removal of an oxygen atom with relatively good yields in the presence of unsaturated alkene. An advantage with the Barton – McCombie procedure is that it does not need exotic reagents to carry out the reaction. Also, it can be used to deoxygenate secondary alcohols. The model compound **340** was reduced to the alcohol (**341**) and converted to thioxo ester **342**. Exposure to tributyltin hydride effected the deoxygenation (Figure 18). The overall yield of 27% for the three step sequence was considered at least acceptable; some of the starting materials were left unreacted and could later be re-subjected to the reaction boosting the yield 60%. Nevertheless, a shorter alternative route was sought.

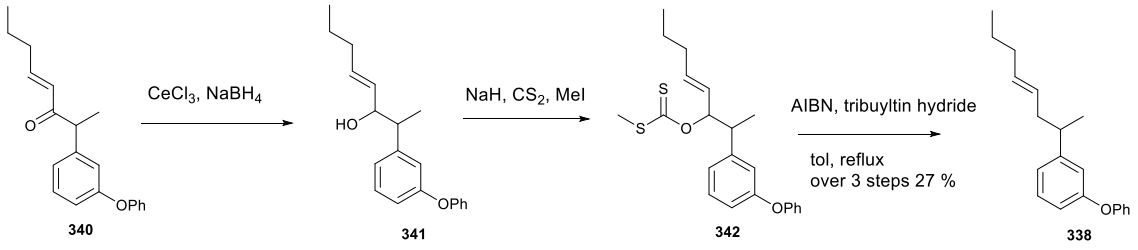


**Figure 18.** Barton – McCombie radical deoxygenation of the model substrate.

The well-known Wolff – Kishner reduction[36] was considered as an alternative. One of the nice features of Wolff-Kishner reduction is that it does not involve radical intermediates, which means that it most likely does not touch alkene moieties present in the substrate. However, the reaction conditions are rather harsh; usually the reaction requires high temperature (up to 200 $^{o}$C), long reaction times (usually a couple of days) and strongly basic conditions (excess of KOH or NaOH). The original Wollf – Kishner reduction procedure has been modified to make the reaction conditions milder and improve yield. Under more or less standard Wolff-Kishner conditions α, β-unsaturated carbonyl compounds form pyrazines and thus such substrates require alternative conditions. The use of preformed semicarbazones (**343**), which are said to undergo reduction under mild reaction conditions[41] afforded the desired product from the model substrate **340** in 47% yield over the two steps (Figure 19A); in contrast, employing the original Wolff-Kishner conditions with hydrazine gave a very messy reaction mixture. Next, the identical preformed semicarbazone reaction conditions were applied to enone **339** (Figure 19B). Unfortunately, the yield was disappointingly low, only 20% over the sequence. Throughout the study toward this natural product synthesis, most of the time the successful reaction conditions found with the model substrates did not prove as successful with the real substrate.

(A)

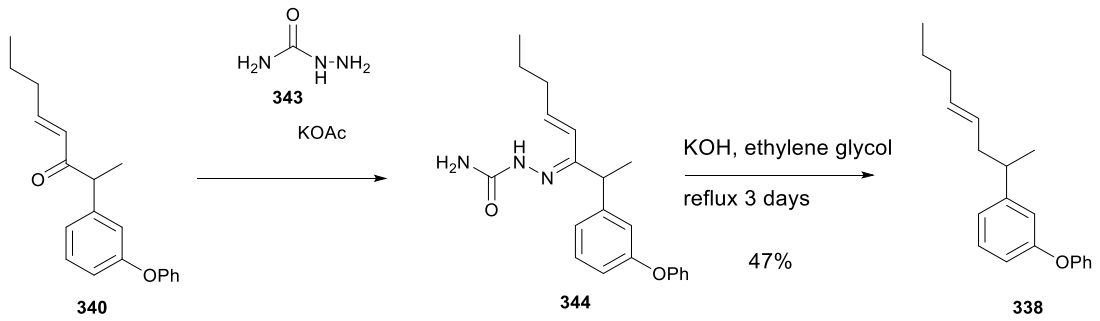


(B)

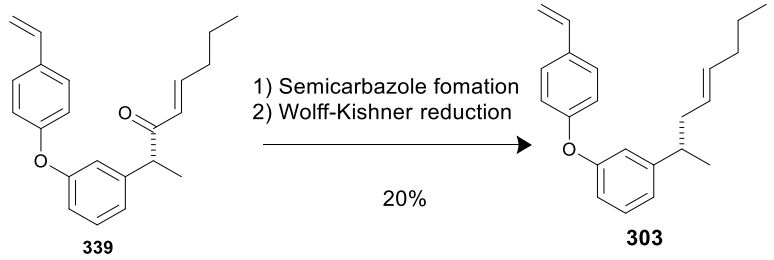


**Figure 19.** (A) Wolff-Kishner reduction with semicarbazone. (B) Semicarbazole procedure applied to the dimeric substrate.

Myers[12] reported that N, N'-bissilylated hydrazine greatly enhanced stability and reactivity relative to simple hydrazines and that the resulting silylated hydrazone undergoes efficient deoxygenation at relatively modest temperatures. This procedure decreases the reaction time from 3 days to overnight as well as reaction temperature (200 $^{o}$C to room temperature). Because of the much milder reaction conditions, the formation of byproducts was minimized with **345** and the desired product **303** was obtained in 75% yield (Figure 20). This is two step reaction but can be done sequentially

in one pot so that only one purification is necessary. The requirements set at the beginning of the optimum deoxygenation step are now cleared, since this provides high yielding one step transformation and alkene groups are not affected at all. Therefore, this was chosen as a part of the total synthesis.

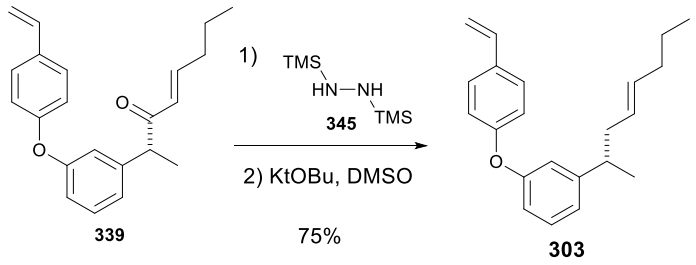


**Figure 20.** Myers modification of Wolff-Kishner deoxygenation worked great on the dimeric substrate.

Having synthesized **303**, Figure 21 shows other possible structural isomers of the antifungal target compound that can in principle be synthesized via a route analogous to that described above using compounds described in Chapter 2 of this thesis. The synthesized **303** was used towards the total synthesis steps described in Figure 3 without any difficulty to reach the final product anti-fungi compound (the detailed procedures are available in the experimental section).

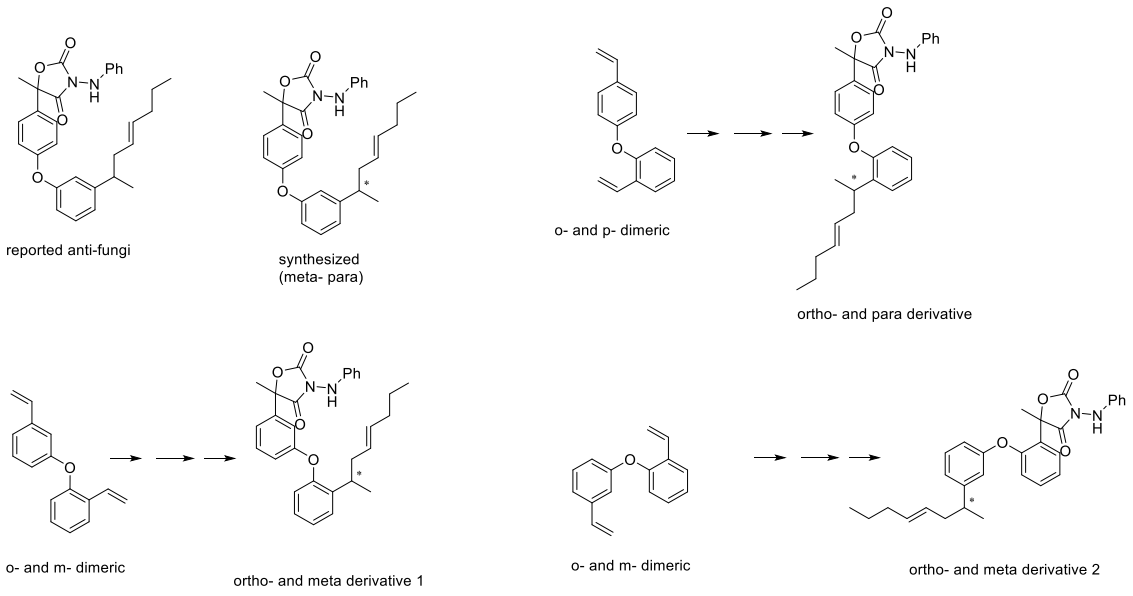


**Figure 21.** Other possible structural isomers of anti-fungi natural products that can be prepared using site selective SALs.

**3.6 Application of site selective hydroboration - conclusions**

In summary, I prepared several hundred milligrams of an enantiomerically pure form of a potent antifungal compound which is in commercial agrochemical. My synthesis, which was based upon a newly developed site-selective hydroboration (see Chapter 2), was completed in 14 steps and 6.4% overall yield from cheap and commercially available benzaldehyde derivatives. This is the first asymmetric total synthesis of this compound. Of all of 14 steps only 2 steps require expensive Rh metals but the catalyst loading was reduced to 0.01 %, which helps keeping the overall synthesis cost down. Negishi coupling of $sp^3 – sp^3$ cross coupling reaction was successfully carried out via boron-zinc exchange method developed by Knochel *et al* to add examples for rather rare $sp^3 – sp^3$ cross coupling literature.

## 3.7 Experimental

### Synthesis toward anti fungi compound using site selective hydroboration as a key step.

Synthesis of acid and acid chloride **339** was previously disclosed[42]. Therefore it is not described in this thesis.

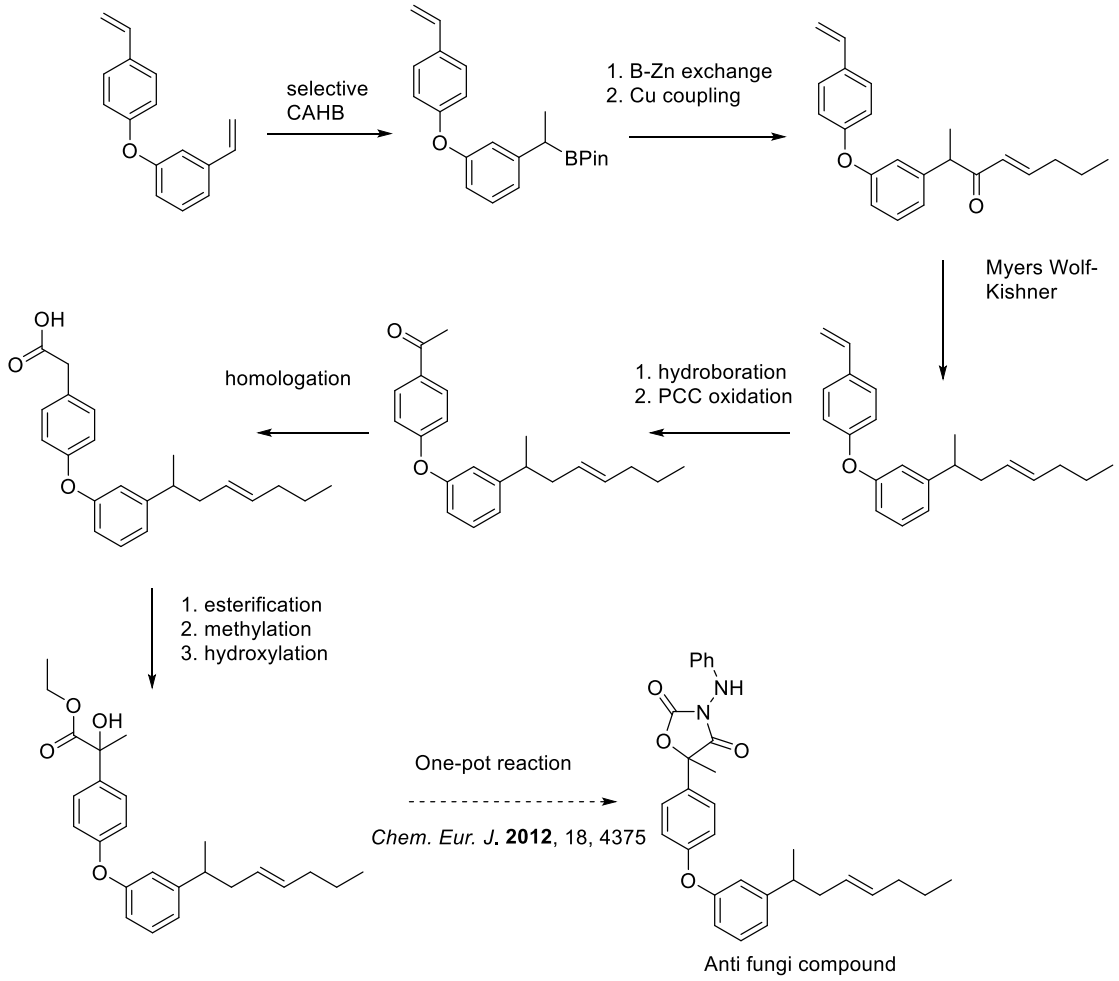

Synthesis of 3-(4-formylphenoxy) benzaldehyde **318**

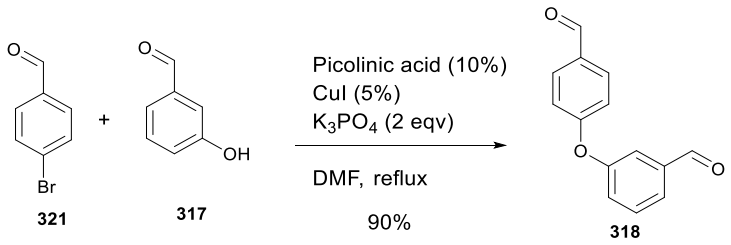


An oven-dried round bottom flask was charged with a magnetic stir bar, copper (I) iodide (5%), picolinic acid (10%), 4-bromobenzaldehyde **321** (1.0 eqv), 3-hydroxybenzaldehyde (1.2 eqv) and $K_3PO_4$ (2.0 eqv). The flask was then evacuated and back-filled with argon. DMF was added by syringe. The flask was placed in a preheated oil bath at 80 ºC and the reaction mixture was stirred vigorously for 24 h. The reaction mixture was cooled to room temperature. Ethyl acetate (10 mL) and $H_2O$ (1 mL) were added and the mixture was stirred. The organic layer was separated and the aqueous layer was extracted twice with ethyl acetate (10 mL). Combined organic layer was dried over $Na_2SO_4$ and filtered. The filtrate was concentrated and the resulting residue was purified via column chromatography on silica gel (10:90 ethyl acetate:hexane) gave the product **318** (90 %): TLC analysis Rf = 0.85 (10:90 ethyl acetate:hexane); $^1$H NMR (400 MHz, $CDCl_3$) δ 10.59 (s, 1H), 10.48 (s, 1H), 7.91 (d, 1H, J = 4.0), 7.44-7.40 (m, 1H), 7.27 (d, 1H, J =8.0), 7.28-6.94 (m, 3H), 6.93 (d, 1H, J = 8.0), 6.66 (d, 1H, J = 8.0) ppm; $^{13}$C NMR (100 MHz, $CDCl_3$) δ 189.6, 189.5, 160.6, 153.7, 136.0, 131.9, 130.3, 128.6, 127.7, 125.9, 125.2, 122.7, 120.4, 116.7, ppm; HRMS (FAB) calcd. for $C_{14}H_{10}O_0$ ($M^+$), 226.0630; found, 226.0742*m/z*.

Synthesis of 1-vinyl-3-(4-vinylphenoxy) benzene **301**

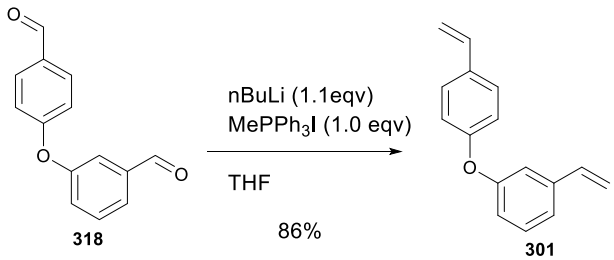

An oven-dried round bottom flask was charged with a magnetic stir bar and $MePPh_3I$ (1.1 eqv) in THF. The solution was cooled to -78°C with dry ice acetone bath and the nBuLi in THF solution (1.6 M) added dropwise over the course of 10 minutes. The resulting mixture was stirred for 30 minutes. A solution containing the compound **318** in THF was prepared into another round bottom flask and added dropwise to the reaction mixture. The acetone dry ice bath was removed and the reaction flask was stirred at room temperature for overnight. The reaction was quenched with an addition of $H_2O$ and the aqueous layer was extracted twice using EtOAc. Combined organic layer was dried over $Na_2SO_4$ and filtered. The filtrate was concentrated and the resulting residue was purified via column chromatography on silica gel (10:90 ethyl acetate:hexane) gave the product **301**. $^1$H NMR (400 MHz, $CDCl_3$) δ 7.50-7.46 (2H, m), 7.39 (1H, t, *J* = 8 Hz), 7.28-7.26 (1H, m), 7.22 (1H, t, *J* = 2.0 Hz), 7.11-7.08 (2H, m), 6.82 (1H, t, *J* = 10.4 Hz), 6.77 (1H, t, *J* = 10.4 Hz), 5.84 (1H, dd, *J* = 17.6, 0.8 Hz), 5.79 (1H, dd, *J* = 17.6, 0.8 Hz), 5.37 (1H, dd, *J* = 6.8, 0.4 Hz), 5.31 (1H, dd, *J* = 10.8, 0.8 Hz) ppm; $^{13}$C NMR (100 MHz, $CDCl_3$) δ 157.50, 157.07, 139.66, 136.38, 136.15, 132.98, 129.95, 1297.74, 123.36, 121.58, 118.94, 118.46, 116.68, 114.81, 114.74, 113.00 ppm; IR (neat) 3087, 3056, 3044 (C-H stretch), 1598, 1574, 1503, 1486 (C=C ring stretch), 1232, 1215 (C-O-C stretch), 1024, 1011, 905 (alkene), 837, 788 (C-H bend), 733, 712 (C=C bend); HRMS (EI) calcd for $C_{16}H_{14}O$ [$M^+$], 222.1045; found: 222.1042 *m/z*.

Selective hydroboration procedure

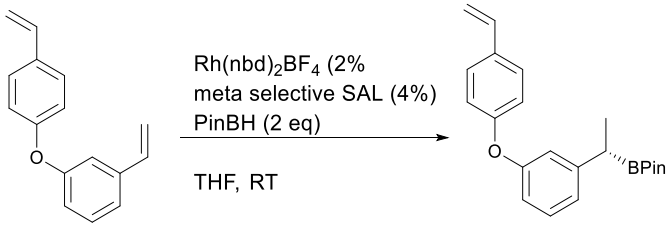


The catalyst mixture was prepared in the glovebox as follow: A solution of S3pTA (21.6 mg, 19.6 x $10^{-3}$ mmol) and R7pTA (20.4 mg, 19.6 x $10^{-3}$ mmol) in DCM (6 mL) was combined with a solution of $ZnEt_2$ (1.28mg, 19.6 x $10^{-3}$ mmol) in DCM (3mL) into a 50 mL

round bottom flask and stirred at ambient temperature (RT, ca. 5 min.) and then a solution of $Rh(nbd)_2BF_4$ (7.4 mg, 20 x $10^{-3}$ mmol) in DCM (2 mL) was added. The resulting mixture was stirred at ambient temperature (0.5 h) after which the volatile solvent was removed under vacuum. The residue was dissolved in THF (6 mL), stirred (0.5 h) and then 0.3mL aliquot of the solution was transferred into a 50 mL round bottom flask. The substrate (450 mg, 1.5 mmol) in THF (10.0mL) was added. The resulting mixture was cooled (0 $^oC$) and a solution of pinacolborane (260 micro L, 3.0 mmol) in THF (5.0 mL) added by syringe pump. The reaction mixture was gradually warmed to RT and stirred (12 h). The reaction mixture was injected to a short silica gel column and washed with ethyl acetate two times. The volatile solvent was removed under reduced pressure to give the boronic ester. This was used for the next step without purification.

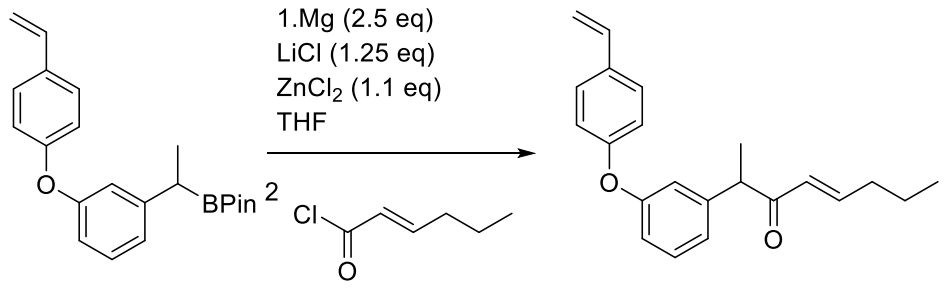


The synthesis of the organozinc reagent is based upon procedures described by Knochel and coworkers; [39]

Magnesium turnings, LiCl and $ZnCl_2$ were added according to Knochel procedure to a dry 50 mL round bottom flask. The boronic ester in THF was added via cannula at 0$^oC$ and stirred for 2 hours.

**Cu coupling procedure**

The solution of the complex CuCN 2LiCl was prepared according to the literature (Organic Syntheses, 1998, 9, 502). The solution of the zinc reagent prepared freshly was transferred to the THF solution of copper cyanide and lithium chloride at – 40$^{o}$C. The resulting solution was warmed to 0$^{o}$C and the acid chloride in THF was added slowly. The reaction mixture was stirred at room temperature overnight. This was quenched with slow addition of sat $NH_4Cl$ solution. The solution was extracted with diethyl ether and combined organics were dried ($MgSO_4$) and concentrated under reduced pressure. Chromatography on silica gel (10:90 ethyl acetate:hexane) gave the product (425 mg, 71 %): TLC analysis Rf = 0.95 (10:90 ethyl acetate:hexane); $^{1}$H NMR (400 MHz, $CDCl_3$) δ 7.35 – 6.88 (9H,m), 6.43 – 6.28 (1H,m), 5.91 – 5.87 (1H, m), 5.16 – 5.13 (2H, m), 2.03 – 2.01 (5H, m), 1.54 – 1.47 (3H, m), 0.96 – 0.91 (3H, m) ppm; $^{13}$C NMR (100 MHz, $CDCl_3$) δ 149.54, 135.31, 131.41, 130.78, 130.05, 128.69, 127.66, 127.65, 122.37, 119.38, 118.71, 118.67, 117.74, 116.24, 112.63, 41.25, 35.96, 28.47, 21.88, 21.46, 13.95 ppm; HRMS (FAB) calcd. for $C_{22}H_{24}O_2$ ($M^+$), 320.1766; found, 320.1674*m/z*.

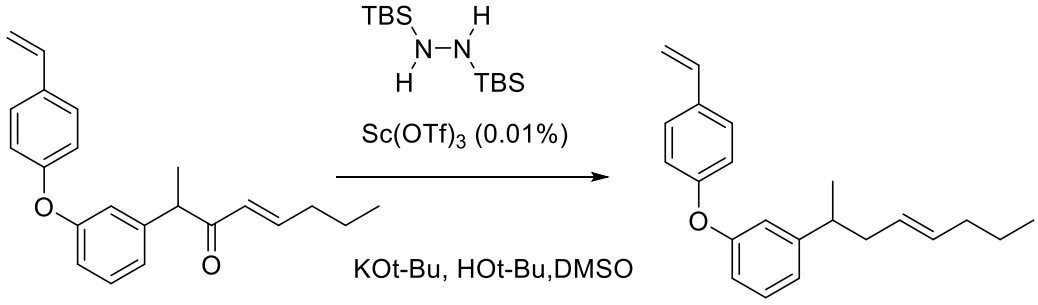


Myers Wolff Kishner reduction procedure (*J. Am. Chem. Soc.* **2004**, 126, 5436)

A freshly prepared solution of scandium trifluoromethanesulfonate in acetonitrile was transferred to a 50 mL round bottom flask. The solvent was removed by Schlenk line. 1.2- Bis(tert-butyldimethylsilyl)hyfrazine was introduced and the reaction flask was cooled in an ice bath. The ketone (425 mg, 1.3 mmol) was added dropwise over 15 min.

The reaction solution was stirred for an additional 15 min at 0°C, then the ice bath was removed, and the reaction mixture was allowed to warm to room temperature. The flask was carefully evacuated with stirring. After stirring under vacuum for 1 h, the flask was immersed in an oil bath (35°C). The reaction mixture was stirred under vacuum at 35°C for 4 h. A separate round bottom flask was charged with potassium tert-butoxide and DMSO was added. The solution was stirred at room temperature until all particles had dissolved. Tert-Butanol was added via syringe and the resulting solution was transferred to the original reaction flask. The reaction mixture was stirred for 24 h and quenched with brine. The reaction mixture was extracted with diethyl ether 3 times and the organic extracts were combined, dried ($MgSO_4$), and removed under reduced pressure. Chromatography on silica gel (10:90 ethyl acetate:hexane) gave the product (305 mg, 75 %): TLC analysis Rf = 0.90 (10:90 ethyl acetate:hexane); $^1$H NMR (400 MHz, $CDCl_3$) δ 7.40 (1H, s), 7.38 (1H, s), 7.26 (1H, s), 7.24 (1H,s), 6.99 – 6.67 (2H, m), 6.92 (1H, m), 6.85 – 6.83 (1H, m), 6.75 – 6.68 (1H, dd, J = 17.6, 10.9 Hz), 5.70 – 5.66 (1H, d, J = 17.0 Hz), 5.42 – 5.29 (2H, m), 5.22 – 5.19 (1H, d, J = 10.9 Hz), 2.78 – 2.72 (1H, h, J = 6.0 Hz), 2.33 – 2.30 (2H, t, J = 7.0 Hz), 1.98 – 1.94 (2H, m), 1.36 – 1.30 (2H, m), 1.27 – 1.26 (3H, d, J = 6.9 Hz), 0.91 – 0.86 (3H, m) ppm; $^{13}$C NMR (100 MHz, $CDCl_3$) δ 157.34, 157.02, 149.70, 136.20, 132.71, 131.16, 129.57, 127.83, 127.65, 122.37, 118.71, 118.67, 117.94, 116.53, 112.82, 40.20, 36.02, 29.53, 22.89, 21.49, 13.94 ppm; HRMS (FAB) calcd. for $C_{22}H_{26}O$ ($M^+$), 306.1984; found, 306.1867*m/z*.

Hydroboration

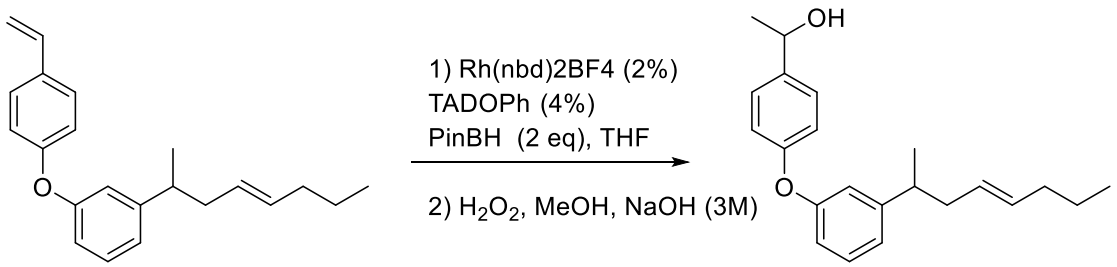

The catalyst mixture was prepared in the glovebox in order to prevent catalyst decomposition. TADOPh (54.6 mg, 0.088 mmol) and $Rh(nbd)_2BF_4$ (16.6 mg, 0.044 mmol) were dissolved in THF (5 mL) into a 100 mL round bottom flask and the resulting catalyst solution was stirred for 30 minutes. The substrate (305 mg, 1.0 mmol) was added and the solution was further stirred for 10 minutes. The reaction mixture was cooled to 0°C and PinBH (175 micro L, 2.0 mmol) in THF (2.0 mL) was added slowly. The resulting reaction mixture was warmed to room temperature gradually and stirred for 8 hours. The reaction was quenched with MeOH (11 mL), NaOH (3M, 15 mL), and $H_2O_2$ (2mL) and the solution was stirred for at least 1 hour. It was extracted with EtOAc 3 times and combined organics were dried ($MgSO_4$) and concentrated. Chromatography on silica gel (10:90 ethyl acetate:hexane) gave the product (280 mg, 87 %): TLC analysis Rf = 0.85 (10:90 ethyl acetate:hexane); $^1$H NMR (400 MHz, $CDCl_3$) δ 7.35 – 7.33 (2H, m), 7.26 – 7.23 (2H, m), 7.00 – 6.93 (3H, m), 6.87 (1H, d, J = 1.5 Hz), 6.82 – 6.80 (1H, d, J = 7.8 Hz), 5.39 – 5.32 (2H, m), 4.91 -4.90 (1H, m), 2.75 – 2.64 (1H, m), 2.29 – 2.18 (1H, m), 1.99 – 1.92 (2H, m), 1.76 (1H, s), 1.62 (1H, m), 1.53 – 1.51 (4H, d, J = 6.4 Hz), 1.34 – 1.30 (2H, m), 1.23 -1.22 (3H, d, J = 6.8 Hz), 0.97 – 0.93 (1H, m), 0.91 – 0.83 (2H, m) ppm; $^{13}$C NMR (100 MHz, $CDCl_3$) δ 156.95, 140.43, 132.40, 132.24, 128.38, 124.92, 117.91, 116.42, 116.32, 41.51, 40.23, 39.92, 37.91, 34.76, 30.65, 27.75, 22.75, 22.29, 21.39, 14.08, 13.70 ppm; HRMS (FAB) calcd. for $C_{22}H_{28}O_2$ ($M^+$), 324.2089; found,324.2088 *m/z*.

PCC procedure

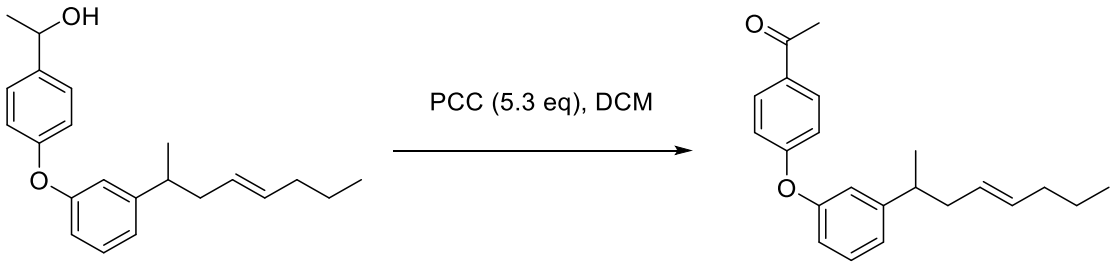


The alcohol (280 mg, 0.86mmol) was added into a 50 mL round bottom flask and PCC (975 mg, 4.52 mmol) was added sequentially. DCM (20 mL) was added to the flask and

the resulting solution was stirred overnight at room temperature. The reaction mixture was quenched with careful addition of sat. $NaHCO_3$. It was extracted with diethyl ether 3 times and combined organics were dried ($MgSO_4$) and concentrated. Chromatography on silica gel (10:90 ethyl acetate:hexane) gave the product (224 mg, 81%): TLC analysis Rf = 067 (10:90 ethyl acetate:hexane); $^1$H NMR (400 MHz, $CDCl_3$) δ 7.2 – 7.22 (3H, m), 7.03 – 6.89 (5H, m), 6.80 – 6.79 (1H, m), 3.66 (2H, s), 3.10 – 3.07 (1H, m), 2.72 – 2.55 (1H, m), 2.32 – 2.19 (1H,m), 2.01 – 1.88 (2H, m), 1.67 – 1.56 (2H, m), 1.31 – 1.30 (2H, m), 1.26 – 1.20 (4H, m) ppm; $^{13}$C NMR (100 MHz, $CDCl_3$) δ 157.15, 151.21, 129.79, 129.50, 127.41, 121.22, 117.51, 117.10, 116.33, 60.90, 44.50, 41.21, 40.07, 40.20, 39.10, 38.21, 35.63, 30.77, 27.44, 22.54, 14.24 ppm HRMS (FAB) calcd. for $C_{22}H_{26}O_2$ ($M^+$), 322.1933; found, 322.1934 *m/z*.

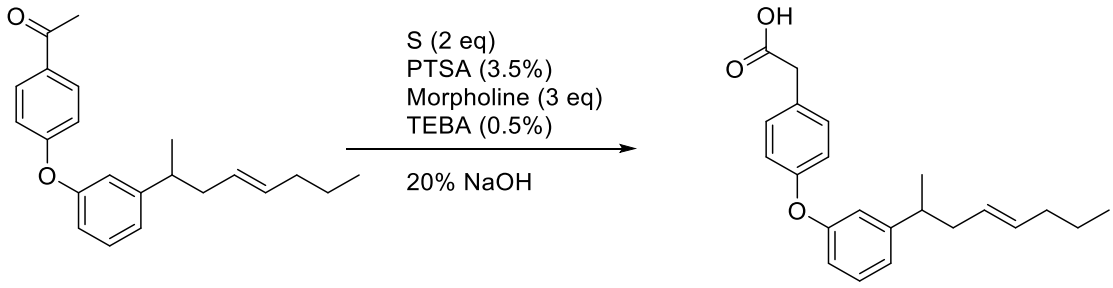


The ketone (240 mg, 0.7 mmol), sulfur (45 mg, 1.4 mmol), morpholine (0.2mL, 2.1 mmol), PTSA (4 mg, 0.25 mmol) were added and it was refluxed in an oil bath (120$^o$C) overnight. The reaction mixture was allowed to cool and 20% NaOH and triethyl benzyl ammonium chloride (TEBA) (8 mg, 0.0035 mmol) were added to the reaction mixture. This mixture was stirred at 100 $^o$C for additional 8 h. The reaction mixture was cooled and filtered. The filtrate was acidified with HCL to pH 6 and then filtered off. The filtrate was further acidified to pH 2. 10% $NaHCO_3$ solution was added and the solution was extracted with EtOAc 3 times. The combined organic layers were dried and concentrated under vacuo. chromatography on silica gel (10:90 ethyl acetate:hexane) gave the product (70 mg, 30 %): TLC analysis Rf = 0.70 (10:90 ethyl acetate:hexane); $^1$H NMR (400 MHz, $CDCl_3$) δ 7.24 – 7.22 (3H, m), 7.00 – 6.87 (5H, m), 6.81 – 6.79 (1H, d, J =

8.1 Hz), 5.38 – 5.31 (2H, m), 3.64 (2H, s), 3.08 – 3.01 (1H, m), 2.75 – 2.58 (1H, m), 2.33 – 2.17 (1H,m), 2.01 – 1.89 (2H, m), 1.62 – 1.52 (2H, m), 1.32 – 1.30 (2H, m), 1.23 – 1.21 (4H, m) ppm; $^{13}$C NMR (100 MHz, $CDCl_3$) ; 157.13, 151.22, 129.77, 129.51, 127.40, 121.20, 117.50, 117.12, 116.30, 60.88, 44.45, 41.25, 40.11, 40.21, 39.12, 38.17, 35.57, 30.71, 27.49, 22.60, 14.25 ppm, HRMS (FAB) calcd. for $C_{22}H_{26}O_3$ ($M^+$), 338.1882; found, 338.1871*m/z*.

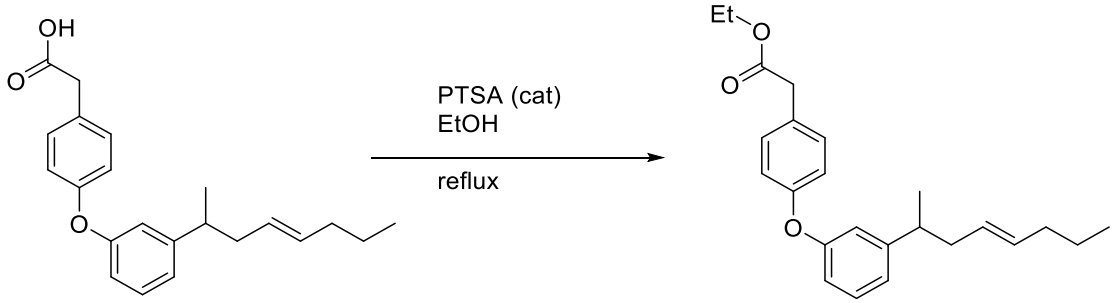


The acid (70 mg, 0.21 mmol) was charged in a dry 25 pear shaped flask and one small chunk of PTSA (cat) was added to the flask. EtOH was added to the flask and refluxed overnight. The solvent was removed under reduced pressure and chromatography on silica gel (10:90 ethyl acetate:hexane) gave the product (47 mg, 61 %): TLC analysis Rf = 0.65 (10:90 ethyl acetate:hexane); $^1$H NMR (400 MHz, $CDCl_3$) δ 7.27 – 6.80 (8H, m), 5.37 – 5.32 (2H, m), 4.18 – 4.09 (1H, m), 3.60 – 3.57 (1H, m), 2.73 – 2.64 (1H, m), 2.28 – 2.20 (1H, m), 2.00 – 1.92 (2H, m), 1.60 – 1.49 (3H, m), 1.32 – 1.22 (9H, m), 0.93 – 0.85 (2H, m) ppm; $^{13}$C NMR (100 MHz, $CDCl_3$) δ 157.14, 151.20, 129.78, 129.51, 127.41, 121.21, 117.54, 117.14, 116.28, 60.87, 44.45, 41.22, 40.10, 40.21, 39.68, 39.13, 38.17, 35.47, 30.61, 27.47, 22.60, 21.39, 14.25 ppm; HRMS (FAB) calcd. for $C_{24}H_{30}O_3$ ($M^+$), 366.2195; found, 366.2188 *m/z*.

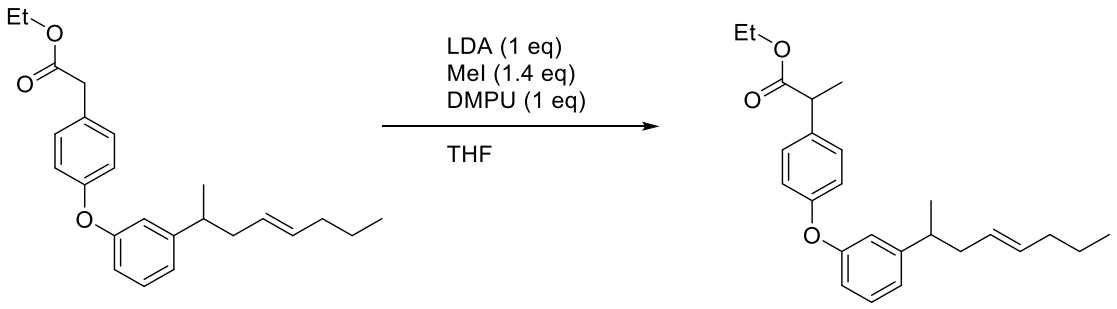


The ester (47mg, 0.13 mmol) was charged in a dry 25 mL pear shaped flask and THF was added. The solution was cooled to – 78 $^{o}$C and a solution of freshly prepared LDA (56 micro L of nBuLi + 14 mg of diisopropylamine in THF) was added dropwise. The reaction mixture was stirred for 1 h, MeI (26mg, 0.18 mmol) was added dropwise, followed by the addition of DMPU (21 micro L). The reaction mixture was stirred overnight and was quenched with addition of water. The mixture was extracted with EtOAc 3 times and the combined organic layers were dried ($MgSO_4$) and concentrated in vacuo. chromatography on silica gel (10:90 ethyl acetate:hexane) gave the product (27 mg, 55 %): TLC analysis Rf = 0.75 (10:90 ethyl acetate:hexane); $^{1}$H NMR (400 MHz, $CDCl_3$) δ 7.27 – 6.80 (8H, m), 5.37 – 5.32 (2H, m), 4.18 – 4.09 (1H, m), 3.60 – 3.57 (1H, m), 2.73 – 2.64 (1H, m), 2.28 – 2.20 (2H, m), 2.00 – 1.92 (2H, m), 1.60 – 1.49 (3H, m), 1.32 – 1.22 (9H, m), 0.93 – 0.85 (3H, m) ppm; $^{13}$C NMR (100 MHz, $CDCl_3$) δ 157.00, 150.22, 130.61, 129.53, 128.80, 122.31, 118.58, 117.98, 116.42, 60.97, 44.96, 41.52, 40.74, 40.23, 39.92, 39.33, 38.19, 34.77, 30.66, 27.75, 22.75, 21.39, 14.25 ppm; δ HRMS (FAB) calcd. for $C_{25}H_{32}O_3$ ($M^+$), 380.2351; found, 380.2345 *m/z*.

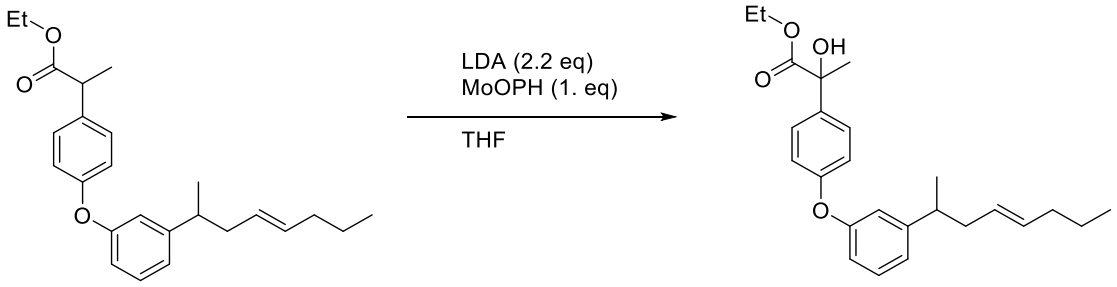

LDA (0.75M in THF) was freshly prepared before its use. An aliquot of 10 mL of LDA solution was transferred to a dry 8 mL vial with septa. The solution was cooled to – 78°C and the ester (27 mg, 0.07 mmol) in THF was added dropwise. After 30min, MoOPH (44 mg, 0.1 mmol) was added over 5 min and the reaction mixture was allowed to warm to room temperature, which was stirred overnight. The reaction mixture was quenched with sat sodium sulfite solution. After 10 min of stirring, the mixture was extracted with diethyl ether 3 times. The combined organics were dried ($MgSO_4$) and filtered. Then the solvent was removed under reduced pressure. Chromatography on silica gel (10:90 ethyl acetate:hexane) gave the product (20 mg, 70 %): TLC analysis Rf = 0.60 (10:90 ethyl acetate:hexane) $^1$H NMR (400 MHz, $CDCl_3$) δ 7.25 – 6.77 (8H, m), 5.35 – 5.32 (2H, m), 4.17 – 4.08 (1H, m), 3.62 – 3.59 (1H, m), 2.74 – 2.64 (1H, m), 2.28 – 2.19 (2H, m), 1.99 – 1.92 (2H, m), 1.63 – 1.51 (3H, m), 1.30 – 1.21 (9H, m), 0.93 – 0.84 (3H, m) ppm; $^{13}$C NMR (100 MHz, $CDCl_3$) δ 156.87, 150.14, 130.14, 129.74, 128.12, 122.11, 118.78, 118.41, 116.10, 60.47, 44.6, 41.52, 40.47, 40.33, 39.72, 39.13, 38.01, 35.77, 30.96, 27.65, 21.65, 21.30, 14.25 ppm; HRMS (FAB) calcd. for $C_{25}H_{32}O_4$ ($M^+$), 396.2301; found, 396.2300 *m/z*.

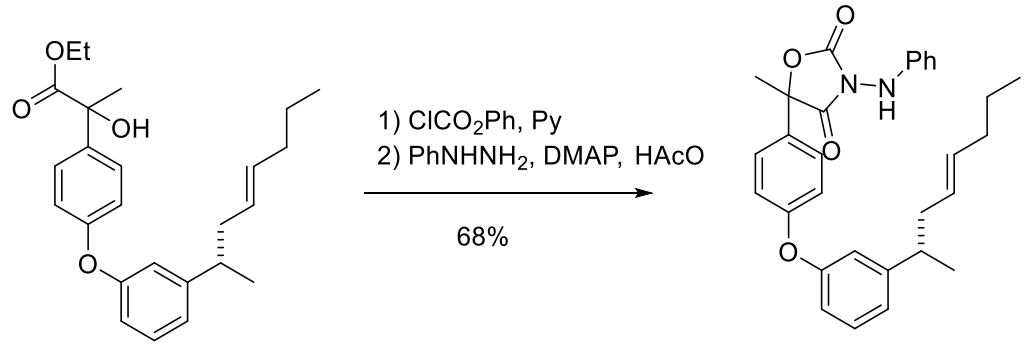


5 Anti fungi compound

To a solution of **5** (20 mg, 0.05mmol) in anhydrous $CH_2Cl_2$ under N2 atmosphere was added pyridine (0.076 mmol). The mixture was cooled to 0°C, and then was added dropwise of phenyl chloroformate (0.06 mmol). An abundant white solid was observed. The reaction mixture was warmed to room temperature and stirred overnight. Then,

water was added and the resulting mixture was extracted with ethyl acetate, dried over MgSO4, filtered off, and the solvents were evaporated to give a solid which was used in the next step without further purification. To a solution of the preceding carbonate in THF was added DMAP (6.1 mg, 0.05 mmol), acetic acid (0.5 mmol), phenyl hydrazine hydrochloride (1.0 mmol) and anhydrous triethylamine (1.0 mmol) in this order. Next, the reaction mixture was refluxed and stirred for 36 h. After cooling the reaction mixture to room temperature, the volatiles were removed under reduced pressure. Afterwards, water and DCM was added, and the resulting mixture was extracted with DCM, dried over MgSO4, filtered off, and the solvents were evaporated. Chromatography on silica gel (10:90 ethyl acetate:hexane) gave the product (16mg, 68 %): TLC analysis Rf = 0.70 (10:90 ethyl acetate:hexane), $^{1}$H NMR (400 MHz, $CDCl_3$) δ 7.60 – 7.40 (5H, m), 7.28 – 6.74 (9H, m), 5.37 – 5.30 (2H, m), 4.18 – 4.08 (1H, m), 3.60 – 3.57 (1H, m), 2.77 – 2.64 (1H, m), 1.99 – 1.94 (2H, m), 1.31 – 1.20 (9H, m), 0.94 – 0.84 (3H, m) ppm; $^{13}$C NMR (100 MHz, $CDCl_3$) δ 172.12, 156.84, 150.10, 130.15, 129.81, 128.10, 122.07, 118.74, 118.47, 116.11, 60.51, 44.54, 41.50, 40.41, 40.30, 39.67, 39.10, 37.9, 35.71, 30.94, 27.69, 25.5 21.65, 21.34, 14.22 ppm; HRMS (FAB) calcd. for $C_{30}H_{32}N_2O_4$ ($M^+$), 484.2362; found, 484.2308 *m/z*.

**3.8 References:**


1. *PCT Int Appl* **1993** WO 9318016 A1 19930916
2. N. D. Antona, P. Lombardi, G. Nicolosi, G. Salvo, "Large scale preparation of enantiopure S-ketoprofen b biocatalysed kinetic resolution*", Process Biochemistry*, **2002**, 38, 373
3. B. Knoche, G. Blaschke, "Investigations on the in vitro racemization of thalidomide by high performance liquid chromatography", *Journal of Chromatography A*, **1994**, 666, 235
4. S. H. Kennedy, H. F. Andersen, R. W. Lam*, "*Comparative efficacy of escitalopram in the treatment of major depressive disorder". *J Psychiatry Neurosci*. **2006**, 31 (2), 122
5. R. Infante, J. Nieto, C. Andres. "Highly Homogeneous Stereocontrolled Construction of Quaternary Hydroxyesters by Addition of Dimethylzinc to α-Ketoesters Promoted by Chiral Perhydrobenzoxazines and $B(OEt)_3$". *Chem. Eur. J*. **2012**, 18, 4375
6. N. Miyaura, A. Suzuki, "Stereoselective synthesis of arylated (*E*)-alkenes by the reaction of alk-1-enylboranes with aryl halides in the presence of palladium catalyst". *J. Chem. Soc. Chem. Commun*. **1979**, 866
7. N. Miyaura, K. Yamada, A. Suzuki, **"**A new stereospecific cross-coupling by the palladium-catalyzed reaction of 1-alkenylboranes with 1-alkenyl or 1-alkynyl halides". *Tetrahedron Lett*. **1979**, 3437
8. N. Miyaura, T. Yanagi, A. Suzuki, "The Palladium-Catalyzed Cross-Coupling Reaction of Phenylboronic Acid with Haloarenes in the Presence of Bases". *Synth. Commun*. **1981**, 11, 513
9. E. Hupe, Isabel. M. Calaza, P. Knochel, "Synthesis and reaction of secondary and primary diorganozinc reagents using a boron–zinc exchange reaction: A useful method for the stereo- and regioselective formation of new carbon-carbon bonds". *J. Organometallic. Chem*. **2003**, 22, 136

10. J. Kishner, "Chemischen Institut der Universität Jena: Methode zum Ersatz des Sauerstoffatoms der Ketone und Aldehyde durch Wasserstoff", *J. Russ. Phys. Chem. Soc*. **1911**, 43, 582
11. L. Wolff, "Diazo anhydride (1,2,3-oxydiazoles or diazooxides) and diazo ketones", *Liebigs Ann. Chem*. **1912**, 394, 23
12. M. E. Furrow, A. G. Myers, "Practical Procedures for the Preparation of N-tert-Butyldimethylsilylhydrazones and Their Use in Modified Wolff-Kishner Reductions and in the Synthesis of Vinyl Halides and gem-Dihalides". *J. Am. Chem. Soc*. **2004**, 126, 5436
13. R. Infante, J. Nieto, C. Andres, "Highly Homogeneous Stereoceontorolled Construction of Quaterary Hydroxyesters by Addition of Dimethylzinc to α-Ketoesters Promoted by Chiral Perhydrobenzoxazines and $B(OEt)_3$", *Chemistry – A European Journal*, **2012**, 18, 4375
14. N. Armestro, I. Lavandera, M. Ferrero, V. Gotor-Fernandez, A. G. Bellettini, J. A. Sternberg, S. Fermandez, V. Gotor, *EU patent*, **2001**, EP1092712
15. L. Del Valle, J. K. Stille, L. S. Hegedus, "Palladium-Catalyzed Coupling of Allylic Acetates with Aryl- and Vinylstannanes", *J. Org. Chem*, **1990**, *55*, 3019-3023.
16. J. K. Stille, A. M. Echavarren, R. M. Williams, J. A. Hendrix, "4-Methoxy-4'-Nitrobiphenyl 1,1'-Biphenyl, 4-methoxy-4'nitro", *Organic Synthesis*, **1998**, 9, 97
17. B. S. Edelson, B. M. Stoltz, E. J. Corey, "A simple and effective procedure for removal of tri-n-butyltin halides from reaction mixtures", *Tetrahedron letters*, **1999**, 40, 6729
18. R. W. Hoffmann, "Wittig and His Accomplishments: Still Relevant Beyond His $100^{th}$ Birthday", *Angew, Chem. Int. Ed*, **2001**, 40, 1411
19. B. P. Clark, C. Thomas, M. Javier, P. T. Gallagher, J. Gilmore, J. J. Masters, G. H. Timms, M. A. Whatton, V. A. Wood, PCT Int Appl **2004** WO 2004052858 A2
20. L. Salvi, N. R. Davis, S. Z. Ali, S. L. Buchwald, "A New Biarylphosphine Ligand for the Pd-Catalyzed Synthesis of Diaryl Ethers under Mild Conditions". *Org Lett*. **2012**, 14, 170

21. D. Maiti, S. L. Buchwald. “Cu-Catalyzed Arylation of Phenols: Synthesis of Sterically Hindered and Heteroaryl Diaryl Ethers”. *J. Org. Chem*. **2010**, 75 (5), 1791
22. N. Miyaura, “Organoboron compounds”, *Top. Curr. Chem*. **2002**, 219, 248
23. N. Miyaura, “Rational Ligand Design in Constructing Efficient Catalyst Systems for Suzuki-Miyaura Coupling”. *Angew. Chem. Int. Ed. Engl*. **2004**, 43, 2201
24. G. A. Molander, C. R. Bernardi, “Suzuki-Miyaura Cross-Coupling Reactions of Potassium Alkenyltrifluoroborates”. *J. Org. Chem*. **2002**, 67, 8424
25. G. A. Molander, B. Biolatto, “Efficient Ligandless Palladium-Catalyzed Suzuki Reactions of Potassium Aryltrifluoroborates”. *Org. Lett*. **2002**, 4, 1867
26. G. A. Molander, B. W. Katona, F. Machrouchi, “Development of the Suzuki-Miyaura Cross-Coupling Reaction: Use of Air-Stable Potassium Alkynyltrifluoroborates in Aryl Alkynylations”. *J. Org. Chem*. **2002**, 67, 8416
27. Y. Yang, S. L. Buchwald, “Ligand-Controlled Palladium-Catalyzed Regiodivergent Suzuki-Miyaura Cross-Coupling of Allyboronates and Aryl Halides”. *J. Am. Chem. Soc*. **2013**, 135, 10642
28. V. Bagutski, A. Ros, V. K. Aggarwal, “Improved method for the conversion of pinacolboronic esters intotrifluoroborate salts: facile synthesis of chiral secondary and tertiary trifluoroborates”. *Tetrahedron*, **2009**, 65, 9956
29. J. Hassan, M. Sevignon, C. Gozzi, E. Schulz, M. Lemaire, “Overview of Carbon-Carbon and carbon-Heteroatom Bond Forming Reactions”. *Chem. Rev*. **2002**, 102, 1359
30. S. L. Zultanski, G. C. Fu, “Nickel-Catalyzed Carbon-Carbon Bond-Forming Reactions of Unactivated Tertiary Alkyl Halides: Suzuki Arylations”. *J. Am. Chem. Soc*. **2013**, 135, 624
31. H. Liu, J. Wei, Z. Qiao, Y. Fu, X. Jiang, “Palladium-Catalyzed Intramolecular Reductive Cross-Coupling of $Csp^2$—$Csp^3$ Bond Formation”. *Chem. Eur. J*. **2014**, 20, 8308

32. K. Endo, T. Ohkubo, T. Ishioka, T. Shibata, “Cross Coupling between p3-Carbon and sp3-Carbon Using a Diborylmethane Derivative at Room Temperature”. *J. Org. Chem*. **2012**, 77, 4826
33. V. B. Phapale, M. G. Ceinos, E. Bunuel, D. J. Cardenas, “Nickel-Catalyzed Cross-Coupling of Alkyl Zinc Halides for the Formation of $C(sp^2)$—$C(sp^3)$ Bonds: Scope and Mechanism”. *Chem. Eur. J*. **2009**, 15, 12681
34. D. L. Clive, J. Wang, “A Tin Hydride Designed To Facilitate Removal of Tin Species from Products of Stannane-Mediated Radical Reactions”, *J. Org. Chem*. **2002**, 67, 1192
35. N. Hadei, E. A. B. Kantchev, C. J. O’Brien, M. G. organ, “The First Negishi Cross-Coupling Reaction of Two Alkyl Centers Utilizing a Pd-N-Heterocyclic Carbene (NHC) Catalyst”. *Org. Lett*. **2005**, 7, 3805
36. H. H. Szmant, C. E. Alciaturi, “Mechanistic aspects of the Wolff-Kishner reaction. 6. Comparison of the hydrazones of benzophenone, fluorenone, dibenzotropone, and dibenzosuberone”, *J. Org. Chem*, **1977**, 42, 1081
37. J. E. Tungen, M. Aursnes, J. Dalli, H. Arnardottir, C. N, Serhan, T. V. Hansen, “Total Synthesis of the Anti-inflammatory and Pro-resolving Lipid Mediator $MaR1_{n-3\ DPA}$ Utilizing an $sp^3$–$sp^3$ Negishi Cross-Coupling Reaction”. *Chem. Eur. J*. **2014**, 20, 14575
38. E. Negishi, *Handbook of Organopalladium Chemistry for Organic Synthesis*, **200**2, 1, 229
39. E. Hupe, P. Knochel, K. J. Szabo, “Mechanism of the Stereoselective Alkyl Group Exchange between Alkylboranes and Alkylzinc Compounds. Quest for Novel Types of Boron-Metal Exchange Reactions”. *Organometallics*, **2002**, 21, 2203
40. T. R. Pettus, M. Inoue, X. T. Chen, S. J. Danishefsky, “A Fully Synthetic Route to the Neurotrophic IIIicinones: Syntheses of Tricycloillicinone and Bicycloillicinone Aldehyde”. *J. Am. Chem. Soc*. **2000**, 122, 6160
41. D. Todd, “Wollf-Kishner reduction”, *Org. React*. **1948**, 4, 378

42. T. H. Chuang, Y. C. Chen, S. Pola, “Use of the Curtus Rearrangement of Acryloyl Azides in the Synthesis of 3,5-Disubstituted Pyridines: Mechanistic Studies*”, J. Org. Chem*. **2010**, 75, 6625
43. K. Okamoto, T. Yamamoto, T. Kanbara, “Efficient Synthesis of Thiobenzanilides by Willgerodt-Kindler Reaction with Base Catalysts”, *Synlett*, **2007**, 2687
44. R. Gamboni, C. Tamm, “Asymmetric Synthesis of α-Hydroxy-Esters via Ester Enolates with Very High Diastereoselectivity”, *Helvitica. Chimica. Acta*, **1986**, 69, 615

# CHAPTER 4. BORANE-ASSISTED HYDROGENATION

## 4.1 Introduction

Under metal catalyzed hydroboration conditions, several competing reaction modes are possible and a typical reaction mixture often contains several products, including the expected hydroboration product, regioisomers of the expected product including products arising via alkene isomerization, and hydrogenation (also referred as reduced product) products  Several research groups study catalyzed hydroboration but not every group formally describes formation of undesired hydrogenation products, although some of those groups make comments in supporting information. In most cases the amount of formation of undesired hydrogenation products is small and ignored as an insignificant side reaction.  However, there are several reports in which the undesired hydrogenation product formation is mentioned. Three examples are shown in Figure 1; these largely agree with observations that the Takacs group has made over the last decade. The most recent mention of this pathway is from a 2004 publication from the Crudden group exploring control of hydroboration regioselectivity based on the use of different borane.[1] The formation of the undesired hydrogenation product is not described in the main manuscript, but the supporting information includes a sentence describing formation of the undesired hydrogenation product in 3% yield from *para*-chlorostyrene (Figure 1A, Crudden case).  The metal precursor used in that study was $Rh(cod)_2BF_4$, and the borane employed was PinBH.  There is no similar discussion for other substrates that are studied in the paper.  A PhD thesis[2] from a member of the Crudden team mentions that the undesired hydrogenation byproducts

are commonly observed during hydroboration reactions, and have been isolated in up to 15% yield. It is surprising that among the 200 pages of that thesis only one sentence was devoted to formation of this byproduct.

Westcott, in 1992, also described the formation of an undesired hydrogenation product. This paper came from an early stage of research into asymmetric hydroboration and Westcott's main objective was to investigate effectiveness of iridium as a catalytic metal in asymmetric hydroboration[3]. Westcott was particularly interested in reactions of 4-vinylanisole. For this study CatBH was used as borane source and several different anion and ligand of metal precursors were used; these included $[Ir(coe)Cl]_2$, $[Ir(cod)Cl]_2$, $[Ir(cod)(py)(PCy_3)][OTf]$, and $[Ir(C_5Me_5)Cl]_2$. All gave the undesired hydrogenation product in amounts ranging from 2% to 10% (Figure 1B, Westcott case).

The last example describing the formation of hydrogenation product comes from Evans, Fu, and Hoveyda.[4] Their 1992 paper described rhodium- and iridium-catalyzed hydroboration of simple alkenes with catecholborane in the presence of $[Ir(cod)(py)(PCy_3)][PF_6]$, $Rh(nbd)(diphos)BF_4$, and $Rh(PPh_3)_3Cl$ (Figure 1C, Evans case). In the footnotes, the authors noted: "During the reaction of less reactive substrates, olefin hydrogenation and isomerization can become significant reaction pathways. Analogous behavior has been observed in the Rh (I) catalyzed hydrosilylation reaction". However, the exact substrates that furnished hydrogenation products were not explicitly indicated in the paper. In summary, the formation of hydrogenation products under metal-catalyzed hydroboration conditions has been observed fairly often whether the borane

source is PinBH or CatBH, the catalyst metal is rhodium or iridium, or the catalyst precursor is neutral (e.g., Rh(I)Cl) or cationic (e.g., Rh(I)$BF_4$).

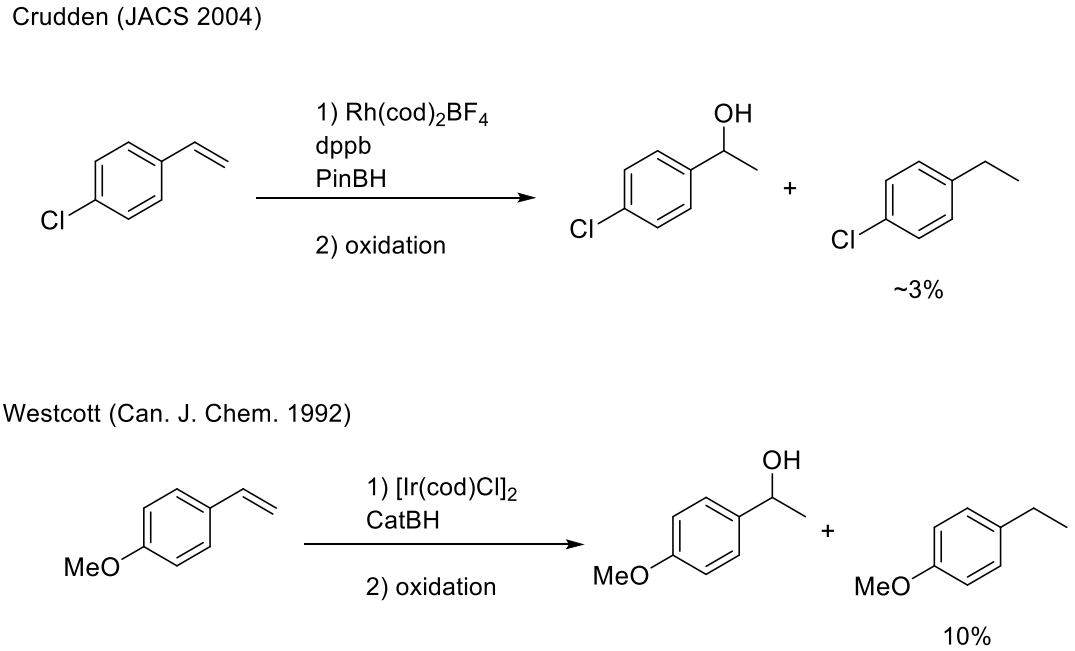


**Figure 1.** Literature examples describing hydrogenation under catalyzed hydroboration conditions.

Group members in Takacs group have consistently observed hydrogenation products under hydroboration conditions; Figure 2 summarizes some recent findings.

The catalyst precursor used for these studies is $Rh(nbd)_2BF_4$, the chiral ligands are typically TADDOL-based phosphite or phosphoramidite, and the borane is either PinBH or TMDBH (Figure 2). Generally speaking, under identical conditions, TMDBH tends to be associated with slower reaction and the generation of a higher fraction of reduced products. The observation that slower hydroboration is associated with more hydrogenation is consistent with the earlier work from Evans et al. The extent of hydrogenation depends on the structure of the substrate and the directing group. The oxime ether directing group facilitates hydrogenation more than other directing groups (i.e., amides or phosphonates, data not shown for the latter). Oxime ether substrates (Figure 2. Substrate **401**, **402**, and **403**) are particularly problematic, furnishing the hydrogenation product as the major product, in one case up to 87% yield, for reactions employing TMDBH. In contrast, when pinBH, a structural isomer of TMDBH, is used, the yield of the hydrogenation product observed from the same substrates decreases to approximately 20%. Substrate **404** contains the oxime ether moiety and gave up to 25% yield with TMDBH[5]. A high yield of hydrogenation product is characteristic of oxime ether containing substrates but reduction is observed for phosphonate substrate **405** and amide substrates **406** and **407**, with hydrogenation products observed in yields sometimes approaching approximately 20 % yield (Figure 2). Therefore, finding way(s) to minimize hydrogenation is a key to boost the yield of the major hydroboration product which would make the methodology more attractive to the chemistry community. Ultimately, understanding of why and how the reduced byproduct is formed could also inform the design of more effective asymmetric hydroboration

catalysts. In this chapter, an investigation into why and how the hydrogenation product is formed, principally by for the reaction of **401** with TMDBH, has been carried out. The preliminary evidence obtained to date and presented herein is used to propose a mechanism to account for formation of the hydrogenation product. As described below, the understanding also lead to a new type of catalytic asymmetric hydrogenation (CAH) reaction.

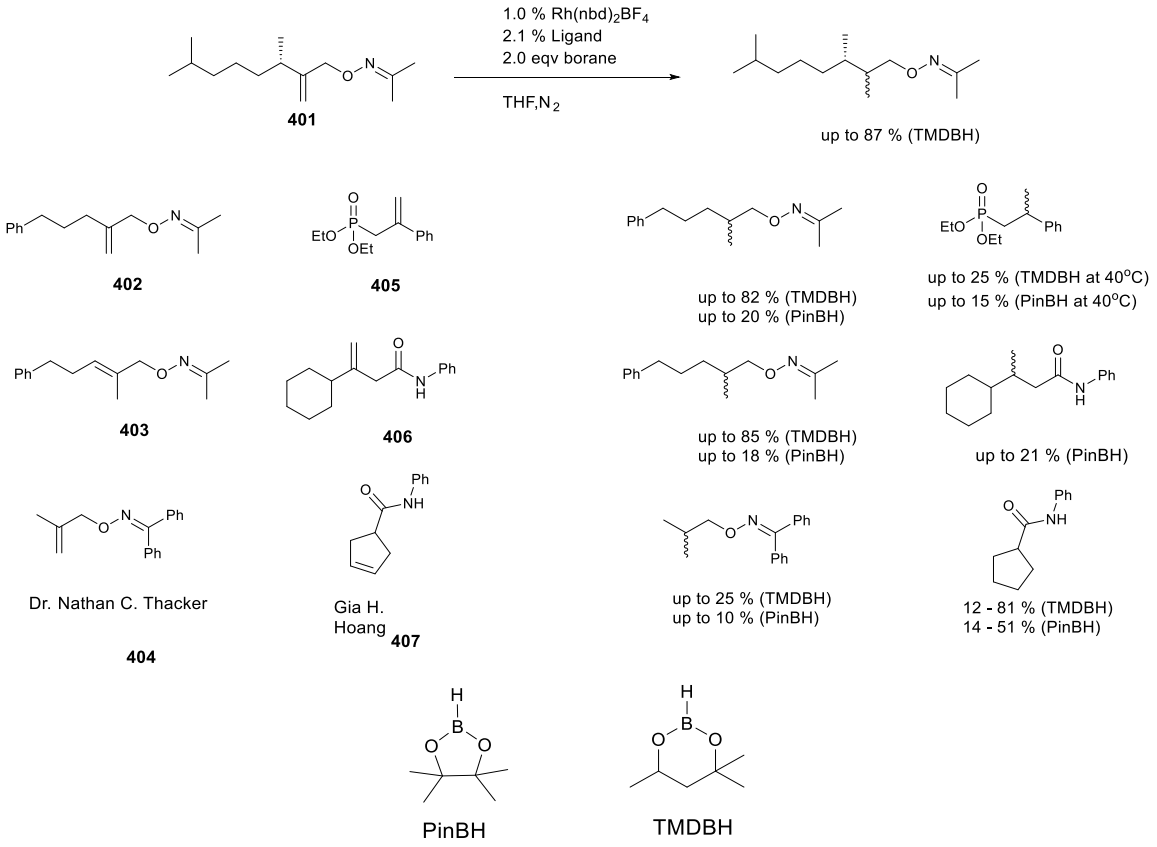


**Figure 2.** A summary of observations from the Takacs groups relevant to the formation of hydrogenation by-product under catalytic asymmetric hydroboration conditions.

**4.2 Identifying the elements which affect generation of hydrogenation product**

With the attention of the Takacs group mainly focused on asymmetric hydroboration, a systematic investigation into the factors that affect the yield of hydrogenation byproducts had for some time been relegated to the back burner. My search for clues into the hydrogenation mechanism under hydroboration conditions started with a careful look at some of the individual reaction components, including the nature of the substrates, the nature of metal precursors, the nature of the borane, ligand effects, solvent effects, influence of the reaction temperature, and eventually the presence or absence of hydrogen (i.e., $H_2$) and to a lesser extent proton sources. The collected observations from the Takacs group (Figure 2), makes clear that hydrogenation can occur for any substrate but that the yield of reduced product varies widely with structure.

I first explored the hypothesis that if the side reaction proceeded via one of the "standard" rhodium-catalyzed hydrogenation mechanisms with $H_2$, then prototypical hydrogenation substrates should give some hydrogenated products under the CAHB conditions or in the presence of $H_2$. Several prototypical substrates were screened under the typical reaction conditions. This included simple alkenes as well as enamide substrate **408**; the latter contains a two point binding functional group and is a common test substrate for catalytic asymmetric hydrogenation (CAH).[7] Surprisingly, the results showed that, other than oxime ether **401**, the substrates tested (i.e., **408**, **409**, and **410**) did not yield hydrogenation products (Figure 3). Under a $N_2$ atmosphere and all of the starting materials from **408**, **409**, and **410** were recovered and no hydroboration

product was obtained (Figure 3). The same results were obtained when **408**, **409**, and **410** were treated with TMDBH under 1 atm or under 50 psi of $H_2$ overnight. Even using Wilkinson's catalyst under $H_2$ (50 psi) did not catalyze the hydrogenation with substrate **408** in presence of TMDBH.

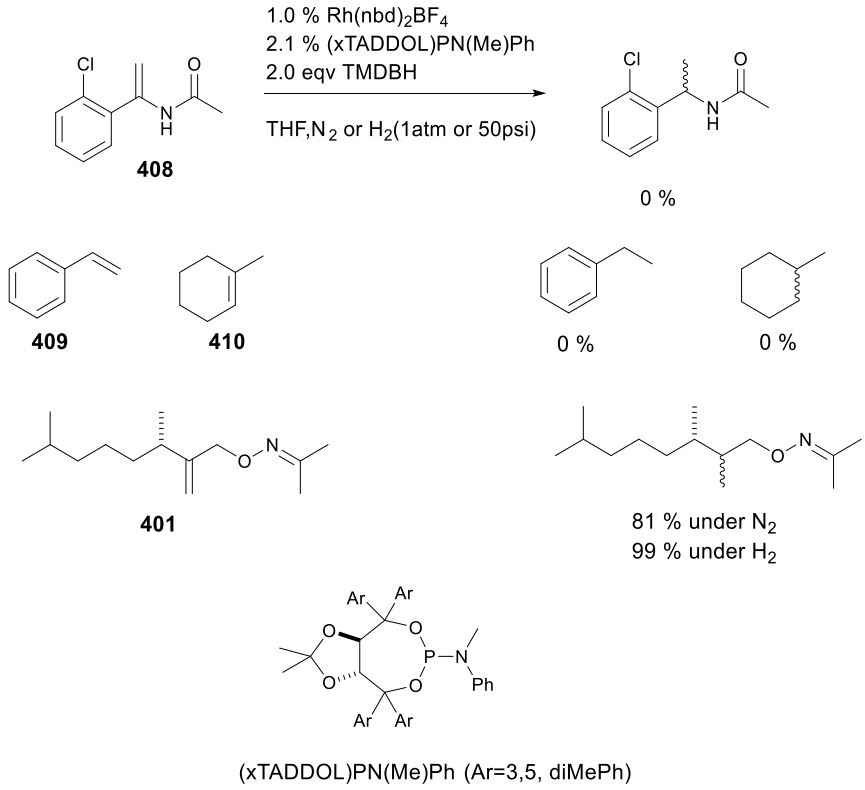


**Figure 3.** Prototypical hydrogenation substrates were not converted to the corresponding hydrogenated products under conditions in with the oxime ether is reduced.

Activation of a catalyst precursor is a critical and often underappreciated step in catalysis. A substrate thought to be non-reactive at times will react when a more reactive substrate first promotes formation of an active catalyst from the catalyst precursor.[6] To test this possibility, the oxime ether containing substrate **401** was first

mixed with the enamide substrate **408** described above then subjected to the reaction conditions under an atmosphere of $H_2$ (Figure 4). However, it was found that only the **401** reacted, while **408** was recovered unchanged (94 % recovered). The experiments shown in Figures 3 and 4 suggest that the hydroboration-associated hydrogenation pathway (with or without added $H_2$) highly depends on the nature of the substrate and not just the presence of two point binding functionalities.

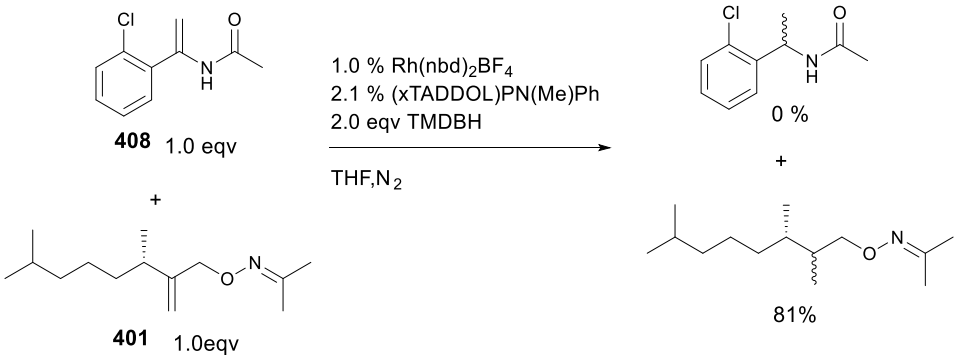


**Figure 4.** Addition of oxime ether substrate did not promote hydrogenation of amide substrate.

In contrast to the enamide substrate **408**, alkenes bearing other polar functionalities underwent competing (or partial) reduction under CAHB/$H_2$ reaction conditions. One of the successful oxime ether containing substrates was taken as a lead structure and derivatives were synthesized in which the oxime ether group is replaced with an alcohol or protected alcohol (e.g., *tert* butyl dimethyl silyl (TMDBS), *tert* butyl diphenyl silane (TBDPS), tri-isopropyl silane (TIPS), and benzyl group (Bn)). When the CAHB by TMDBH is run under an atmosphere of $N_2$, oxime ether substrate **411** gives an 87% yield of the hydrogenation product. However, removal of the oxime ether group substantially lowers the yields of hydrogenated product (Figure 5). Only 11% of the

hydrogenation product is formed in the case of the bulkiest protecting group (TIPS protected alcohol **404**). As the size of silyl protecting groups diminishes, the yield of reduction increases up to a maximum of 33% for the TBDMS ether. As in the case of the oxime ether, running reactions under a $H_2$ atmosphere also markedly increased the yield of the reduction product. The highest yield (60%) was obtained for the TBDMS ether **411**. The benzyl ether **413** also underwent hydrogenation when the reaction was run under $N_2$ in 20% yield. However, the corresponding unsaturated alcohol **415** was not reduced under those conditions. The latter result seems likely related to the fact that this alcohol has an acidic proton available to react with TMDBH. It should be noted that this same argument could in principle be used for the experiment described in Figure 3, in which the enamide substrate **408** has an acidic proton. However, the results of the competition experiment negate this argument. From this set of experiments, we tentatively conclude that the presence of a directing group with the capacity for two point binding can speed up the hydrogenation pathway but its presence does not grantee a highly efficient hydrogenation pathway under the typical hydroboration conditions.

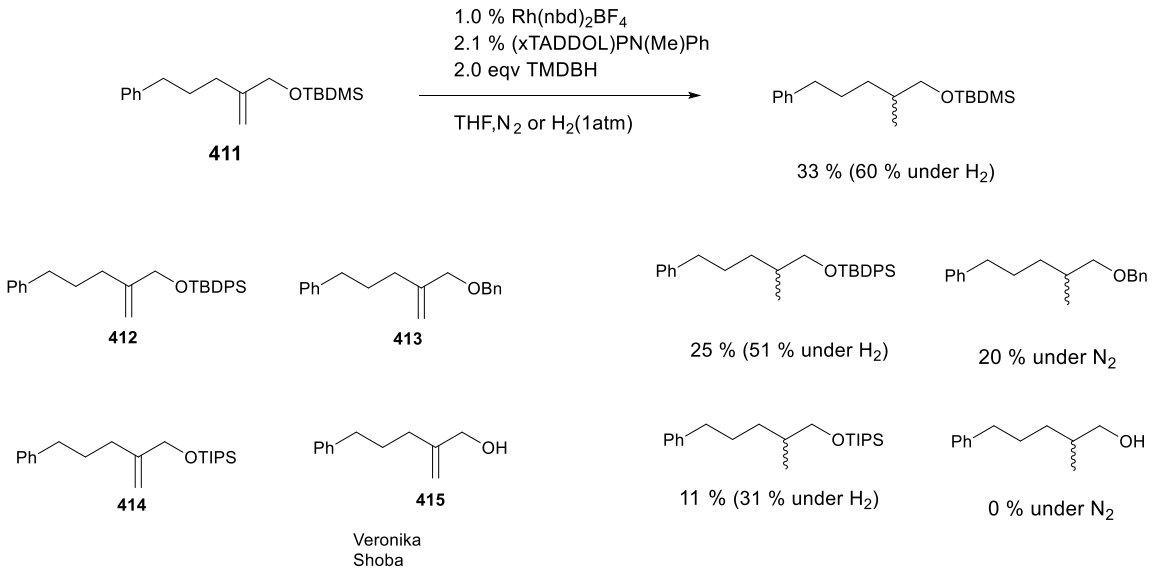


**Figure 5.** Influence of a polar "directing group" on the yield of reduced product.

It is the norm to screen various types of ligands to study the effect of ligands on reactivity and selectivity. Here several types of ligands, including TADDOL based phosphite, phosphoramidite, BINOL based phosphoramidite, and P-N iPr PHOX ligands, were screened (Figure 6). The purpose is to get an idea of which ligands perform the best in terms of generating hydrogenation product and not necessarily to screen every available ligand in the lab. Using unsaturated oxime **401** as a substrate, we found that phosphoramidite ligands promote more hydrogenation than phosphite ligands; for example, (xTADDOL)POPh (**416**) gave 35% reduced product (ca 46% of starting material was recovered unreacted) while (xTADDOL)PN(Me)Ph (**417**) was completely consumed, furnishing 83% of the hydrogenation product. The same result was observed with a BINOL-derived phosphoramidite (i.e., (BINOL)PN(Me)Ph **418**). The P, N iPrPHOX **419** ligand exhibited poor reactivity with a rhodium or iridium catalyst precursor. Due to the

relative ease of preparation of TADDOL-based vs BINOL-based phosphoramidites and the comparable results obtained with each, the remaining experiments described in this chapter were conducted using (xTADDOL)PN(Me)Ph (**417**).

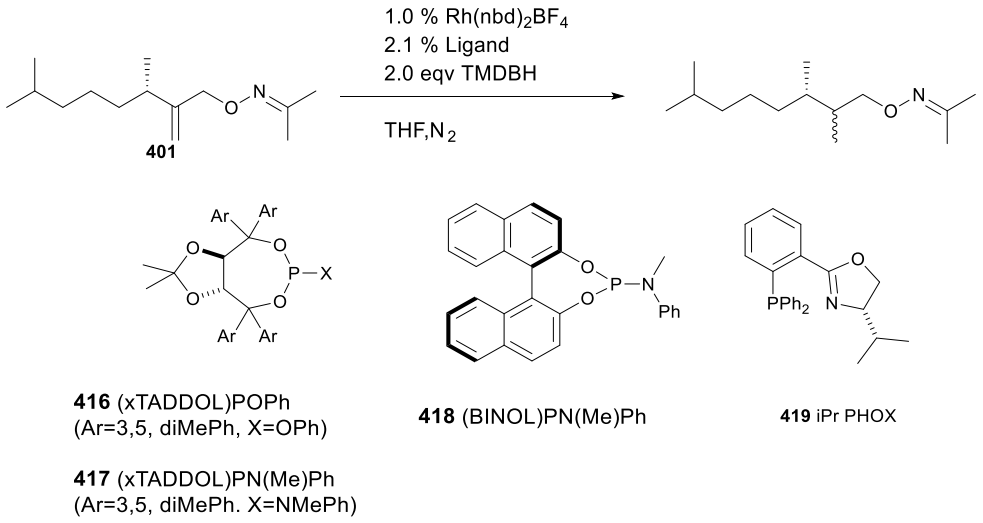


| | | Ligands | | | |
|---|---|---|---|---|---|
| | | **416** | **417** | **418** | **419** |
| Yield (%) | starting material | 46 | 0 | 0 | 67 |
| | Reduced | 35 | 83 | 84 | 27 |

**Figure 6.** Phosphoramidite ligands facilitate the hydrogenation pathway.

With a good ligand selected, we turned our attention to evaluating metal precursors that might promote hydrogenation pathway more efficiently. Several available iridium catalyst precursors (i.e., $Ir(cod)_2BF_4$, $[Ir(nbd)Cl)_2]$ were screened but showed no reactivity so in this section of the chapter, only rhodium catalyst precursors were shown (Figure 7). Both cationic (i.e., $(Rh(nbd)_2BF_4$ and $Rh(cod)_2BF_4)$) and neutral (i.e., $([Rh(nbd)Cl]_2$ and $[Rh(nbd)OEt]_2)$) rhodium catalyst precursors were screened. The neutral Rh (I) catalyst precursors did not show any reactivity at all. It was surprising to

find that, while $Rh(nbd)_2BF_4$ gave an 83% yield of the hydrogenation product, the reaction using $Rh(cod)_2BF_4$ did not go to completion; 39% of starting material remained unreacted in addition to the 34% of hydrogenation product.

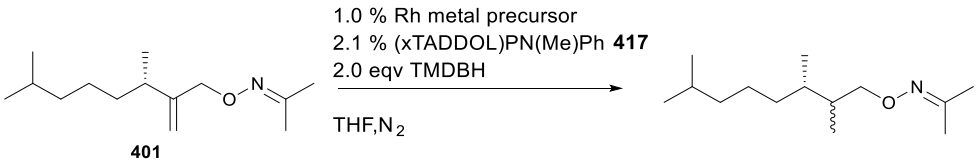


| | | Metal precursors | | | |
|---|---|---|---|---|---|
| | | $Rh(nbd)_2BF_4$ | $Rh(cod)_2BF_4$ | $[Rh(nbd)Cl]_2$ | $[Rh(nbd)OEt]_2$ |
| Yield (%) | starting material | 0 | 39 | 88 | 96 |
| | Reduced | 83 | 34 | 5 | 0 |

**Figure 7.** The influence of the Rh complex used as a catalyst precursor.

Since catalysts formed from $Rh(cod)_2BF_4$ showed lower reactivity than those prepared from $Rh(nbd)_2BF_4$, the effect of nbd ligand addition was investigated to see if it would improve hydrogenation product yield. The reaction was set up as follow. $Rh(cod)_2BF_4$ and (xTADDOL)PN(Me)Ph (**417**) were weighed out and mixed in a glove box to ensure that the active catalyst is formed. Then, varying amounts of nbd were added (i.e., 0, 1, 2, 3, and 5 equivalents with respect to Rh) in THF and the reaction mixture was stirred for additional length of time before the addition of an oxime ether substrate. Afterwards, TMDBH was added to start the reaction. Addition of the first equivalent of nbd improves the hydrogenation yield but further addition of nbd did not show further improvement (Figure 8). Compared to the optimum rhodium precursor $Rh(nbd)_2BF_4$, the addition of nbd to $Rh(cod)_2BF_4$ did not result in the same hydrogenation yield; only

50% hydrogenation was obtained. However, the results might also relate to the age of the Rh precursor. The $Rh(cod)_2BF_4$ used had been stored for fairly long time before its use and that might have affected its performance. In fact, Evans reported that commercially purchased rhodium metal precursors are often partially oxidized, and when this is the case, lower reactivity and inferior selectivity are obtained[7].

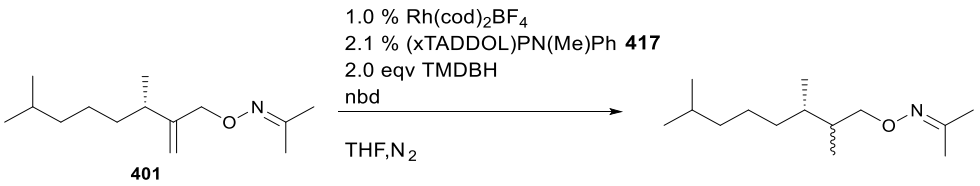


| | Amount of nbd | | | | |
|---|---|---|---|---|---|
| | 0% | 1% | 2% | 3% | 5% |
| starting material | 39 | 18 | 16 | 17 | 19 |
| reduced | 34 | 50 | 50 | 52 | 54 |
| hydroboration | 13 | 11 | 7 | 10 | 9 |

**Figure 8.** Pre-coordinated ligand in the Rh (I) catalyst precursor is found to be an important factor for hydrogenation.

Having established the best rhodium precursor and ligand, the effect on the ratio of metal to ligand was investigated. Although the recent norm in the Takacs group has been to use a 1 : 2 ratio of metal : ligand for asymmetric hydroboration, the hydrogenation pathway may involve a different metal complex. It was therefore important to go back to the basics and test the effect of metal to ligand ratio. Without any ligand, hydrogenation occurred only to the extent of 2%; most of the starting material was untouched and recovered (82% starting material) (Figure 9). In the

presence of 1.0 equivalent of ligand the reaction gave an 88% yield of the hydrogenation product. It is interesting to note that these results are slightly better than the results obtained with 2.0 equivalents of ligand relative to Rh (I). When the amount of ligand was increased to 3.0 equivalents (Figure 9) or more (data not shown), the rate of reaction dropped rather precipitously. This results from varying the metal/ligand ratio are interesting and suggest that only one ligand per rhodium is necessary for efficient hydrogenation. Recently a group member, Veronika Shoba, observed that the hydrogenation reaction (under a different set of reaction conditions) proceeded faster with 1 to 1 ratio of metal to ligand compared to a 1 to 2 ratio. Further investigations will be needed to resolve this question with meaningful conclusions. The data reported in this chapter generally use the traditionally employed 1 to 2 ratio unless it is indicated.

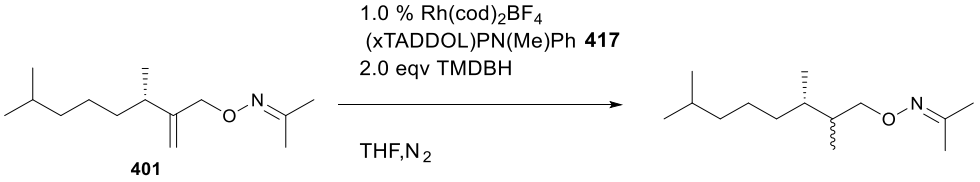


401

| | | Ligand (%) | | | |
|---|---|---|---|---|---|
| | | 0 | 1.0 | 2.0 | 3.0 |
| Yield (%) | starting material | 82 | 0 | 0 | 10 |
| | Reduced | 2 | 88 | 83 | 75 |

**Figure 9.** Effect of metal to ligand ratio in hydrogenation pathway under hydroboration.

TMDBH was found to be better than pinBH at promoting the hydrogenation pathway under hydroboration condition. I questioned, how much borane is needed for hydrogenation. It has been the case to use 2.0 equivalents of borane for hydroboration

reactions involving typical two point binding substrates for CAHB. In order to justify the appropriate amount that is required for efficient hydrogenation, the following experiments were conducted in which incremental increases in the amount of TMDBH was used to check the effects. First of all, TMDBH is absolutely necessary for hydrogenation pathway to take place. At least 2.0 equivalents of TMDBH was needed to react starting material and this gave 83% of hydrogenation product with 15:85 diastereoselectivity (Figure 10). Adding more than 2.0 equivalents of TMDBH addition resulted in a quantitative yield of hydrogenation product having slightly better diastereoselectivity (11 : 89). While the diastereoselectivity was slightly increased by adding more TMDBH, for the purpose of studying the hydrogenation pathway mechanism 2.0 equivalents of TMDBH was chosen as a standard condition. A possible reason for the increase in yield with increasing amounts of TMDBH may be that TMDBH is consumed in part to generate $H_2$ gas in situ and used as the hydrogen source for hydrogenation mechanism; excess TMBDH could compensate for any loss of $H_2$ from the reaction mixture.

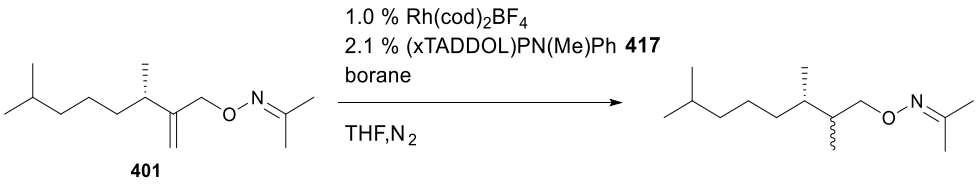


| | | TMDBH (eqv) | | | | | |
|---|---|---|---|---|---|---|---|
| | | 0 | 0.5 | 1.0 | 2.0 | 4.0 | 6.0 |
| yield % (dr) | starting material | 99 | 63 | 31 | 0 | 0 | 0 |
| | alkene reduction | 0 | 25 (30:70) | 55 (25:75) | 83 (15:85) | 99 (12:88) | 99 (11:89) |

**Figure 10.** Higher TMBH loading resulted in higher yield and diastereoselectivity.

During the course of study it was found that performing the reactions under an atmosphere of $H_2$ gas drastically improved hydrogenation product yields. A separate reaction kinetic study showed that the rate of the reaction is in agreement with the amount of $H_2$ gas present in the reaction flask. Therefore, it was my interest to investigate the effect of a limited amount of TMDBH in combination with a $H_2$ atmosphere. The use of 1.0 and 2.0 equivalents of TMBH under 1 atm of $H_2$ gas pushed the reaction to completion and resulted in exclusively the hydrogenation product (99%) (Figure 11). When the amount of TMDBH was reduced to 0.1 and 0.2 equivalents, majority of the starting material was left and only 12% and 29% of hydrogenation product was observed, respectively. However, 50 psi of $H_2$ gas in hydrogenation chamber led to dramatic yield improvement to 99% (Figure 11). This is interesting in two regards. First, most of the hydrogen source for hydrogenation must come from $H_2$ gas not TMDBH. Secondly, TMDBH can be used as catalytic amount, which suggests that

it is possible to use TMDBH as a catalyst to afford hydrogenation product in the mechanism. However, recall that in the absence of borane, there is not hydrogenation even under 50 psi of $H_2$ and that diastereoselection is reduced under a hydrogen atmosphere. These observations encouraged me to perform labeling studies which are described later in the chapter.

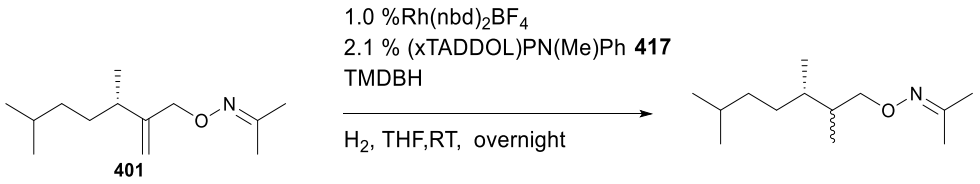


401

| TMDBH (eqv) | 0.1 | 0.2 | 0.1 | 0.2 | 1 | 2 |
|---|---|---|---|---|---|---|
| $H_2$ | 1 atm | 1 atm | 50 psi | 50 psi | 1 atm | 1 atm |
| starting material | 78 | 71 | 0 | 0 | 0 | 0 |
| reduced | 12 | 29 | 99 | 99 | 99 | 99 |
| dr | 30:70 | 31:69 | 31:69 | 30:70 | 26:74 | 20:80 |

**Figure 11.** Catalytic amount of TMDBH can be used under pressurized $H_2$ gas.

After observing marked differences under $N_2$ and $H_2$ atmospheres, and taking note of hydrogenation with even 0.1 equivalents of TMBH, an investigation to probe the mechanism(s) responsible was performed by using TMDBD or $D_2$ as deuterium source. The reaction was run under a $D_2$ atmosphere (1 atm) and the deuterium distribution in the product was analyzed by NMR and GCMS. Two key pieces of information were learned from this experiment. First, only one of the two positions of alkene moiety was incorporated deuterium from $D_2$ gas; the other site was untouched based on integration of the $^1$H NMR spectrum (Figure 12 A). Figure 12 B is an H NMR spectra of the

hydrogenated product and red rectangles indicates integrations relevant to this discussion. The signals at 3.85 and 3.79 ppm correspond to the methylene group adjacent to the oxime ether moiety. The protons with chemical shifts at 1.57 ppm and 0.8 ppm correspond to the methine hydrogen and terminal methane hydrogens, respectively (Figure 12 B). The spectra which was obtained under the reaction condition with $D_2$ as deuterium source (Figure 12 C) shows the some deuterium incorporations (10 and 17%) into protons adjacent to the oxime ether moiety and 100% incorporation into the terminal methane group. This suggests that all of the methine hydrogen (i.e., the site where deuterium was not incorporated) must come from TMDBH. Secondly, alkene isomerization took place in the course of the reaction as evidenced by deuterium incorporation onto the oxygen-substituted carbon; the data show 17% and 10% of deuterium atom incorporation into each of the sites on the methylene group. The second point is nothing new and group members in Takacs group have observed some levels of alkene isomerization in the past with various substrates. When TMDBD was used in place of TMDBH under $N_2$ it was found that deuterium was incorporated at the tertiary position with 100% incorporation (Figure 13 A, B, & C). In addition, 53% incorporation of deuterium was observed in the methyl substituent. The methylene group (bearing the oxygen) also showed 31% deuterium incorporation but only in one of the positions. The experiments in Figures 12 and 13 suggest that a hydrogen/deuterium from TMDBH/TMDBD is incorporated into the tertiary position. The presence of $D_2$ partially puts deuterium on the methyl group, and alkene isomerization leads to the remaining deuterium adding to the methylene bearing oxygen. It is worth mentioning

that the labeling study with this substrate was rather complex in that it produces several deuterium-containing species. Ms. Veronika Shoba has observed similarly complex deuteration pattern with a related substrate under different conditions.

(A)

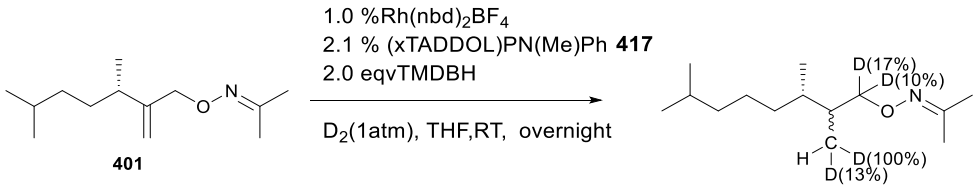


(B)

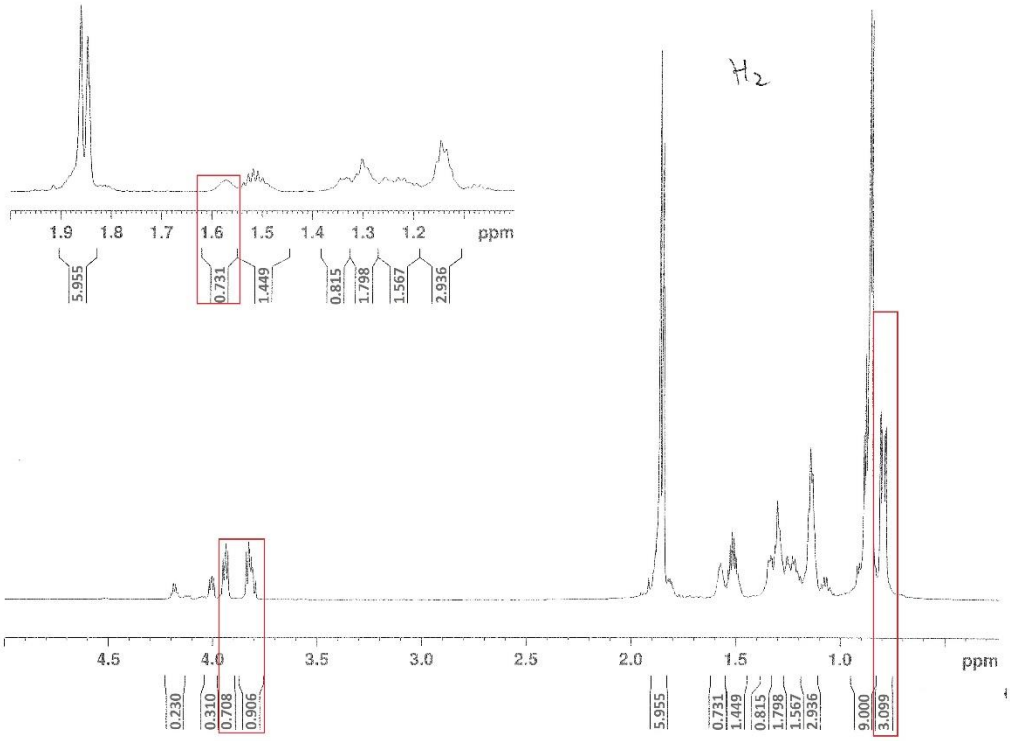


(C)

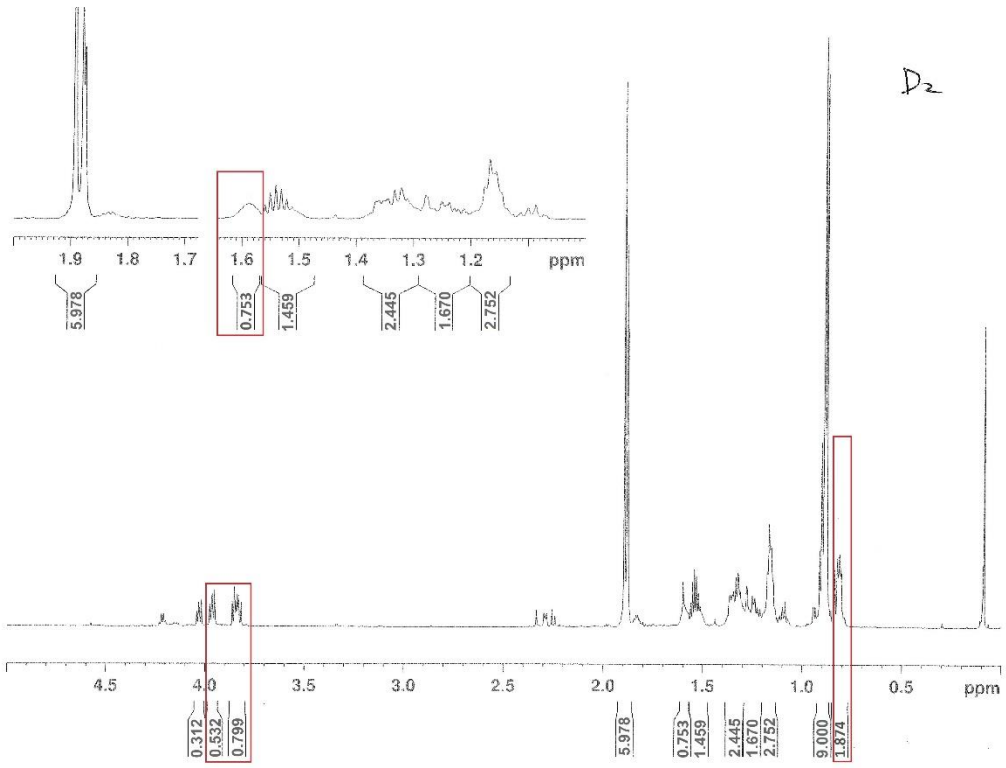


**Figure 12.** (A) Deuterium study with $D_2$. (B) H NMR spectra of the hydrogenation product. (C) H NMR of the hydrogenation product under $D_2$.

(A)

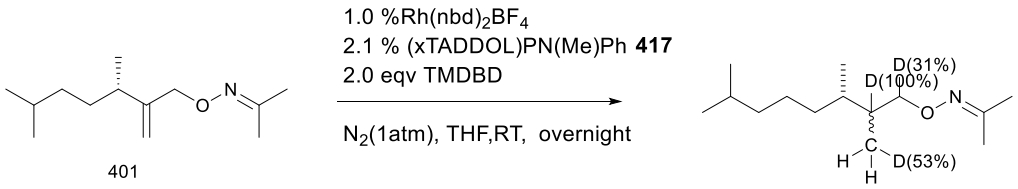


401

(B)

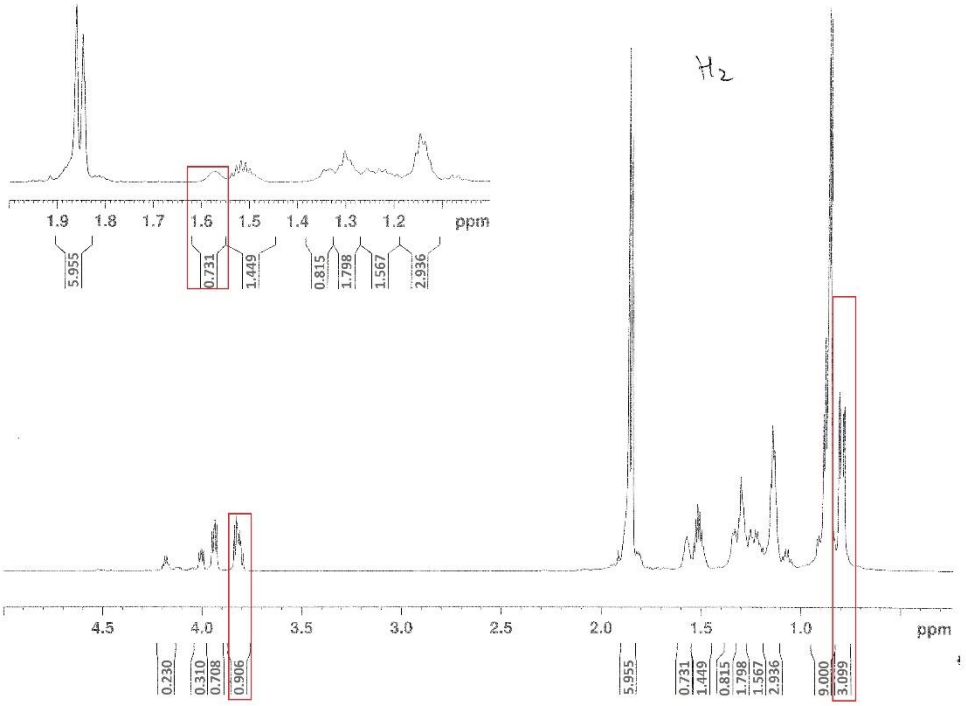
H2
1.9 1.8 1.7 1.6 1.5 1.4 1.3 1.2 ppm
5.955
0.731
1.449
0.815
1.798
1.567
2.936
4.5 4.0 3.5 3.0 2.5 2.0 1.5 1.0 ppm
0.230
0.310
0.708
0.906
5.955
0.731
1.449
0.815
1.798
1.567
2.936
9.000
3.099

(C)

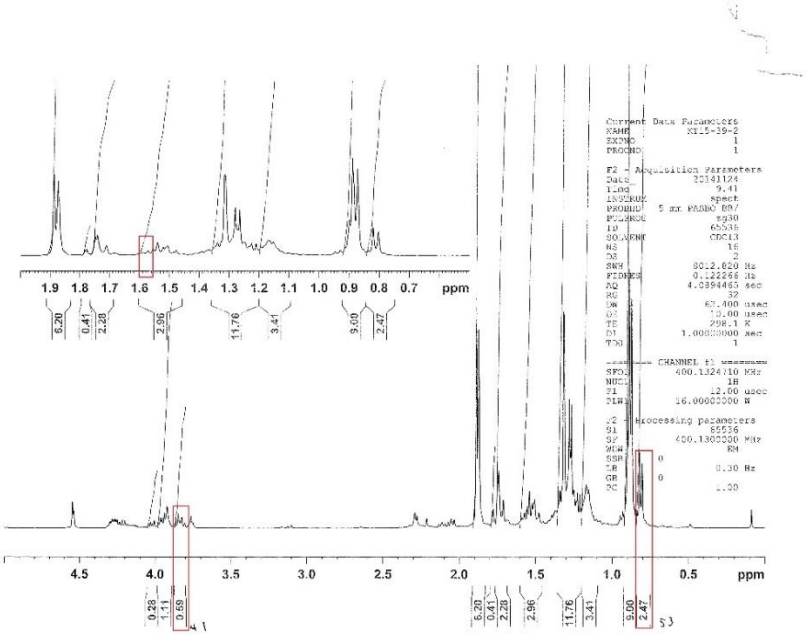
1.9 1.8 1.7 1.6 1.5 1.4 1.3 1.2 1.1 1.0 0.9 0.8 0.7 ppm
6.20
0.41
2.28
2.96
11.76
3.41
9.00
2.47
4.5 4.0 3.5 3.0 2.5 2.0 1.5 1.0 0.5 ppm
0.28
1.11
0.58
6.20
0.41
2.28
2.96
11.76
3.41
9.00
2.47

**Figure 13.** (A) Deuterium study with TMDBD. (B) H NMR spectra of the hydrogenation product. (C) H NMR of the hydrogenation product with TMDBD.

Previously a substrate bearing a benzophenone-derived oxime ether moiety was shown to undergo *ortho*-C-H activation of a phenyl substituent under asymmetric hydroboration conditions[5]. Although the oxime ether group employed in this thesis does not contain phenyl group where *ortho*-C-H activation is prone to occur, it is important to verify that C-H activation on the oxime actually does not happen under the conditions used in this study. The hexadeuterated oxime ether substrate **420** was prepared and reduced with TMDBH (Figure 14). I find no evidence for that H/D-exchange (i.e., no C-H activation) occurred during the reaction.

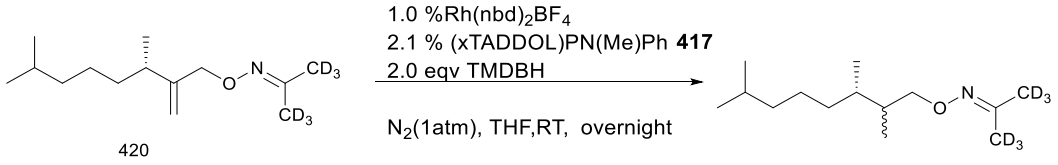


**Figure 14.** C-H activation not observed with oxime ether moiety.

**4.3 Proposed mechanism for hydrogenation pathway**

The experiments described above implicate molecular $H_2$ in mechanism leading to alkene reduction. The next question is whether $H_2$ is involved in rate determining step of hydrogenation pathway under hydroboration conditions. If so, a rate difference should be observed when comparing reactions run under $H_2$ versus $D_2$. Preliminary evidence that this is the case was obtained using a ReactIR instrument to monitor the reaction[8] progress for both consumption of TMDBH (Figure 15 A) and generation of the hydrogenated product (Figure 15 B). Blue and red line graphs (data taken every 10 seconds) show the data obtained from reaction under $D_2$ and $H_2$, respectively. Indeed, as expected, a significant rate difference is observed, indicating the involvement of molecular $H_2$ in the rate-determining step. Both past experimental results and computational study carried out by Dr. Zhao-Di Yang in the Takacs group[9] suggest that the rate determining step of hydroboration is reductive elimination step from a rhodium-boryl complex to form the carbon-boron bond. Perhaps rate-determining reaction with $H_2$ intercepts an intermediate in that same pathway leading to hydrogenation.

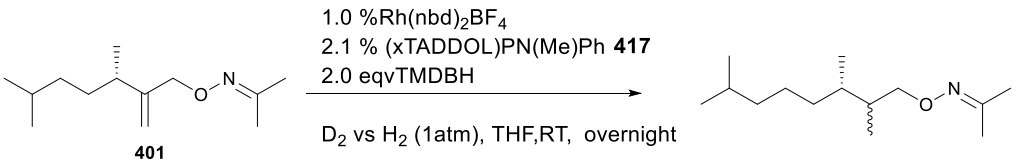
1.0 %Rh(nbd)2BF4
2.1 % (xTADDOL)PN(Me)Ph 417
2.0 eqvTMDBH
D2 vs H2 (1atm), THF,RT, overnight
401

(A)

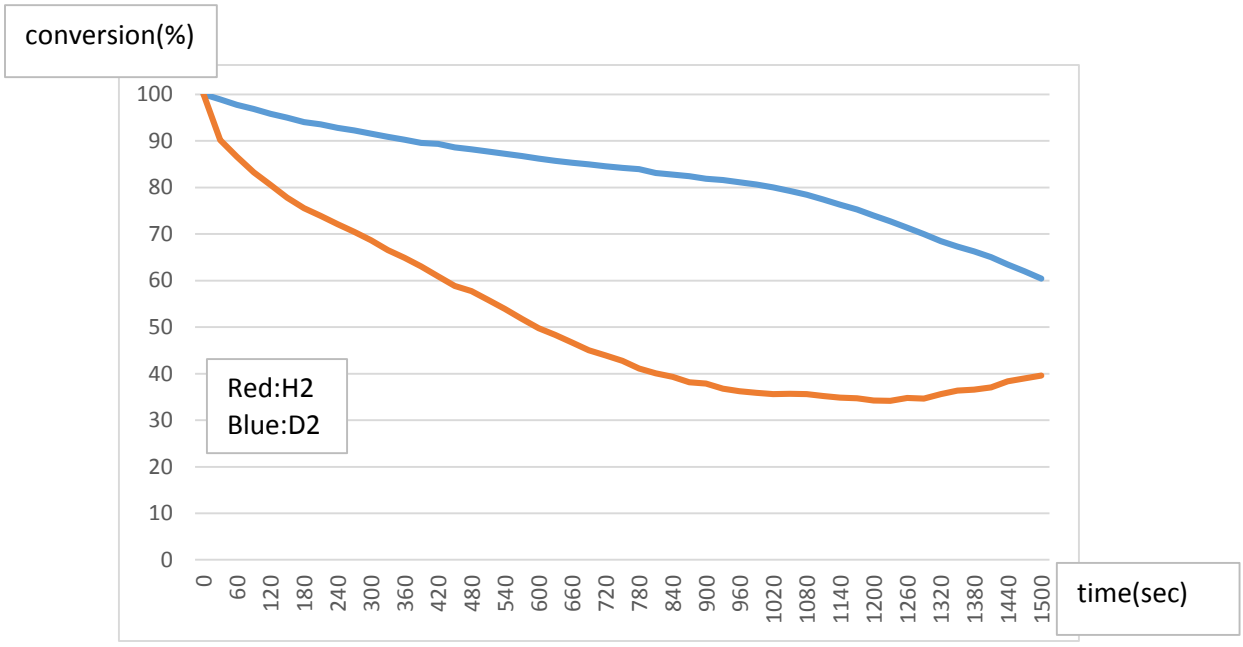
conversion(%)
100
90
80
70
60
50
40
30
20
10
0
Red:H2
Blue:D2
0
60
120
180
240
300
360
420
480
540
600
660
720
780
840
900
960
1020
1080
1140
1200
1260
1320
1380
1440
1500
time(sec)

(B)

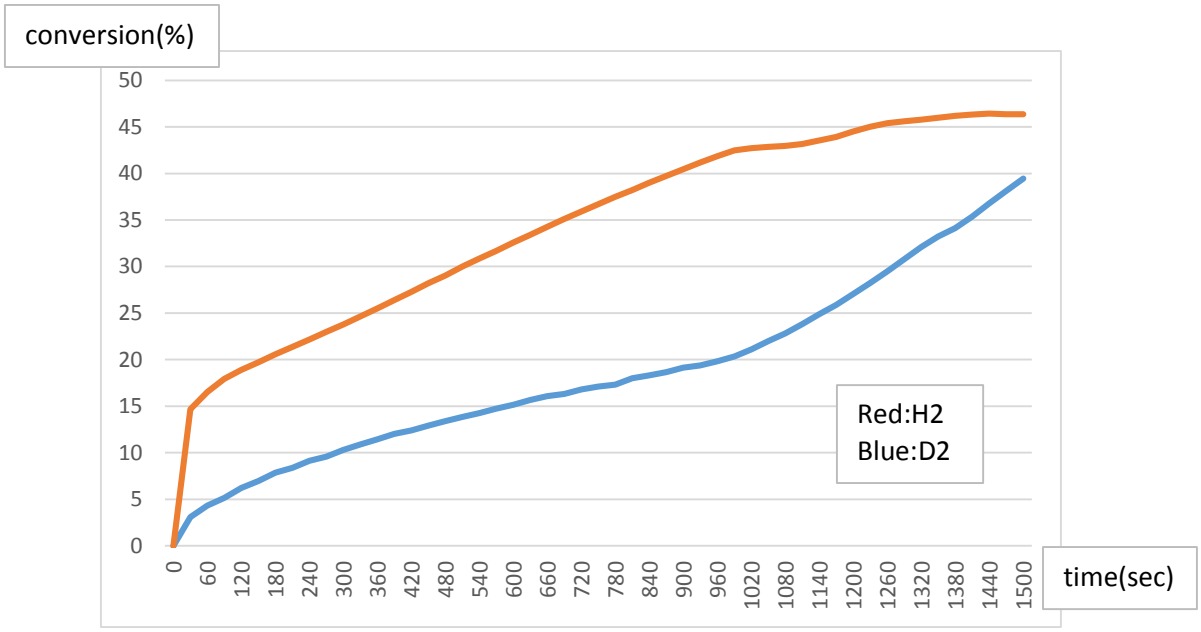
conversion(%)
50
45
40
35
30
25
20
15
10
5
0
Red:H2
Blue:D2
0
60
120
180
240
300
360
420
480
540
600
660
720
780
840
900
960
1020
1080
1140
1200
1260
1320
1380
1440
1500
time(sec)

**Figure 15.** Rate comparison between $D_2$ and $H_2$ condition. (A) Consumption of TMDBH over time. (B) Generation of hydrogenation product over time.

Two mechanisms are considered at this point. One mechanism involves intercepting an intermediate **425** along the catalyzed hydroboration pathway with molecular hydrogen, providing the hydrogen source for hydrogenation; the second instead envisions a second molecule of TMDBH intercepting that intermediate **425** and thereby providing the hydrogen for hydrogenation (Figure 22). The first proposed mechanism is shown in Figure 16 and is adapted from computational work[8] with an amide substrate. The cycle starts with alkene coordination between the rhodium catalyst **421** and substrate **422** via two point binding. Then oxidative addition of TMDBH to the rhodium catalyst **423** forms a rhodium hydride species **424**, which undergoes migratory insertion of the alkene into the Rh-H bond delivering hydride to methine position as is indicated by the TMDBD deuteration experiment. Intermediate **425** is poised for carbon-carbon bond formation via reductive elimination but competing reaction with molecular hydrogen via sigma bond metathesis is proposed to generate TMDBH while replacing the (pin)B-Rh by H-Rh giving intermediate **426**. Reductive elimination then affords the hydrogenation product **427** and regenerates the rhodium catalyst (Figure 16). Note that the hydrogen incorporated from $H_2$ gas ends up on primary position (i.e., methyl group) which is consistent with deuterium labeling under an atmosphere of $D_2$.

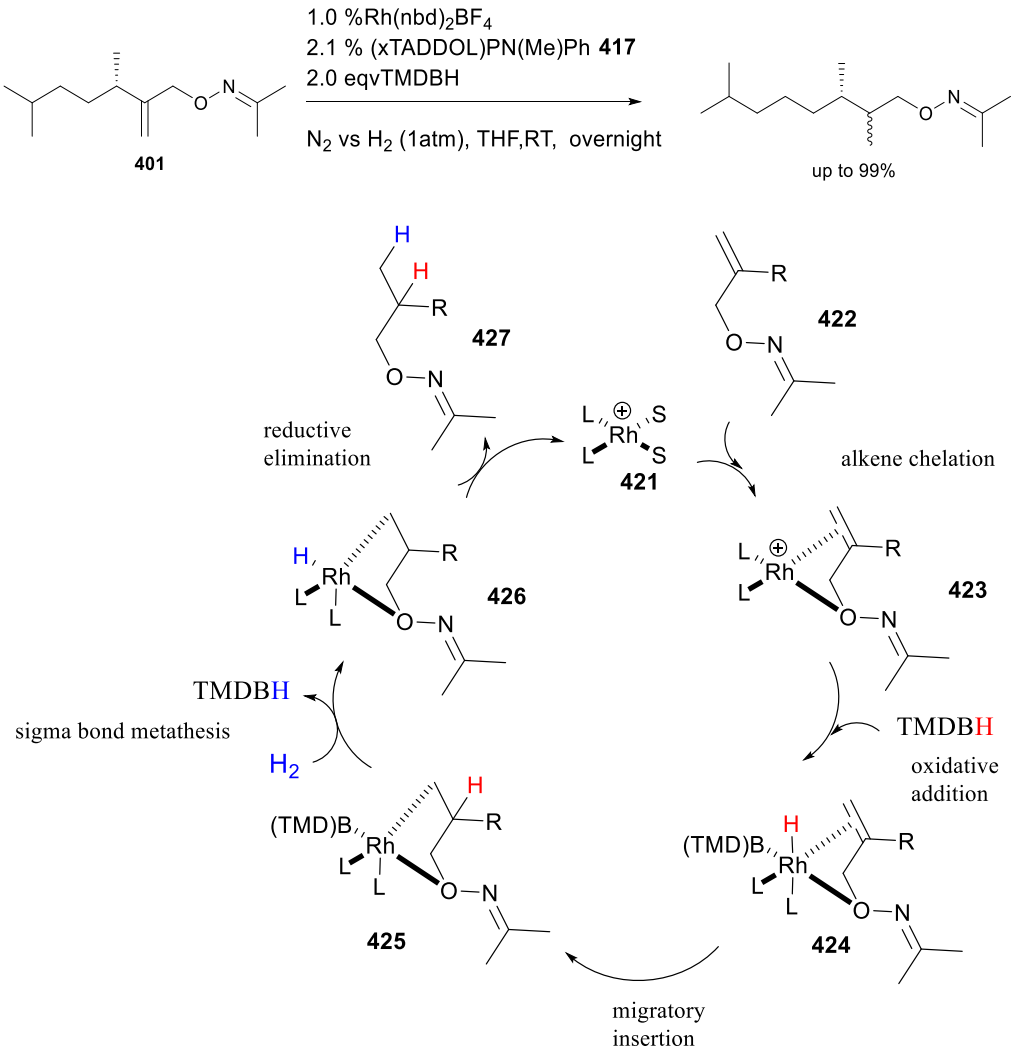


**Figure 16.** Proposed mechanism 1 for hydrogenation pathway under hydroboration. Alternatively, the rhodium may be complexed to nitrogen suggested by some preliminary computational studies by Zhao-Di.

In support of the proposed mechanism, I note that similar sigma bond metathesis reactions with various metals, including rhodium and iridium, have been well documented[10-22]. Campos et al[17] reported the hydrogenolysis of the iridium-methyl bond of a iridium complex where the σ -$H_2$ intermediate **2** was observed spectroscopically upon treating iridium complex **1** with $H_2$ gas (Figure 17). DFT

calculation using the PBE0 functional with the Stuttgart basis set was found to be in better agreement with experiment. In the proposed mechanism it is reasonable to suggest σ -bond metathesis of $H_2$ with rhodium complex **425** to generate the resulting rhodium complex **426** and TMDBH. The TMDBH formed by σ -bond metathesis can be recycled in the mechanism. This TMDBH recyclability agrees with the observation that reaction with only a limited amount of TMDBH (0.1 equivalents) under $H_2$ pressure afforded the hydrogenation product yield quantitatively.

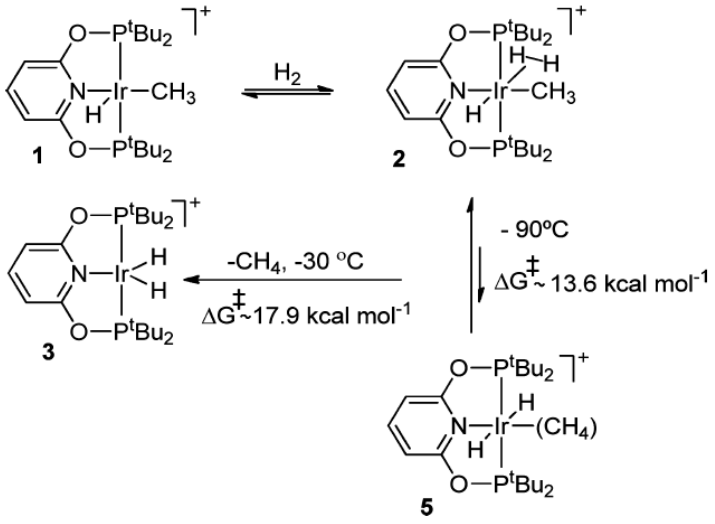


**Figure 17.** σ-bond metathesis of molecular hydrogen with iridium complex (permission obtained from the publisher).

As mentioned above, a computational study using density functional theory carried out by Dr. Zhao-Di Yang et al[9] investigated the rhodium-catalyzed hydroboration of a cyclic γ, δ- unsaturated amide substrate by pinBH in the presence of a caged phosphite ligand. In that study, geometry optimizations were carried out utilizing the

basis set 6-31 +G** for C, O, P, B, N, and H and LANL2DZ for Rh atoms. The same method of calculation was used to address whether sigma bond metathesis with a molecule of $D_2$ provides a feasible mechanistic pathway starting from the previously calculated intermediate **Im2a** (Figure 18 and 19). Two approaches of $D_2$ to an **Im2a** were considered (Figure 18). Pathway 1 is defined by the axial approach to the rhodium center, while pathway 2 is defined by the perpendicular side approach to the rhodium center.

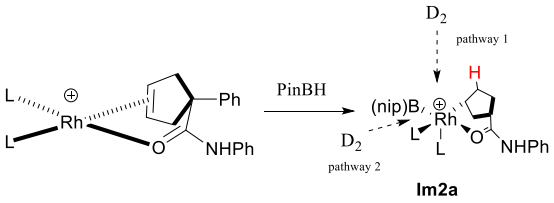


**Figure 18.** Computational study focused on two $D_2$ addition pathway.

The calculation by Dr. Yang starts with **Im0** (Figure 18A), a square planar tetra coordinate rhodium (I) complex optimized in a previous computational study[9]. PinBH adds to **Im0** via oxidative addition followed by migratory insertion to form **Im2a**. Then $D_2$ approaches to the rhodium complex **Im2a** to form **Im3a** via **TS2a**. **Im3a** undergoes sigma bond metathesis with $D_2$ by transient interaction between B atom from TMDB and the D atom from $D_2$ molecule (**TS3a**) resulting in the formation of **Im4a** and generating PinBD, which leaves from the catalytic cycle. **Im4a** undergoes isomerization (**TS4a**) via amide bond to form **Im5a**. **Im5a** then undergoes reductive elimination step to form the C-D bond in the hydrogenation product **D**.

Figure 19B illustrates the potential energy diagram of mechanism shown in Figure 19A. The energy diagram suggests that sigma bond metathesis via **TS3a** is overall rate determining but relatively facile.

(A)

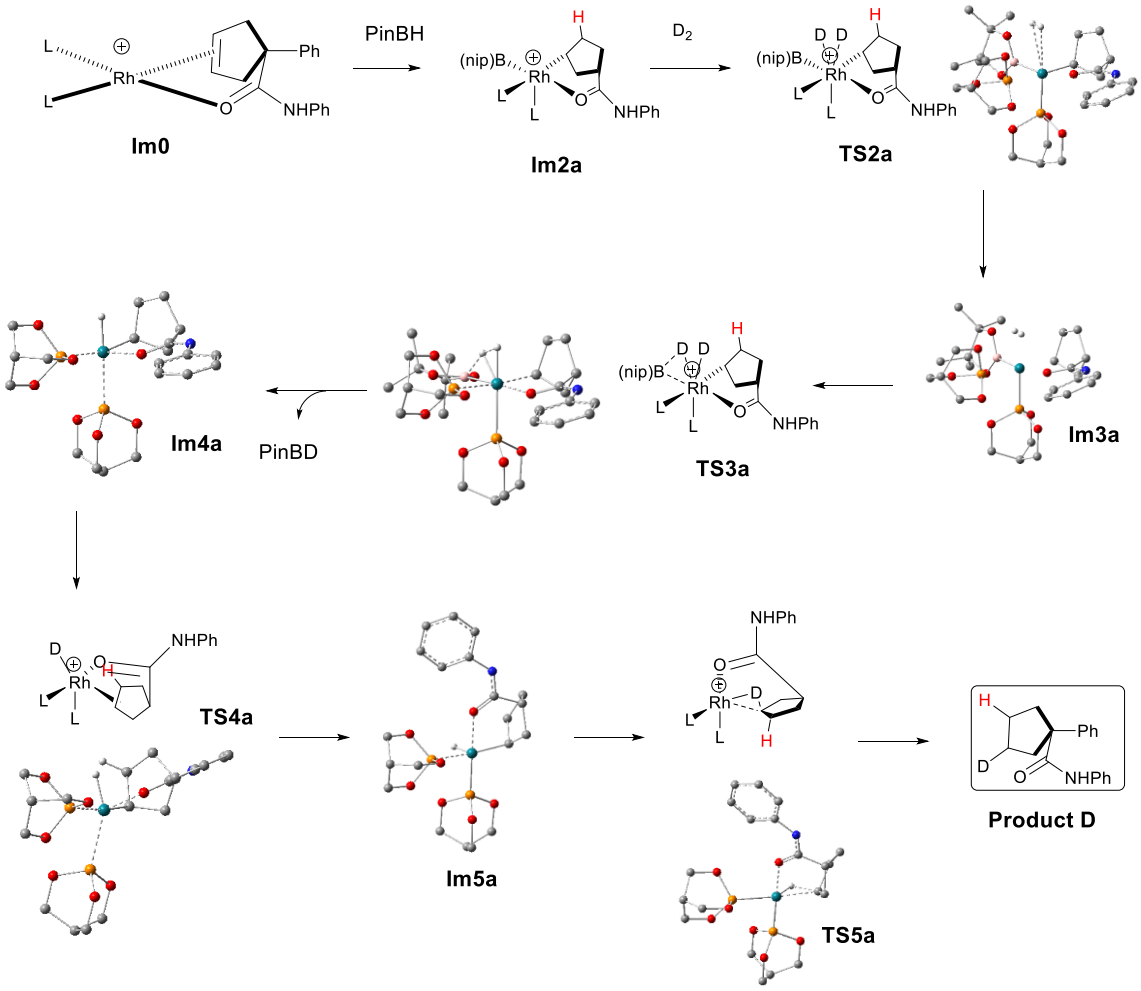

(B)

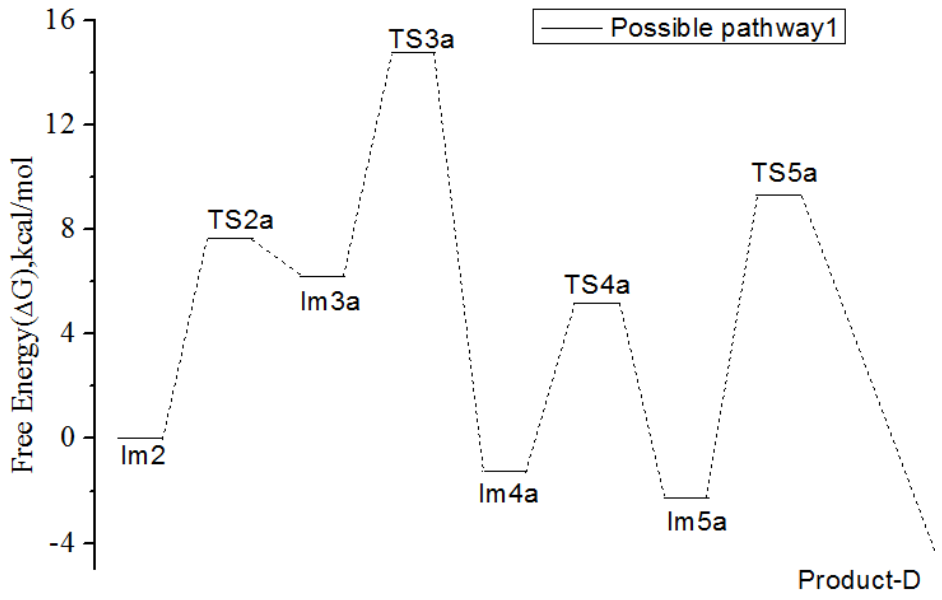


**Figure 19.** (A) Calculated intermediate and transition state structures for pathway 1. (B) The corresponding energy diagram of pathway 1.These structures and figures was created by Dr. Zhao-Di.

An alternate side-on approach of $D_2$ (pathway 2) was also considered but found to involve a significantly higher energy transition state. The computational study starts with **Im2** after oxidative addition of PinBH followed by migratory insertion step (Figure 20A). Calculating an optimum structure of the side-on $D_2$ approach was not trivial and the energy needed to get to **Im3b** and structures thereafter was very high compared to pathway 1 (Figure 19A). Therefore, Dr. Yang decided to stop the calculation and made the conclusion that the lower energy pathway 1 is more likely (Figure 19B). Based on the computational work done by Dr. Yang, the mechanism involving with $D_2$ or $H_2$ sigma bond metathesis (Figure 16) is proposed to be a feasible pathway for the formation of

the hydrogenation product under hydroboration conditions with the presence of $D_2$ or $H_2$ gas.

(A)

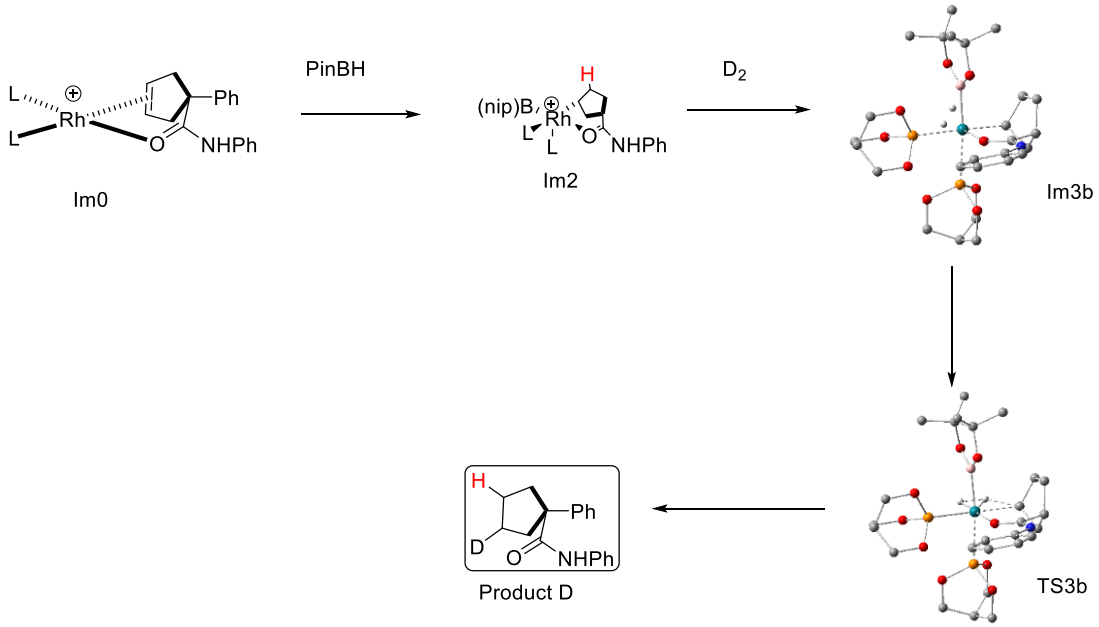


(B)

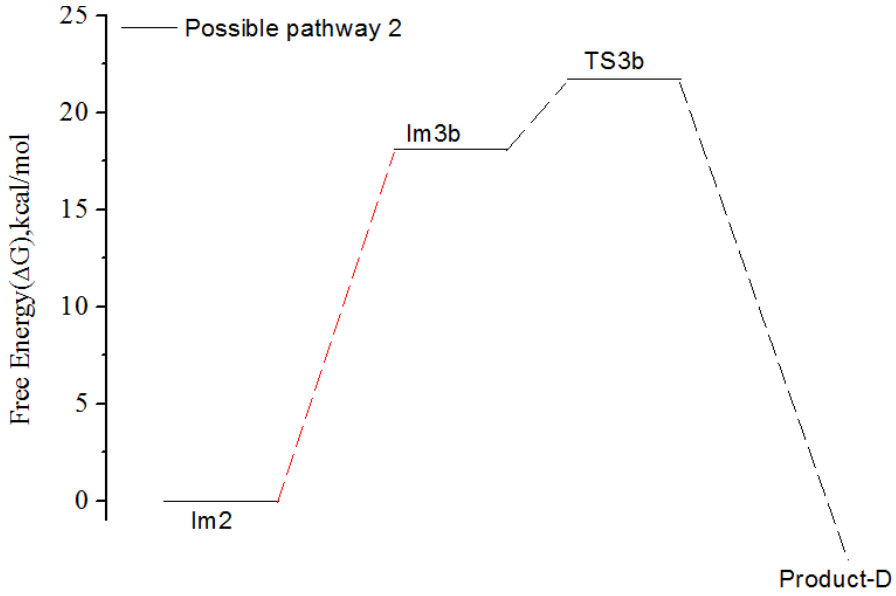

**Figure 20.** (A) Calculated intermediate and transition state structures for pathway 2. (B) Energies of reactant, intermediate, transition state, and products for pathway 2. These structures and figures was created by Dr. Zhao-Di.

The second proposed mechanism differs from the first described above (Figure 16) in featuring a sigma bond metathesis with TMDBH (not $H_2/D_2$). There are several published studies that show that borane compounds can participate in sigma bond metathesis[13, 19, and 24]. Hartwig et al[19] reported experimental and computational studies on boron assisted σ -bond metathesis pathway for alkane borylation with Fe and W species (Figure 21). First an alkane σ -complex **A** is formed followed by transfer of a hydrogen from the alkyl group to the boron via σ -bond metathesis transition state **σ -CAM**. This leads to intermediate **B**, which cannot undergo direct formation of the final alkylboronate ester due to the trans geometry of the alkyl and boryl groups. The complex **B** undergoes an σ -rotation to locate both the boryl and alkyl groups to cis position (**B'**). B-C bond formation occurs through an σ -bond metathesis to yield the intermediate **C** where elimination of alkylboronate ester occurs favorably. Compared to the mechanism based upon sigma bond metathesis with $H_2$, this mechanism seems less likely. It does not account for the fact that an atmosphere of $H_2$ significantly increases the reaction rate and yield of hydrogenation product. However, there might be a possibility that the mechanism under $N_2$ and $H_2$ are different.

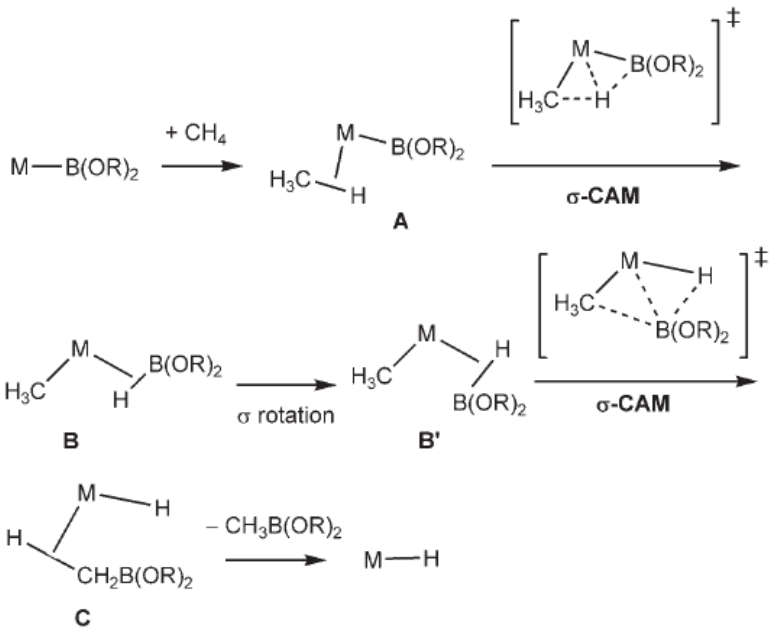


**Figure 21.** Borane σ -bond metathesis proposed by Hartwig et al. (permission obtained from the publisher)

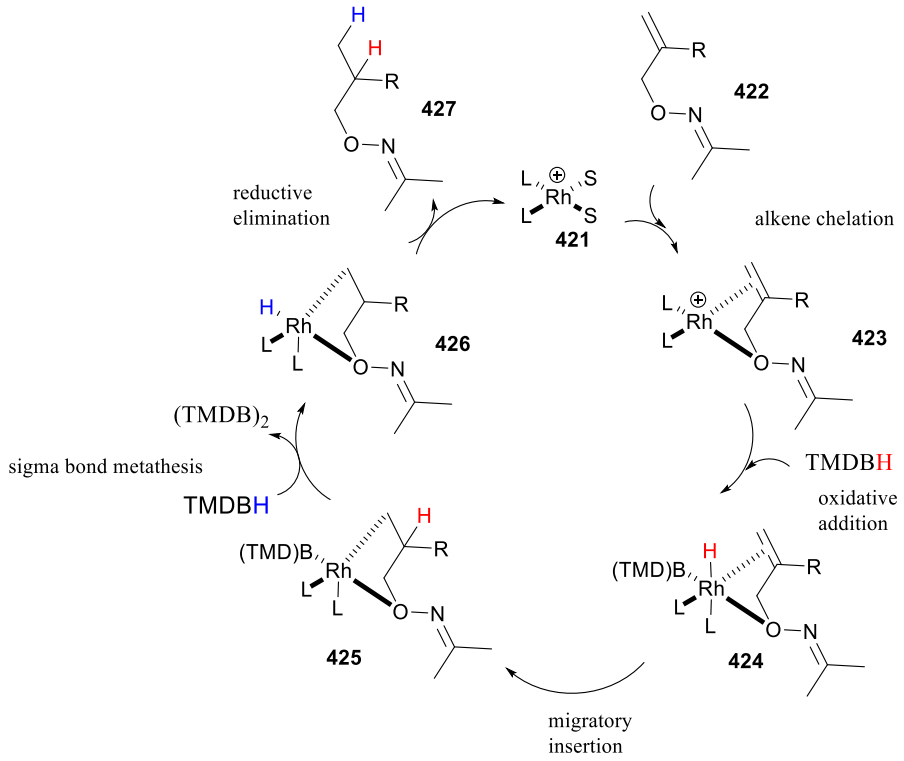


**Figure 22.** Proposed mechanism 2 for hydrogenation pathway under hydroboration. Alternatively, the rhodium may be complexed to nitrogen suggested by some preliminary computational studies by Zhao-Di.

The following section of this chapter discusses observations that support the proposed mechanism involving $H_2$ sigma bond metathesis (Figure 16). In order for the proposed mechanism to be operative, $H_2$ must be present. Nonetheless, the rhodium-catalyzed hydroboration of the oxime ether substrates by TMDBH gives up to 87% yield of the hydrogenation product. An obvious question is whether $H_2$ gas is generated during the reaction under the typical hydroboration conditions with TMDBH under a $N_2$ atmosphere. NMR spectroscopy was employed to search for evidence of $H_2$ gas formation during the reaction, a resonance for $H_2$ is generally observed at 4.55 ppm in the $^1$H NMR[25] spectrum. However, oxime ether substrates and TMDBH have multiple

peaks grouped in a small region around 3.0 – 4.5 ppm on $^1$H NMR, which makes analysis of $H_2$ peak difficult and unreliable. Therefore, deuterium NMR (D NMR) was used instead. TMDBD was used as a deuterium source based on the assumption that $D_2$ gas generation is most likely stem from TMDBD. By D NMR, only deuterium-containing compounds would show up in the spectrum; this makes analysis and identification of $D_2$ easy. The D NMR of THF was taken as a reference based upon the natural abundance level of deuterium. THF exhibits peaks at 3.65 and 1.8 ppm (Figure 23 A). $D_2$ gas from a cylinder was bubbled into this THF solvent via a metal needle for a few minutes to make certain that $D_2$ is present in the solution; a D NMR spectrum recorded immediately afterwards shows a new peak at 4.6 ppm consistent with $D_2$ (Figure 23 B). Furthermore, it was observed that in the absence of oxime ether substrate, the combination of rhodium metal, ligand, and TMDBD in THF generated the same $D_2$ peak (Figure 24 A); in addition, visible bubble formation was observed in the NMR tube. As soon as a substrate was introduced to this solution, the $D_2$ peak was no longer observed.

Although it took some trial and error and several attempts to get the D NMR spectra described above, these two simple experiments suggest two important conclusions. One is that during a reaction under normal asymmetric hydroboration condition $D_2$ generation is possible. Secondly, $D_2$ generated in the solution is quickly consumed by reaction with substrate, which means that the hydrogenation pathway is very efficient. These data coupled with the fact that TMDBH(D) can be used catalytically under a moderate pressure of hydrogen (Figure 11) and a high level computational study support the possibility of sigma bond metathesis of $H_2/D_2$ account for the

reduction product (Figure 19); thus, taken together the preliminary experimental data suggest that it is likely that the proposed mechanism (Figure 16) is operative. However, one important question has not been answered fully, how $H_2$/ $D_2$ is generated from TMDBH(D).

(A)

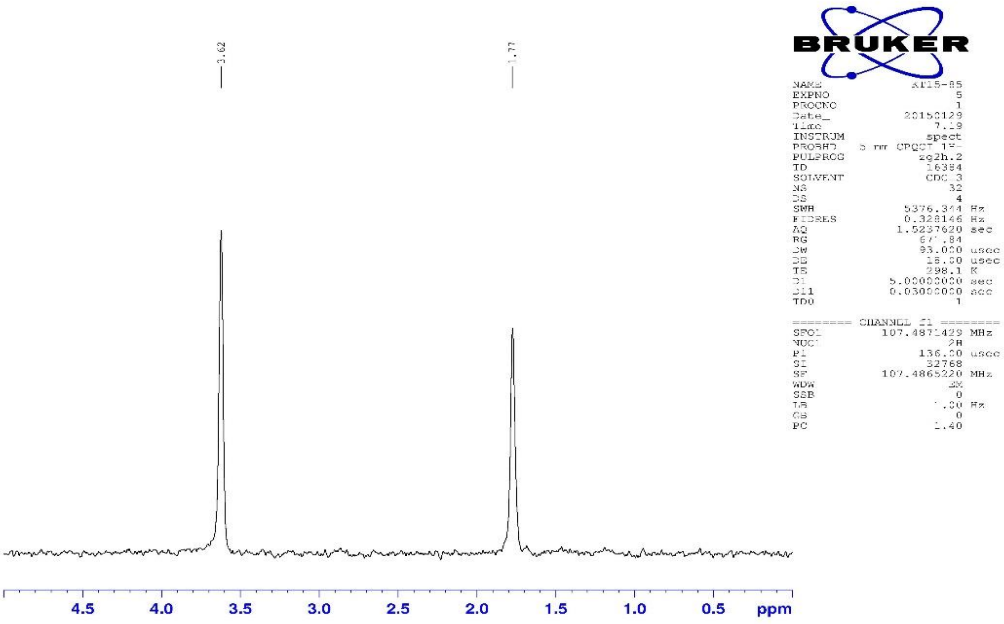

(B)

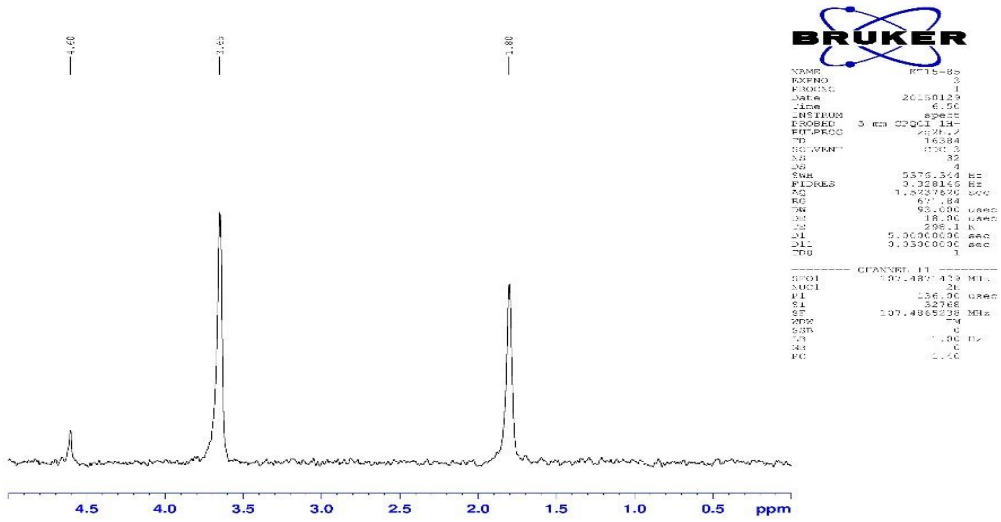


**Figure 23.** (A) Spectra on D NMR with THF. (B) Spectra on D NMR with THF + $D_2$.

(I)

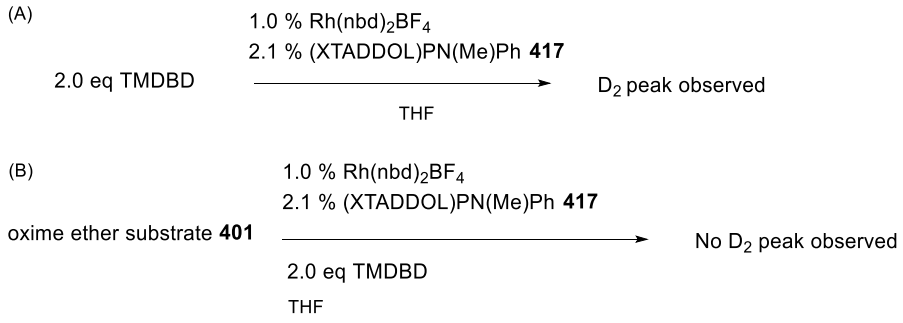


(II)

(A)

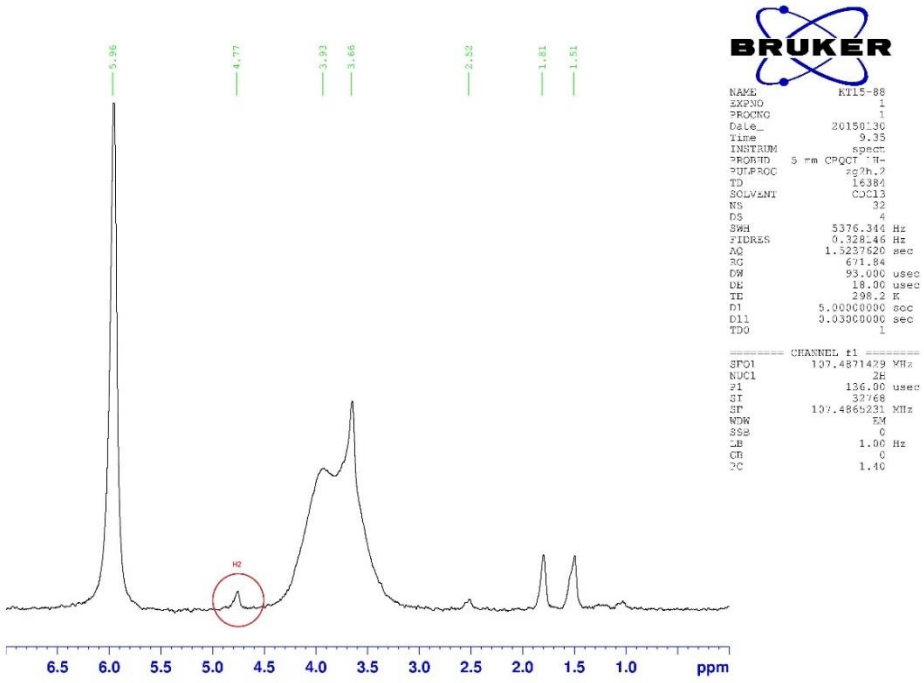
5.96
4.77
3.93
3.66
2.52
1.81
1.51
H2
6.5 6.0 5.5 5.0 4.5 4.0 3.5 3.0 2.5 2.0 1.5 1.0 ppm
BRUKER
NAME KT15-88
EXPNO 1
PROCNO 1
Date_ 20150130
Time 9.35
INSTRUM spect
PROBHD 5 mm CPQCI 1H-
PULPROG zg2h.2
TD 16384
SOLVENT CDCl3
NS 32
DS 4
SWH 5376.344 Hz
FIDRES 0.328146 Hz
AQ 1.5237620 sec
RG 671.84
DW 93.000 usec
DE 18.00 usec
TE 298.2 K
D1 5.00000000 sec
D11 0.03000000 sec
TD0 1
======== CHANNEL f1 ========
SFO1 107.4871429 MHz
NUC1 2H
P1 136.00 usec
SI 32768
SF 107.4865231 MHz
WDW EM
SSB 0
LB 1.00 Hz
GB 0
PC 1.40

(B)

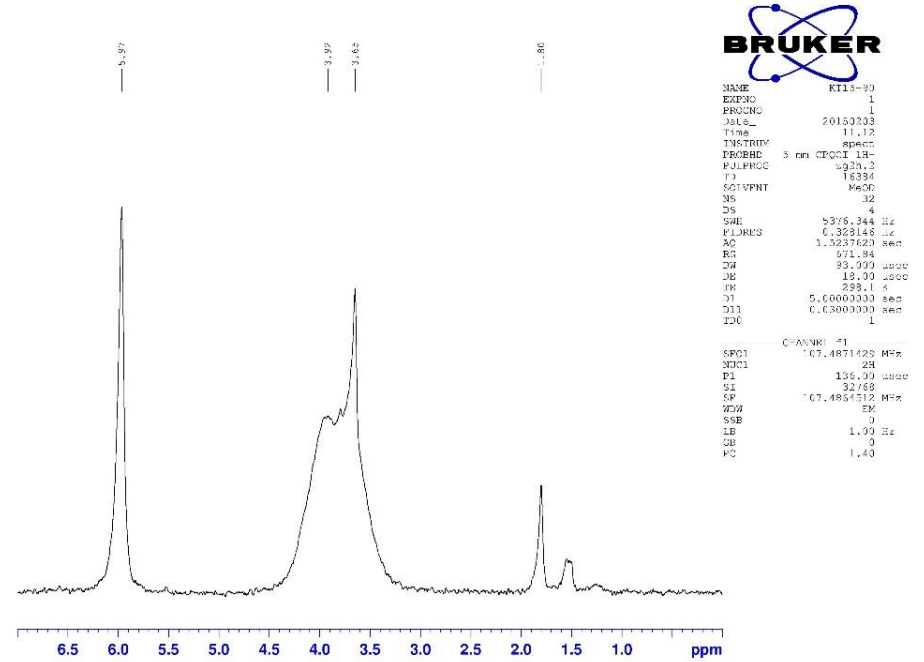
5.97
3.97
3.68
1.80
6.5 6.0 5.5 5.0 4.5 4.0 3.5 3.0 2.5 2.0 1.5 1.0 ppm
BRUKER
NAME KT15-90
EXPNO 1
PROCNO 1
Date_ 20150203
Time 11.12
INSTRUM spect
PROBHD 5 mm CPQCI 1H-
PULPROG zg2h.2
TD 16384
SOLVENT MeOD
NS 32
DS 4
SWH 5376.344 Hz
FIDRES 0.328148 Hz
AQ 1.5237620 sec
RG 671.84
DW 93.000 usec
DE 18.00 usec
TE 298.1 K
D1 5.00000000 sec
D11 0.03000000 sec
TD0 1
======== CHANNEL f1 ========
SFO1 107.4871429 MHz
NUC1 2H
P1 136.00 usec
SI 32768
SF 107.4854512 MHz
WDW EM
SSB 0
LB 1.00 Hz
GB 0
PC 1.40

**Figure 24.** (I) $D_2$ peak appearance on D NMR depending on reaction condition. (II) D NMR spectra for condition (A) and (B).

Several possible routes for $H_2$ generation are shown in Figure 25. First, TMDBH can react with $H_2O$ to generate TMDBOH adduct and $H_2$; TMDBOH can react with another molecule of TMDBH to form TMDBOBTMD and $H_2$[27] (Figure 25 A). This transformation requires the presence of $H_2O$, and under normal hydroboration conditions, no $H_2O$ is added to the reaction. Despite efforts to eliminate moisture as much as possible in the lab, a literature study found that solvent THF can have up to 50 ppm of $H_2O$, even after distillation from sodium metal/benzophenone with refluxing overnight[26]. Considering this information and calculating the amount of moisture that might be present in reaction mixture, it was estimated[27] that total water content can be as high as 4% relative to the amount of oxime ether substrate. It is important to point out that this estimate is a minimum amount and the amount of water in the reaction mixture could be higher.

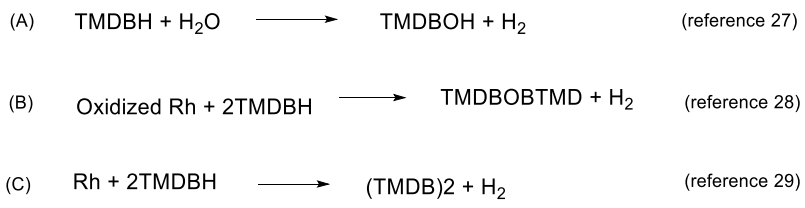


**Figure 25.** Four possible modes of $H_2$ generation.

While the level of $H_2O$ in the reaction mixture alone are unable to account for the full conversion of TMDBH into $H_2$, the generation of $H_2$ from TMDBH and $H_2O$ was nonetheless investigated. It was reported that PinBOH reacts with PinBH to form PinBOBPin along with $H_2$[28]. Therefore, it should be possible to achieve the same transformation with the isomeric borane TMDBH. This was confirmed by the reaction of TMDBOH (synthesized from equimolar TMDBH and $H_2O$ in THF) with TMDBH; this indeed leads to TMDBOBTMD and $H_2$ (Figure 26 A). The formation of TMDBOBTMD was confirmed by both $^{11}B$ NMR and GCMS. The consumption of TMDBH and generation of TMDBOBTMD by reaction with $H_2O$ were monitored by $^{11}B$ NMR over the course of 6 hours collecting data at one hour intervals. The results were presented in Figure 26 B. As expected, one $H_2O$ molecule reacts with two TMDBH to afford TMDBOBTMD with generation of two $H_2$ molecules. This reaction monitoring data suggests that the reaction of TMDBOH with TMDBH to give TMDBOBTMD is slower than the reaction of TMDBH with $H_2O$ to give TMDBOH. The consumption of TMDBH in presence of equimolar $H_2O$ is very fast (took only 5 min) and generation of $H_2$ was easily visible through a NMR tube as gas bubbles. The reaction can take as long as 6 hours with lesser amounts of water; still a rate that is competitive with a typical hydroboration reaction. This experiment suggests that the presence of 4% $H_2O$ relative to oxime ether substrate could result in consumption of 8% of TMDBH to generate $H_2$ and byproduct TMDBOBTMD. Of course, this number could be further increased depending on the condition of certain experiment day and other factors affecting moisture content of reaction mixture.

(A)

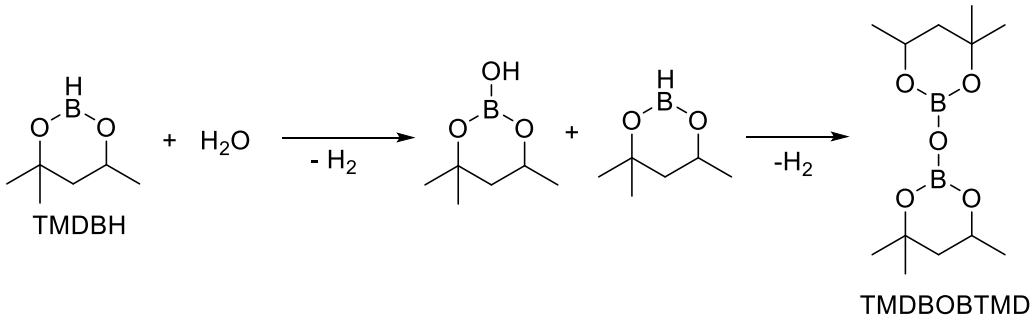


(B)

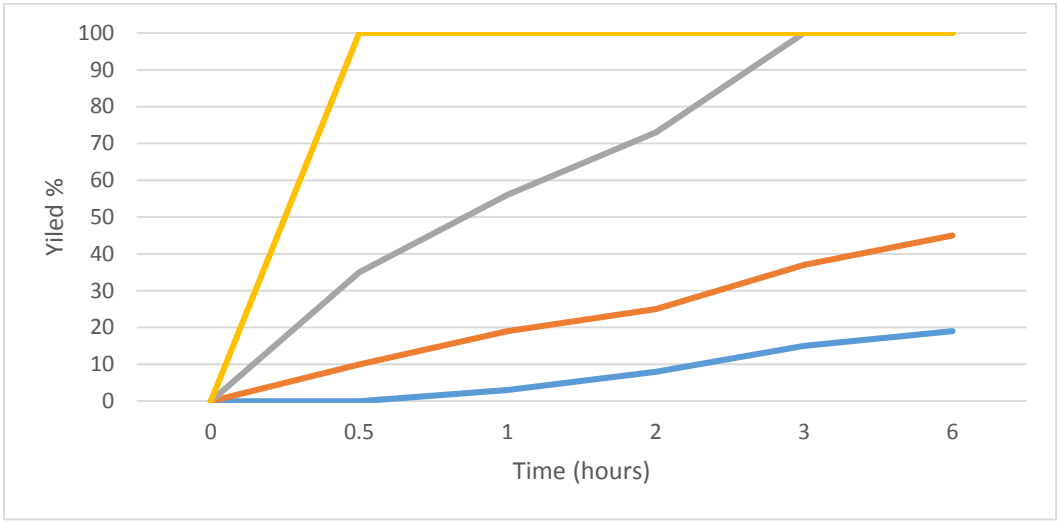


| | time (hours) | | | | | |
|---|---|---|---|---|---|---|
| $H_2O$ (eqv) | 0 | 0.5 | 1 | 2 | 3 | 6 |
| 0.1 | 0 | 0 | 3 | 8 | 15 | 19 |
| 0.3 | 0 | 10 | 19 | 25 | 37 | 56 |
| 0.5 | 0 | 35 | 56 | 73 | 100 | 100 |
| 1.0 | 0 | 100 | 100 | 100 | 100 | 100 |

(C)

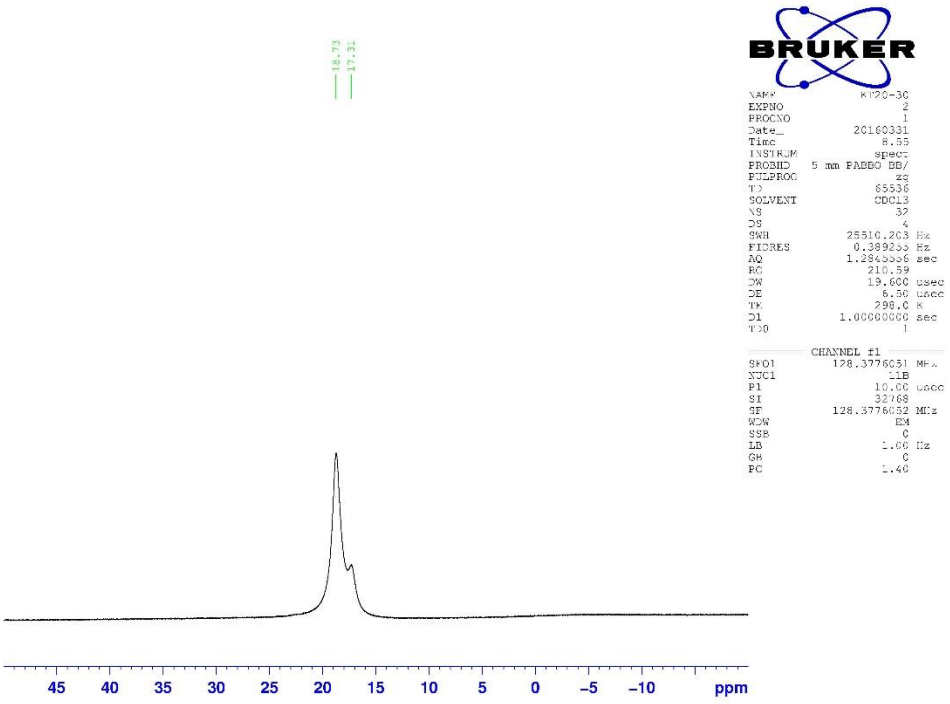


**Figure 26.** (A) Reaction of TMDBH with $H_2O$. (B) Reaction profile of TMDBOBTMD generation. (C) TMDBOBTMD $^{11}B$ NMR spectra

If $H_2O$ is replaced with $D_2O$, the reaction with TMDBH would form DH exclusively. As expected, a resonance for HD was found in the D NMR spectrum at 4.85 ppm in THF. When TMDBH and $D_2O$ were combined under hydroboration conditions with oxime ether substrate, deuterium is incorporated into both the methyl and methine positions with a roughly 1.5:1 distribution in the reduced product (Figure 27). Recall that the reaction of the oxime ether with TMDBH under $D_2$ (1 atm) resulted in no incorporation of deuterium at the methine, only in the methyl group (Figure 12). This can be understood by recognizing that sigma bond metathesis with HD can result in the partial

formation of TMDBD which can enter another cycle to deliver deuterium onto methine position.

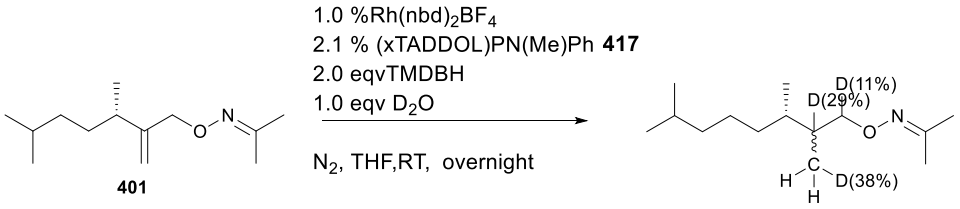


**Figure 27.** Added $D_2O$ as a source of deuterium incorporation in reduction of oxime ether.

It is worth noting that the one mode of $H_2$ generation described above (Figure 25 B) does not require presence of rhodium catalyst. Although later experiments suggest that the rhodium catalyst is needed to generate $H_2$ under hydroboration reaction conditions, it would be an oversimplification to rule out this mechanism on these grounds. It is possible that those two mechanisms operate in conjunction with other $H_2$ generating mechanisms.

The second potential mode of generating $H_2$ during the reaction that was considered involves rhodium catalysis (Figure 25 B & C). It has been noted that most commercially purchased rhodium metals were found to contain some fraction of oxidized rhodium[7]. The presence of oxidized rhodium has been shown to enable a reaction with borane to form $H_2$ gas and borane adducts[28] (Figure 25 B). This process starts with treatment of rhodium (I) precursor with dioxygen to form rhodium (III)-

peroxo complex. The latter reacts with the Lewis acidic boron compounds, here I suggest TMDBH, by oxygen transfer to give a rhodium complex and borane adduct (Figure 28). The boron adduct which would be produced here is TMDBOH. This can react with another molecule of TMDBH to form TMDBOBTMD along with $H_2$ (Figures 25A and 26) thus supplying $H_2$ needed for the hydrogenation. Hydrogen generation by oxidized rhodium is less likely because of the fact that only 1% of $Rh(nbd)_2BF_4$ is used in this study, which can produce 1% of hydrogen gas by the interaction with TMDBH. This is far too little to account for over 80% of hydrogenation product.

With regard to the third potential mode of generating $H_2$ under hydroboration conditions, Braunschweig et al[29] reported an efficient catalytic transition metal catalyzed synthesis of diboranes. $(pinB)_2$ and $(catB)_2$ were prepared with either homogeneous or heterogeneous transition metal catalysts, including Pt, Pd, Ni, and Rh, from the corresponding boranes precursors, pinBH and catBH, respectively. The highest TON reported for Rh catalyzed diborane synthesis is 6,500. This supports the possibility that the rhodium catalyst can very efficiently generate $H_2$ and $(TMDB)_2$ from TMDBH. To test whether the rhodium catalyst precursor used for hydroboration also generates $H_2$ from TMDBH, a series of control reactions were set up with the same procedure described in Braunschweig paper[29], which in this case GCMS was used to detect $(TMDB)_2$. The results in Figure 28 showed that both Rh on alumina and $Rh(nbd)_2BF_4$ catalyzed the formation of $(TMDB)_2$ and $H_2$, although TON observed were significantly lowered than those found by Braunschweig for $(pinB)_2$ and $(catB)_2$. Docosane $(CH_3(CH_2)_{20}CH_3)$ was used as internal standard for GCMS analysis to quantify $(TMDB)_2$

diborane generated. Considering the Takacs group experience on the relative reactivity of borane compounds including CatBH, PinBH, and TMDBH, it seems reasonable that TMDBH is the least reactive borane source among the three. This is perhaps one of the reasons that TON for converting TMDBH to $(TMDB)_2$ is significantly lower. Nonetheless, the important finding here is that $(Rh(nbd)_2BF_4)$ does generate $H_2$ in THF solution. $H_2$ gas was visible as gas bubbles in the solution as well.

In the Braunschweig paper, the formation of $(pinB)_2$ was accompanied by several side products, among which pinBOH and $(pinB)_2O$ were identified by mass spectrometry and NMR. Similar observations have been made with my system; TMDBH was converted to TMDBOH and $(TMDB)_2$ by reacting with $(Rh(nbd)_2BF_4)$ as confirmed by mass spectrometry (Figure 32). In addition to my studies and those of Braunschweig and I, the groups of Bettinger[30] and Stephan[31] also reported the formation of the same byproducts when working with pinBH. In addition, Braunschweig mentioned that the continuous removal of diborane $(catB)_2$ and $(pinB)_2$ from the reaction mixture greatly enhanced TON from 95 to 11,600 and from 93 to 1,850, respectively. So under the right circumstance hydrogen gas can be generated rapidly in rhodium-catalyzed hydroboration reactions.

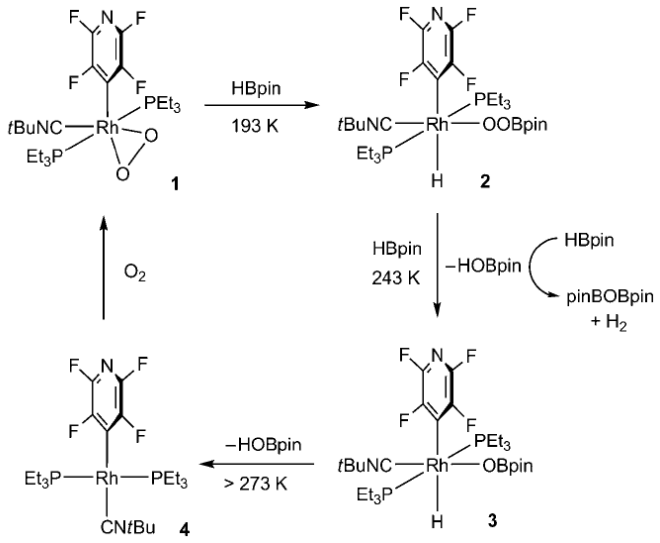


**Figure 28.** Reproduced from *Angew. Chem. Int. Ed*. **2008**, 47, 8867 scheme 2 (permission obtained).

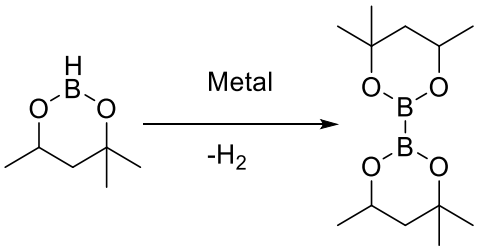


| Metal | Time | TON |
|---|---|---|
| Rh on alumina (0.05%) | 20 h | 190 |
| $Rh(nbd)_2BF_4$ (0.05%) | 20 h | 80 |

**Figure 29.** $(TMDB)_2$ diborane synthesis with rhodium metals. Reaction condition: 0.05% of metal was mixed with neat TMDBH and after 20 h the reaction mixture is analyzed by GCMS. Note that the resulting $(TMDB)_2$ diborane was not removed during the reaction.

In order to provide further evidence for $H_2$ generation during the reaction, the boron byproducts of rhodium-catalyzed $H_2$ generation process were explored further. A series of possible boron compounds were prepared according to published procedures and characterized by $^{11}B$ NMR; the chemical shift data are summarized in Figure 30. As is apparent from the graph, several of these boron compounds have very similar $^{11}B$ chemical shifts, for example, TMDB-O-BTMD (18.65 ppm), $B_2TMD_3$ (18.67 ppm) and TMDBOH (18.67 ppm). Note that $B_2TMD_3$ was a result of ligand promoted trimerization.[43] $^{11}B$ NMR tends to generate broad peaks due in part to the fact that the material used to make NMR tubes is borosilicate glass. As a result, it is hard to distinguish peaks within the very similar chemical shifts by $^{11}B$ NMR. Three boron compounds (TMDBOH, $(TMDB)_2$, and $B_2TMD_3$) were added under hydroboration condition either with $N_2$ or $H_2$ atmosphere to determine their effectiveness in promoting hydrogenation of the oxime ether substrates. TMDBOH added in place of TMDBH, under otherwise standard hydroboration conditions under a $N_2$ or $H_2$ atmosphere, did not catalyze the reaction at all (Figure 31 I). Similar results were obtained with $(TMDB)_2$ and $B_2TMD_3$ (figure 31 II & III); no hydrogenation product was formed.

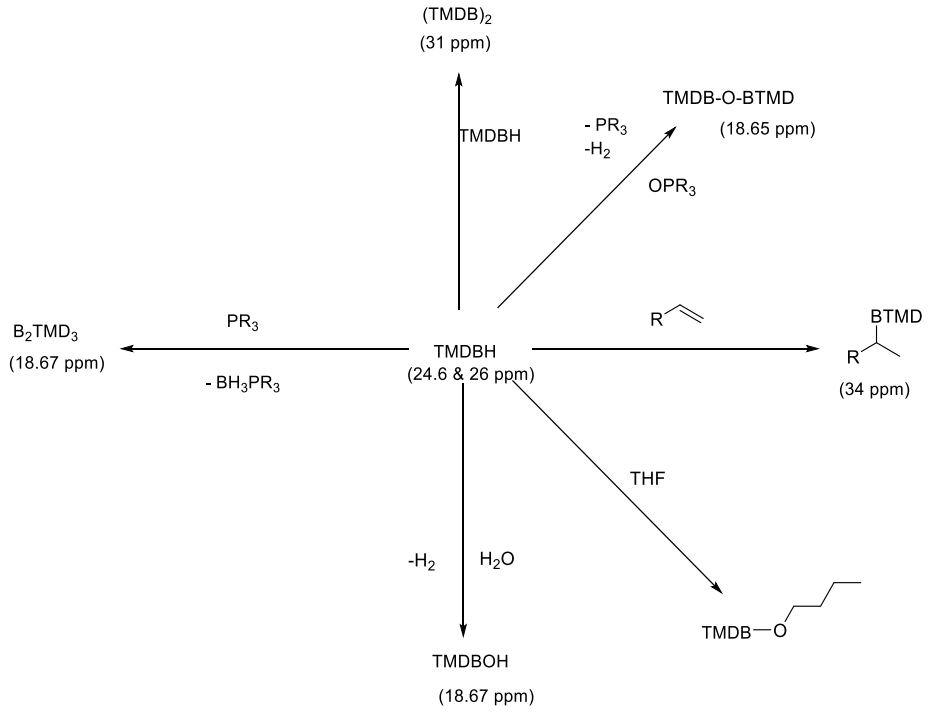


**Figure 30.** $^{11}B$ NMR chemical shifts of boron-containing species that can be formed under hydroboration.

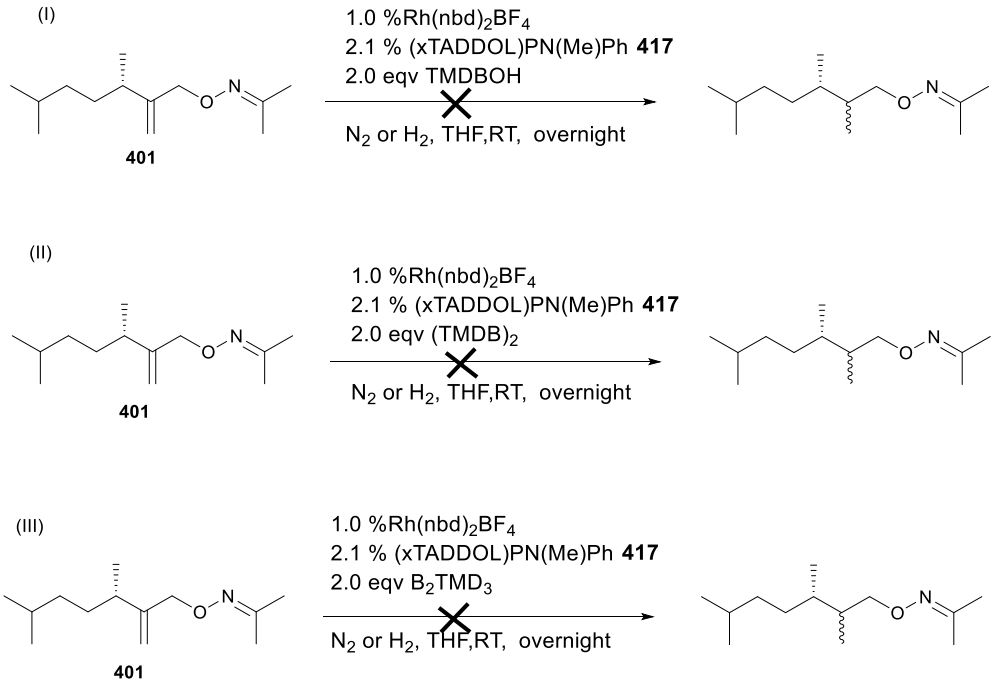


**Figure 31.** Control reactions with various TMDBH derivatives.

Next, a reaction mixture was analyzed by $^{11}B$ NMR and GCMS at the end of the reaction to identify which boron containing species were present that might provide clues for understanding the hydrogenation pathway mechanism. These observations provided evidence that two boron containing species were present in the crude reaction mixture (Figure 32 A). GCMS confirmed the presence of TMDBOH and $(TMDB)_2$ diboron with the ratio of 10 and 90%.[44] Surprisingly no peak at 29 ppm, the shift at which $(TMDB)_2$ diboron should be observed, was seen (see Figure 33). $^{11}B$ NMR only showed one broad peak between 19-16.5 ppm. Within this region of the spectra, a resonance of TMDBOH would be expected. A similar ratio of boron-containing compounds was observed when TMDBH was treated with equimolar $H_2O$. This gave the exact same B NMR spectra and GCMS identified the presence of TMDBOH and $(TMDB)_2$ dimer in a 40% to 60% ratio (Figure 32 B). An important question was raised from this experiment. What happened to a peak of $(TMDB)_2$ dimer that would normally appear around 30 ppm?

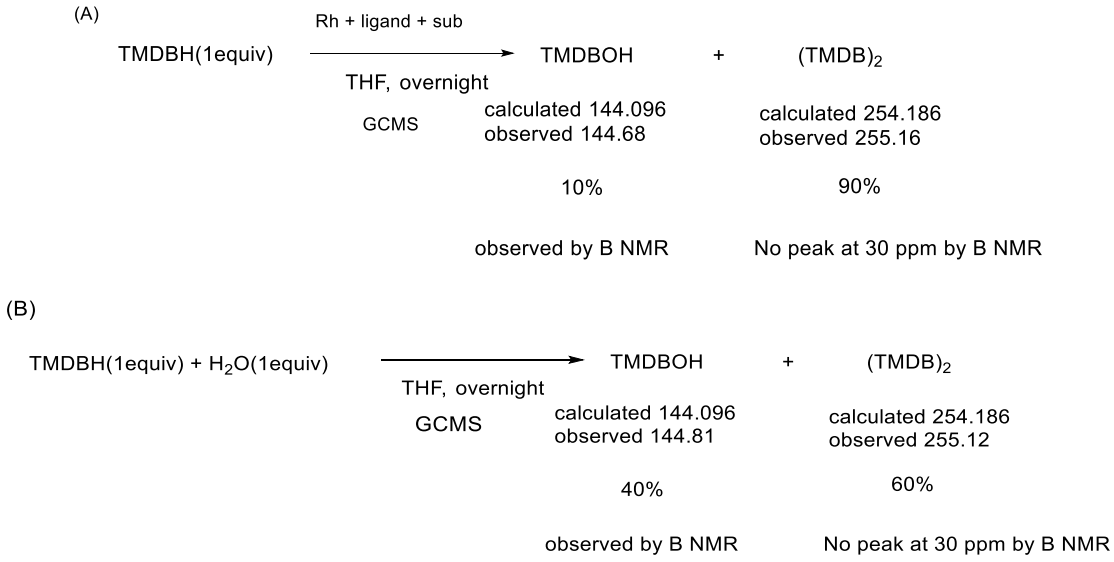

(C)

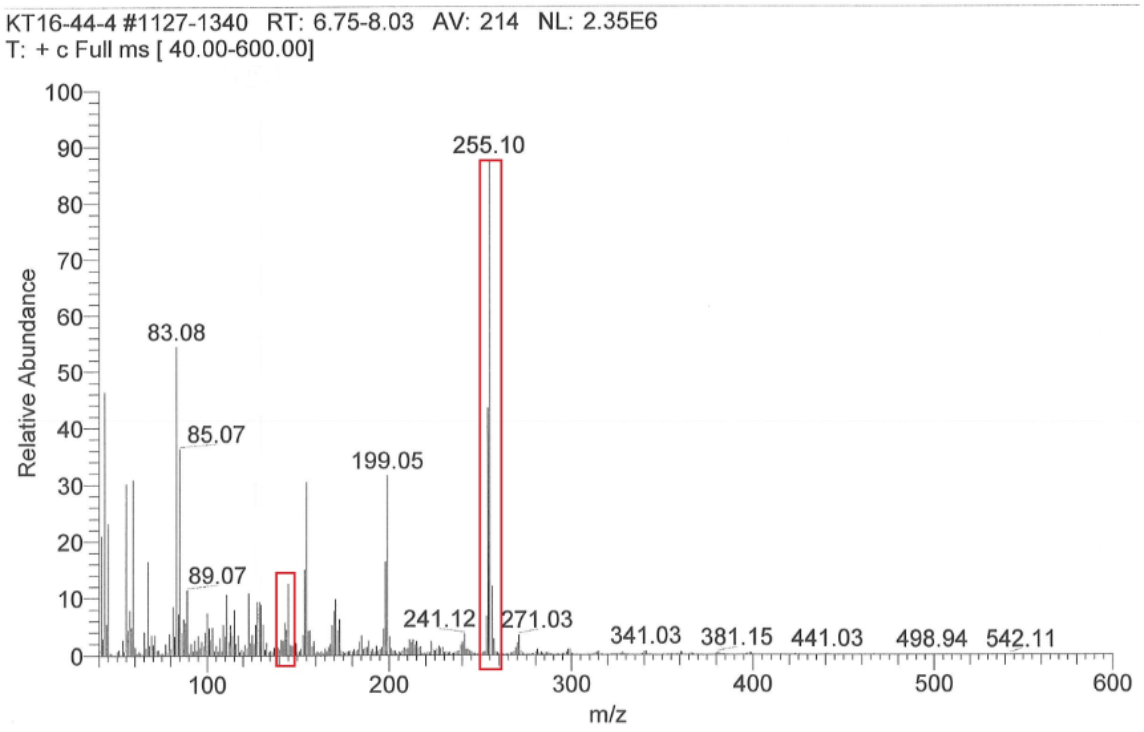


**Figure 32.** Analysis by B NMR and GCMS of the reaction mixture after overnight with (A) typical hydroboration condition and (B) control reaction with TMDBH and $H_2O$. (C) GCMS spectra of (A) showing 90:10 ratio of $(TMDB)_2$/TMDBOH.

It has been the experience in the Takacs group that bis(pinacolato)diboron does not catalyze hydroboration under the conditions described in this thesis. As a result, there has been little study of the reactivity of this reagent. $(TMDB)_2$ diboron was prepared from 2-methyl 2, 4,- pentanediol by an adaptation of the method[30 & 31] used to synthesize bis(pinacolato)diboron; $(TMDB)_2$ diboron was mixed with 2% $Rh(nbd)_2BF_4$ in THF overnight and the reaction monitored by B NMR. Surprisingly, the peak observed on B NMR after overnight reaction time was not the resonance at 29.19 ppm indicative of $(TMDB)_2$ diboron but a newly generated broad peak at 18.41 ppm (Figure 33 B). This

latter peak corresponds to the peak observed after the borane-assisted hydrogenation reaction of the oxime ether substrates. As an aside, a similar outcome was observed upon treating $(pinB)_2$ with $Rh(nbd)_2BF_4$ in THF. This demonstrates that a species we previously thought to be unreactive under the reactions condition is in fact reactive. When TMDBH was subjected to same condition in presence of $Rh(nbd)_2BF_4$, the same peak was again observed by B NMR (Figure 34), which suggests that transformations of $(TMDB)_2$ and TMDBH lead to the same boron-containing compound. The identity of this boron containing compound is under investigation. The sample was submitted for electric ionization mass spec analysis and showed the mass of 141.0860 (calculated mass: 254.1861) which suggests that this molecule was easily fragmented upon ionization.

(A)

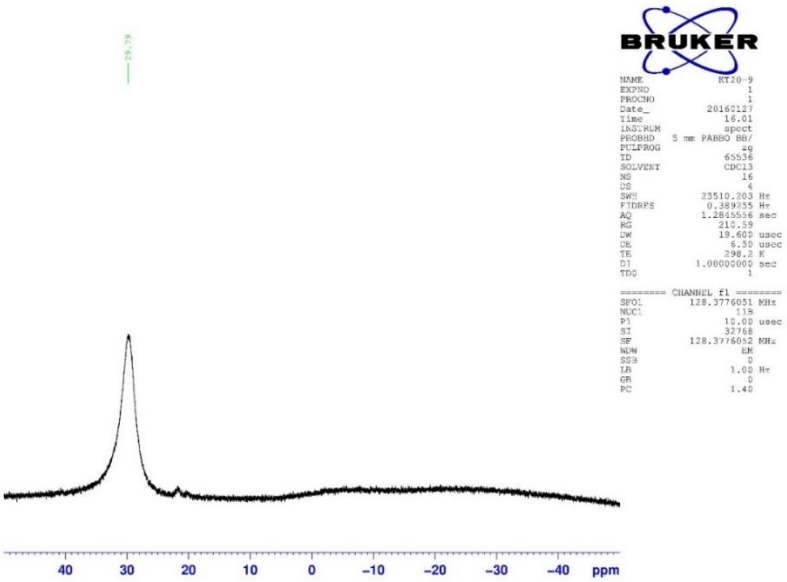

(B)

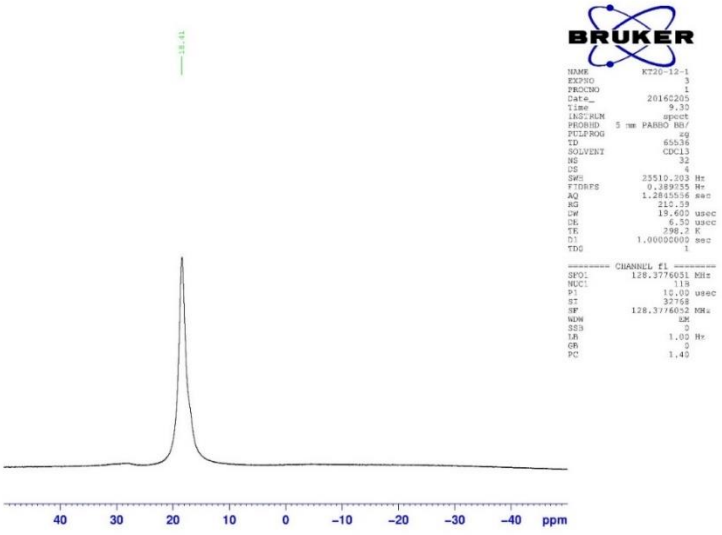


**Figure 33.** (A) $(TMDB)_2$ peak on B NMR. (B) $(TMDB)_2$ with $Rh(nbd)_2BF_4$ after overnight.

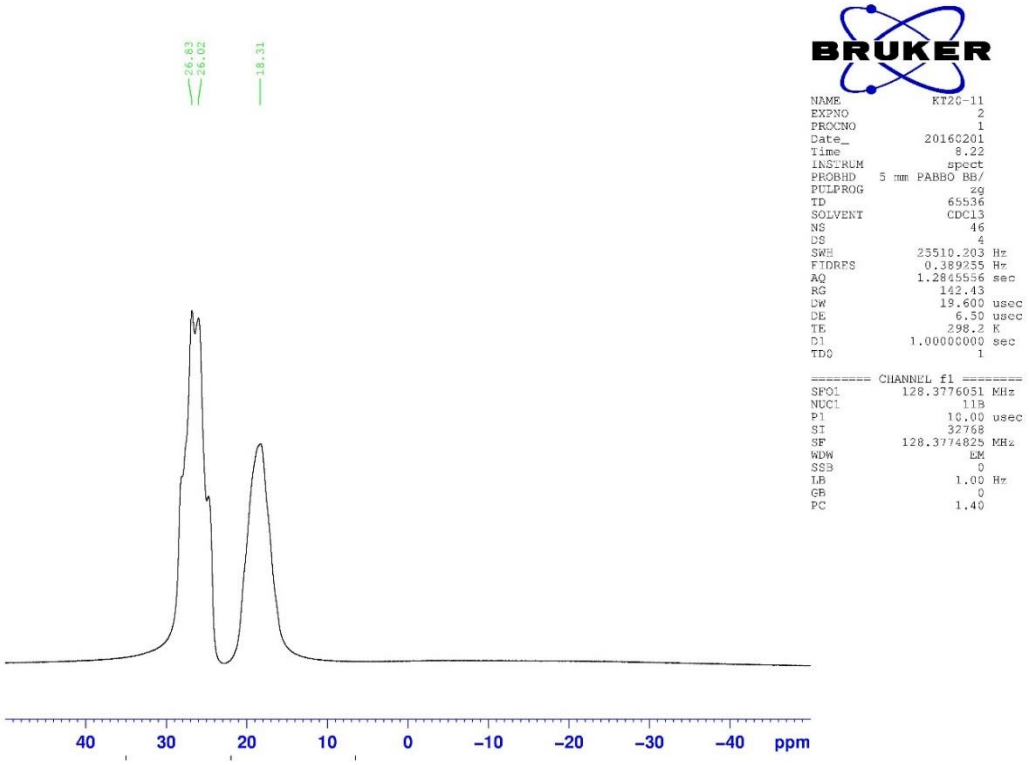


**Figure 34.** B NMR of TMDBH with $Rh(nbd)_2BF_4$ after 4 hours.

The observation of 10% TMDBOH can be accounted for in part by residual water contained in the THF reaction solvent, which was reported to be at least 4% relative to TMDBH, as discussed above. Braunschweig[29] reported the observation of PinBOH and PinBOBPin with their system in which reaction equipment was flame dried and the reaction was run under inert condition to exclude contacts of moisture and oxygen. Although they did not disclose the amount of each side products in their publications, it supports that even carefully designed and executed experiments can admit enough oxygen sources to form PinBOH and PinBOBPin. Therefore, it is not surprising to see

TMDBOH formation in my reaction mixture at the end of the reaction. Another factor to facilitate the formation of TMDBOH is presence of oxidized rhodium metal. Salomon[28] reported the formation of PinBOH with oxidized rhodium metal. It is highly possible that those two elements are responsible for the observation of 10% TMDBOH in the reaction mixture by GCMS.

Based on the data provided above, it is clear that under the condition utilized for catalytic asymmetric hydroboration generates hydrogen gas. The typical reaction condition requires 2.0 equivalents of TMDBH relative to the amount of oxime ether substrate to achieve above 80% yield of reduced product. This in turns translates into the formation of 1.0 equivalent of hydrogen gas from 2.0 equivalents of TMDBH and most of hydrogen gas is consumed very efficiently to afford hydrogenation product. The formation of $H_2$ in THF above 0.0033 M[45] will result in gas bubble at room temperature. Though a reaction vial used in this study has an air tight cap, I would not be surprised that some of the evolved gas escape from the reaction vial. However, the efficiency of consuming hydrogen gas is very high so this observation leads me to believe that there is some manner by which hydrogen gas is stabilized. In fact, when hydrogen gas is deliberately generated from addition of water to TMDBH containing solution, hydrogen gas is still present after overnight. So hydrogen gas is most likely stabilized in the solution which prevent it from escaping to the atmosphere. Mendez et al[42] reported a computational study on the stability of $H_2$ gas with several borane species. In the study the computational methods used were BLYP, MP2, and CCSD(T) and it showed that the strength of interaction between the boron site and the hydrogen molecule is related to

the Lewis acidity of the boranes. This can be affected by the size and electronic nature of the boranes. Specifically, they were able to observe and confirm the interaction between $BH_3$ an $H_2$, which lead to the stable complex $H_3B$-$H_2$ in gas phase. In addition, $CF_3BH_2$ was used to increase the acidity of the borane and it was found that stability of the complex was increased compared to $BH_3$. Although attempts to further confirm such a stabilized complex failed with fluoroboranes and hyroxyboranes, those still showed weakly bounded van der Waals complexes, which suggests that hydrogen gas is perhaps also stabilized by complexation with those boranes. The fact that hydroxyboranes $(HO)_2BH$ are similar to TMDBH and the fact that Lewis acid- base interaction was observed between TMDBH and THF (shown in Figure 39) suggest that hydrogen gas generated under catalytic asymmetric hydroboration condition is perhaps stabilized in the reaction mixture accounting for the unexpectedly high yields of hydrogenation products with stoichiometric, not excess, hydrogen. Although the computational study conducted by Mendez et al[42] was gas phase, it suggests the possibility of hydrogen gas being stabilized by boron species.

One additional consideration was briefly explored. In the past decade, seminal work by Piers[37] and others[31-34] have demonstrated that hydrogenation can be catalyzed by frustrated Lewis pairs (FLP), which are Lewis acids and bases that are sterically prevented from interaction. It allows hydrogenation to proceed under mild condition with high yields, which shares the characterization with hydrogenation pathway under hydroboration condition. But it usually does not require a metal as hydrogenation catalyst to accomplish highly reactive hydrogenation of various substrates[35]. In

addition, hydrogenation with FLP requires $H_2$ gas to promote the reaction and relatively high temperature (above 80$^oC$) and high $H_2$ pressure. In that context, FLP hydrogenation is rather different from hydrogenation pathway under hydroboration condition discussed in this thesis. Therefore, FLP type mechanism is assumed to be absent in hydrogenation pathway.

**4.4 Miscellaneous observations**

In this section of the chapter, several other miscellaneous discoveries regarding hydrogenation pathway are discussed. First, as mentioned above in several places, efficient hydrogenation has been observed not only in the presence of $H_2$ gas but also upon addition of $H_2O$. Based on a series of experiments, it is found that adding $H_2O$ to TMDBH as the source of hydrogen significantly increase the rate of hydrogenation. Under the standard hydroboration condition with an oxime ether substrate, the addition of 1.0 or 2.0 equivalents of $H_2O$ results in full conversion of the starting material to hydrogenation product (Figure 35, entry 1). Under conditions for which the reaction time without added water is about 2 hours, reaction with added $H_2O$ is complete within 30 minute (ReactIR, data not shown). However, adding a large excess of $H_2O$ leads to no reaction (Figure 35, entry 3). It seems reasonable that under such conditions, no TMDBH remains as required in the proposed mechanism for the hydrogenation pathway.

D NMR showed that as soon as $H_2O$ or $D_2O$ was added to a solution containing TMDBH(D), $D_2$ and HD evolution occurs; it is visible as hydrogen bubbles in the NMR tube. In order to confirm that hydrogen from reaction between TMDBH and $H_2O$ is indeed essential, TMDBH was mixed with $H_2O$ and then the solution was degassed by freeze-pump-thaw to remove any $H_2$. Adding rhodium, ligand and an oxime ether substrate to the degassed solution gave no hydrogenation product formation (Figure 35, entry 4). Thus, I conclude that it is indeed the hydrogen gas which generated by the reaction between TMDBH and $H_2O$ that is responsible for generating hydrogenation

product. However, it should be noted that adding $H_2$ gas after the freeze-pump-thaw did not lead to any hydrogenation product either (Figure 35, entry 5); I conclude that the species formed by the reaction between TMDBH and $H_2O$ (presumed to be TMDBOH) does not act as a hydrogenation catalyst. To confirm this conclusion, TMDBOH added in place of TMDBH did not promote hydrogenation (Figure 35, entry 6). Adding a hydrogen atmosphere to the latter had no effect either (Figure 35, entry 7). Another possible side product that could potentially catalyze the reaction, TMDB-O-BTMD, was similarly tested; it too did not promote the reaction (Figure 35, entry 8) even with an atmosphere of $H_2$ gas (Figure 35, entry 9).

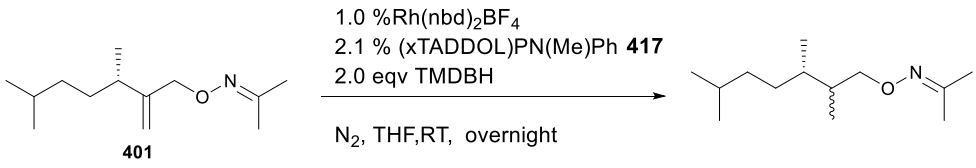


| entry | conditions | Yields (%) |
|---|---|---|
| 1 | 1 eqv $H_2O$ | 99 |
| 2 | 2 eqv $H_2O$ | 99 |
| 3 | 10 eqv $H_2O$ | 0 |
| 4 | 2 eqv $H_2O$ + freeze pump thaw | 0 |
| 5 | 2 eqv $H_2O$ + freeze pump thaw + $H_2$ (1atm) | 0 |
| 6 | 2 eqv TMDBOH (instead of TMDBH) | 0 |
| 7 | 2 eqv TMDBOH + $H_2$ (1atm) | 0 |
| 8 | 2 eqv TMDB-O-BTMD | 0 |
| 9 | 2 eqv TMDB-O-BTMD + $H_2$ (1atm) | 0 |

**Figure 35.** $H_2O$ promote hydrogenation pathway.

It was found that with the addition of stoichiometric $H_2O$, pinBH also effects reduction that, at least qualitatively, is much faster than the corresponding reduction in the presence of TMDBH. This is perhaps due to the fact that $H_2$ gas is generated much faster from the combination of pinBH with $H_2O$. It seems that the rate of $H_2$ generation is directly related to the rate of hydrogenation. The reaction proceeds to completion usually within 30 minutes at room temperature. This is quite remarkable in comparison with many hydrogenations that require high temperature and high pressure and could be valuable aspect of this unusual reduction procedure.

PinBH and TMDBH, although they are structural isomers, can give very different results in terms of reactivity, regioselectivity and enantioselectivity in catalyzed hydroboration. As mentioned above, their hydrogenation reaction rates under hydroboration also differ due to the rate difference of hydrogen production with $H_2O$. Similar observations have been made by other groups[36]. In this section, it is my goal to explore why PinBH and TMDBH are much different in their reactivity, especially with respect to the hydrogenation pathway. This study was done by D NMR and $^{11}B$ NMR and required a set of reference chemical shifts of the possible deuterium or boron containing species. Each individual chemical compounds were prepared, purified, and characterized by NMR to construct chemical shift tables shown in Figure 36 A & B.

(A)

| Reagents | D chemical shift in ppm |
|---|---|
| THF | 3.65 & 1.8 |
| $D_2O$ | 2.64 |
| TMDBD | 4.23 |
| $D_2$ | 4.6 |
| HD | 4.85 |
| PinBD | 3.96 |
| d-hydrogenation product | 0.8 |

(B)

| Reagents | B chemical shift in ppm |
|---|---|
| TMDBH | 25.04 |
| TMDBD | 23.72 |
| PinBH | 28.08 |
| PinBD | 26.73 |
| $B_2Pin_3$ | 21.42 |
| $B_2TMD_3$ | 18.67 |
| Hydroboration product | 34.4 |
| PinBOH | 22.85 |
| $(PinB)_2$ | 31.07 |
| TMDBOH | 18.67 |

**Figure 36.** (A) List of D chemical shifts. (B) List of B chemical shifts.

TMDBD in THF showed unusual behavior by D NMR analysis. The TMDBD peak can be found 4.23 ppm (Figure 36 A) as a single peak in solvents such as DCM and toluene. However, the D NMR spectrum of TMDBD in THF, showed the expected TMDBD peak 4.23 ppm and another peak at 5.98 ppm along with deuterated THF peaks (Figure 37). No such a peak was observed with PinBH in THF. Similarly, a peak at 5.98 ppm was observed in diethyl ether and DME, but its relative abundance in those

solvents was not as great as in THF. It seem plausible that the peak at 5.98 ppm (D NMR spectrum) may be a TMDBD•THF adduct. However, the peaks observed by $^{11}B$ NMR are not shifted compared to other solvents such as DCM. Thus if coordination to THF is indeed important, $^{11}B$ NMR suggests that THF is coordinated to deuterium atom of TMDBD not to the Lewis acidic boron atom (Figure 38).

(A)

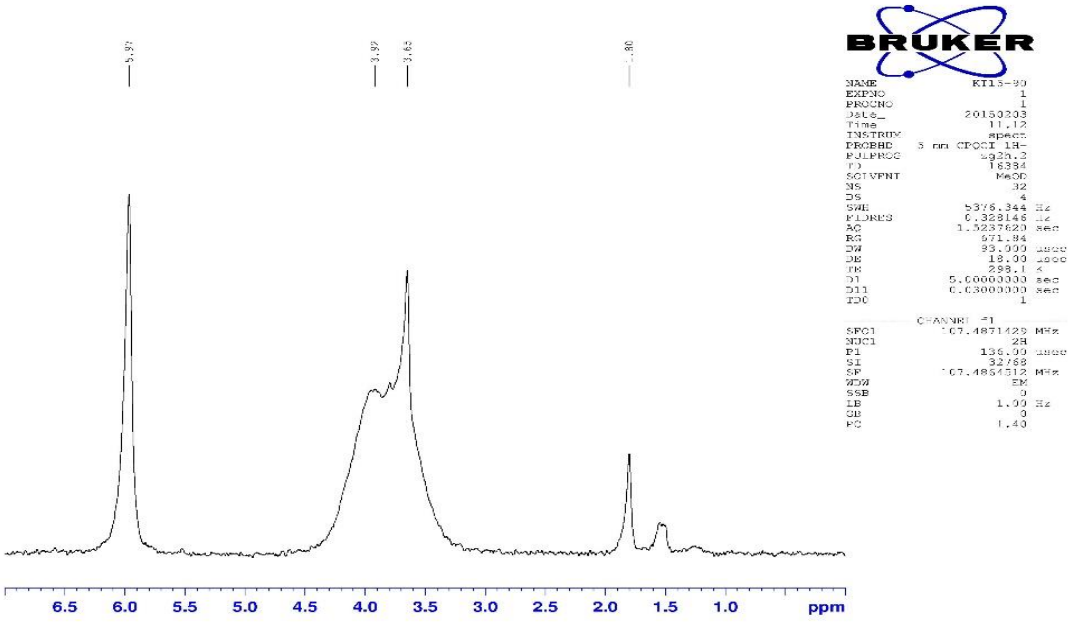

(B)

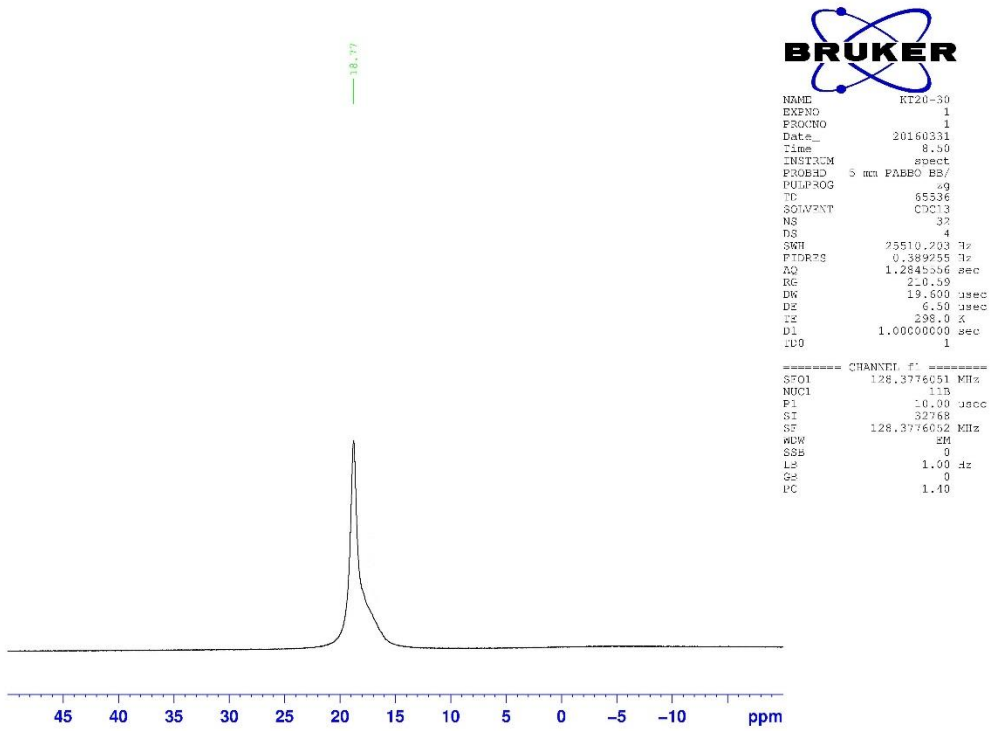


**Figure 37.** (A)D NMR spectra of TMDBD in THF. (B) B NMR spectra of TMDBD

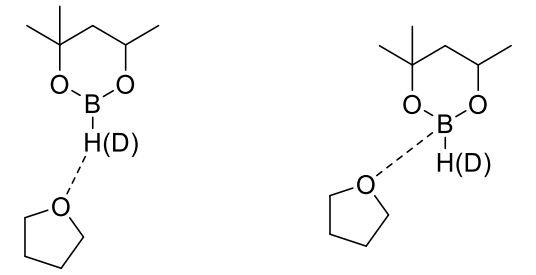


D shift change

B shift change
(not observed)

**Figure 38.** Possible TMBH (D) coordination to THF molecule.

**4.5 Conclusions**

In conclusion, the oxime ether substrates have been shown to undergo hydrogenation under hydroboration conditions in excellent yield using TMDBH as the borane. The reaction conditions for successful hydrogenation require the rhodium catalyst precursor, ligand and a borane. If any one of these components is missing, the hydrogenation becomes sluggish or does not proceed. Adding a hydrogen source, either directly in the form of $H_2$ gas or indirectly in the form of $H_2O$, promotes hydrogenation by increasing yield and reaction rate. Under $H_2$ pressure (50 psi) the reaction went to completion even with only 0.1 equivalents of TMDBH; this shows that TMDBH can be used catalytically. NMR studies revealed that $H_2$ gas evolution occurs by several different pathways (Figure 39 II). One of them is the reaction of TMDBH with $H_2O$ in THF, perhaps residual moisture in the reaction solution. I noted that it has been reported that even when THF was refluxed overnight with sodium metal and benzophenone at least 50 ppm of water remains, equivalent to 4% $H_2O$ relative to the oxime ether substrate under typical reaction conditions. Furthermore, Braunschweig reported that side products indicative of presence of water in the reaction were observed in his reactions even when extra care was taken to exclude adventitious moisture. A second mode by which $H_2$ can be generated under the hydroboration reaction conditions is rhodium-catalyzed dimerization of TMDBH. When $Rh(nbd)_2BF_4$ and TMDBH are mixed, hydrogen gas was evolved. Thirdly, based on literature oxidized rhodium complexes may react with TMDBH to form of TMDBOH and $H_2$. These three modes of generation of $H_2$ gas may all be operative at the same time contributing to the hydrogenation

pathway. However, considering the data and spectral evidence collected in this thesis chapter, a major driving force for hydrogen generation seems to be the presence of $H_2O$ and the rhodium-catalyzed dimerization.

Based on $^{11}B$ and D NMR experiments (see Figure 36 & 37), THF seems to coordinate to a proton of TMDBH. Also this interaction suggests the existence of Lewis acid-base property of TMDBH and THF. Mendez and the coworkers reported the stabilization of hydrogen gas by boranes. This may explain why hydrogen gas is used very efficiently – stoichiometrically - in the hydrogenation pathway.

Dr. Yang's computational study indicates that $H_2$ sigma bond metathesis hydrogenation pathway is feasible (Figure 39 I), which agrees with experimental results presented in this thesis. The hydrogenation mechanism discussed in this thesis is different from traditional hydrogenation reaction[41]. In addition, the reaction conditions are mild; neither high temperature nor high pressure is required. Additionally, the hydrogen source is not limited to hydrogen gas but can be TMDBH alone or borane in combination with water. Those are more environmentally friendly choices of hydrogen sources and it does not require special handlings such as hydrogen cylinders; from the safety standpoint, there is a potential advantage for some applications. Although most of the evidence collected in this thesis study suggests that $H_2$ σ-bond metathesis mechanism is likely present, it is possible that the pathway leading to the hydrogenated product could be a combination of the two mechanism discussed in this chapter. Furthermore, based on the preliminary observations of the rates of the hydrogenation pathway under $N_2$ and $H_2$ (1 atm or 50 psi) or in presence of $H_2O$ monitored by the

ReactIR instrument there is no reason to speculate that those undergo the exact same mechanism. The further development of this chemistry as a synthetic method and the search for more evidence for the mechanism is currently under investigation in the Takacs group.

(I)

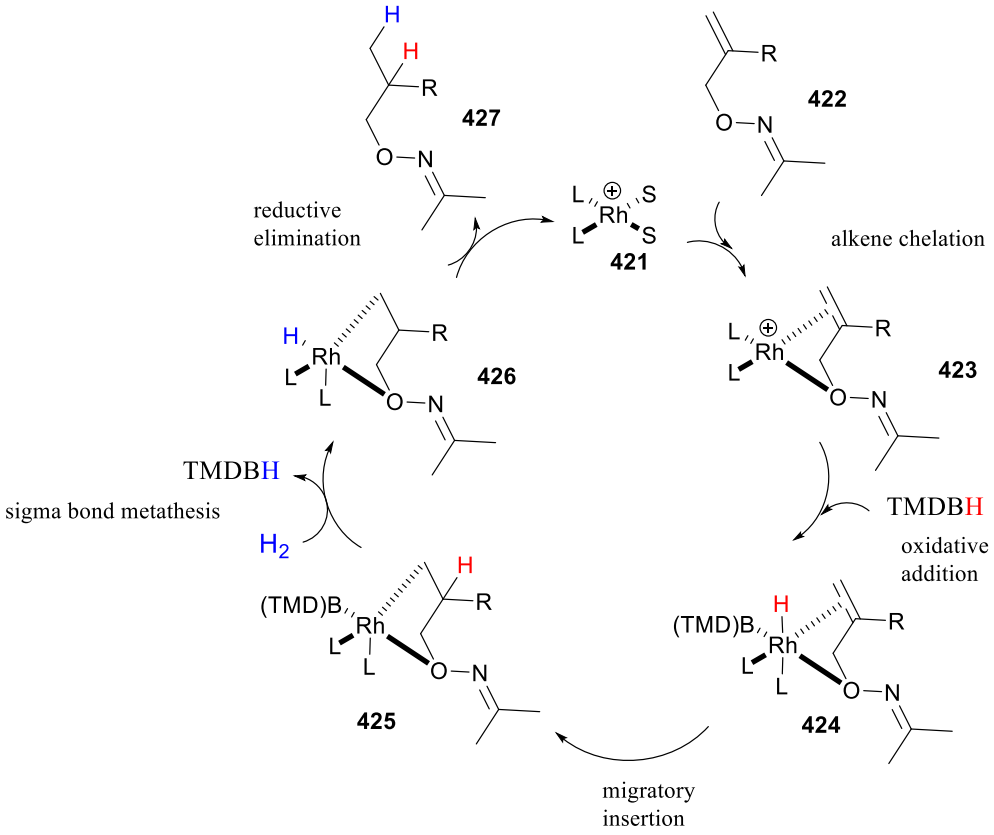


(II)

(A) $TMDBH + H_2O \longrightarrow TMDBOH + H_2$ (reference 27)

(B) Oxidized Rh + 2TMDBH $\longrightarrow$ $TMDBOBTMD + H_2$ (reference 28)

(C) Rh + 2TMDBH $\longrightarrow$ $(TMDB)2 + H_2$ (reference 29)

**Figure 39.** (I) Current proposed mechanism of hydrogenation pathway under hydroboration condition. (II) Different hydrogen generation pathways.

**4.6 Experimental**

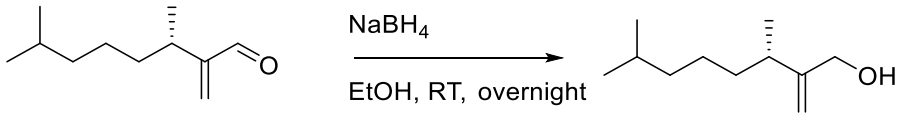


***a*. Preparation of citronellal derived alcohol.** To a 100 mL round-bottom flask was added the aldehyde (5.30 g, 31.5 mmol) (this aldehyde was prepared according to a reported (give reference/footnote) procedure described in JOC 2003, 68, 6451). The mixture was dissolved in EtOH (50 mL) and $NaBH_4$ (1.20g, 31.5 mmol) was added slowly at 0$^o$C. The mixture was stirred at room temperature for overnight. The solvent was removed under reduce pressure and extracted with EtOAc. The combined organic layers dried ($MgSO_4$) and concentrated (5.00 g, 93 %). The alcohol was used without purification for the next step.

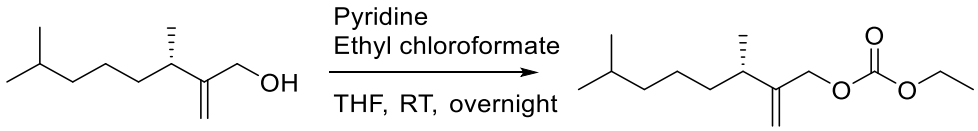


**Preparation of citronellal derived ester.** To a 100 mL round-bottom flask was added the alcohol (5.00 g, 29.4 mmol). The mixture was dissolved in THF (100 mL). Pyridine (4.70 mL, 58.8 mmol) and ethyl choloroformate (5.59 mL, 58.8 mmol) was added sequentially. The mixture was stirred at room temperature for overnight. The reaction was quenched with water. The solvent was extracted with EtOAc. The combined organic layers dried ($MgSO_4$) and concentrated. Flash chromatography (hexane:EtOAc = 90:10) afforded the product (4.60 g, 65 %) as clear oil: $^1$H NMR (400 MHz, $CDCl_3$) δ 5.07 (1H, d, J = 1.0 Hz), 4.96 *1H, d, J = 1.0 Hz), 4.59 (2H, s), 4.23 -4.17 (2H, dq, J = 7.1, 2.24 Hz), 2.21 – 2.17 (1H, m), 1.53 – 1.41 (2H, m), 1.33 – 1.25 (6H, m), 1.16- 1.13 (2H, m), 1.07 -1.04 (3H,dd, J = 6.9, 2.2 Hz), 0.86 – 0.84 (3H, dd, J = 6.6, 2.2 Hz) ppm; 13C NMR (100 MHz, $CDCl_3$) δ 155.22,148.36, 111.47, 69.05, 64.07, 39.14, 37.18, 35.82, 28.00, 25.11. 22.73, 19.86, 14.39 ppm; HRMS (FAB,) calcd. for $C_{14}H_{26}O_3$ ($M^+$), 242.1882; found, 242.1883*m/z*.

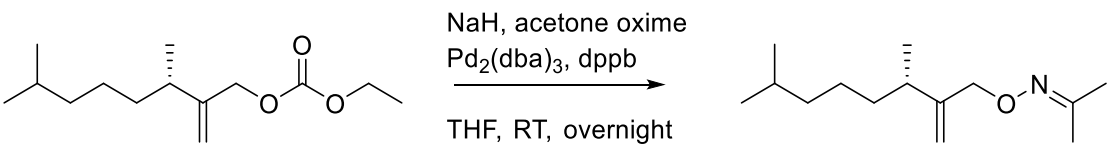


**Preparation of citronellal derived oxime ether.** To a 100 mL round-bottom flask was added acetone oxime (1.66 g, 2.09 mmol) in THF (50 mL). To a separate 50 mL round-bottom flask was added NaH (0.50 g, 2.09 mmol) in THF (20mL). The flask containing acetone oxime was cooled to 0 $^{o}$C and NaH (2.09 mmol) in THF was added via cannula needle and the mixture was stirred for 20 min at 0$^{o}$C. To another 100 mL round-bottom flask was added both $Pd_2(dba)_3$ (0.23g, 0.475 mmol) and dppb (0.48 g, 1.14mmol) in THF (10mL) and the reaction mixture was stirred for 10 min at RT. Then the ester (4.60 g, 19.0 mmol) was added to the catalyst containing reaction mixture. The solution of acetone oxime was added slowly to this catalyst reaction mixture. The mixture was stirred at room temperature for overnight. The reaction was quenched with sat. NH4C solution. The solvent was extracted with EtOAc. The combined organic layers dried ($MgSO_4$) and concentrated. Flash chromatography (hexane:EtOAc = 90:10) afforded the product (5.38 g, 74 %) as clear light yellow oil: $^{1}$H NMR (400 MHz, $CDCl_3$) δ5.03 (1H, d, J = 1.48 Hz), 4.92 (1H, d, J = 1.48 Hz), 4.53 (2H, s), 1.90-1.89 (6H, d, J = 2.76 Hz), 1.56 -1.45 (2H, m), 1.31 – 1.26 (4H, m), 1.18 – 1.13 (3H, m), 1.08 – 1.06 (3H, d, J = 6.92 Hz), 0.88 (3H, s), 0.87 (3H, s) ppm ppm ; 13C NMR (100 MHz, $CDCl_3$) δ 154.6,150.9, 110.1, 75.15, 39.13, 37.28, 35.88, 27.94, 25.14, 22.66, 21.86,19.97, 15.72 ppm; HRMS (FAB) calcd. for $C_{14}H_{27}NO$ ($M^{+}$), 225.2093; found, 225.2087 *m/z*.

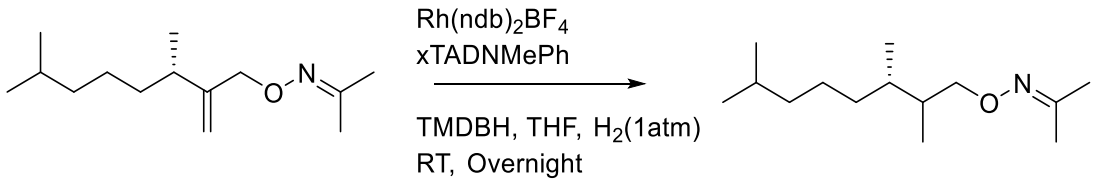


**Preparation of citronellal derived oxime ether reduced product.** To a 25 mL pear shaped flask was added Rh catalyst (0.0067 mmol of Rh and 0.0134 mmol of ligand) in THF (1.0 mL). Citronellal derived oxime ether substrate (150 mg, 0.67 mmol) was added to the catalyst mixture and the reaction mixture was stirred for 10 min. $H_2$ balloon was introduced. TMDBH (170 mg, 1.34 mmol) was added one portion and the reaction mixture was stirred overnight at room temperature. The reaction mixture was passed through a pad of silica gel and washed with EtOAc. Solvent was removed under reduced pressure. Flash chromatography (hexane:EtOAc = 90:10) afforded the product (142 mg, 93 %) as clear oil: $^1$H NMR (400 MHz, $CDCl_3$) δ4.03 – 3.93 (1H, m), 3.85 -3.79 (1H, m), 1.87 – 1.85 (6H, m), 1.58 – 1.48 (2H, m), 1.36 – 1.26 (3H, m), 1.17 – 1.13 (3H, m), 0.88 – 0.86 (9H, m), 0.81 -0.79 (3H, d, J = 6.64 Hz) ppm; 13C NMR (100 MHz, $CDCl_3$) δ 39.20, 36.11, 34.97, 33.59, 27.96, 25.21, 22.68, 22.63,21.86, 15.52,14.67, 11.60 ppm; HRMS (FAB) calcd. for $C_{14}H_{29}NO$ ($M^+$), 227.2249; found, 227.2239*m/z*.

Deuterated citronellal derived oxime ether synthesis

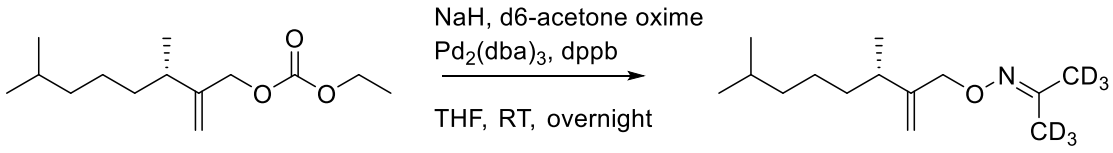


**Preparation of deuterated citronellal derived oxime ether.** To a 100 mL round-bottom flask was added d6- acetone oxime (1.73 g, 2.09 mmol) in THF (50 mL). To a separate 50 mL round-bottom flask was added NaH (0.52 g, 2.09 mmol) in THF (20mL). The flask containing acetone oxime was cooled to 0 $^o$C and NaH in THF was added via cannula needle and the mixture was stirred for 20 min at 0$^o$C. To another 100 mL round-bottom flask was added both $Pd_2(dba)_3$ (0.24g, 0.475 mmol) and dppb (0.50 g, 1.14mmol) in THF

(10mL) and the reaction mixture was stirred for 10 min at RT. Then the ester (4.80 g, 19.0 mmol) was added to the catalyst containing reaction mixture. The solution of acetone oxime was added slowly to this catalyst reaction mixture. The mixture was stirred at room temperature for overnight. The reaction was quenched with sat. NH4C solution. The solvent was extracted with EtOAc. The combined organic layers dried ($MgSO_4$) and concentrated. Flash chromatography (hexane:EtOAc = 90:10) afforded the product (5.50 g, 76 %) as clear light yellow oil: $^1$H NMR (400 MHz, $CDCl_3$) δ5.01 (1H, d, J = 1.4 Hz), 4.90 (1H, d, J = 1.4 Hz), 4.51 (2H, s), 2.20 (1H, m), 1.53 – 1.44 (2H, m), 1.27 - 1.26 (3H, m), 1.14 – 1.13 (2H, m), 1.07 – 1.05 (3H, d, J = 6.9 Hz), 0.87 – 0.85 (6H, m) ppm ; 13C NMR (100 MHz, $CDCl_3$) δ 150.99, 110.19, 75.24,39.23, 37.38, 35.99,28.04,25.24, 22.75, 20.08 ppm; HRMS (FAB) calcd. for $C_{14}H_{21}D_6NO$ ($M^+$), 231.2469; found, 231.2467 *m/z*.

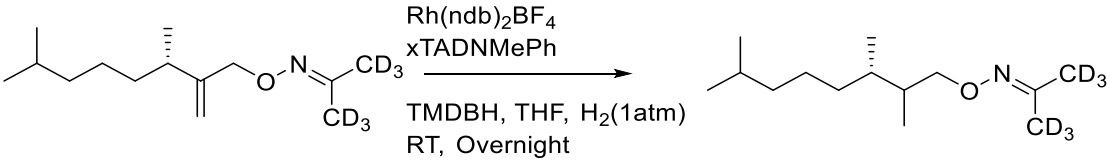


**Preparation of citronellal derived oxime ether reduced product.** To a 25 mL pear shaped flask was added Rh catalyst (0.0067 mmol of Rh and 0.0134 mmol of ligand) in THF (1.0 mL). Citronellal derived deuterated oxime ether substrate (150 mg, 0.67 mmol) was added to the catalyst mixture and the reaction mixture was stirred for 10 min. $H_2$ balloon was introduced. TMDBH (170 mg, 1.34 mmol) was added one portion and the reaction mixture was stirred overnight at room temperature. The reaction mixture was passed through a pad of silica gel and washed with EtOAc. Solvent was removed under reduced pressure. Flash chromatography (hexane:EtOAc = 90:10) afforded the product (142 mg, 93 %) as clear oil: $^1$H NMR (400 MHz, $CDCl_3$) δ4.03 – 3.93 (1H, m), 3.85 -3.79 (1H, m), 1.58 – 1.48 (2H, m), 1.36 – 1.26 (3H, m), 1.17 – 1.13 (3H, m), 0.88 – 0.86 (9H, m), 0.81 -0.79 (3H, d, J = 6.64 Hz) ppm ; 13C NMR (100 MHz, $CDCl_3$) δ 150.99, 110.19, 75.24,39.23, 37.38, 35.99,28.04,25.24, 22.75, 20.08 ppm; HRMS (FAB) calcd. for $C_{14}H_{29}NO$ ($M^+$), 233.2626; found,233.2614 *m/z*.

TMDBD was previously prepared by Dr. Nathan C. Thacker and the procedure is in the PhD thesis.

**4.7 References:**


1. C. M. Crudden, Y. B. Hleba, A. C. Chen, “Regio- and enantiocontrol in the room-temperature hydroboration of vinyl arenes with pinacol borane”. *J. Am. Chem. Soc*. **2004**, 126, 9200
2. PhD thesis of Y. B. Hleba, “Transition Metal Catalyzed Hydroborations with Pinacolborane: New Applications and Mechanistic Investigations”, Queen’s University, **2007**
3. S. A. Westcott, T. B. Marder, R. T. Baker, J. C. Calabrese, “Reactions of catecholborane with iridium complexes: molecular structure of trans-$IrHCl(CO)(Bcat)(PPh_3)_2$”. *Can. J. Chem*. **1993**, 71, 930
4. D. A. Evans, G. C. Fu, A. H. Hoveyda, “Rhodium(I)- and iridium(I)-catalyzed hydroboration reactions: scope and syntheticapplications”. *J. Am. Chem. Soc*. **1992**, 114, 6671
5. N. C. Thacker, V. M. Shoba, A. E. Geis, J. M. Takacs, “Surprisingly facile C-H activation in the course of oxime-directed catalytic asymmetric hydroboration”. *Tetrahedron. Letters*. **2015**, 56, 3306
6. G. L. Hoang, Z. D. Yang, S. M. Smith, R. Pal, J. L. Miska, D. E. Perez, L. S. W. Pelter, X. C. Zeng, J. M. Takacs, “Enantioselective Desymmetrization via Carbonyl-Directed Catalytic Asymmetric Hydroboration and Suzuki-Miyaura Cross-Coupling”, Org. Lett, 2015, 17, 940
7. N. C. Thacker, S. A. Moteki, J. M. Takacs, “Ligand Scaffold Optimization of a Supramolecular Hydrogenation Catalyst: Analyzing the Influence of Key Stractural Subunits on Reactivity and Selectivity”. *ACS Catal*. **2012**, 2, 2743
8. D. G. Blackmond, “Reaction Progress Kinetic Analysis: A Powerful Methodology for Mechanistic Studies of Complex Catalytic Reactions”, *Angew, Chem. Int. Ed*, **2005**, 44, 4302
9. D. A. Evans, G. C. Fu, A. H. Hoveyda, “Rhodium(I)-Catalyzed Hydroboration of Olefins. The Documentation of Regio- and Stereochemical Control in Cyclic and Acyclic Systems," *J. Am. Chem. Soc*. **1988**, 110, 6917

10. Z. Yang, R. Pal, G. L. Hoand, X. C. Zeng, J. M. Takacs, “Mechanistic Insights into Carbonyl-Directed Rhodium-Catalyzed Hydroboration: b Initio Study of a Cyclic γ, δ-unsaturated Amide”. *ACS Catal*. **2014**. 4, 763
11. M.Arrowsmith, M. S. Hill, T. Hadington, G. K. Kohn, C. Weetman, “Magnesium-Catalyzed Hydroboration of Pyridines”. *Organometallics*, **2011**, 30, 5556
12. A. Anaby, B. Butschke, Y. David, L. J. W. Shimon, G. Leitus, M. Feller, D. Milstein, “B–H Bond Cleavage via Metal–Ligand Cooperation by Dearomatized Ruthenium Pincer Complexes”. *Organometallics*, **2014**, 33, 3716
13. R. Waterman, “σ-Bond Metathesis: A 30-Year Retrospective”. *Organometallics*. **2013**, 32, 7249
14. X. Wan, X. Wang, Y. Luo, S. Takami, M. Kubo, A. Miyamoto, “Theoretical Investigation on Functionalization of Alkanes by a Rhodium Complex Catalyst”. *Organometallics*, **2002**, 21, 3703
15. S. Miu, M. B. Hall, “Inter- and Intramolecular C−H Activation by a Cationic Iridium(III) Center via Oxidative-Addition Reductive-Elimination and σ-Bond Metathesis Pathways”. *J. Am. Chem. Soc*. **1998**, 120, 6169
16. H. Zhao, L. Dang, T. B. Marder, Z. Lin, “DFT studies on the mechanism of the diboration of aldehydes catalyzed by copper(I) boryl complexes”. *J. Am. Chem. Soc*. **2008**, 130, 5586
17. J. Campos, S. Kundu, D. R. Pahls, M. Brookhart, E. Carmona, T. R. Cundari, “Mechanism of Hydrogenolysis of an Iridium–Methyl Bond: Evidence for a Methane Complex Intermediate”. *J. Am. Chem. Soc.* **2013**, 135, 1217
18. M. V. Campian, E. Clot, O. Eisenstein, U. Helmstedt, N. Jasim, R. N. Perutz, A. C. Whitewoo, D. Williamson, “Stereochemical Nonrigidity of a Chiral Rhodium Boryl Hydride Complex: A σ-Borane Complex as Transition State for Isomerization”. *J. Am. Chem. Soc*, **2008**, 130, 4375
19. C. E. Webster, Y. Fan, M. B. Hall, D. Kunz, J. F. Hartwig, “Experimental and Computational Evidence for a Boron-Assisted, σ-Bond Metathesis Pathway for Alkane Borylation”. *J. Am. Chem. Soc*. **2003**, 125, 858

20. B. Goldfuss, P. Knochel, L. O. Bromm, K. Knapp, "C-H Activation by Direct Borane-Hydrocarbon Dehydrogenation: Kinetic and Thermodynamic Aspects". *Angew. Chem. Int. Ed*. **2000**, 39, 4136
21. Y. Li, G. He, E. B. Kantchev, "Mechanistic Study on Rh-Catalyzed Stereoselective C—C/C—H Activation of *tert*-Cyclobutanols". *Phys. Chem. Chem. Phys*. **2014**, 16, 24250
22. M. Armelin, M. Schlangen, H. Schewarz, "On the Mechanisms of Degenerate Ligand Exchange in $[M(CH_3)]^+/CH_4$ Couples (M=Fe, Co, Ni, Ru, Rh, Pd, Os, Ir, Pt) as Explored by Mass Spectrometric and Computational Studies: Oxidative Addition/Reductive Elimination versus σ-Complex-Assisted Metathesis". *Chem. Eur. J*. **2008**, 14, 5229
23. R. N. Pernutz, S. S. Etienne, "Multiplication of Human Natural Killer Cells by Nanosized Phosphonate-Capped Dendrimers". *Angew. Chem. Int. Ed*. **2007**, 46, 2575
24. C. C. Chong, H. Hirao, R. Kinjo, "A Concerted Transfer Hydrogenolysis: 1,3,2-Diazaphospholene-Catalyzed Hydrogenation of N=N Bond with Ammonia-Borane", *Angew. Chem. Int. Ed*. **2014**, 53, 3342
25. J. Y. –C. Chen, A. A. Marti, N. J. Turro, K. Komatsu, Y. Murata, R. G. Lawler, "Comparative NMR Properties of $H_2$ and HD in Toluene-$d_8$ and in $H_2$/HD@$C_{60}$". *J. Phys. Chem. B*. **2010**, 114, 14689
26. D. D. G. Williams, M. Lawton, "Drying of Organic Solvents: Quantitative Evaluation of the Efficiency of Several Desiccants". *J. Org. Chem*. **2010**, 75, 8351
27. Calculation of THF moisture: The amount of THF used for each reaction was 1.0 mL. 50 ppm water of 1.0 mL is 0.05 mg, which is 0.00278 mmol. Each reaction used 0.06655 mmol of the oxime ether substrate. The water content relative to the substrate is 4.0%.
28. M. A. Salomon, T. Brawn, "Stepwise oxygenation of pinacolborane by a rhodiumperoxo complex: detection of an intermediate metal borate and perborate", *Angew. Chem. Int. Ed*. **2008**, 47, 8867

29. H. Braunschweig, F. Guethlein, “Transition-Metal-Catalyzed Synthesis of Diboranes(4)”. *Angew. Chem. Int. Ed*. **2011**, 50, 12613
30. H. F. Bettinger, M. Filthaus, H. Bormemann, I. M. Oppel. “Metal-free conversion of methane and cycloalkanes to amines and amides by employing a borylnitrene”. *Angew. Che. Int. Ed*. **2008**, 47, 4744
31. S. Hawkeswood, D. W. Stephan. “Syntheses and reactions of the bis-boryloxide $O(Bpin)_2$ (pin = $O_2C_2Me_4$)”. *Dalton Trans*. **2005**, 2182
32. S. M. Marcuccio, C. M. Moorhoff, *PCT Int. Appl*. 2004076467, 10 sep **2004**
33. Q. Liu, *Faming Zhuanli Shenquing*, 102718787, 10 oct **2012**
34. Y. Xu, C. A. Rettenmeier, G. T. Plundrich, H. Wadepohl, M. Enders, L. H. Gade, “Borane-Bridged Ruthenium Complex Bearing a PNP Ligand: Synthesis and Structural Characterization”. *Organometallics*, **2015**, 34, 5113
35. G. C. Welch, J. D. Masuda, D. W. Stephan, “Phosphonium−Borate Zwitterions, Anionic Phosphines, and Dianionic Phosphonium−Dialkoxides via Tetrahydrofuran Ring-Opening Reactions”. *Inorg. Chem*. **2006**, 45, 478
36. G. C. Welch, D. W. Stephan, “Facile Heterolytic Cleavage of Dihydrogen by Phosphines and Boranes”. *J. Am. Chem. Soc*. **2007**, 129, 1880
37. D. J. Parks, W. E. Piers, “Tris(pentafluorophenyl)boron-Catalyzed Hydrosilation of Aromatic Aldehydes, Ketones, and Esters”. *J. Am. Chem. Soc*. **1996**, 118, 9440
38. D. W. Stephan, “Frustrated Lewis pairs”: a concept for new reactivity and catalysis. *Org. Biomol. Chem*. **2008**, 6, 1535
39. D. W. Stephan, “Frustrated Lewis Pairs: From Concept to Catalysis”. *Acc. Chem. Res*. **2015**, 48, 306
40. C. M. Crudden, D. Edwards, “Catalytic asymmetric hydroboration. Recent advances and applications in carbon-carbon bond-forming reactions”. *Eur. J. Org. Chem*. **2003**, 4695
41. R. Noyori, “Asymmetric catalysis: science and opportunities”. *Angew. Chem. Int. Ed*. **2002**, 41, 2008

42. M. Mendez, A Cedillo, “Stability and Bonding in the Borane-$H_2$ Complexes”. *International Journal of Quantum Chemistry*. **2012**, 112, 3564
43. M. Arrowsmith, M. S. Hill, G. K. Kohn, “Magnesium Catalysis of Imine Hydroboration”, *Chem. Eur. J*. **2013**, 19, 1041
44. In order to confirm that $(TMDB)_2$ is not formed due to the GC injection port, prepared TMDBOH and $(TMDB)_2$ are injected separately and the masses observed were: 144.81 (TMDBOH) and 255.13 $(TMDB)_2$ and the calculated masses are 144.0958 (TMDBOH) and 254.1861 $(TMDB)_2$
45. E. Brunner, “Solubility of Hydrogen in 10 Organic Solvents at 298.15, 323.15, and 373.15 K”, *J. Chem. Eng. Data*, **1985**, 30, 269. Mole fraction solubility of $H_2$ in THF at room temperature (25$^o$C) was reported as 0.00027. Assuming that total mole is 1.0 mol, THF mole fraction is 1.0 – 0.00027 = 0.99973. Weight of $H_2$ = 0.00027 x 2 = 0.00054 g. Weight THF = 0.99973 x 72 = 71.98 g. The volume of THF = 71.98 g/ (0.89 g/mL) = 0.08087764 L. Therefore, the molarity of $H_2$ in THF is calculated as follow: 0.00027mol/0.08087764L = 0.0033M.

# CHAPTER 5. DISCUSSION OF DEVELOPMENT OF NEW SAL CATALYSTS

## 5.1 Introduction

Hayashi and Kumada introduced ferrocene based *P, N*-ligands for asymmetric reactions in 1982[1], and an increasing number of reports now routinely describe the utility of chiral *P*, *N*-ligands. *P*, *N*-ligands have properties that can complement those of *P, P*- ligands and have been effectively expanded substrate scopes in many asymmetric reactions due to their unique nature [4-6]. For example, *P*, *N*-ligands are widely used in in asymmetric allylic substitution reactions, a reaction in which the nature of π-allylpalladium transition state is often highly symmetric. The unsymmetric nature of *P*, *N*-ligands is thought to help differentiate the termini of the allylic systems, improving regio- and enantioselectivity over traditional *P*, *P*-ligands[2]. The highly efficient regioselectivity comes from trans effect of *P*, *N*-ligands where atoms complexed trans to phosphorus atom become more electrophilic than the one trans to nitrogen atom of a ligand[3]. Iridium-catalyzed reactions, especially C-H activation, are another area in which *P*, *N*-ligands have attracted much interest in recent years; the reaction scope has expanded rapidly[7] including applications to C-H borylation[8].

The unique properties of the *P, N*-ligands led us to wonder if their incorporation within the Takacs SAL-derived supramolecular catalysts might hold significant advantages in terms of reactivity or selectivity. There had been attempts to develop such a ligand system in Takacs group in the past, but the progress has ceased before the project could investigate the full potential as an effective ligand system. This chapter

reports on the successful development of a supramolecular SAL based upon a *P*,*N*-ligand and some encouraging preliminary results on catalytic asymmetric hydroboration of 1, 1, disubstituted alkenes, a challenging class of substrates.

**5.2 New SAL development – Supramolecular SAL *P, N*-ligand synthesis**

The Takacs group has successfully used phosphite and phosphoramidite ligands in catalytic asymmetric hydroboration.[9-12] However, to date the reported SAL-derived supramolecular catalysts have used mostly phosphite ligands[13-15]. Access to supramolecular catalysts with phosphoramidite ligating groups would most likely expand the substrate and reaction scopes with the possibility for achieving high enantioselectivity. Therefore, I first considered adapting the existing synthetic route shown in Figure 1 for the possibility to include phosphoramidite ligands. The bisoxazoline unit, tethers, and ligating groups are separately prepared and assembled by first attaching bisoxazoline unit to tethers by alkylation and then phosphorylating phenols to attach the ligating groups.

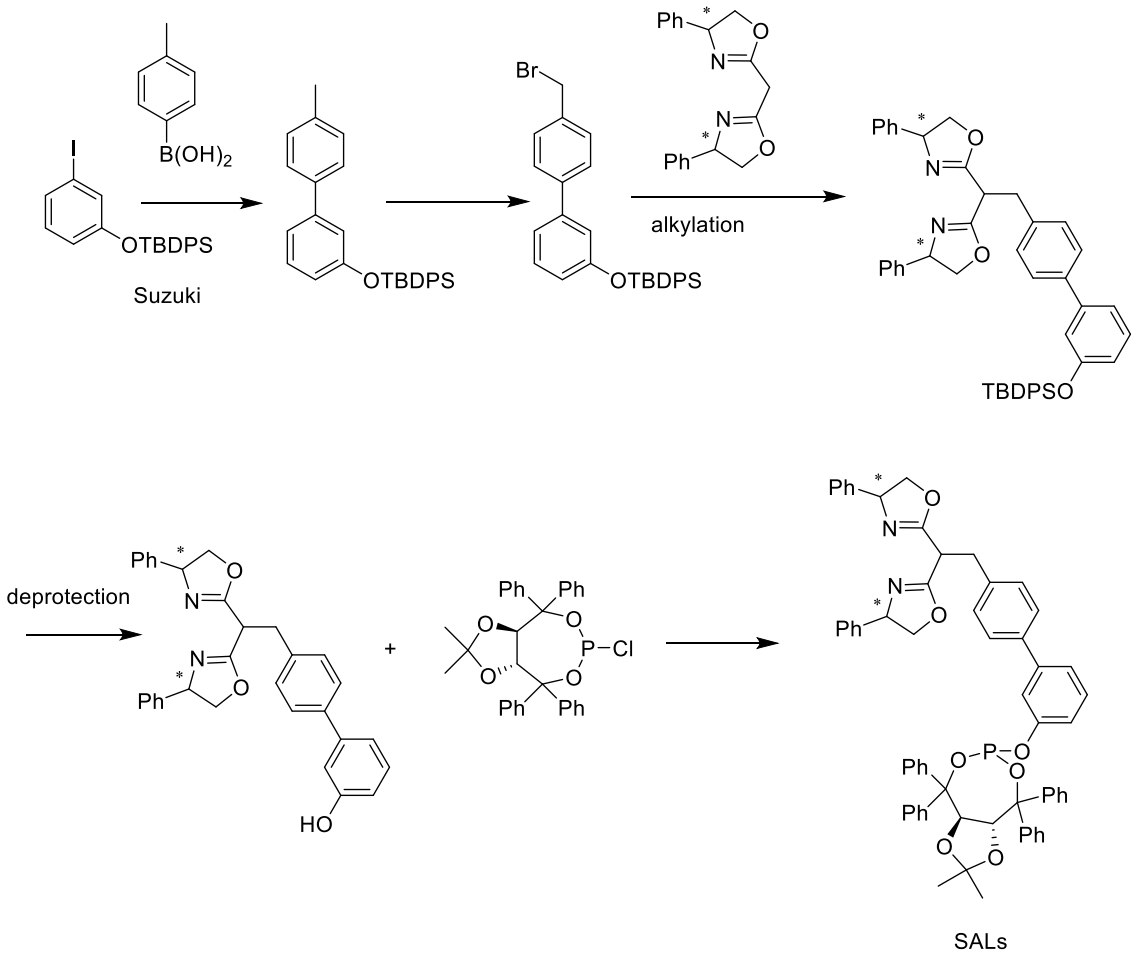


**Figure 1.** Typical supramolecular SAL synthesis scheme.

Preparation of phosphoramidite ligands **503** would require synthesis and phosphorylation of tethers that incorporate the amine substituent **501** (Figure 2). However, two issues arose. One, the synthesis of nitrogen containing SAL tether **501** proved to be problematic; the overall yield was very low. Secondly, the polarity of the resulting phosphoramidite **503** made purification almost impossible. One potential solution to the purification problem would be to use reversed phase silica gel, but the cost of this media discouraged such an effort. I considered a potential synthetic route

that would install the phosphoramidite moiety at an earlier stage. However, this introduces the likelihood of oxidizing phosphoramidite ligand during the course of the synthesis with poor prospects for recovery. For such reasons, the preparation of SALs bearing desirable phosphoramidite ligating groups has not been a trivial task.

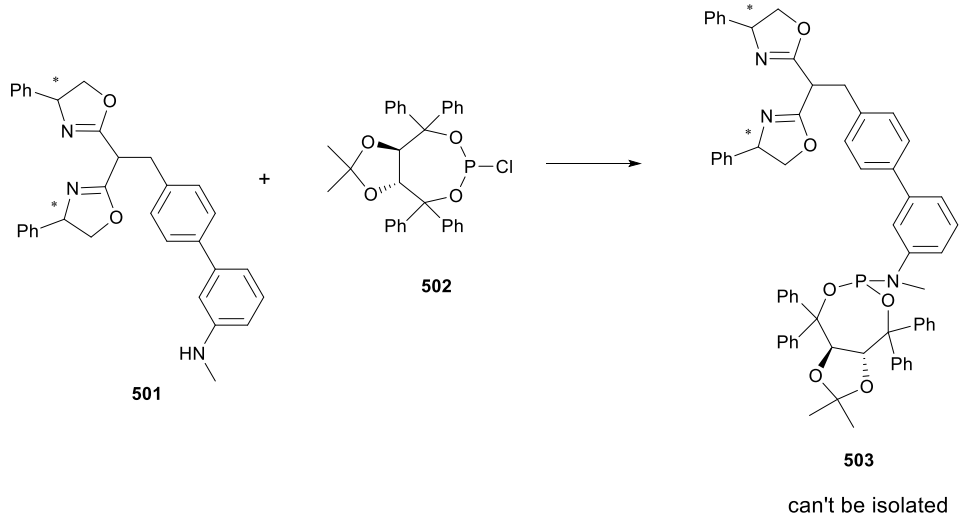


**Figure 2.** Challenge of preparing SAL phosphoramidite ligands SAL phosphoramidite ligands were not able to be isolated.

It seemed that the next logical thing to consider was the possibility to include stable nitrogen containing ligands. Some potential chiral nitrogen containing ligands would require multistep synthesis, so for the purpose of exploring new synthetic routes some simple pyridine derivatives were first examined. Several routes were explored to attach the pyridine moiety to an SAL tether-building subunit. First, the most obvious route is to attach pyridine group at the end of the synthesis, analogous to phosphite SAL synthesis. However, the presence of bisoxazoline unit in the substrate **508** inhibited

reactivity of coupling reaction between pyridine moiety and tether due to the fact that bisoxazoline unit is known to chelate metals strongly so that it prevents other ligands to chelate the metal, which destroys efficient coupling reaction (Figure 3). This reaction did not proceed even when zinc metal was used to form complex with bisoxazoline moieties where bisoxazoline is now unable to chelate metal that is used to catalyze the reaction.

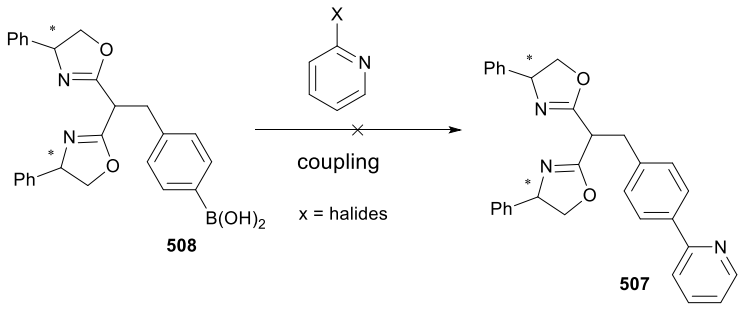


**Figure 3.** Installation of N containing group to SAL at the last stage did not proceed.

Thus the second approach was to prepare a pyridyl derivative and convert it via alkylation of the bisoxazoline. Accordingly, the substituted pyridine derivative **504** was prepared via Stille coupling as shown in Figure 4. Other coupling procedures, including Suzuki, Negishi, and Kumada couplings, were not satisfactory. Unfortunately, conditions were not found to convert **505** to the benzylic bromide **506** under the bromination condition including NBS, $CBr_4$, or $Br_2$. A new synthetic approach was required.

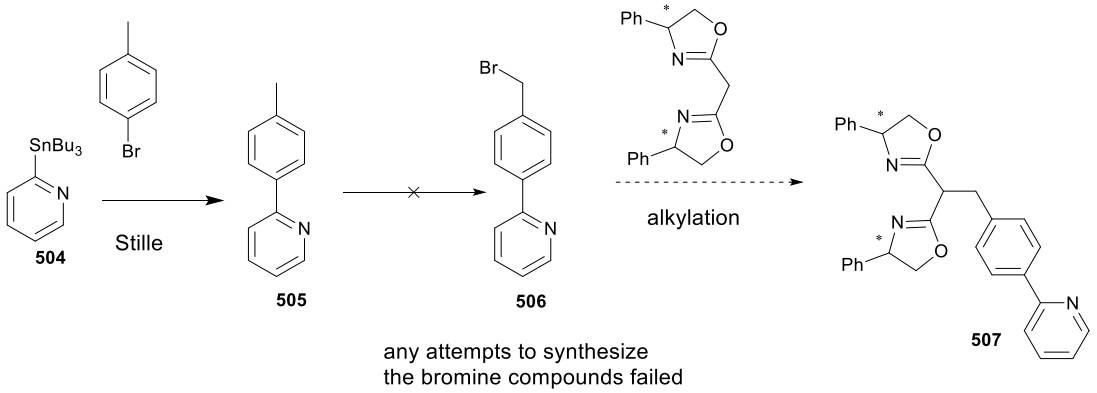


**Figure 4.** Pyridine moiety decreases reactivity toward many synthetic routes that were used to give high yield for preparing SAL. Presence of pyridine moiety negatively impacts synthetic approaches to SAL.

A significant amount of time and effort was therefore directed to come up with a totally new synthetic scheme for SAL synthesis. (Figure 5). The synthesis starts with a halogenated pyridine derivative; iodo compound **509** was usually chosen because of higher reactivity. There are several procedures for preparing tin compound **510** via transmetallation; most involves with treating the iodo compound with *n*-BuLi and then quenching with tri-*n*-butyltin chloride.[16] However, the yield obtained was lower than anticipated and the need for higher yielding condition lead to exploring an alternative procedure to convert the iodo pyridine to the corresponding tin compound **510** via the zinc intermediate[17] using $COCl_2$ and allyl bromide to activate the zinc. Tin compound **510** was then coupled with the cheap, commercially-available 3-bromobenzaldehyde (**511**) via Stille coupling to afford the biaryl product **512** in good yield of 72%. It is worth pointing out again that other coupling conditions (Suzuki, Negishi, and Kumada) did not lead to practically useful yields.

3-Bromobenzaldehyde route was chosen for two reasons. First, this substrate undergoes Stille coupling in good yield. Secondly, Knoevenagel condensation with dicyanomethane installs a bisnitrile group which provided a useful precursor of the required bisoxazoline unit. It can be noted that 3-iodobenzaldehyde could also be used and gave somewhat higher yield in the Stille coupling. However, 3-bromobenzaldehyde **511** is much cheaper so I decided to stick with the bromo compound. The conversion of aldehyde **512** to bisnitrile compound **513** via Knoevenagel condensation worked satisfactorily (82% yield). The next step required a reagent strong enough to reduce alkene but selective enough not to reduce nitrile groups. The reagent selected was ammonium borane[18] and showed very good yield compared to alternatives such as hydrogenation under $H_2$ or transfer hydrogenation and afforded compound **514** (78%). Surprisingly, converting the dinitrile to the bisoxazoline proved to be the easiest step; it required the least amount of time to optimize the reaction conditions.[19] This resulting homoleptic $(box)_2Zn$ complex **515** which was stable and could be readily purified by silica gel chromatography.

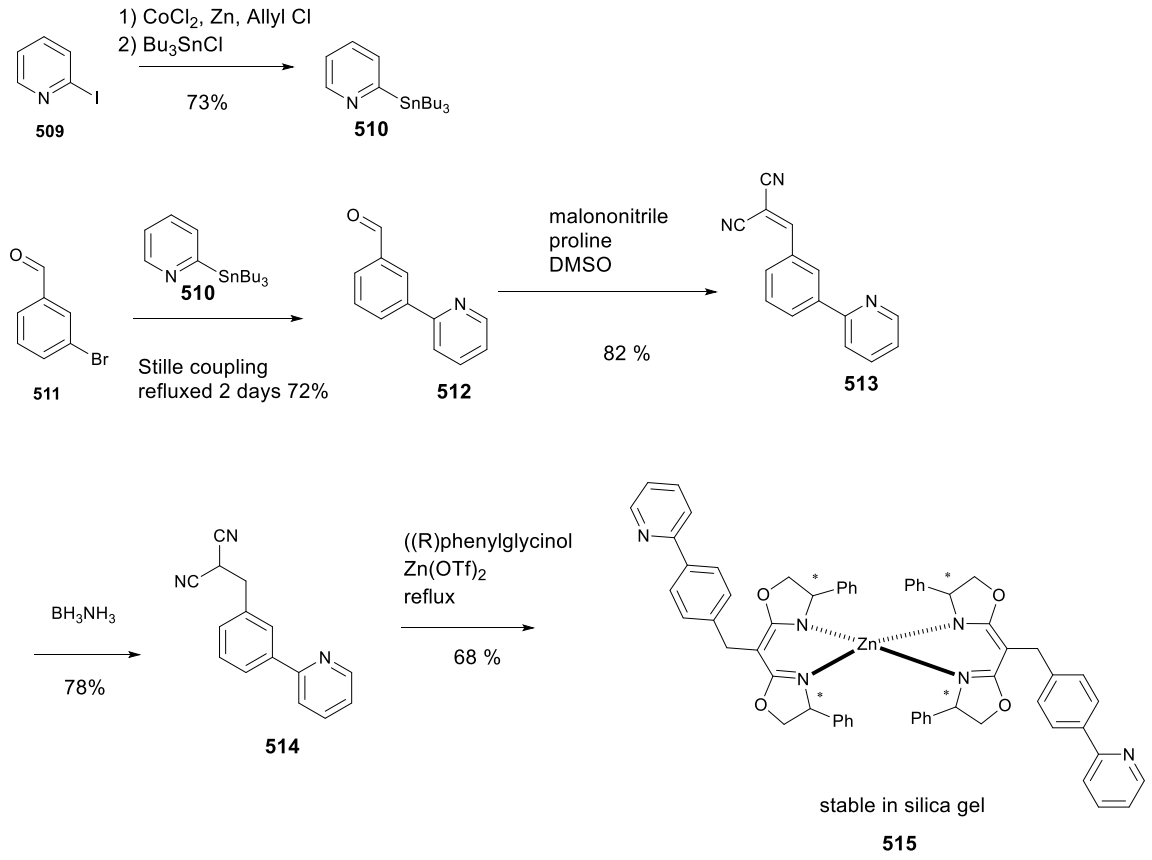


**Figure 5.** Complete synthetic route for pyridine containing SALs.

Several pyridine SAL derivatives shown in Figure 6 were prepared according to the synthetic pathway shown above. The 4-(dimethylamino)pyridyl derivative (i.e., SAL **A**) was prepared to explore the effect of a more electron rich ligand and was also briefly used by Dr. Nathan Thacker to explore potential supramolecular acylation catalysts. SAL **B**, **C**, and **D** differ in the position of the nitrogen atom in the pyridine ring. Since these nitrogen containing SALs are achiral, TADDOL based phosphite containing SALs were combined with SAL **A**, **B**, **C**, or **D** to prepare a series of chiral SAL-derived supramolecular catalysts which I briefly examined for rhodium-catalyzed hydroboration.

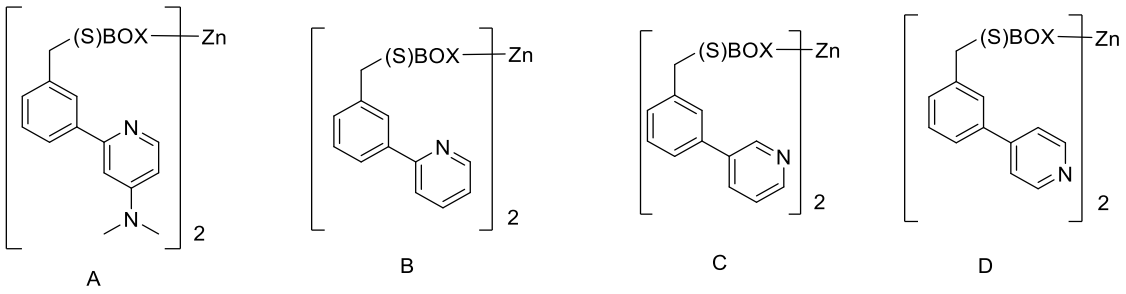


**Figure 6.** A variety of pyridine moiety containing SALs were synthesized.

**5.3 New SAL development – Screening with 1, 1-disubstituted alkenes**

A number of highly efficient asymmetric catalysts have been developed for hydroboration but only a few have been effective for the hydroboration of 1, 1-disubstituted alkenes (i.e., methylidenes) such as α-methyl styrene or limonene. [20]. Methylidenes have proven to be difficult to substrates for asymmetric hydroboration. Two successful approaches have been published. Soderquist developed reagents for stoichiometric hydroboration based upon 9 BBD and showed their effectiveness on certain 1, 1-disubstituted alkenes. The results showed that the highest enantioselectivity obtained for α-methyl styrene is 78% ee and for limonene is 76% de; the latter results is the highest level of diastereoselectivity reported in the literature for limonene substrate[20]. Meanwhile, Hoveyda group published the work on utilization of copper catalysts based upon N-heterocyclic carbene (NHC)- for asymmetric hydroboration of α-methyl styrene derivatives. In that communication, they obtained the highest enantioselectivity reported up to date for α-methyl styrene (86% ee)[21].

The, new pyridine-containing SAL system described the above was briefly investigated as a ligand for metal-catalyzed asymmetric hydroboration. Preparation of catalyst precursor incorporating SALs **A**-**D** starts with making both homoleptic zinc complexes of nitrogen containing SALs and TADDOL based SALs. An equimolar amount of each complex is combined in solution. The mixture rapidly equilibrates to form the heteroleptic zinc complex, the structure of which was confirmed by NMR, high resolution MS, and GPC. The introduction of rhodium (I) completes the preparation of self-assembled supramolecular catalysts. Preliminary screening results were obtained

with 3 SAL-derived catalysts that were available at the time. The reaction conditions were optimized in terms of metal precursors, boranes, and solvents.

As mentioned above, the highest level of diastereoselectivity obtained for the hydroboration of limonene reported to date is 76% de using a stoichiometric reagent. It is my pleasure to report that a new SAL-derived supramolecular catalyst incorporating *P*, *N*-ligating groups gives 89% de in a catalytic asymmetric hydroboration (Figure 7, entry 2). Even higher selectivity (94% ee) can be obtained by lowering the reaction temperature to – 20 $^{o}$C. In comparison, a ligating group without SAL backbone scaffolds ((TADDOL)POPh) gave 73% d.e. under the same conditions (Figure 7, entry 1). The increase from 73% de with monodentate ligands to 89% de with the supramolecular catalysts is an indication that the combination of SAL backbone scaffold and pyridine moiety enhances the diastereoselectivity of the catalyst.

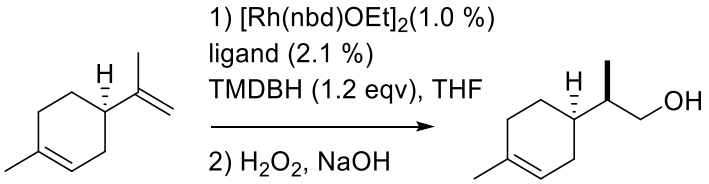


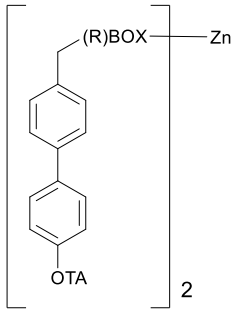


SAL (R15TA)

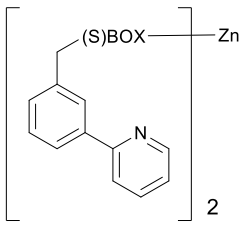


B

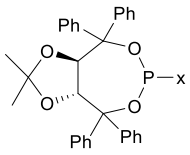


(TADDOL)POPh (x=OPh)

TA (x=SAL)

| entry | ligand | Temperature | Yield (%) | % de |
|---|---|---|---|---|
| 1 | (TADDOL)POPh | RT | 80 | 73 |
| 2 | SAL (R15TA) + B | RT | 99 | 89 |
| 3 | SAL (R15TA) + B | -20 | 99 | 94 |

**Figure 7.** Catalytic asymmetric hydroboration of (*S*)-limonene.

As for α-methyl styrene, it proved more challenging to induce high enantioselectivity. In this case, SAL **A** when combined with SAL (R15TA) was found to give the most effective catalyst. The highest enantioselectivity obtained from the small preliminary screening was 67% ee (Figure 8, entry 2) at room temperature and 78% ee at – 20 $^{o}$C. While this is unfortunately not as high as the enantioselectivity reported by Hoveyda (86% ee), the supramolecular catalyst again gave improved results when compared to monodentate ligand (TADDOL)POPh.

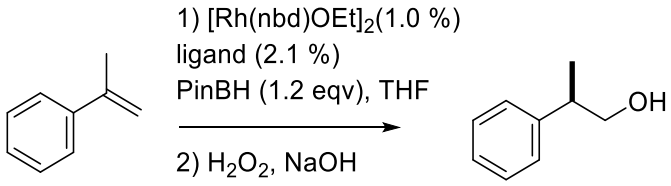

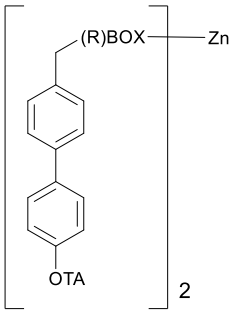


SAL (R15TA)

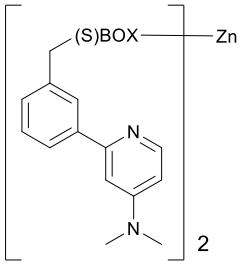


A

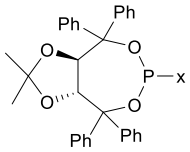


(TADDOL)POPh (x=OPh)

TA (x=SAL)

| entry | ligand | Temperature | Yield (%) | % ee |
|---|---|---|---|---|
| 1 | (TADDOL)POPh | RT | 96 | 45 |
| 2 | SAL (R15TA) + A | RT | 99 | 67 |
| 3 | SAL (R15TA) + A | -20 | 99 | 78 |

**Figure 8.** Catalytic asymmetric hydroboration of α-methyl styrene.

**5.4 New SAL development – Conclusions**

This chapter describes the preparation of several new pyridine based SAL synthesis which required the development of a completely new synthetic route in order to generate the pyridine-containing ligands. The new ligands proved effective in preparing chiral SAL-derived supramolecular *P*, *N*- catalysts for CAHB of the challenging 1, 1, disubstituted alkenes. A small preliminary screen found a catalyst that promotes the efficient hydroboration of limonene with up to 94% de, exceeding the highest de reported in the literature. A more challenging substrate, α-methyl styrene, gave up to 78% ee, approaching the highest level of enantioselectivity in the literature to date (86% ee). In both cases, the supramolecular scaffold increases the level of stereoselectivity by approximately 20% compared to comparable ligands lacking the scaffold. It should be noted that only handful of catalysts and two representative 1, 1-disubstituted alkenes were used for this survey. The possibility of identifying even more effective through a more extensive optimization of the catalyst scaffold is very plausible. It is hoped that the synthetic route developed will facilitate further development of chiral SAL-derived supramolecular *P*, *N*- catalysts for new reactions and broad substrate scope.

**5.5 Experimental:**

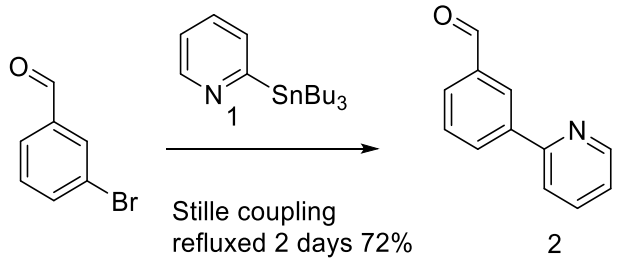


Stille coupling was performed to afford the coupled N containing aldehyde. To a 25 mL round bottom flask, tris(dibenzylideneacetone)dipalladium (5 mol %) and triphenyl phosphine (20 mol %) were dissolved in 5 mL of dry toluene. This mixture was stirred for 30 minutes. To a 50 mL round bottom flask, 3-bromobenzaldehyde (1 equivalent) and tin compound 1 (1 equivalent) were weighted out and dry toluene was introduced into the flask, which was stirred for 10 minutes. Via a dry cannula needle the catalyst solution was transferred into the flask containing substrates. The resulting reaction mixture was refluxed for 2 days. The solution was cooled down and the solvent was removed. The coupled product 2 was purified by flash chromatography on silica (40:60 ethyl acetate: hexane) to give 2 (72 %) as clear oil: $^{1}$H NMR (400 MHz, $CDCl_3$) δ 10.13 (1H, s), 8.8-8.7 (1H, s), 8.6-8.5 (1H, s), 8.2-8.3 (1H, s), 8.0-7.9 (2H, s), 7.8 (1H, s), 7.7-7.6 (1H, s), 7.3-7.2 (1H, s) ppm; 13C NMR (100 MHz, $CDCl_3$) δ 192.4, 156.1, 150.0, 140.4, 137.2, 137.0, 132.9, 129.9, 129.6, 128.6, 122.9, 120.8 ppm; HRMS (FAB, 3-NBA matrix) calcd. for $C_{12}H_9NO$ ($M^+$), 183.0684; found, 183.0247*m/z*.

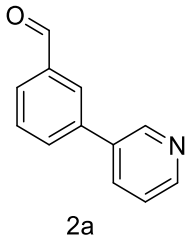


2a

A coupled product 2a was synthesized using the same aldehyde and meta-substituted tributyltinpyridine. $^{1}$H NMR (400 MHz, $CDCl_3$) δ 10.2 (1H, s), 8.8-8.7 (1H, s), 8.6-8.5 (1H, s), 8.2-8.3 (1H, s), 8.0-7.9 (2H, s), 7.8 (1H, s), 7.7-7.6 (1H, s), 7.3-7.2 (1H, s) ppm; 13C NMR (100 MHz, $CDCl_3$) δ 192.3, 156.0, 150.1, 140.4, 137.2, 137.1, 132.8, 129.9, 129.7,

128.6, 122.9, 120.8 ppm; HRMS (FAB, 3-NBA matrix) calcd. for $C_{12}H_9NO$ ($M^+$), 183.0684; found, 183.0159*m/z*.

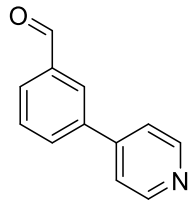


2b

A coupled product 2b was synthesized using the same aldehyde and para-substituted tributyltinpyridine. $^1$H NMR (400 MHz, $CDCl_3$) δ 10.2 (1H, s), 8.8-8.7 (2H, s), 8.2 (1H, s), 8.0-7.9 (2H, s), 7.7 (1H, m), 7.7-7.6 (2H, m), 7.6 (2H, s) ppm; 13C NMR (100 MHz, $CDCl_3$) δ 192.3, 156.1, 150.1, 140.4, 137.2, 137.0, 132.8, 129.8, 129.7, 128.6, 122.8, 120.8 ppm; HRMS (FAB, 3-NBA matrix) calcd. for $C_{12}H_9NO$ ($M^+$), 183.0684; found, 183.0318*m/z*.

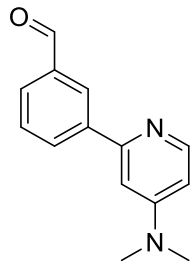


2c

A coupled product 2c was synthesized using the same aldehyde and N, N, dimethyl ortho-substituted tributyltinpyridine. $^1$H NMR (400 MHz, $CDCl_3$) δ 10.1-10.2 (1H, s), 8.4 (1H, s), 8.3 (1H, m), 8.2 (1H, m), 8.0-7.9 (1H, m), 7.6 (1H, m), 7.0 (1H, s), 6.7-6.6 (1H, m), 3.1 (6H, s) ppm; 13C NMR (100 MHz, $CDCl_3$) δ 192.8, 156.3, 150.0, 141.4, 137.2, 137.5, 133.9, 129.9, 129.6, 128.6, 127.9, 122.8, 112.4 ppm; HRMS (FAB, 3-NBA matrix) calcd. for $C_{14}H_{14}N_2O$ ($M^+$), 226.1106; found, 226.3158 *m/z*.

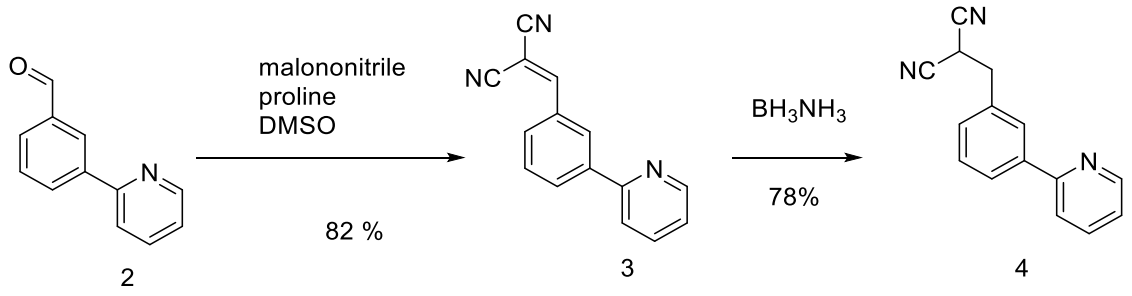


2 3 4

Knoevenagel condensation was used to install di nitrile group to afford a compound 3. The Stille coupled aldehyde s (1 equivalent) and malononitrile (1 equivalent) were placed into a round bottom flask. To this flask EtOH was added along with piperidine (5 drops) as a catalyst. The reaction was stirred overnight and the resulting mixture contained some particles. The solid was filtered off using vacuum filtration and rinsed with extra EtOH to get rid of yellow color. The yellow color contained in the solid is impurities and it was essential to remove the yellow impurities to obtain higher yields for the following step. The white solid 3 was dried overnight under vacuum and used it for the next step without purification. Borane ammonia (1 equivalent) and alkene 3 were placed in a flask in THF. The reaction was stirred overnight. The solvent was concentrated and flash chromatography afforded the title compound 4. $^1$H NMR (400 MHz, $CDCl_3$): δ 8.7 (1H, s), 8.0 (2H, m), 7.8-7.7 (2H, m), 7.5 (1H, m), 7.4 (1H, m), 7.3-7.2 (1H, m), 4.1 (1H, m), 3.3 (2H, m), 3.1 (6H, s) ppm; 13C NMR (100 MHz, $CDCl_3$) δ 157.0, 155.3, 150.0, 141.1, 133.0, 129.1, 127.6, 112.7, 105.6, 103.9, 36.5, 25.0 ppm; HRMS (FAB, 3-NBA matrix) calcd. for $C_{15}H_{11}N_3$ ($M^+$), 233.0953; found, 233.0811 *m/z*.

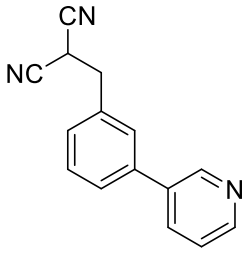


4a

The compound 4a was prepared the same way. $^1$H NMR (400 MHz, $CDCl_3$): δ 8.9 (1H, s), 8.6 (1H, s), 7.9 (1H, m), 7.7-7.4 (5H, m), 4.1 (1H, m), 3.4 (2H, m) ppm; 13C NMR (100

MHz, $CDCl_3$) δ 157.1, 155.2, 150.0, 141.0, 133.1, 129.4, 127.9, 112.4, 105.6, 103.9, 36.7, 25.1 ppm; HRMS (FAB, 3-NBA matrix) calcd. for $C_{15}H_{11}N_3$ ($M^+$), 233.0953; found, 233.0670 *m/z*.

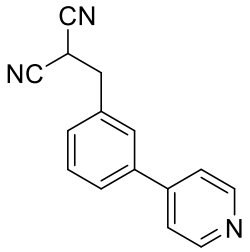


4b

The compound 4b was prepared the same way. $^1H$ NMR (400 MHz, $CDCl_3$): δ 8.9 (1H, s), 8.6 (1H, s), 7.9 (1H, m), 7.6 (2H, m), 7.5-7.4 (3H, m), 4.1 (1H, m), 3.4 (2H, m) ppm; 13C NMR (100 MHz, $CDCl_3$) δ 157.0, 155.2, 149.9, 141.1, 133.2, 129.4, 127.8, 112.4, 105.6, 103.7, 36.5, 25.1 ppm; HRMS (FAB, 3-NBA matrix) calcd. for $C_{15}H_{11}N_3$ ($M^+$), 233.0953; found, 233.0751 *m/z*.

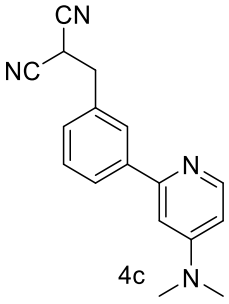


4c

The compound 4c was prepared the same way. $^1H$ NMR (400 MHz, $CDCl_3$): δ 8.4-8.3 (1H, s), 7.9 (2H, m), 7.5 (1H, m), 7.4-7.3 (1H, m), 6.9 (1H, s), 6.5 (1H, m), 4.0 (1H, s), 3.4 (2H, m), 3.2-3.1 (6H, s) ppm; 13C NMR (100 MHz, $CDCl_3$) δ 157.1, 155.2, 149.8, 141.3, 133.2, 129.5, 127.9, 112.4, 105.8, 103.8, 39.4,36.5, 25.0 ppm; HRMS (FAB, 3-NBA matrix) calcd. for $C_{17}H_6N_4$ ($M^+$), 276.1375; found, 276.2165 *m/z*.

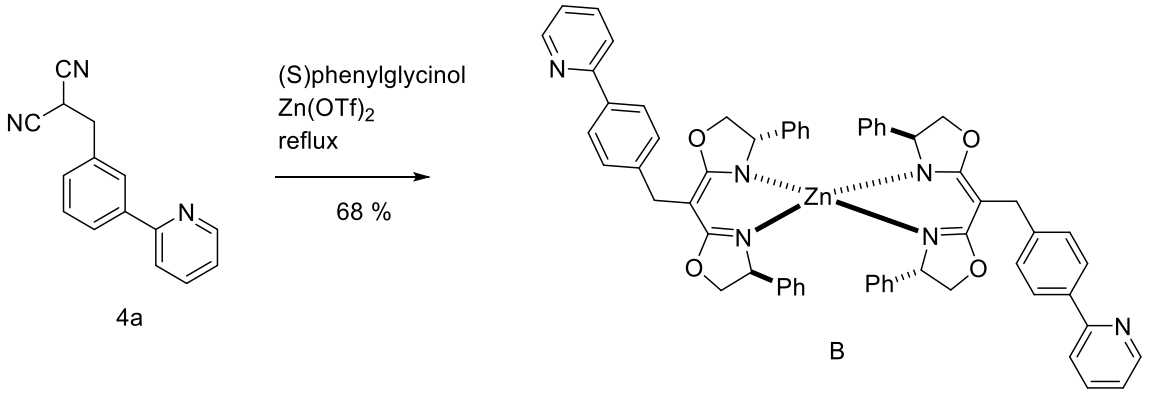


Dinitrile compound 4a (1 equivalent) was mixed with (S) phenylglycinol (2 equivalents) and zinc triflate (1 equilavent) in chlorobenzene, which was refluxed overnight. The solvent is concentrated via rotovap and flash chromatography was done to afford the hemolytic title compound B. $^1$H NMR (400 MHz, $CDCl_3$): δ 8.9 (1H, s), 8.6 (1H, s), 7.9 (1H, m), 7.6-7.2 (13H, m), 7.0 (2H, s), 5.2 (2H, s), 4.7 (2H, m), 4.3-4.0 (3H, m), 3.5 (2H, m) ppm; 13C NMR (100 MHz, $CDCl_3$) δ 165.7, 165.6, 157.3,149.7, 149.5, 142.1, 141.9, 139.7, 138.6, 137.1, 136.9, 129.9, 129.0, 128.8, 128.7, 128.6, 127.8, 127.7,127.6,127.1, 126.9, 126.8, 126.7, 126.3, 125.5, 122.3, 122.2, 121.1, 120.7, 75.6, 75.3, 69.7, 41.5, 36.0 ppm; HRMS (FAB, 3-NBA matrix) calcd. for $C_{62}H_{52}N_6O_4Zn$ ($M^+$), 1008.3342; found, 1008.4321 *m/z*.

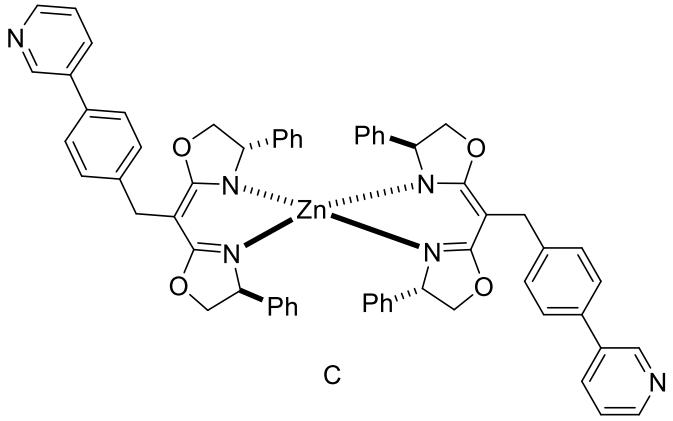


The complex C was prepared the same method. $^1$H NMR (400 MHz, $CDCl_3$): δ 8.9 (1H, s), 8.7 (1H, s), 8.0 (1H, m), 7.6-7.1 (13H, m), 7.0 (2H, s), 5.3 (2H, s), 4.7 (2H, m), 4.4-4.0 (3H, m), 3.4 (2H, m) ppm; 13C NMR (100 MHz, $CDCl_3$) δ 165.8, 165.6, 157.2,149.8, 149.5, 142.0, 142.0, 139.8, 138.6, 137.1, 137.0, 129.9, 129.0, 128.9, 128.8, 128.6, 127.9, 127.7,

127.6, 127.1, 127.0, 126.9, 126.7, 126.3, 125.5, 122.2, 122.0, 121.1, 120.7, 75.5, 75.3, 69.8, 41.5, 36.1 ppm; HRMS (FAB, 3-NBA matrix) calcd. for $C_{62}H_{52}N_6O_4Zn$ ($M^+$), 1008.3342; found, 1008.3322 *m/z*.

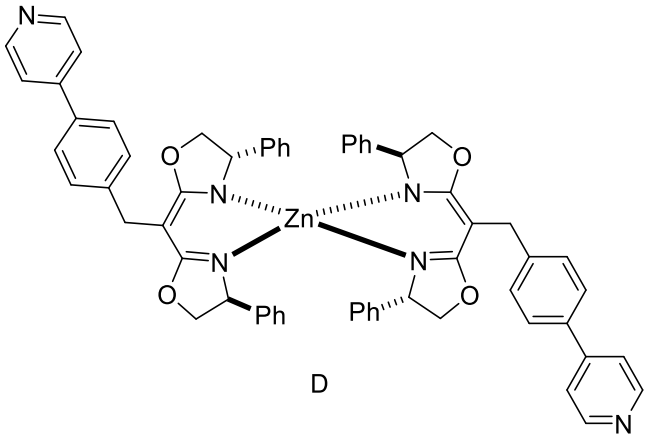


D

The complex D was prepared the same method. $^1$H NMR (400 MHz, $CDCl_3$): δ 8.7 (1H, s), 7.8-7.2 (17H, m), 7.0 (1H, s), 5.2 (2H, s), 4.7 (2H, m), 4.3-4.1 (2H, m), 3.5 (2H, m) ppm; 13C NMR (100 MHz, $CDCl_3$) δ 165.6, 165.5, 157.3, 149.8, 149.5, 142.1, 141.9, 139.6, 138.5, 137.1, 137.0, 129.9, 128.9, 128.8, 128.7, 128.6, 127.8, 127.7, 127.6, 127.1, 126.9, 126.8, 126.7, 126.2, 125.5, 122.3, 122.2, 121.1, 120.7, 75.5, 75.0, 69.6, 41.5, 36.0 ppm; HRMS (FAB, 3-NBA matrix) calcd. for $C_{62}H_{52}N_6O_4Zn$ ($M^+$), 1008.3342; found, 1008.4218 *m/z*.

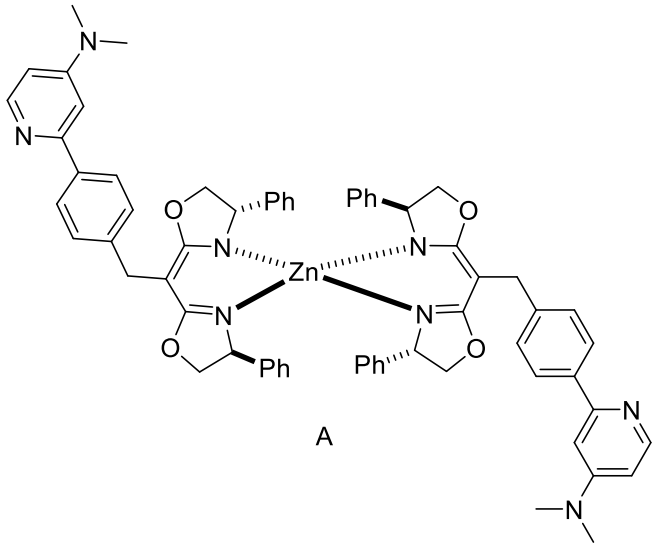

A

The complex A was prepared the same method. $^{1}$H NMR (400 MHz, $CDCl_3$): δ 9.0-8.7 (1H, broad), 8.2 (1H, s), 7.8 (2H, m), 7.5-7.4 (3H, m), 7.4-7.3 (9H, s), 7.2-7.0 (3H, m), 6.8 (2H, m), 6.6 (1H, m), 5.2 (2H, m), 4.7-4.6 (2H, m), 4.2-4.1 (2H, m), 3.8 (1H, m), 3.5 (2H, m), 3.1 (6H, s), 2.6 (1H, s) ppm; 13C NMR (100 MHz, $CDCl_3$) δ 165.9, 165.8, 157.2, 149.7, 149.4, 142.1, 141.8, 139.7, 138.6, 137.0, 136.9, 129.8, 129.0, 128.8, 128.7, 128.6, 127.8, 127.7, 127.6, 127.0, 126.9, 126.8, 126.7, 126.6, 125.5, 122.2, 122.1, 120.9, 120.7, 75.4, 75.3, 69.7, 41.5, 39.3, 36.0, 25.1 ppm; HRMS (FAB, 3-NBA matrix) calcd. for $C_{66}H_{62}N_8O_4Zn$ ($M^+$), 1094.4185; found, 1094.0048 *m/z*.

**5.6 Reference:**


1. T. Hayashi, M. Kumada, “Asymmetric Synthesis Catalysed by Transition-Metal Complexes with Functionalised Chiral Ferrocenylphosphine Ligands”, *Acc. Chem. Res*. **1982**, 15, 395
2. Z. Lu, S. Ma, “Metal-Catalyzed Enantioselective Allylation in Asymmetric Synthesis”, *Angew. Chem. Int. Ed*. **2008**, 47, 258
3. R. H. Crabtree, *The organometallic chemistry of the transition metals*. Wiley, **2009**, fifth edition
4. M. Magre, M. Biosca, O. Pamies, M. Dieguez, “Expanded Scope of the Asymmetric Hydrogenation of Minimally Functionalized Olefins Catalyzed by Iridium Complexes with Phosphite–Thiazoline Ligands”, *ChemCatChem*. **2015**, 7, 114
5. E. Fernandez, P. J. Guiry, K. P. T. Connole, J. M. Brown, “Quinap and Congeners: Atropos PN ligands for Asymmetric Catalysis”, *J. Org. Chem*. **2014**, 79, 5391
6. S. J. Roseblade, A. Pfaltz, “Iridium-catalyzed asymmetric hydrogenation of olefins”, *Acc. Chem. Res*. **2007**, 40, 1402
7. X. Chen, K. M. Engle, D. H. Wang, J. Q. Yu, “Palladium(II)-Catalyzed C—H Activation/C—C Cross-Coupling Reactions: Versatility and Practicality”, *Angew. Chem. Int. Ed*. **2009**, 48, 5094
8. M. A. Larsen, C. V. Wilson, J. F. Hartwig, “Iridium-Catalyzed Borylation of Primary Benzylic C-H Bonds Without Directing Group: Scope, Mechanism, and Origins of Selectivity”, *J. Am. Chem. Soc*, **2015**, 137, 8633
9. S. M. Smith, M. Uteuliyev, J. M. Takacs, “Catalytic asymmetric hydroboration of *β*,*γ*-unsaturated Weinreb amides: striking influence of the borane”, *Chem. Commun*, **2011**, 47, 7812
10. S. M. Smith, J. M. Takacs, “Remarkable Levels of Enantioswitching in Catalytic Asymmetric Hydroboration”, *Org. Lett*. **2010**, 12, 4612

11. S. M. Smith, G. L. Hoang, R. Pal, M. O. B. Khaled, L. S. W. Pelter, X. C. Zeng, J. M. Takacs, “γ-Selective directed catalytic asymmetric hydroboration of 1,1-disubstituted alkenes”, *Chem. Commun*. **2012**, 48, 12180
12. Z. Yang, R. Pal, G. L. Hoang, Z. C. Zeng, J. M. Takacs, “Mechanistic Insights into Carbonyl-Directed Rhodium-Catalyzed Hydroboration: ab Initio Study of a Cyclic γ,δ-Unsaturated Amide”, *ACS Catal*. **2014**, 4, 763
13. J. M. Takacs, D. S. Reddy, S. A. Moteki, D. Wu, H. Palenda, “Mechanistic Insights into Carbonyl-Directed Rhodium-Catalyzed Hydroboration: ab Initio Study of a Cyclic γ,δ-Unsaturated Amide”, *J. Am. Chem. Soc*. **2004**, 126, 4494
14. J. M. Takacs, K. Chaiseeda, S. A. Moteki, D. S. Reddy, D. Wu, K. Chandra, “Rhodium-catalyzed asymmetric hydrogenation using self-assembled chiral bidentate ligands”, *Pure. Appl. Chem*. **2006**, 78, 501
15. S. A. Moteki, K. Toyama, Z. Liu, J. Ma, A. E. Holmes, J. M. Takacs, “Two-stage optimization of a supramolecular catalyst for catalytic asymmetric hydroboration”, *Chem. Commun*. **2012**, 48, 263
16. L. Brandsma, H. D. Verkruijsse, Preparative Polar Organometallic Chemistry I. Berlin, Springer-Verlag, **1987**
17. A. S. Y. Lee W. C. Dai, “Facile and highly efficient sonochemical synthesis of organostannane via Barbier reaction”, *Tetrahedron*, **1997**, 53, 859
18. M. Nguyen, V. S. Nguyen, M. H. Matus, G. Gopakumar, D. A. Dixon, “Molecular mechanism for $H_2$ release from $BH_3NH_3$, including the catalytic role of the Lewis acid $BH_3$”, *J. Phys. Chem. A.* **2007**, 111, 679
19. B. Barsten, W. Konrad, M. Zehnder, T. Ranff, “Synthesis of Optically Active Bis(2-oxazolines): Crystal Structure of a 1,2-Bis(2-oxazolinyl)benzene $ZnCl_2$ Complexes”, *Chemische Benrichte*, **1991**, 124, 1173
20. Z. Gonzalez, J. G. Roman, E. Gonzalez, J. Martinez, J. R. Medina, K. Matos, J. A. Soderquist, “9-Borabicyclo[3.3.2]decanes and the Asymmetric Hydroboration of 1, 1-Disubstituted Alkenes”, *J. Am. Chem. Soc.* **2008**, 130, 9218

21. R. Corberan, N. W. Mszar, A. H. Hoveyda, “NHC-Cu-Catalyzed Enantioselective Hydroboration of Acyclic and Exocyclic 1,1-Disubstituted Aryl Alkenes”, *Angew. Chem. Int. Ed*. **2011**, 50, 7079